ENGINEERING RESEARCH INSTITUTE
UNIVERSITY OF MICHIGAN
ANN ARBOR

THE TRAJECTRON, AN EXPERIMENTAL DC MAGNETRON

Technical Report No. 18
Electron Tube Laboratory
Department of Electrical Engineering

BY

W. W. PETERSON

Approved by: W. G. DOW

G. HOK

Project 2009

CONTRACT NO. DA-36-039 sc-15450
SIGNAL CORPS, DEPARTMENT OF THE ARMY
DEPARTMENT OF THE ARMY PROJECT NO. 3-99-13-022
SIGNAL CORPS PROJECT 27-112B-0

Submitted in partial fulfillment of the requirements for the Degree of Doctor of Philosophy in the University of Michigan

May 1954

ABSTRACT

An experimental study of the dc cylindrical magnetron is described. An electron beam parallel to the axis of the magnetron is injected into the magnetron space charge close to the cathode surface at one end. The beam is deflected by the fields in the magnetron, and its exit point shows on a fluorescent screen at the other end of the magnetron. Through a study of the beam deflection, significant information about the electric field in the magnetron can be obtained.

According to the most widely used theory of the dc magnetron in the cutoff condition, the space charge is confined to a region between the cathode and a maximum radius commonly called the Hull radius. Experimental results indicate that the amount of space charge outside the Hull radius, far from being negligible, exceeds that within the Hull radius in many cases. The space charge outside the Hull radius consists primarily of electrons whose momentum or energy have been changed from initial values by collisions or irregularities in the fields, in such a manner that these electrons are trapped within the magnetron. Such space charge has sometimes been called secular space charge.

Calculations of beam electron orbits indicate that if the space charge in the magnetron agreed with the classical theory of the magnetron, it would be possible to determine from a study of the beam spot observed in these experiments which of the several possible types of orbits actually occur. Attempts to determine which of the classically possible orbits occur, or to find evidence of transitions from one type of orbit to another, indicate that the actual behavior does not correspond to any of the classically predicted behavior. There is apparently so much secular space charge relative to that in the stream emitted from the cathode that the latter has very little effect on the probing beam.

Control experiments are described. On the basis of these experiments, the electron probe technique and its limitations are discussed.

ACKNOWLEDGEMENTS

The author is indebted to the members of his doctoral committee, especially to Professor W. G. Dow, the chairman, for encouragement and for many valuable suggestions. Mr. J. R. Black and the personnel of the University of Michigan, Electron Tube Laboratory contributed invaluable advice and assistance in the design and construction of the trajectron. The author wishes to express his appreciation to Miss Priscilla L. Woodhead and the others who have assisted in the preparation of the text.

The author also wishes to acknowledge his indebtedness to the U. S. Signal Corps for their support of this research.

TABLE OF CONTENTS

TABLE OF CONTENTS (Cont'd)

LIST OF ILLUSTRATIONS

LIST OF ILLUSTRATIONS (cont.)

LIST OF ILLUSTRATIONS (cont.)

LIST OF ILLUSTRATIONS (cont.)

THE TRAJECTRON--AN EXPERIMENTAL DC MAGNETRON

CHAPTER I

INTRODUCTION

1.1 The Problem

The purpose of the research reported in this dissertation was to learn as much as possible about the potential distribution, space-charge distribution, and electron orbits in a cylindrical dc magnetron having a relatively large diameter cathode, by means of an experimental technique involving the use of an electron beam as a probe.

The trajectron, the dc magnetron used in the experiments, consisted of concentric cylindrical anode and cathode placed in the magnetic field of a solenoid. An electron gun was placed within the vacuum envelope with the magnetron diode and diode and positioned so that the beam electrons entered one end of the diode close to the cathode surface and parallel with the axis of the cathode. The exit point of the beam showed on a fluorescent screen placed at the other end of the diode. The electric field in the magnetron was studied through the deflection which it caused the beam to undergo.

According to the most widely used theory of the dc magnetron in the cutoff condition the space charge is confined to a region between the cathode and a maximum radius commonly called the Hull radius. The results of the trajectron experiment indicate that the space charge outside the Hull

radius is by no means negligible. In fact, rough calculations based on trajectron experiments for a typical situation in which the Hull radius was located approximately one-fifth of the distance from the cathode to the anode show the quantity of space charge outside the Hull radius to be several times the amount inside the Hull radius. This and other conclusions relative to the dc magnetron are discussed in detail in Chapter V and summarized in Chapter VI.

The initial plan was to interpret the data from the trajectron in the following simple manner: if initial velocities of both the beam electrons and the electrons emitted from the magnetron cathode and end effects in the magnetron diode could be neglected, the forces would be the same for beam electrons as for emitted electrons. The radial and angular displacements of the beam in a given transit time would then be the same as for emitted electrons in the same time. Thus, as the beam velocity was varied, the beam spot would trace the orbits of emitted electrons on the fluorescent screen. In control experiments[1] there was reasonably good agreement between the theoretical electron orbits and observed deflection of the beam when a non-emitting cathode was used. However, when an emitting cathode was inserted and the emitted current became space-charge-limited, the situation was changed markedly. The electron beam then entered the diode in a region of weak electric field and was deflected into a region of strong field. It has been both shown theoretically and observed in the trajectron that the beam defocuses under these circumstances. The defocussing effect is so important that the beam deflection cannot then be interpreted as being identical with the deflection of emitted electrons.

---

1 See Chapter IV.

However, it was found possible by use of more refined studies of electron beam motion to draw significant conclusions relative to the potential distribution and space-charge distribution.

In addition to these semi-quantitative conclusions, careful study of the beam motion in the trajectron contributes to an intuitive understanding of the character of the fields in the dc magnetron and the resulting electron motion. For example, it becomes clear that the electrons' canonical momentum (and hence their initial tangential velocity or initial radial position) is much more important than initial radial velocity.[1] Likewise, a more vivid understanding of the effects of the potential minimum on the motion electrons is obtained from the photographs and discussion of the trajectron data with emitting cathode and no magnetic field.[2]

1.2 Outline of Previous Work on the DC Magnetron

1.2.1 Introduction. The dc magnetron is a diode, usually with the anode and cathode surfaces concentric cylinders. It is operated with a positive voltage on the anode and in a uniform magnetic field parallel to the axis of the diode.[3] The anode current as a function of anode voltage of a typical dc magnetron is shown in Figure 1.1. The current is very small below a "cutoff voltage." As the anode voltage is increased through this cutoff range, the current rises rapidly. Above cutoff voltage the current is only slightly less than it would be in the absence of a magnetic field.

---

[1] This was also noticed by Twiss. See Refs. 44 and 45.

[2] See ection 4.5.

[3] The arrangement of electrode in a dc magnetron is illustrated in Fig. 2.4. A simplified drawing of the trajectron appears in Fig. 3.1.

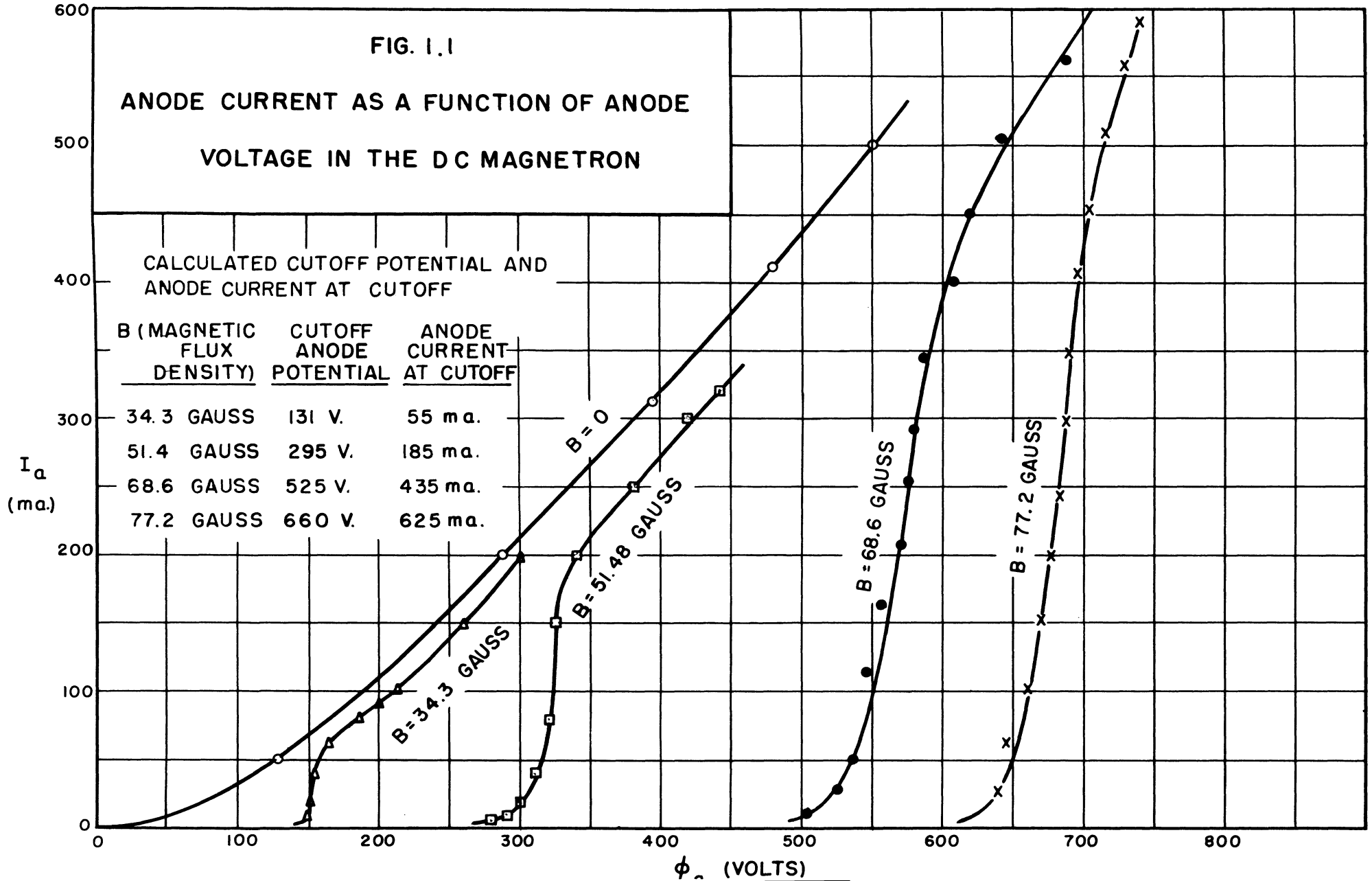
FIG. 1.1
ANODE CURRENT AS A FUNCTION OF ANODE VOLTAGE IN THE DC MAGNETRON
CALCULATED CUTOFF POTENTIAL AND ANODE CURRENT AT CUTOFF
B (MAGNETIC FLUX DENSITY) | CUTOFF ANODE POTENTIAL | ANODE CURRENT AT CUTOFF
34.3 GAUSS | 131 V. | 55 ma.
51.4 GAUSS | 295 V. | 185 ma.
68.6 GAUSS | 525 V. | 435 ma.
77.2 GAUSS | 660 V. | 625 ma.
B=0
B=34.3 GAUSS
B=51.48 GAUSS
B=68.6 GAUSS
B=77.2 GAUSS
I_a (ma.)
ϕ_a (VOLTS)
0
100
200
300
400
500
600
700
800

Most of the theoretical studies of magnetrons have been based on one of two idealizations of a practical magnetron, the infinite cylindrical magnetron, or the infinite planar magnetron. It has been possible to solve the equations of motion for electrons in these ideal magnetrons if initial velocities and electron collisions are neglected. For a magnetron in the cutoff condition several types of electron orbits are indicated by the theory. In one type, which in this dissertation is called the B_0 or single-stream solution, the electrons move in circles concentric with the cylindrical cathode (or in straight lines parallel to the planar cathode). In all other types the electrons move out from the cathode to a maximum radius and then back again to the cathode in a cycloid-like path. These are called double-stream solutions. The radial velocity may vanish or nearly vanish at a number of almost evenly spaced points between the cathode and the maximum radius. The solution with no such point is called the B_1 solution. If there is one such point, it is the B_2 solution; and if there are k such points, it is the B_{k+1} solution. The idea is illustrated in Figure 1.2.[4]

In the planar magnetron and under some conditions in the cylindrical magnetron, several or even infinitely many different solutions are theoretically possible with the same anode voltage and magnetic field. No adequate answer to the question of which of these solutions actually occurs has yet been given.

---

[1] The orbits sketched in Figure 1.2 are not accurate. Orbits drawn from actual solutions of the equations of motion appear in Figures 2.7 and 2.8.

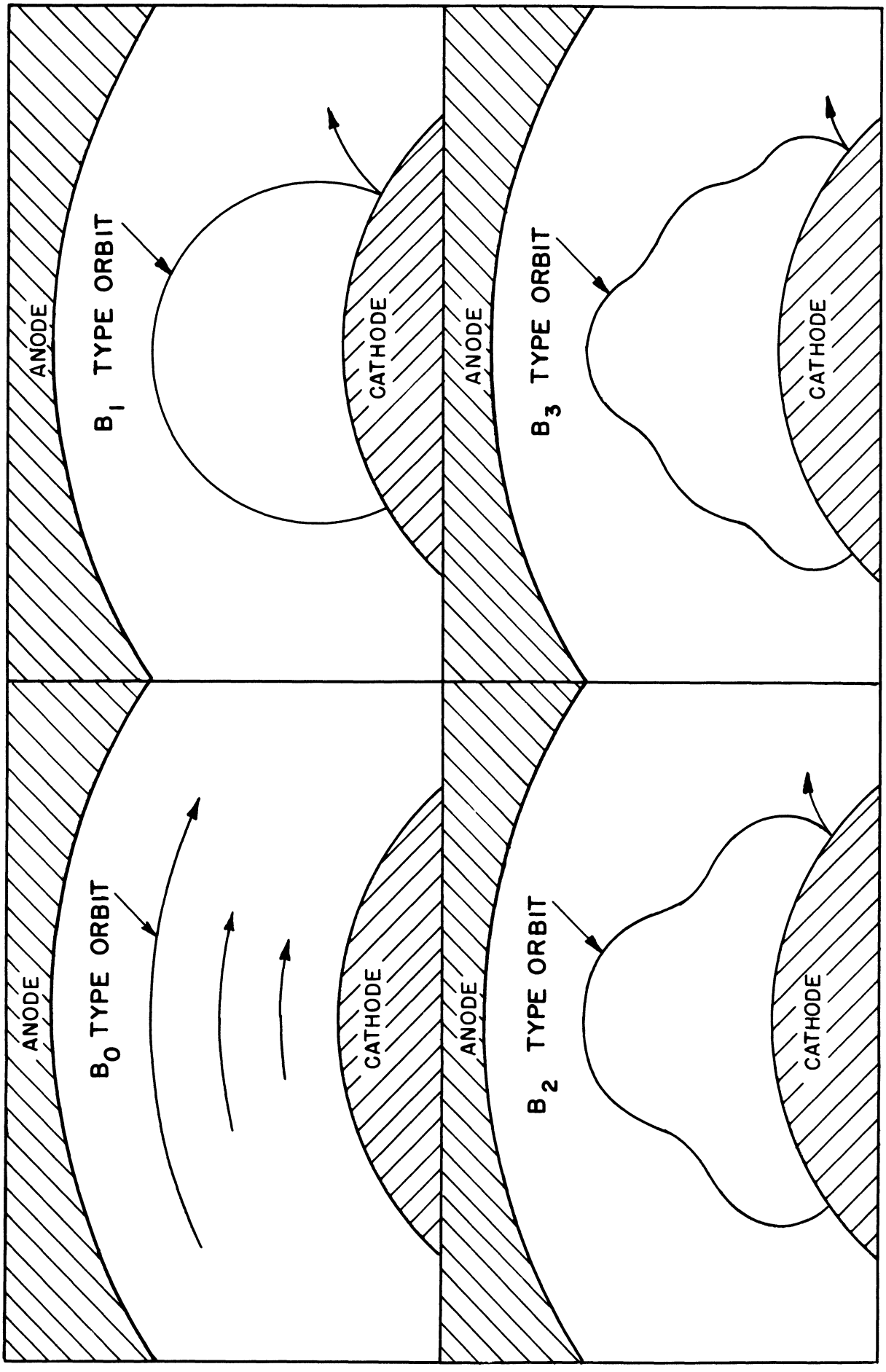

FIG. I.2 THEORETICAL TYPES OF ORBITS IN A DC MAGNETRON

The study of trajectron data has shown that none of these solutions is more than a crude approximation for the magnetron operating below cutoff.

1.2.2 Theoretical Work. In 1921 the classic paper of A. W. Hull introduced the magnetron to the scientific world.[5] After thirty-three years, after many studies by very capable men, there are still fundamental questions about even the dc magnetron which remain unanswered.

In his original paper Hull included both experimental and theoretical results. He derived the equations of motion and stated the cutoff condition for both the planar and cylindrical cases. He speculated that the orbits were of the double-stream type. Then in 1924, in a paper presented to the American Physical Society,[6] he described a solution of the equations of motion for the cylindrical magnetron in which the electrons move in circular paths concentric with the cathode and anode, i.e., the B_o or single-stream solution.

The equations of motion which Hull presented were derived on the assumption that initial velocities and electron collisions are negligible. They are the "self-consistent field" equations; i.e., they take into account the space charge of the moving electrons. Much of the theoretical effort on the static magnetron has been on obtaining the solution of these equations. This problem has been solved satisfactorily. The solution is presented in Chapter II, since it forms the basis for much of the discussion of the data obtained from the trajectron.

---

[1] Ref. 26.

[2] Ref. 27.

The earliest step towards the solution of the magnetron equations appears to have been presented by W. E. Benham in 1935.[1] He derives the equations of motion for the planar magnetron with the total current to the anode a known function of time. The equations are reduced to the following:

$$\ddot{x} + \omega^2 x = J , \tag{1.1}$$

where x is the distance from the cathode, ω is the cyclotron angular frequency,[2] and J is the current density to the anode, which may be a function of time. The dots represent differentiation with respect to time. Benham gave the solution for x as a function of time for the two important cases

$$J = J_o , \text{ and}$$

$$J = J_o + j_1 \sin pt. \tag{1.2}$$

These solutions did not play a prominent part in his paper, and he did not carry them to the logical conclusion by giving expressions for potential distribution, space charge density, and the electron orbits. The solution for a sinusoidally varying anode current did not appear in the literature again until Brillouin rediscovered it ten years later and discussed it very thoroughly.[3]

The solution for constant current was presented the same year, derived independently, by S. J. Braude.[4] Braude did discuss the electron orbits, potential distribution, and space charge distribution. He failed

---

1 Ref. 3.

2 $\omega = eB/m$, where B is the magnetic flux density, e the charge, and m the mass of an electron.

3 Ref. 8.

4 Ref. 6.

to fit his solution properly to the physical boundary conditions, and came to the erroneous conclusion that there could be no cutoff in the planar magnetron. The error was pointed out by Lewi Tonks,[1] and the solution for the planar magnetron was complete. The solutions have been derived and discussed by many authors since.[2]

The equations for the cylindrical magnetron cannot be integrated in terms of any commonly used functions. Therefore, only approximate or numerical solutions can be obtained. Most of the solutions given have been applicable only to the cylindrical magnetron with large ratio of anode radius to cathode radius.[3] The first satisfactory solution applicable to the entire range of anode radius to cathode radius ratio was that obtained by W. P. Allis, derived during the World War II research program.[4] This solution, together with some numerical solutions of Hartree[5] and the differential analyser solutions obtained by Brillouin,[6] have given a definitive picture of the solution for the cylindrical magnetron. A lucid derivation and description of the solutions for both the planar and cylindrical magnetrons are presented in two papers by Leon Brillouin and Felix Bloch.[7]

---

1 Ref. 43.

2 Bethenrod, Ref. 4; Boutry and Delcroix, Ref. 5; Delcroix, Ref. 12; Moullin, Ref. 34; Page and Adams, Ref. 35; Pidduck, Ref. 37; Slater, Ref. 39; Watanabe and Katsura, Ref. 49.

3 Glagolev, Ref. 22; Möller, Ref. 32; Page and Adams, Ref. 36; Pidduck, Ref. 37.

4 Ref. 1.

5 Ref. 24.

6 Ref. 9.

7 Refs. 8 and 9.

Solutions obtained by neglecting initial velocities and collisions fail completely to explain the small flow of current when the anode potential is below cutoff. (See Figure 1.1.) A number of authors have attempted to find the explanation of this phenomenon. Harvey[1] describes theoretical studies of the effects of finite rather than infinite geometry. Several authors have discussed the effects of initial velocities.[2] A few have attacked the difficult problem of including the random interaction effects of electrons.[3] The possibility of oscillation and noise amplification in the space charge has been studied.[4] All of these factors seem to enter the problem, and their relative importance has not yet become clear.

By far the most satisfactory study of the effects of initial velocities is that of Twiss.[5] The equations involved are quite complicated. Twiss has done a remarkable job of finding the nature of the solutions without actually solving the equations. The most important results are as follows: the tangential initial velocities are far more important than normal initial velocities; when tangential initial velocities are considered, the solution must be of the double-stream type; and the initial velocities, although they account for a small current to the anode below cutoff, do not account for currents as large as are observed.

---

1 Ref. 25.

2 Fechner, Ref. 20; Twiss, Refs. 44 and 45; Watanabe and Katsura, Ref. 49.

3 Gabor, Ref. 21; Hok, Refs. 28 and 29; Lindsay and Sims, Ref. 31.

4 e.g. Guénard and Huber, Ref. 23; Warnecke, Huber, Guénard, and Doehler, Refs. 46 and 47.

5 Refs. 44 and 45.

The recent paper by G. Hok[1] is the best discussion of the magnetron from the point of view of statistical mechanics. Unfortunately, as both Twiss and Hok point out, the dc magnetron is not in or even near statistical equilibrium, nor is it in the state studied by Twiss, where electron collisions are neglected. Rather it is somewhere between. Nevertheless, the ideas presented by Hok and Twiss are a step closer to the actual conditions than previous studies. A discussion of some of Hok's concepts and their implications with respect to the electron orbits is given in Chapter II.

1.2.3 Experimental Studies of the DC Magnetron. In his original paper, Hull described many detailed observations of the behavior of the magnetron.[2] His experiments included investigation of the effect of filament heating current, anode voltage, filament temperature, anode diameter, electrode alignment, magnetic field alignment, and gas pressure. He studied the magnetron with concentric cylindrical anode and cathode both with the cathode at the center and with the anode at the center. In all cases the ratio of the radius of the outside electrode to the radius of the inside electrode was much larger than one.

Harvey[3] also described experiments on the effect of misalignment of electrodes and magnetic field. He compared curves in the neighborhood of cutoff for various anode voltages and magnetic fields. He pointed out that if the disagreement with the theoretical curve were caused by the

---

1 Refs. 28 and 29.

2 Ref. 26.

3 Ref. 25.

initial velocity distribution, the actual cutoff curve would approach the ideal as the anode voltage is increased. His experiments indicated that this did not occur.

Möller obtained an estimate of the current of the rotating space charge in the magnetron by measuring the small change it produces in the axial magnetic field.[1] He reported the measured current nine per cent weaker than predicted for the B_1 solution. He stated that this was within the limits of experimental error. More recently Wasserman[2] conducted a similar experiment and reported agreement within fifteen per cent of the B_0 solution. The tubes used in both of these experiments had filamentary cathodes. This is not a promising technique for distinguishing between the various types of solutions because it requires measuring a very weak magnetic field in the presence of a strong magnetic field (in Möller's case, 0.7 gauss in 5000). Also, the magnetic fields for the various solutions are probably very nearly the same. The current of the moving space charge parallel to the cathode of a planar magnetron with given anode voltage and magnetic field is the same for the whole series of solutions, B_0, B_1, B_2, and so on.

The potential distribution in a dc magnetron with filamentary cathode was measured by Engbert[3] with a probe. The probe potential was varied until the deflection of the wire as observed with a microscope was

---

1 Ref. 33.

2 Ref. 48.

3 Ref. 19.

zero, and this potential was presumed to be the potential at that point in the tube. Control experiments with no magnetic field were run. The potential distribution curves found experimentally with no emission, temperature-limited emission, and space-charge-limited emission agreed very well with theory. The experimentally determined potential distribution in the magnetron, when normalized with respect to anode potential, was found to be almost independent of anode voltage, magnetic field, and filament emission over a wide range if the anode voltage was kept near but somewhat below cutoff. The potential curve was parabolic near the cathode, but nearly linear near the anode. The data did not appear accurate enough to permit calculation of space-charge distribution, making comparison with theory difficult.

Another phenomenon of the dc magnetron, noticed by a number of workers, was studied in some detail by Linder and Wigdortschik.[1] In a dc magnetron with a filamentary cathode, the current to a small probe was measured as a function of probe potential. The experiments indicated that the electrons in the space charge had a Maxwellian distribution of velocities with average energy approximately 4 percent of the anode voltage. Linder showed that this random energy was much too large to be explained by collisions of electrons with ions or other electrons. He suggested that the high temperature of the space charge may be due to some sort of oscillation such as plasma oscillations.

An experimental measurement of the field in a dc magnetron by an electron-optical method was carried out by Reverdin.[2] A beam of electrons was passed through a wire mesh, through the magnetron diode, and then through another mesh. Images of both meshes were focused on a fluorescent

---

1 Linder, Ref. 30; Wigdortschik, Refs. 50; Spiwak and Zrebny, Ref. 40.

2 Ref. 38.

screen, and from their relative positions the electric field could be calculated. The magnetron diode had a filamentary cathode. Three different space-charge distributions were observed: one had its maximum near the cathode and fell off gradually with increasing radius; another had a maximum roughly at the edge of the space charge cloud; and the third was time-varying.

The method described in this dissertation was first used by Svensson.[1] His work is reported very briefly, and can be considered no more than the introduction of a promising technique. This technique was employed and appraised in the experiment reported herein.

The anode current as a function of anode voltage was studied carefully by Delcroix in a series of tubes with guard rings and with the ratio of anode radius to cathode radius ranging from 1.25 to 7.5.[2] Delcroix noticed discontinuities in the anode current as the anode voltage was varied. The voltage at which these occurred was roughly proportional to the square of the magnetic field, and they occurred in the range of anode voltage in which changes might be expected from one theoretical type of space charge to another (as B_1 to B_2, for example). Delcroix identified regions of operation indicated by these discontinuities and suggested that these regions are very likely the regions in which particular theoretical types of space charge occur.

In a very thorough paper, Guénard and Huber[3] described a series of experiments designed to investigate the possibility that amplification can occur in magnetron-type space charge without the presence of a slow-wave structure. Most of the experiments were carried out with a linear

---

[1] Ref. 42. [2] Refs. 14, 15, and 16. [3] Ref. 23.

magnetron. The electrons were emitted from an electron gun, passed through a region of crossed electric and magnetic fields, and were removed from the tube at a collector electrode. In one experiment an rf wave was introduced near the electron gun and rf power was taken from the tube at a point near the collector. Amplification of 20 db. was observed in tubes of this type. In another experiment, the current to a probe was measured as a function of probe potential. The measurements showed large components of randomly distributed velocity at a point which electrons reached from the electron gun after a few Larmor periods.

If amplification occurs in the space charge, then oscillations would be expected when this stream of electrons is closed on itself, as in the dc cylindrical magnetron. Such oscillations were observed, and the frequency of observed oscillations agreed quite well with theoretical predictions.

CHAPTER II

THEORY OF THE DC MAGNETRON

2.1 Introduction

In this chapter the theoretical background necessary for interpreting the data obtained from the trajectron is presented. This is not intended to be a complete exposition of the theory of the dc magnetron. Only phases of the theory which will come up in discussion of the design or the results of the trajectron experiment are discussed. The idea behind the trajectron was to measure electron trajectories, and the mechanism used for obtaining data in the trajectron was the trajectory of a beam of electrons. Therefore it is fitting that the electron trajectory be emphasized and discussed at length, while the potential and space charge distributions play a secondary role.

Most of the chapter is devoted to the solution of the magnetron equations for the case of no initial velocities or discrete electron interactions. The resulting solutions, which are described qualitatively on page 5, are discussed in more detail and some graphs of solutions are presented.

In all these solutions, the space charge is confined to a region between the cathode and a maximum radius, called the Hull radius. The trajectron experimental results indicate that there is space charge outside the Hull radius. The explanation lies in the fact that conservation of energy and angular momentum was assumed for individual electrons in the deviation of these solutions. Actually electron

collisions may occur, and electron energy and momentum are subject to changes. As a result of such a change, an electron may traverse an orbit confined to the region between the anode and the cathode, but not necessarily inside the Hull radius. The space charge observed to be outside the Hull radius in the trajectron is undoubtedly made up of such electrons, which are called "secular electrons." The concept of secular space charge is discussed in Section 2.6.1, and in Section 2.6.2 the effects of secular space charge on the orbits in the stream of electrons emitted from the cathode are investigated.

The units used in all equations are MKS unless otherwise noted. When numerical values of magnetic flux density B or the ratio ϕ_a/B^2 of anode voltage to flux density squared, B is measured in Gauss.

2.2 The Motion of an Electron in the Fields of a Planar Magnetron

The planar magnetron consists of parallel planar cathode and anode with a uniform magnetic field parallel to the cathode. A rectangular coordinate system is used in describing the motion of electrons in the planar magnetron, with the y axis perpendicular to the cathode and the z axis parallel to the magnetic field, as illustrated in Figure 2.1. The electric potential ϕ is assumed constant in time and dependent only upon the y coordinate; notice that this includes assuming the existence of a steady state. The magnetic field is assumed uniform and parallel to the z axis, with flux density B.

It is most convenient to derive the equations of motion from the Lagrangian.[1] The Lagrangian for an electron in an electromagnetic field can be written

$$L = T + \phi + e\vec{A}\cdot\vec{v} \quad . \tag{2.1}$$

where T is the kinetic energy, ϕ the electric potential, $\vec{A}$ the vector

[1]Goldstein, Ref. E, p. 19.

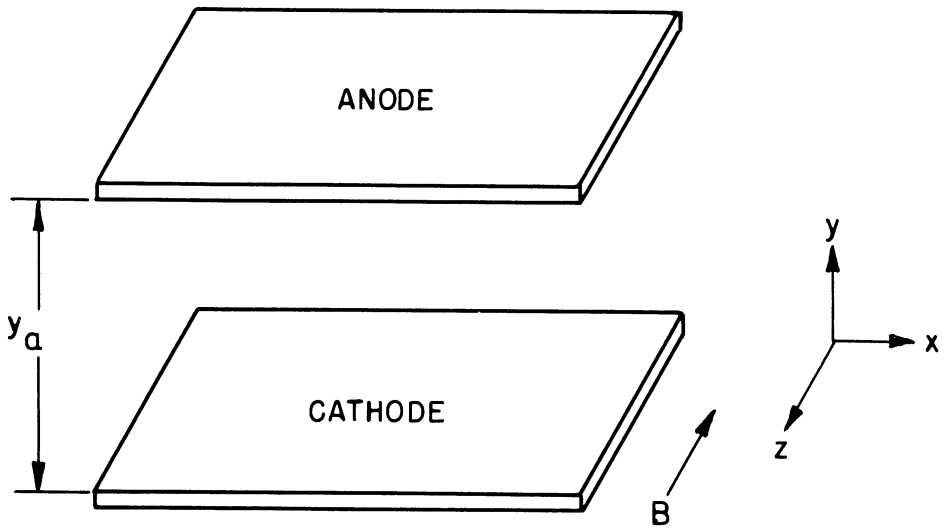

FIG. 2.1

COORDINATE ARRANGEMENT USED IN THE DISCUSSION OF THE PLANAR MAGNETRON

potential of the magnetic field, and m is the mass of an electron.[1]

A suitable choice for the vector potential $\vec{A}$ is as follows:

$$A_y = Bx$$
$$A_x = A_z = 0 \quad . \tag{2.2}$$

With this choice of $\vec{A}$, curl $\vec{A}$ has a component only in the z direction and that component has strength B.

In the rectangular coordinate system, the kinetic energy T can be written

$$T = \frac{m}{2}(\dot{x}^2 + \dot{y}^2 + \dot{z}^2) \quad , \tag{2.3}$$

where the dot denotes differentiation with respect to time, and m is the mass of an electron. Thus the Lagrangian can be written

$$L = \frac{m}{2}(\dot{x}^2 + \dot{y}^2 + \dot{z}^2) + e\phi(y) - eBx\dot{y} \quad , \tag{2.4}$$

and the equations of motion are

$$\frac{d}{dt}\frac{\partial L}{\partial \dot{x}} - \frac{\partial L}{\partial x} = 0 \quad ,$$
$$\frac{d}{dt}\frac{\partial L}{\partial \dot{y}} - \frac{\partial L}{\partial y} = 0 \quad , \text{ and}$$
$$\frac{d}{dt}\frac{\partial L}{\partial \dot{z}} - \frac{\partial L}{\partial z} = 0 \quad . \tag{2.5}$$

If the expression (2.4) is substituted for L, equation (2.5) becomes

$$m\ddot{x} + e B\dot{y} = 0 \quad , \tag{2.6a}$$
$$m\ddot{y} - e B\dot{x} - \frac{ed\phi}{dy} = 0 \quad , \text{ and} \tag{2.6b}$$
$$m\ddot{z} = 0. \tag{2.6c}$$

These are the equations of motion of an electron in the magnetron in

---

[1] A reader not familiar with Lagrangian mechanics may proceed to equation (2.6).

the ordinary Newtonian form, with the forces due to the magnetic field included.[1]

Energy and momentum integrals can be derived from equations (2.6) for an arbitrary potential field and for arbitrary initial conditions. These equations will be used in Chapters IV and V in discussing the motion of the electron beam in the magnetron diode as well as in finding the self-consistent field solution for the planar magnetron.

The solution of equation (2.6c) is

$$z = \dot{z}_o\, t + z_o \quad , \tag{2.7}$$

where $\dot{z}_o$ is the initial z component of velocity and z_o the initial z displacement. Equation 2.6a can be integrated once to

$$m\dot{x} + e\, B_y = P_x \tag{2.8}$$

where P_x is a constant of integration. If there were no magnetic field, the x-component of linear momentum would be constant, because the electric field has no x-component. This equation expresses the corresponding relation with the magnetic field present, and P_x is usually called the generalized or canonical momentum. P_x can be found in terms of initial velocity and displacement by considering its initial value

$$P_x = m\dot{x}_o + eBy_o \quad , \tag{2.9}$$

where $\dot{x}_o$ is the initial x-velocity and y_o is the initial y-displacement.

There is one more integration which can be carried out at this point. Multiplying (2.6a) by $\dot{x}$, (2.6b) by $\dot{y}$, and (2.6c) by $\dot{z}$, and adding gives

$$m\ddot{x}\dot{x} + m\ddot{y}\dot{y} + m\ddot{z}\dot{z} - e\,\frac{d\phi}{dy}\,y = 0 \quad . \tag{2.10}$$

---

[1] See, for example, Dow, Ref. B, p. 46.

This can be integrated to

$$\frac{m}{2}(\dot{x}^2 + \dot{y}^2 + \dot{z}^2) - e\phi(y) = E \quad , \tag{2.11}$$

where E is a constant of integration called the total energy. The equation expresses conservation of energy for this problem. The total energy for any electron can be expressed in terms of initial velocity and position by considering the initial value of E.

$$E = \frac{m}{2}(\dot{x}_o^2 + \dot{y}_o^2 + \dot{z}_o^2) - e\phi(y_o) \quad , \tag{2.12}$$

where $\dot{x}_o$, $\dot{y}_o$, and $\dot{z}_o$ are the components of initial velocity and y_o is the initial y-displacement.

2.3 The Planar DC Magnetron

The plan of this solution is to asuume that electrons are emitted from the cathode at a uniform rate. The local variations of the potential due to the discrete nature of electrons are neglected, but the average effect of the space charge is brought in through Poisson's equation. All electrons are assumed to have congruent orbits. Then the equations of motion are written and solved for any one electron.

The initial conditions assumed for this electron are

$$x_o = y_o = z_o = \dot{x}_o = \dot{y}_o = \dot{z}_o = 0 \quad , \tag{2.13a}$$

i.e., at time t = 0 the electron is at rest on the cathode surface. Then equation (2.7) becomes

$$z \equiv 0 \quad . \tag{2.13b}$$

Since $\dot{x}$ and y are initially zero, P_x is zero. It is convenient to denote by ω_L the Larmor angular frequency, which is defined as

$$\omega_L = \frac{eB}{2m} \quad . \tag{2.14}$$

Then (2.9) can be written

$$\dot{x} = -2\omega_L y \quad . \tag{2.15}$$

With these initial conditions, equation (2.12) becomes

$$m\left(\frac{\dot{x}^2}{2} + \frac{\dot{y}^2}{2}\right) = +e\phi \quad , \tag{2.16}$$

where the constant E has been chosen to make $\phi = 0$ on the cathode.

Substituting (2.15) in (2.16) to eliminate x yields

$$\phi = +\frac{m}{2e}\left(4\omega_L^2 y^2 + \dot{y}^2\right) \quad . \tag{2.17}$$

Since $\dot{y}^2$ must be equal to or greater than zero, an electron cannot reach any region in the magnetron where the potential is less than $\frac{2m\,\omega_L^2\,y^2}{e}$. The symbol y_h denotes the greatest distance from the cathode that an electron emitted from the cathode with zero velocity could reach. This distance y_h can be found by solving the equation

$$\phi(y_h) = \frac{2m\,\omega_L^2\,y_h^2}{e} \quad . \tag{2.18}$$

It follows also that if an electron is to reach the anode,

$$\phi_a \geq \phi \text{ cutoff} = \frac{m}{2e}\left(4\omega_L^2 y_a^2\right) \quad . \tag{2.19}$$

So far, nothing has been required of the potential ϕ except that it depend only upon y. This is to be a self-consistent field solution. Hence the effect on the potential of the space charge due to the moving electrons themselves is to be included. The potential ϕ must satisfy Poisson's equation:

$$\nabla^2\phi = -\frac{\rho}{\epsilon_o} \tag{2.20}$$

where ρ is the space charge density, and ϵ_o is the permitivity of a vacuum. Since ϕ depends only upon y, this reduces to

$$\frac{d^2\phi}{dy^2} = -\frac{\rho}{\epsilon_o} \quad . \tag{2.21}$$

Since the space charge is assumed to be flowing from the cathode at a constant rate, the current per unit area must be a constant. The following relationship must hold between electric current density J and space charge density ρ:

$$J = \rho\dot{y}, \quad \text{or} \quad \rho = \frac{J}{\dot{y}} \tag{2.22}$$

This is the case if the electrons all leave the cathode and go to the anode with positive radial velocity. Another case is important. The electrons may move out to some radius, cease radial motion, and return to the cathode. The net current would be zero, since there would be equal current density for flow in each direction. Equation (2.22) can still be applied for this case if J is interpreted as the sum of absolute values of the two currents, i.e., twice the emitted current. The $\dot{y}$ will have the same magnitude for both streams; since ϕ and $\dot{x}$ are both functions of y only, it follows from (2.16) that the magnitude of $\dot{y}$ depends only upon y.

The magnetron is assumed to be space charge limited. This requires that the potential gradient be zero at the cathode, or

$$\frac{d\phi}{dy} = 0 \text{ where } y = 0 \quad . \tag{2.23}$$

The equations necessary for the self-consistent field solution are summarized below:

$$m\ddot{y} - eB\dot{x} - e\frac{d\phi}{dy} = 0 \quad , \tag{2.66}$$

$$\dot{x} = -2\omega_L y \quad , \tag{2.15}$$

$$\frac{d^2\phi}{dy^2} = -\frac{\rho}{\epsilon_o} \quad , \tag{2.21}$$

$$\rho = \frac{J}{\dot{y}} \quad . \tag{2.22}$$

The initial conditions are

$$x_o = y_o = z_o = \dot{x}_o = \dot{y}_o = \dot{z}_o = 0 \quad , \tag{2.13}$$

and

$$\frac{d\phi}{dy} = 0 \quad \text{where } y = 0 \quad . \tag{2.23}$$

One simple solution of the equations is that called the B_o or single-stream solution. Suppose the y velocity is identically zero for electrons at every distance from the cathode out to some y_h. Then for any particular electron, y is constant. By (2.15) the x-velocity is constant, $2\omega_L y$, for any given electron, and thus

$$x = -2\omega_L y t \quad . \tag{2.24}$$

The potential distribution can be found from the energy integral (2.17):

$$\phi = +\frac{m}{2e}(\dot{x}^2+\dot{y}^2) = +\frac{2m\omega_L{}^2 y^2}{e} \tag{2.25}$$

The space charge density can be found from Poisson's equation (2.21) to be

$$\rho = \frac{4m\,\epsilon_o\omega_L{}^2}{e} \tag{2.26}$$

The current density in the y direction is zero, since $\dot{y} = 0$. Thus all the equations are satisfied.

All of the other self-consistent field solutions, called double-stream solutions, are derived as follows. Equation (2.21) can be

written

$$\frac{dF}{dy} = \frac{\rho}{\epsilon_o} \tag{2.27}$$

where F is the y-component of electric field. Multiplying both sides by $\dot{y}$ and noting (2.22)

$$\frac{dF}{dy} \cdot \dot{y} = \frac{dF}{dt} = \frac{\rho \dot{y}}{\epsilon_o} = \frac{J}{\epsilon_o} \tag{2.28}$$

The term $\frac{dF}{dt}$ is the time rate of change of electric field which an electron experiences while moving through the field. The field itself is not changing with time, of course. Equation (2.28) can be integrated, since J is constant, as follows:

$$F = \frac{Jt}{\epsilon_o} \quad . \tag{2.29}$$

The constant of integration was chosen to make F zero on the cathode in accordance with (2.23).

Equation (2.6b) can be written

$$m\ddot{y} + eB\dot{x} = eF \quad . \tag{2.30}$$

Equation (2.15) can be used to eliminate $\dot{x}$, and F is eliminated by using (2.29). Then

$$\ddot{y} + \frac{eB}{m} \cdot 2\omega_L y = \frac{eJ}{m\epsilon_o} t \quad , \text{ or}$$

$$\ddot{y} + 4\omega_L{}^2 y = \frac{eJ}{m\epsilon_o} t \quad . \tag{2.31}$$

An obvious particular solution of this linear differential equation is

$$y = \frac{eJ}{4\omega_L{}^2 m\epsilon_o} t \quad ,$$

and thus the general solution is

$$y = \frac{eJ}{4\omega_L{}^2 m\epsilon_o} t + C_1 \sin 2\omega_L t + C_2 \cos 2\omega_L t$$

where C_1 and C_2 are constants of integration. The condition y = 0 when

$t = 0$ requires C_2 to be zero. The condition $\dot{y} = 0$ when $t = 0$ requires C_1 to be $-\frac{eJ}{8\omega_L^3 m\epsilon_o}$, and thus the solution of (2.28) is

$$y = \frac{eJ}{8\omega_L^3 m\epsilon_o}(2\omega_L t - \sin 2\omega_L t) \quad . \tag{2.32}$$

For convenience, let

$$\frac{W}{2\pi} = \frac{eJ}{8\omega_L^3 m\epsilon_o} \quad . \tag{2.33}$$

Then (2.29) becomes

$$y = \frac{W}{2\pi}(2\omega_L t - \sin 2\omega_L t) \quad , \tag{2.34}$$

and

$$\dot{y} = \frac{\omega_L W}{\pi}(1 - \cos 2\omega_L t) \quad , \tag{2.35}$$

The y-velocity vanishes when $2\omega_L t$ is any multiple of 2π. The points where $\dot{y}$ vanishes are spaced W units apart on the y-axis.

The x-displacement can be found from equation (2.15):

$$\dot{x} = -2\omega_L y \quad , \text{ or}$$

$$x = \int_0^t \left[-2\omega_L y\right] dt \quad . \tag{2.36}$$

Substituting for y from equation (2.34) and integrating yield

$$x = -\frac{W}{2\pi}(2\omega_L^2 t^2 - 1 + \cos 2\omega_L t) \quad . \tag{2.37}$$

The boundary conditions at the cathode are met by these solutions. However, when the anode voltage is specified, another set of boundary conditions must be met. Consider first the cutoff magnetron.

The electrons are confined to the region between $y = 0$ and $y = y_h$ where

$$\phi\,(y_h) \;=\; +\frac{m}{2e}\,(4\omega_L{}^2 y_h^2) \quad . \tag{2.18}$$

Inside this region the potential distribution is given by (2.17), and between $y = y_h$ and the anode, there is no space charge, so that the potential is linear. Both ϕ and its derivative must be continuous inside the magnetron, and in particular at the boundary of the space charge.

The potential at the boundary given by (2.18) holds for both single-stream and double-stream solutions. The potential gradient at the boundary for the single-stream solution is, from (2.25),

$$\left(\frac{d\phi}{dy}\right)_{y_h} \;=\; \frac{d}{dy}\left[\left(+\frac{m}{2e}\cdot 4\omega_L{}^2 y^2\right)\right]_{y_h} \;=\; +\frac{4m\omega_L{}^2 y_h}{e} \tag{2.38}$$

The potential gradient at the boundary of the double-stream solution can be found from (2.29) to be

$$\frac{d\phi}{dy} \;=\; -F \;=\; -\frac{Jt}{\epsilon_o} \quad . \tag{2.29}$$

J can be eliminated by using (2.33)

$$\frac{d\phi}{dy} \;=\; -t\cdot\frac{8\omega_L{}^3 m}{e}\cdot\frac{W}{2\pi} \tag{2.39}$$

At the space-charge boundary $\dot{y} = 0$, and so $2\omega_L t$ is a multiple of 2π, say $2\pi n$. Then y_h must be nW. Eliminating t and W yields

$$\frac{d\phi}{dy} \;=\; +\frac{4m\omega_L{}^2 y_h}{e} \tag{2.40}$$

which is the same as equation (2.38). Thus regardless of which solution applies, the potential distribution is linear between y and the anode; and at y_h, ϕ, and $\frac{d\phi}{dt}$ satisfy (2.37) and (2.38). Thus the anode potential is

$$\phi_a \;=\; -\frac{4m\omega_L{}^2 y_h{}^2}{2} - \frac{4m\omega_L{}^2 y_h}{e}\,(y_a - y_h) \quad . \tag{2.41}$$

The y_h as a function of anode voltage can be found by solving this equation. The anode voltage determines only y_h, and the boundary conditions are completely satisfied by the single-stream (or B_0) solution, or the double-stream solution with $W = y_h/n$ where n is any integer.

The solution with $W = y_h$ is called the B_1 solution. If $W = y_h/2$, this is a B_2 solution, and in general $W = y_h/n$ gives the B_n solution. The orbits of the B_1 and B_2 solutions and the potential distribution of the B_0, B_1 and B_2 solutions are shown in Figures 2.2 and 2.3. Theoretically one cannot say for a double-stream solution whether an electron will go through or turn around at a point inside the space-charge region where $\dot{y} = 0$. The electrons are illustrated as going through.

The emission current required for the single-stream solution is zero. For the double-stream solutions it is given by equation (2.33). (Note that for a cutoff magnetron the emission current density is J/2.)

The cutoff voltage for the magnetron is given by (2.19). Presumably any double-stream solution could occur, and as the voltage is decreased toward the cutoff voltage, the current would approach the value given by (2.33). There should be absolutely no anode current if the anode voltage is below cutoff.

2.4 The Motion of an Electron in the Field of a Cylindrical Magnetron

The cylindrical magnetron consists of concentric cylindrical cathode and anode with a uniform magnetic field parallel to the axis of the tube. A cylindrical coordinate system is used, with the z-axis the axis of the tube, as illustrated in Figure 2.4. The electric potential is assumed constant in time and dependent only upon the r and z coordinates. The magnetic flux density will be denoted by B.

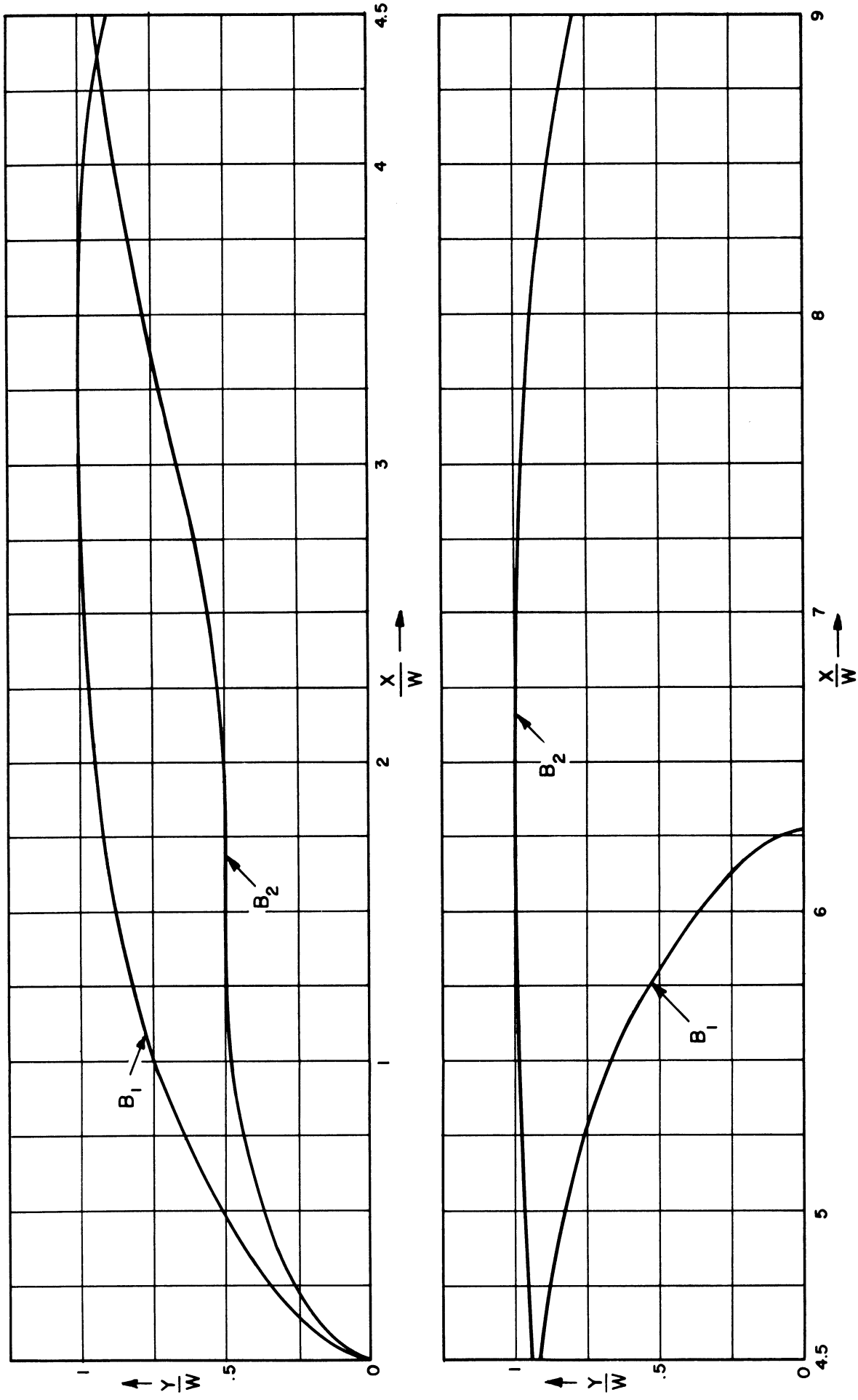

FIG. 2.2 DOUBLE-STREAM ELECTRON ORBITS IN THE PLANAR MAGNETRON

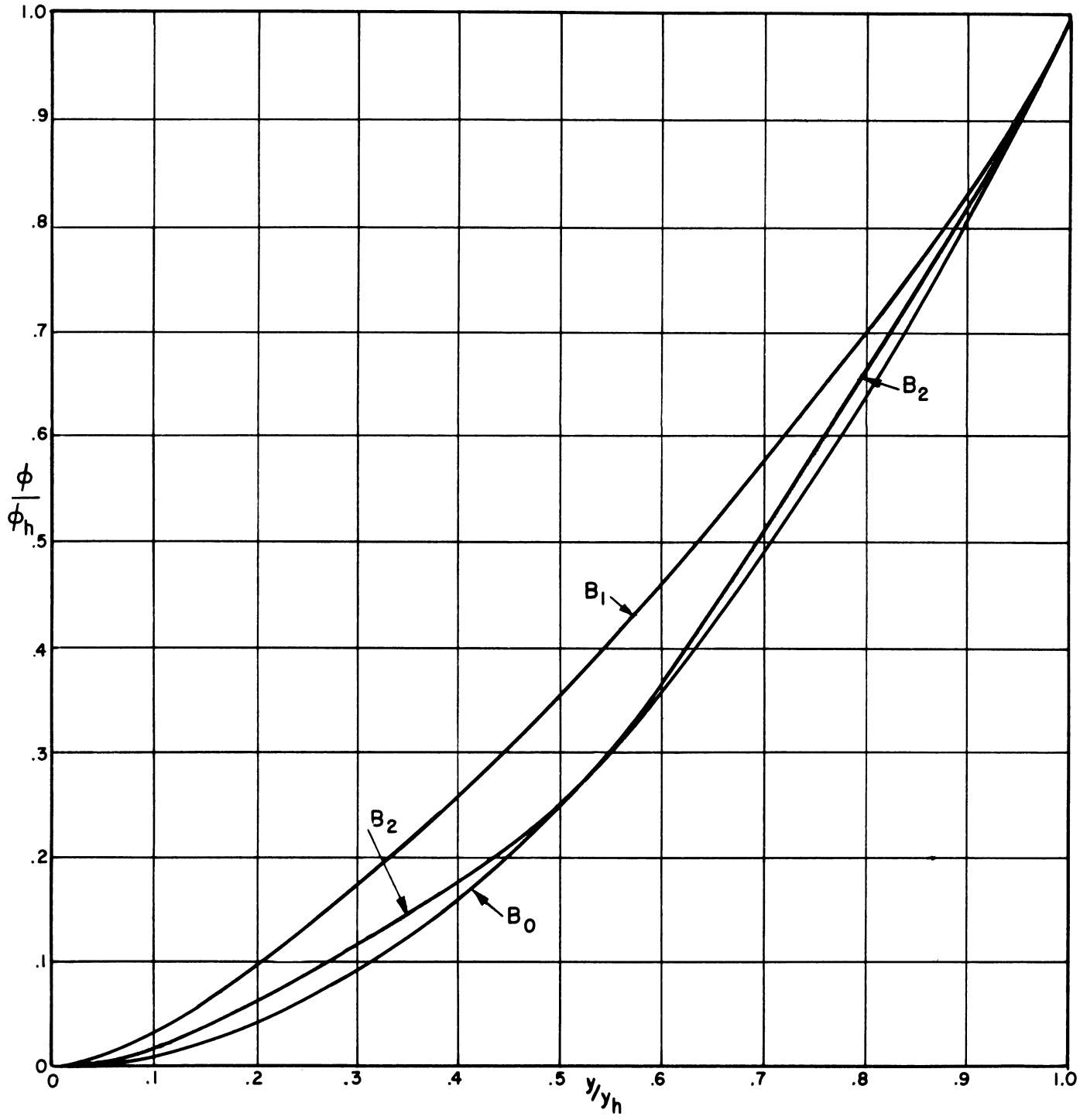

FIG. 2.3

POTENTIAL DISTRIBUTION IN A PLANAR MAGNETRON

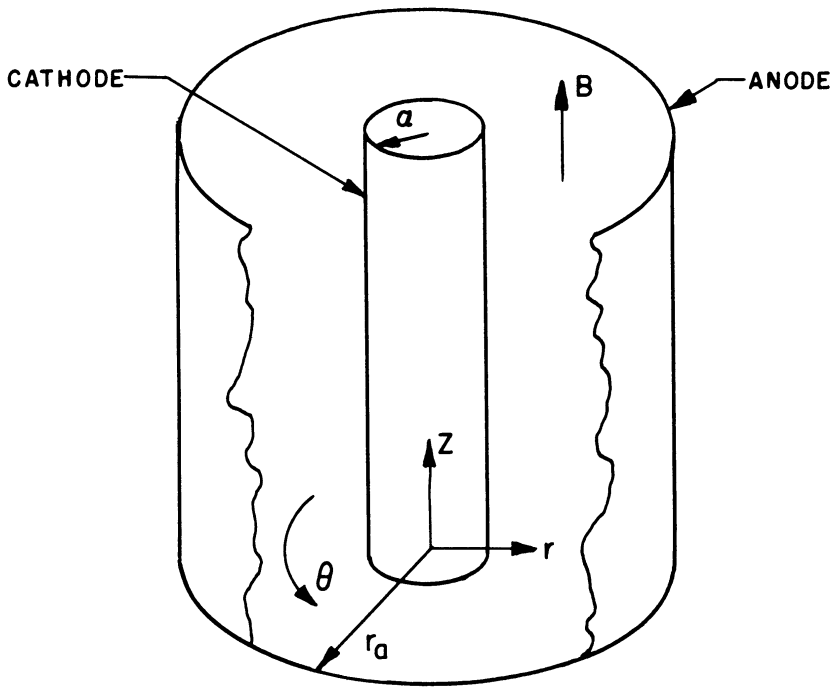

FIG. 2.4

COORDINATE ARRANGEMENT USED IN THE DISCUSSION OF THE CYLINDRICAL MAGNETRON

Again it is convenient to derive the equations of motion from the Lagrangian.[1] A suitable choice for the vector potential $\vec{A}$ is

$$A_z = A_r = 0 ,$$
$$A_\theta = \frac{Br}{2} . \tag{2.42}$$

With this choice of $\vec{A}$, curl $\vec{A}$ has no component in the r or θ direction, and the z-component is constant, equal to B. In the cylindrical coordinate system the kinetic energy T can be written

$$T = \frac{m}{2} (\dot{r}^2 + r^2\dot{\theta}^2 + \dot{z}^2) \tag{2.43}$$

where the dot denotes differentiation with respect to time, and m is the mass and e the charge of an electron. Thus the Lagrangian equation (2.1) can be written

$$L = \frac{m}{2} (\dot{r}^2 + r^2\dot{\theta}^2 + \dot{z}^2) + e\phi(r) - \frac{eBr^2\dot{\theta}}{2} \tag{2.44}$$

The equations of motion are

$$\frac{d}{dt} \left(\frac{\partial L}{\partial \dot{r}}\right) - \frac{\partial L}{\partial r} = 0 , \tag{2.45}$$

$$\frac{d}{dt} \left(\frac{\partial L}{\partial \dot{\theta}}\right) - \frac{\partial L}{\partial \theta} = 0 , \text{ and} \tag{2.46}$$

$$\frac{d}{dt} \left(\frac{\partial L}{\partial \dot{z}}\right) - \frac{\partial L}{\partial z} = 0 .$$

On substituting the expression (2.44) for L in (2.45), they become

$$m\ddot{r} - mr\dot{\theta}^2 - e\frac{\partial \phi(r,z)}{\partial r} + eBr\dot{\theta} = 0 \tag{2.46a}$$

$$\frac{d}{dt} \left(m r^2 \dot{\theta} - \frac{eBr^2}{2}\right) = 0 \tag{2.46b}$$

$$m\ddot{z} = e\frac{\partial \phi(r,z)}{\partial z} \tag{2.46c}$$

[1]The reader not familiar with the Lagrangian may simply omit this paragraph.

Equations (2.46a and (2.46c) are the equations of motion in Newtonian form.[1] Notice that the second term in (2.46a) is present because of the curvilinear coordinate system; it is essentially centrifugal force.

$$m r \ddot{\theta} + 2 m \dot{r} \dot{\theta} - eB\dot{r} = 0 \qquad (2.47)$$

which is also in Newtonian form. Here the second term is centrifugal force and the third the force due to the magnetic field.

Energy and momentum integrals can be found from equations (2.46) for an arbitrary potential field and for arbitrary initial conditions. These equations will be useful in discussing the motion of the electron beam in the magnetron diode as well as in finding the self-consistent field solution for the cylindrical magnetron.

Equation (2.46b) can be integrated to

$$mr^2\dot{\theta} - \frac{eBr^2}{2} = P_\theta \qquad (2.48)$$

where P_θ is a constant of integration. This equation can be interpreted as a generalization of conservation of angular momentum. P_θ is called the generalized, or canonical, angular momentum.

P_θ can be expressed in terms of initial conditions by considering equation (2.45) at time t = 0.

$$P_\theta = mr_o^2 \dot{\theta}_o - \frac{eBr_o^2}{2} , \qquad (2.49)$$

where r_o is the initial radial displacement and $\dot{\theta}_o$ is the initial angular velocity of the electron with respect to the axis of the cathode.

---

[1] See, for example, Dow, Ref. B, p. 54.

The energy integral can be obtained by multiplying (2.46a) by $\dot{r}$, 2.47 by $r\dot{\theta}$, (2.46c) by $\dot{z}$, and adding. The result is

$$m\ddot{r}\dot{r} + mr^2\dot{\theta}\ddot{\theta} + mr\dot{\theta}^2\dot{r} + m\ddot{z}\dot{z} - \dot{r}\frac{\partial \phi}{\partial r} - \dot{z}\frac{\partial \phi}{\partial z} = 0. \quad (2.50)$$

This equation can be integrated once with respect to time, yielding

$$\frac{m}{2}(\dot{r}^2 + r^2\dot{\theta}^2 + \dot{z}^2) - e\phi(r,z) = E \quad (2.51)$$

where E is a constant of integration called the total energy. The total energy for any electron can be found in terms of intial conditions by considering equation (2.51) at time t = 0 as follows:

$$E = \frac{m}{2}(\dot{r}_o^2 + r_o^2\dot{\theta}_o^2 + \dot{z}_o^2) - e\phi(r_o, z_o). \quad (2.52)$$

where $\dot{r}_o$ and $\dot{z}_o$ are the initial r and z components of velocity, r_o and z_o are initial r and z displacements, and $\dot{\theta}_o$ is the initial value of $\dot{\theta}$.

2.5 The Cylindrical D C Magnetron

The derivations of this section are analogous to those given in Section 2.3 for the planar magnetron. The solutions are very similar, though there are several important differences.

In this section the electric field is assumed to depend only upon r. The local variations of the potential due to the discrete nature of the electrons are neglected, but the average effect of space charge is

brought in through Poisson's equation. All electrons are assumed to have congruent orbits and the equations of motion are solved for any one of them.

The initial conditions for this electron are assumed to be

$$r_o = a, \theta_o = z_o = \dot{r}_o = \dot{\theta}_o = \dot{z}_o = 0 , \tag{2.53}$$

where r_o, θ_o, z_o are initial values of r, θ, and z, and $\dot{r}_o$, $\dot{\theta}_o$, and $\dot{z}_o$ are initial values of $\dot{r}$, $\dot{\theta}$, and $\dot{z}$ respectively, and a is the cathode radius.

Since ϕ does not depend upon z, $\frac{\partial \phi}{\partial z} = 0$, and equation (2.46c) can be integrated immediately. In view of the initial conditions, (2.53), the solution is

$$z \equiv 0 . \tag{2.54}$$

Since r is initially a, the cathode radius, and $\dot{\theta}$ is initially zero,

$$P_\theta = - \frac{e B a^2}{2} , \tag{2.55}$$

and (2.45) can be rewritten as follows:

$$\dot{\theta} = \omega_L \left(1 - \frac{a^2}{r^2}\right) , \tag{2.56}$$

where $\omega_L = eB/2m$ as before.

With the initial conditions (2.53), E is found from equation (2.52) to be zero (if ϕ is assumed to be zero at the cathode.) Then the energy integral (2.51) becomes

$$\frac{m\dot{r}^2}{2} + \frac{m\, r^2\, \dot{\theta}^2}{2} + \frac{m\dot{z}^2}{2} = e\phi\,(r) \quad . \tag{2.57}$$

Equation (2.56) can be used to eliminate $\dot{\theta}$ from (2.57), and $\dot{z} = 0$, so that

$$\frac{m\dot{r}^2}{2} + \frac{mr^2\,\omega_L^{\,2}}{2}\left(1 - \frac{a^2}{r^2}\right) = e\,\phi\,(r) \quad , \tag{2.58}$$

Since $\dot{r}^2$ must be equal to or greater than zero, an electron cannot reach any region in the magnetron where

$$\phi < \frac{mr^2\,\omega_L^{\,2}}{2e}\left(1 - \frac{a^2}{r^2}\right)^2 \tag{2.59}$$

The maximum radius from the cathode that an electron emitted from the cathode with zero velocity could reach is called the Hull radius and denoted by r_h. The Hull radius can be found by solving the equation

$$\phi\,(r_h) = \frac{m\, r_h^{\,2}\,\omega_L^{\,2}}{2e}\left(1 - \frac{a^2}{r_h^{\,2}}\right)^2 \quad . \tag{2.60}$$

It follows also that if an electron is to reach the anode,

$$\phi_a \geq \phi_{cutoff} = \frac{m}{2e}\,\omega_L^{\,2}\, r^2\left(1 - \frac{a^2}{r^2}\right)^2 \quad . \tag{2.61}$$

So far nothing has been required of the potential ϕ except that it be a function of r only. Now the conditions on ϕ which make this a "self-consistent field" solution are introduced. The potential ϕ must satisfy Poisson's equation

$$\nabla^2\phi = -\frac{\rho}{\epsilon_o} \quad , \tag{2.62}$$

which in cylindrical coordinates becomes

$$\frac{1}{r}\frac{d}{dr}\left(r\,\frac{d\phi}{dr}\right) = -\frac{\rho}{\epsilon_o} \quad , \tag{2.63}$$

since ϕ is a function of r only.

Since the space charge is assumed to be flowing from the cathode at a constant rate, the current per unit length of the tube must be constant. The current per unit length I and current density J are related as follows:

$$I = 2\pi r\, J(r) \quad . \tag{2.64}$$

Because of the symmetry, J can depend only on r. The space charge density is related to J by the equation

$$J = \rho \dot{r} \, , \tag{2.65}$$

and therefore

$$I = 2\pi r\, \dot{r} \rho \quad . \tag{2.66}$$

Again this is the case if the tube is not cut off and the electrons are all moving toward the anode. If the tube is cut off, half the electrons are moving out and half are moving back toward the cathode. The net current is zero. Equation (2.66) still applies, however, if I is taken as the sum of the magnitudes of the inward and outward currents, or twice the emission current.

The magnetron is assumed to be space-charge-limited, and hence the potential gradient at the cathode is zero, i.e.,

$$\frac{d\phi}{dr} = 0 \qquad \text{where } r = a \, . \tag{2.67}$$

With this, all the equations and boundary conditions required to determine r and θ as functions of time have been presented. The necessary equations are summarized as follows:

$$m\ddot{r} - mr\,\dot{\theta}^2 - e\frac{d\phi}{dr} + e\,Br\dot{\theta} = 0 \tag{2.46a}$$

$$\dot{\theta} = \omega_L \left(1 - \frac{a^2}{r^2}\right) \tag{2.56}$$

$$\frac{1}{r}\frac{d}{dr}\left(r\frac{d\phi}{dr}\right) = -\frac{\rho}{\epsilon_o} \tag{2.62}$$

$$I = 2\pi r\, \dot{r} \rho \tag{2.66}$$

with the boundary conditions

$$r = a,\ \theta = z = \dot{r} = \dot{\theta} = \dot{z} = 0 \text{ when } t = 0, \text{ and} \qquad (2.53)$$

$$\phi = \frac{d\phi}{dr} = 0 \text{ where } r = a\ . \qquad (2.67)$$

These equations can be solved for r and θ as functions of time, and for electric potential and space charge distributions.

Again a simple solution for the equations is that called the single-stream solution. Suppose the r-velocity is identically zero for electrons at every distance from the cathode out to some maximum radius r_h. Then for any electron, r is constant, and the electrons move in circles concentric with the cathode. By (2.56), the angular velocity is constant, $\omega_L\left(1 - \frac{a^2}{r^2}\right)$, and so

$$\theta = \omega_L t\left(1 - \frac{a^2}{r^2}\right)\ . \qquad (2.68)$$

The potential distribution can be found from the energy integral (2.57) to be

$$\phi = \frac{m}{2e}\left(\dot{r}^2 + r^2\dot{\theta}^2 + \dot{z}^2\right) = \frac{m\omega_L{}^2 r^2}{2e}\left(1 - \frac{a^2}{r^2}\right)^2\ . \qquad (2.69)$$

The space-charge density can be found from Poisson's equation (2.63) to be

$$\rho = \frac{2m\,\omega_L{}^2\epsilon_o}{e}\left(1 + \frac{a^4}{r^4}\right)\ . \qquad (2.70)$$

The current density in the r direction is zero, since y = 0. All the equations are satisfied.

Next the double-stream solutions are considered. Equation (2.63) can be written

$$\frac{1}{r}\frac{d}{dr}(rF) = \frac{\rho}{\epsilon_o} \qquad (2.71)$$

where F is the radial component of electric field. Multiplying both sides

by $r\dot{r}$, and using (2.66) to eliminate ρ,

$$\dot{r}\,\frac{d}{dr}(rF) = \frac{d}{dt}(rF) = \frac{\rho r\dot{r}}{\epsilon_o} = \frac{I}{2\pi\epsilon_o} \quad . \tag{2.70}$$

The term $\frac{d}{dt}(rF)$ is the time rate of change in electric field which an electron experiences while moving through the field. The field itself is not changing with time, of course. Equation (2.72) can be integrated since I is a constant.

$$rF = \frac{It}{2\pi\epsilon_o} \quad . \tag{2.73}$$

The constant of integration was chosen to make F zero on the cathode in accordance with (2.67).

Equation (2.46a) can be written

$$m\ddot{r} - mr\dot{\theta}^2 + e\,Br\dot{\theta} = eF, \text{ or}$$

$$\ddot{r} - r\,(\dot{\theta} - \omega_L)^2 + \omega_L^{\,2}\, r = \frac{eF}{m} \tag{2.74}$$

Equation (2.56) can be used to eliminate $\dot{\theta}$, and F can be eliminated by using (2.73).

$$\ddot{r} - \frac{\omega_L^{\,2}\, a^4}{r^3} + \omega_L^{\,2}\, r = \frac{eIt}{2\pi m\,\epsilon_o\, r} \quad . \tag{2.75}$$

The problem has been reduced to the problem of solving an ordinary differential equation. Unfortunately, the equation cannot be solved in terms of well known functions. All the necessary information about the solutions has been obtained, however, through the efforts of Allis on an approximate solution, which was checked with numerical solutions by Hartree and differential analyser solutions by Brillouin.[1]

---

1. Allis, Ref. 1; Slater, Ref. 39; Hartree, Ref. 24; Brillouin, Ref. 9.

In solving (2.75) it is important to eliminate as many parameters as possible by introducing dimensionless variables. Let

$$R = \frac{r}{a}, \quad T = \omega_L t, \text{ and } b = \frac{eI}{2\pi m \epsilon_o \omega_L^3 a^2}. \tag{2.76}$$

Then (2.75) can be written

$$\frac{d^2R}{dT^2} + R - \frac{1}{R^3} = \frac{bT}{R}, \tag{2.77}$$

and the boundary conditions become

$$R = 1, \quad \frac{dR}{dT} = 0 \quad \text{when } T = 0. \tag{2.78}$$

Solutions of this equation were obtained on the electronic differential analyser at the University of Michigan.[1] Some of the solutions are shown in Figure 2.5. They are in substantial agreement with those obtained by Allis and Brillouin. The solutions obtained by Brillouin on the MIT differential analyser are more accurate, since that is a much more elaborate machine. However, these solutions show clearly the nature of the solutions of equation (2.77).

When the solutions were run on the differential analyser, both R and dR/dT were recorded. The tapes shown in Figure 2.5 include the curves of both quantities. For some solutions,

$$\theta = \int_o^t \dot{\theta} dt = \int_o^T (1 - \frac{1}{R^2}) \, dT \tag{2.79}$$

was also recorded. Some examples of these curves are shown in Figure 2.6. They give the orbit parametrically.

In Figures 2.7 and 2.8 the data have been replotted showing R as a function of θ, which is the orbit. Note that for small values of R_h,

[1] The method of solution is discussed in Appendix 2.

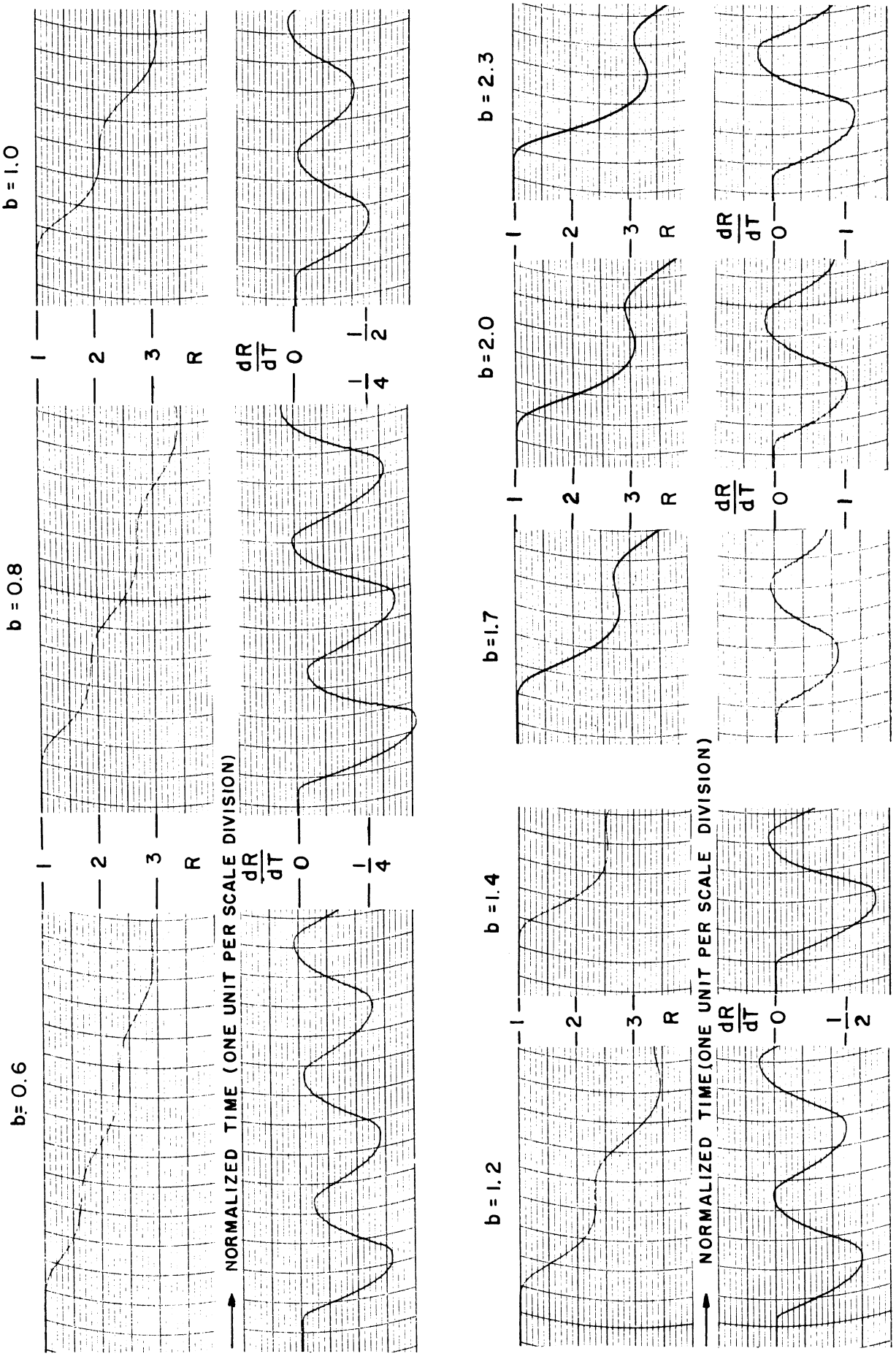

FIG. 2.5 NORMALIZED RADIUS AS A FUNCTION OF TIME FOR ELECTRON ORBITS IN THE CYLINDRICAL MAGNETRON (DIFFERENTIAL ANALYSER SOLUTIONS)

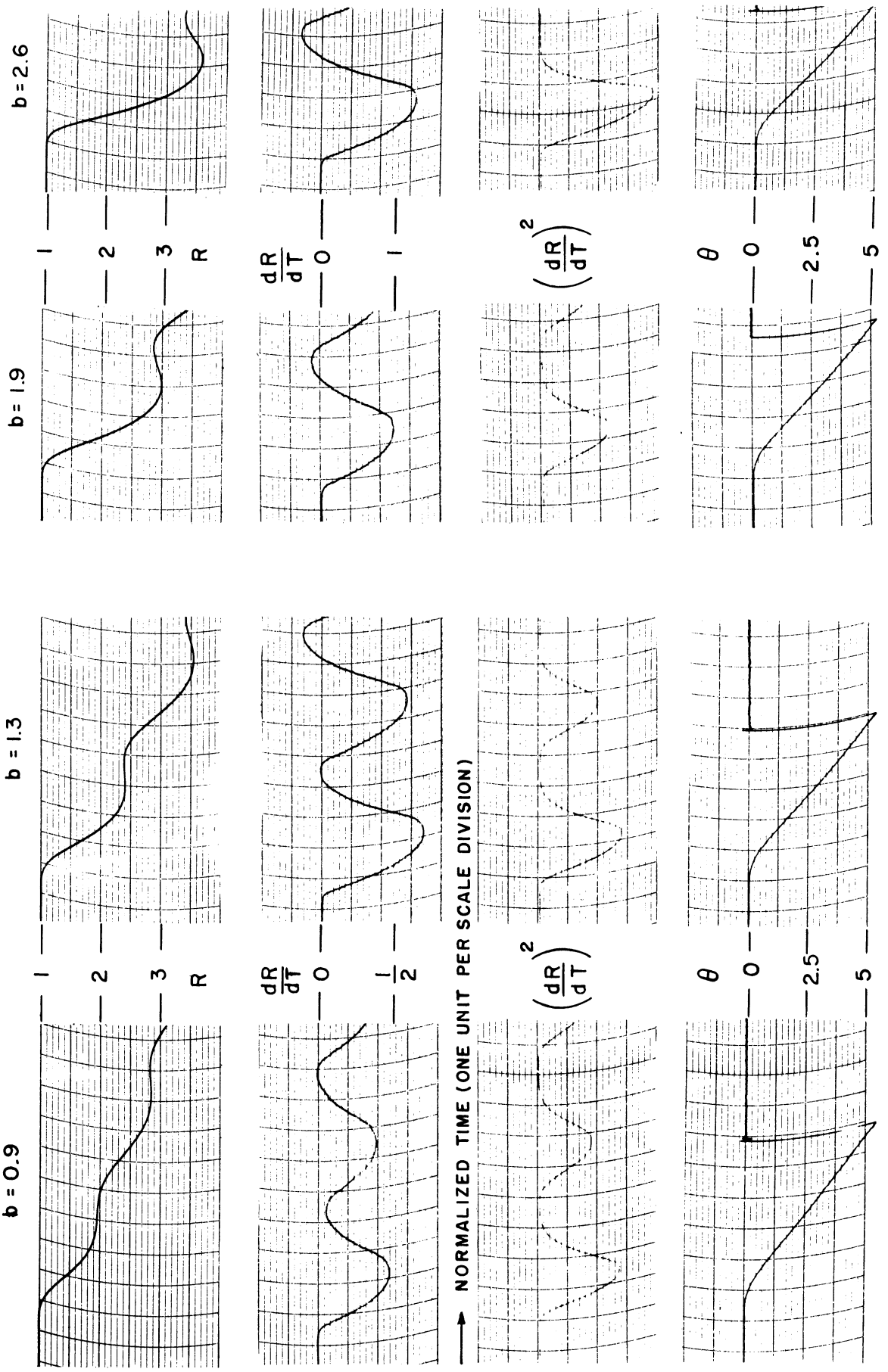

FIG. 2.6 NORMALIZED RADIUS AS A FUNCTION OF TIME FOR ELECTRON ORBITS IN THE

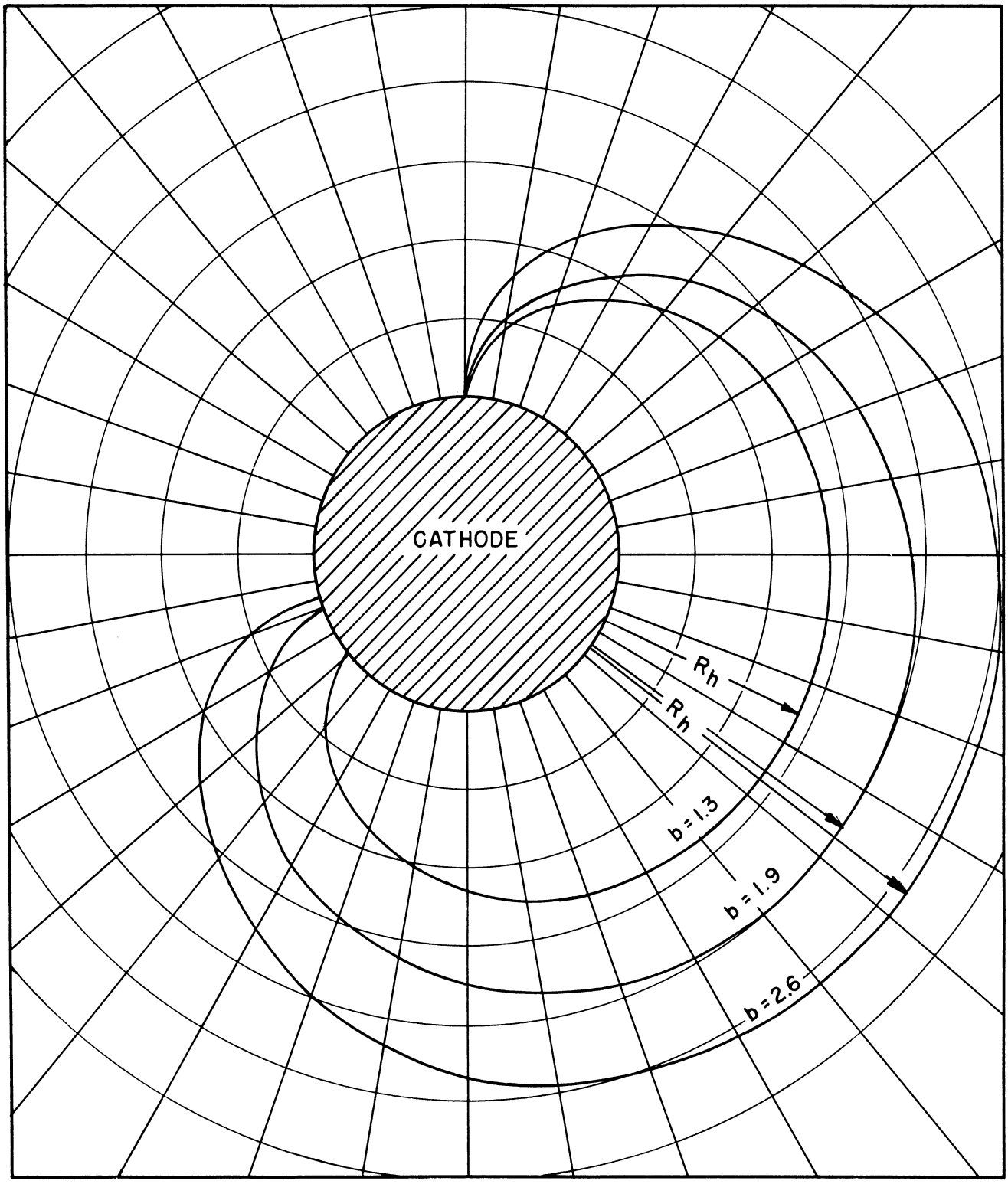

FIG. 2.7

ELECTRON ORBITS FOR B_1 SOLUTION

(THIS TYPE OF ORBIT OCCURS ONLY FOR $R_h \leq 2$)

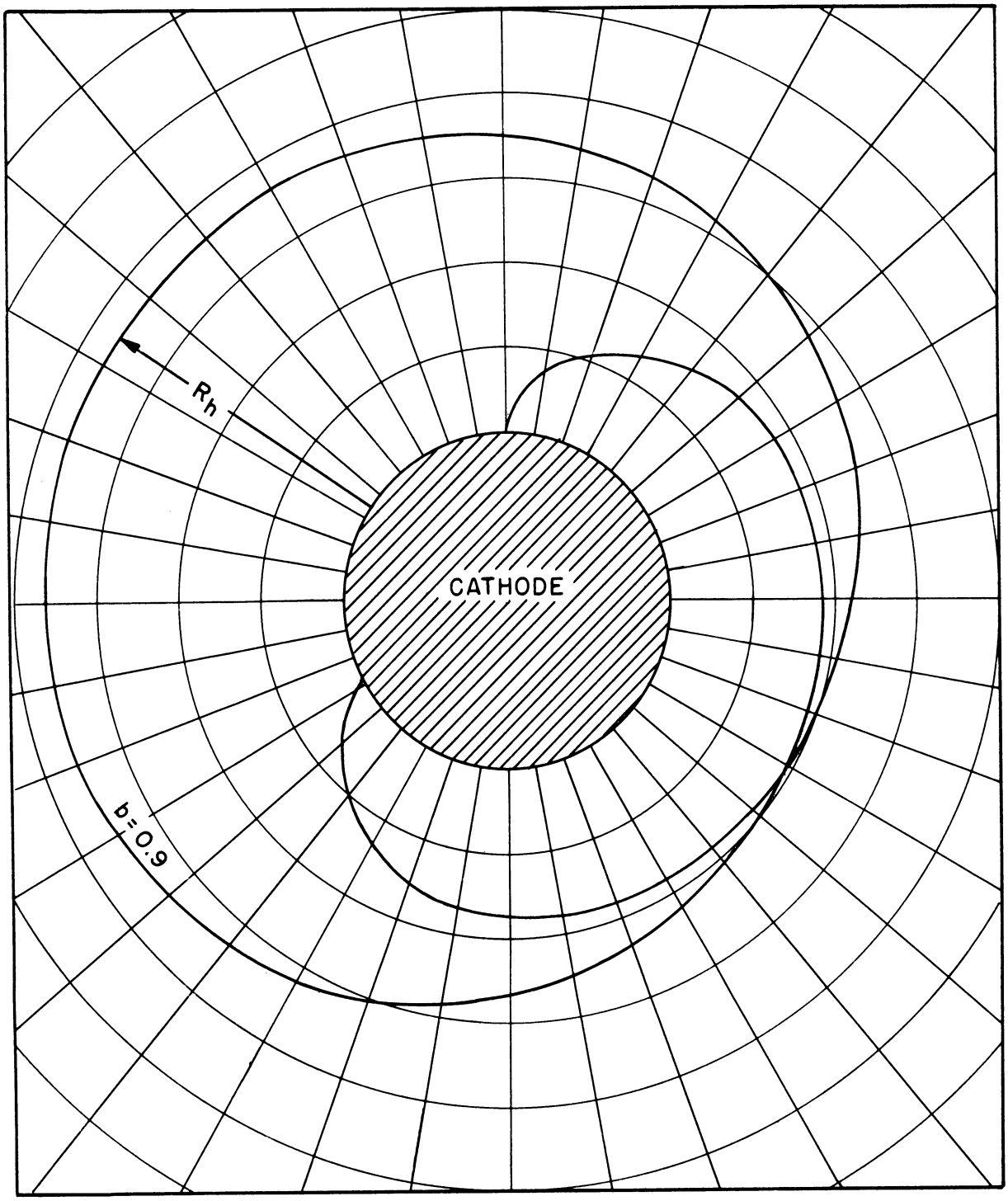

FIG. 2.8

ELECTRON ORBITS FOR B_2 SOLUTION

(THIS TYPE OF ORBIT OCCURS ONLY FOR $2.2 \leq R_h \leq 2.9$)

the B_1 and B_2 solutions do not occur; this phenomenon is discussed on page 46.

For small values of b, the electron radial velocity oscillates between small and large values as the electron moves outward, just as the electron velocity oscillated between zero and a maximum value in the planar case of the B_n solutions with n greater than one. Each successive minimum velocity is nearer zero, until finally the radial velocity actually reaches zero and apparently becomes negative. For the solutions shown, in the case of b = 0.6, there are two minima before dR/dT becomes zero, and for b = 0.8 or 1.0 there is one. For b = 1.2 or greater there is no minimum before dR/dT reaches zero.

In equation (2.58), the energy integral,

$$\frac{m\dot{r}^2}{2} + \frac{m\, r^2 \omega_L{}^2}{2}\left(1 - \frac{a^2}{r^2}\right) = e\,\phi\,(r)\,, \qquad (2.58)$$

$\dot{r}^2$ is a single valued function of r. The magnitude of $\dot{r}$ for an electron moving outward and for an electron moving back toward the cathode are the same. Therefore, if an electron moving outward ever ceases outward radial motion and starts moving back, it moves back in the mirror image of its outward path. Thus the differential analyser solutions have no connection with the physical problem beyond the point where $\dot{R} = 0$.

If the electrons cease radial motion and start returning to the cathode before they reach the anode, the magnetron is said to be operating below cutoff. The radius at which the radial velocity vanishes is called the Hull radius, R_h; there can be no space charge between the Hull radius and the anode. The Hull radius R_h as a function of b, the parameter in the differential equation (2.77), is plotted as a solid

curve in Figure 2.9.[1] The parameter b is proportional to the current emitted from the cathode. It can be varied physically by varying the anode voltage, but b is not a single-valued function of the anode voltage, and hence is not determined uniquely by the anode voltage. The relationship between b, R_h, and the anode voltage is discussed in the next few pages.

Important constants for a number of solutions are listed in Table 2.1. This table is taken from Allis' report.[2]

Discontinuities in R_h as b is increased occur when the next earlier minimum in the $\dot{R}$ curve reaches the axis, and there is one less minimum before $\dot{R}$ becomes zero. The double-stream solution is called the B_1 solution if $\dot{R}$ has no minimum inside the space charge region. It is called B_2 if there is one minimum, B_3 if there are two, and so forth. From Figure 2.9 it can be seen that for $b > 0.96$ the B_1 solution occurs. For $0.96 > b > 0.6$ the B_2 solution occurs. For $0.6 > b > .41$ the B_3 solution occurs. Also, the B_1 solution can occur for any value of R_h greater than about 2. The B_2 solution can occur only if $2.1 < R_h < 2.7$ approximately; the B_3 occurs in the range $2.15 < R_h < 2.6$, and so forth. No double-stream solution is possible in the curoff magnetron if $R_h < 2$. The single-stream (B_0) solution is possible for any value of R_h.

The Hull radius in the cutoff magnetron for a given anode voltage can be found from the condition that the potential and its gradient must be continuous. The space charge density between $R = R_h$ and the anode is zero, and therefore the potential is logarithmic in that region. It is a solution of Laplace's equation:

---

[1]This figure is for the most part copied from a figure in the report by W. P. Allis, Ref. 1.

[2]Ref. 1.

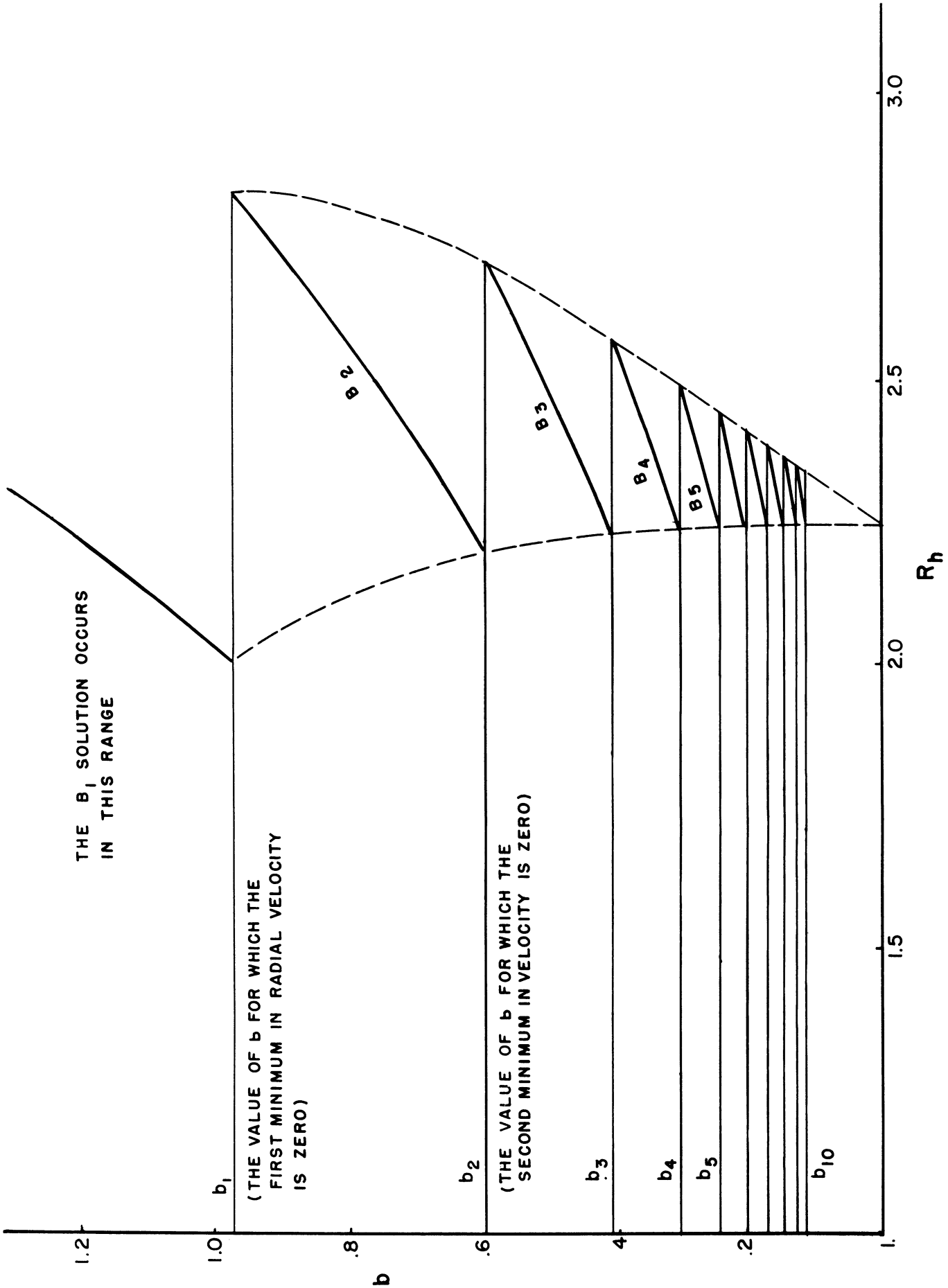

FIG. 2.9 HULL RADIUS AS A FUNCTION OF b

TABLE 2.1

DATA FOR SOME SOLUTIONS OF THE CYLINDRICAL MAGNETRON EQUATION

Solution Type*	b	R_h	bT_h**	$-R_h''$**	Author***
10	.125	2.312	5.01	.07	H,A
4	.354	2.436	5.68	.03	H
3	.415	2.279	5.01	.00	H
3	.545	2.627	6.54	.08	H
2	.590	2.226	4.76	.00	H
2	.605	2.254	4.83	.03	H
2	.762	2.540	6.00	.12	H
2	.867	2.722	6.83	.16	H
2	.957	2.871	7.53	.20	H
1	.957	2.023	3.84	-.04****	H
1	1.00	2.067	3.87	.08	H
1	1.17	2.241	4.49	.15	H
1	1.20	2.270	4.50	.21	A
1	1.71	2.741	6.10	.47	H
1	2	2.992	7.1	.57	A
1	2.8	3.618	9.7	.91	A
1	2.83	3.622	9.66	.94	H
1	4	4.406	13.5	1.36	A
1	6	5.512	19.5	1.96	A
1	8	6.437	25.3	2.49	A
1	12	7.949	35.7	3.46	A

*An n in this column indicates that the B_n type occurs.

**T_h is the normalized time required for an electron to reach the Hull radius from the cathode, and R_h'' is the normalized acceleration experienced at the Hull radius.

***This column indicates whether the data were taken from Hartree's numerical solutions or Allis's approximate solutions.

****Allis referred to this positive value of R_h'' as "dubious." Equation (2.93) shows that R_h'' must be negative.

$$\nabla^2 \phi = \frac{1}{r}\frac{d}{dt}\left(r\frac{d\phi}{dr}\right) = 0 \tag{2.80}$$

Laplace's equation can be integrated for this case as follows:

$$\begin{aligned} r\frac{d\phi}{dr} &= C_1 \\ 0 &= C_1 \ln r + C_2 \end{aligned} \tag{2.81}$$

where C_1 and C_2 are constants of integration. If F_h and ϕ_h are the electric field strength and pot tial at r_h, then the continuity of ϕ and F requires that

$$\begin{aligned} C_1 &= -F_h r_h \\ C_2 &= \phi_h + F_h \ln r_h \end{aligned} \tag{2.82}$$

Consider first the single-stream solution. By (2.69)

$$\phi = \frac{m\omega_L^2 r^2}{2e}\left(1 - \frac{a^2}{r^2}\right)^2 \tag{2.69}$$

in the space charge region. Therefore

$$\begin{aligned} -F_h &= \left.\frac{d\phi}{dr}\right|_{r_h} = \frac{m\omega_L^2}{e}\left(r_h - \frac{a^4}{r_h^3}\right) . \\ \phi_h &= \frac{m\omega_L^2 r_h^2}{2e}\left(1 - \frac{a^2}{r_h^2}\right)^2 . \end{aligned} \tag{2.83}$$

The potential outside the space charge region, and in particular at the anode, is obtained by substituting (2.83) and (2.82) in (2.81).

$$\phi_a = \frac{m\omega_L^2 r^2}{2e}\left[\left(1 - \frac{a^2}{r_h^2}\right)^2 + 2\left(1 - \frac{a^4}{r_h^4}\right)\ln\frac{r_a}{r_h}\right], \tag{2.84}$$

This equation can be written

$$\frac{\phi_a}{B^2} = \frac{e a^2}{8m} R_h^2\left[\left(1 - \frac{1}{R_h^2}\right)^2 + 2\left(1 - \frac{1}{R_h^4}\right)\ln\frac{R_a}{R_h}\right], \tag{2.85}$$

and ϕ_a/B^2 as a function of R_h is plotted in Figure 2.10.

For the double-stream solution, ϕ_h can be obtained from the energy integral (2.58), since $\dot{r} = 0$ at $r = r_h$.

$$\phi_h = \frac{m \omega_L^2 r^2}{2e} \left(1 - \frac{a^2}{r_h^2}\right)^2 , \qquad (2.86)$$

the same as in the single stream case. The electric field can be obtained from the differential analyser solutions and (2.73).

$$r_h F_h = \frac{I t_h}{2\pi \epsilon_o} \qquad (2.87)$$

where t_h is the time at which $\dot{r}$ becomes zero. Putting this in dimensionless form gives

$$a F_h = \frac{I T_h}{2\pi R_h \omega_L \epsilon_o} = \frac{m \omega_L^2 a^2}{2e} \frac{2bT_h}{R_h} , \text{ and}$$

$$\phi_h = \frac{m \omega_L^2 a^2}{2e} R_h^2 \left(1 - \frac{1}{R_h^2}\right)^2 . \qquad (2.88)$$

Then the anode voltage can be found by substituting these expressions in (2.82) and (2.81).

$$\phi_a = \frac{m \omega_L^2 a^2}{2e} \left[R_h^2 \left(1 - \frac{1}{R_h^2}\right)^2 + 2bT_h \ell n \frac{R_a}{R_h} \right] , \qquad (2.89)$$

or

$$\frac{\phi_a}{B^2} = \frac{e a^2}{8m} R_h^2 \left[\left(1 - \frac{1}{R_h^2}\right)^2 + \frac{2b T_h}{R_h^2} \ell n \frac{R_a}{R_h} \right] . \qquad (2.90)$$

The time T_h when $\dot{R}$ becomes zero can be found from differential analyser solutions, and ϕ_a/B^2 is plotted in Figure 2.10 for the B_1 and B_2 solutions with the R_a appropriate for the trajectron. Note that several types of solutions, B_1, B_2, etc., may be possible with a given anode voltage, but, unlike the planar magnetron case, the various types of solutions result in slightly different Hull radii r_h.

In order for the double-stream solution and the single-stream solution to have the same anode voltage for a given r_h, it is necessary

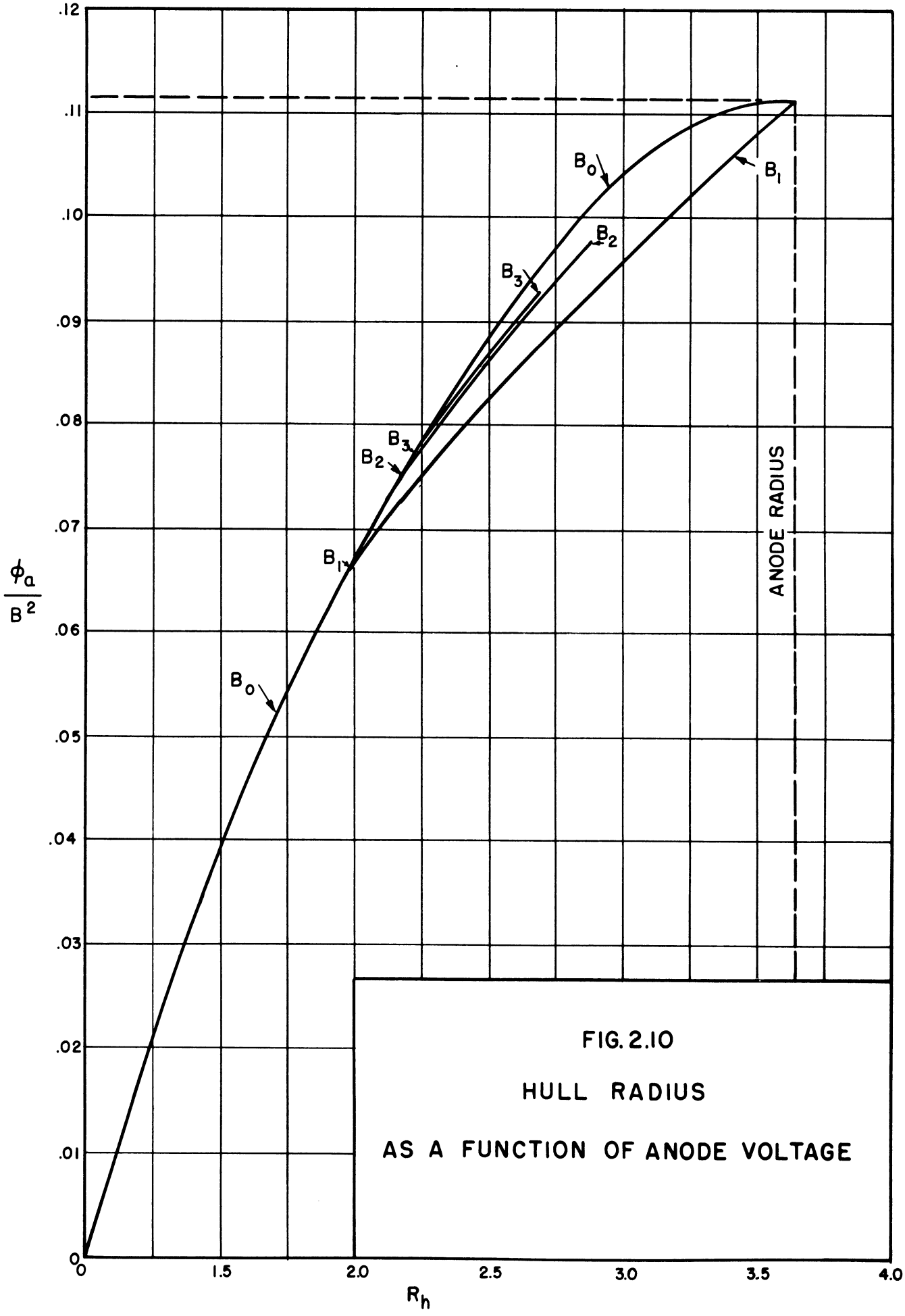

FIG. 2.10

HULL RADIUS

AS A FUNCTION OF ANODE VOLTAGE

and sufficient that the F_h for the two cases be the same, since the ϕ_h is always the same for a given r_h. By (2.58), for either type of solution,

$$e\phi = \frac{m}{2}\left[\dot{r}^2 + \omega_L^2 r^2 \left(1 - \frac{a^2}{r^2}\right)^2\right], \qquad (2.58)$$

and therefore

$$F_h = -\frac{d\phi}{dr} = -\frac{m}{2e}\left(\frac{d\dot{r}^2}{dr} + \frac{d}{dr}\left[\omega_L^2 r^2 \left(1 - \frac{a^2}{r^2}\right)\right]\right). \qquad (2.91)$$

The second term is the same for both types of solution. The first term is zero in the single-stream case, since $\dot{r} \equiv 0$. If $d\dot{r}^2/dr = 0$ at $r = r_h$ in the double-stream case, then ϕ_a is the same in both cases. But

$$\frac{d(\dot{r}^2)}{dr} = \frac{\frac{d(\dot{r}^2)}{dt}}{\frac{dr}{dt}} = \frac{2\dot{r}\frac{d\dot{r}}{dt}}{\dot{r}} = \frac{2d\dot{r}}{dt} \qquad (2.92)$$

and this is to be zero when $\dot{r} = 0$. Thus in a double-stream solution if the $\dot{r}$ curve becomes tangent to the axis, the Hull radius is the same as for the single-stream case. This is why the curves for the double-stream solutions start on the curve for the single-stream solution in Figure 2.9. In any case,

$$\frac{d(\dot{r})^2}{dr} = \frac{2d\dot{r}}{dt} \leqq 0 \qquad \text{when } \dot{r} = 0, \qquad (2.93)$$

since $\dot{r}$ must approach zero from the positive side. Therefore the gradient at the edge of a double-stream space charge cloud is no larger than that at the edge of a single-stream cloud. For the same Hull radius, the double-stream solution generally has less space charge and a lower anode potential.

As the anode voltage is decreased the cutoff occurs at the point where $\dot{r}$ becomes zero at the anode radius, i.e., the anode radius becomes the Hull radius. The cutoff voltage is given by (2.61). Presumably, any solution could occur at cutoff if it is possible for that

solution to have $\dot{r} = 0$ at the anode radius. As the anode voltage is decreased toward cutoff, the current should approach the value given by (2.76).

2.6 Secular Space Charge

2.6.1 The Concept of Secular Space Charge. The idea of electrons in the "secular" region of phase space, introduced by Hok in his Space Charge Equilibrium in a Magnetron-A Statistical Approach,[1] is very helpful in interpreting the trajectron data. Therefore this concept will be defined and discussed here.

The state of any electron in a cylindrical magnetron at a given time can be described by giving the coordinates of its position and the three components of its momentum. It is convenient to use the canonical momentum, which is, with the choice of magnetic vector potential used in the previous section, equation (2.42),

$$\begin{aligned} P_r &= \frac{\partial L}{\partial \dot{r}} = m\dot{r} \\ P_\theta &= \frac{\partial L}{\partial \dot{\theta}} = m r^2 (\omega_L - \dot{\theta}) \\ P_z &= \frac{\partial L}{\partial \dot{z}} = m\dot{z} \quad . \end{aligned} \tag{2.94}$$

The state of the electron is given by six numbers, and hence the state can be thought of as a point in six dimensional space. This is called the representation in phase space.

If the potential field in the magnetron is constant in time and dependent only upon the radius, the equations of motion are the same as those of Section 2.3, with $\frac{\partial \phi}{\partial z} = 0$.

---

[1] Ref. 28 or 29.

By equation (2.49), P_θ is constant. The energy integral is, from equation (2.51),

$$\frac{m\,\dot{r}^2}{2} + \frac{mr^2\,\dot{\theta}^2}{2} + \frac{m\,\dot{z}^2}{2} - e\,\phi(r) = E\,. \qquad (2.96)$$

This equation can be rewritten in terms of the momenta:

$$\frac{P_r^2}{2m} + \frac{(P_\theta - m\omega_L\,r^2)^2}{2mr^2} + \frac{P_z^2}{2m} - e\phi(r) = E\,. \qquad (2.97)$$

If an electron in a certain state would eventually reach the cathode, or if it could have reached its state by starting from the cathode, that state is called accessible from the cathode. The totality of all states which are accessible from the cathode form a region of the phase space, which Hok calls the cathode-accessible region. Likewise, there is an anode-accessible region, comprising all states which could be reached by electrons starting on the anode or states from which electrons may reach the anode.

Electrons can obviously be in either accessible region. It is possible for an electron to be in both regions, as for example most electrons in the magnetron with the anode voltage above cutoff. It is also possible for an electron to be in neither region. For example, the electrons in the single-stream (B_o) solution travel in circles concentric with the cathode, never reaching the cathode or anode. Hok calls the region in phase space which is in neither accessible region the secular region.

The energy integral can be used to determine whether or not an electron is in the cathode- or anode-accessible region. The equation (2.97) for the energy can be solved for P_r^2 as follows:

$$\frac{P_r^2}{2m} = e\phi(r) + E - \frac{P_z^2}{2m} - \frac{(P_\theta - m\omega_L\,r^2)^2}{2mr^2}\,. \qquad (2.98)$$

If an electron is at radius r_o with constants of motion P_θ, P_z, and E, and if it is in the cathode-accessible region, it must be able to reach the cathode in a finite time, or it must have come from the cathode to r_o in a finite time. Hence,

$$\int_a^{r_o} \frac{dr}{\dot{r}} = \int_a^{r_o} \frac{m dr}{P_r} = \text{transit time} \qquad (2.99)$$

must be a finite real number. Since P_r as a function of r is given by equation (2.98) which in turn is completely specified by the three constants of motion of the electron P_θ, P_z, and E, for a given potential distribution, knowledge of the three constants P_θ, P_z, and E suffices for determining whether or not an electron is in the cathode-accessible region. Note that it is necessary that $P_r^2 \geq 0$ everywhere between r_o and a, and it is sufficient that $P_r^2 > 0$ everywhere between r_o and a for an electron at r_o to be in the cathode-accessible region of phase space. It can be determined whether or not an electron is in the anode-accessible region by a completely analogous method.

Twiss[1] argues that if initial velocities are taken into account in the cutoff magnetron, the electron motion must be of the double-stream, and probably even the single-swarm (B_1) type. The time which such an electron spends in the magnetron between the time when it is emitted and the time it reaches the cathode again is not much greater than $4\pi n/\omega_L$ for the B_n solution.[2] Generally, one would not expect electrons in the cathode-accessible region of the phase space to spend more time in the magnetron than a few Larmor periods $2\pi/\omega_L$.[3] This would also be true of

---

[1] Ref. 44.

[2] This can be seen from the solution of the magnetron equations given in Section 2.3. See the curves in Fig. 2.5 and the data in Table 2.1.

[3] Any period is theoretically possible; for example, the B_n solution with n arbitrarily large may occur, and thus the time spent in the tube might be arbitrarily large.

electrons in the anode-accessible region. Electrons in the secular region, however, would stay in the magnetron indefinitely.

The above discussion assumes each electron moves in a potential field which is independent of time and dependent only on the r-coordinate in space. This is not the actual case, of course. The electrons are emitted in a random manner, and have, when they are emitted, a random distribution of velocities. There are bound to be small variations in space charge density which will cause variations in time and space from the strictly radial potential field. It must also be remembered that the space charge is made up of electrons, discrete particles, and very near any electron there is a sharp depression in the potential. If two electrons pass very near each other, each is deflected by the field of the other; this is a collision. The collisions are not accounted for if the potential is assumed strictly radial. Furthermore, it is possible that oscillations may occur due to phenomena like plasma oscillations or space charge waves, and as a result, the potential may change in time.

Thus an electron may experience changes in P_z, P_θ, and E. It is even possible for an electron to change its position in phase space into or out of any particular region. Not enough is known about the magnetron for a good estimate to be made of the frequency or magnitude of the changes or the rate of flow of electrons in or out of the various regions of phase space. In the cutoff magnetron the anode current, which probably is a large fraction of the flow of electrons into the anode accessible region, is only a very small fraction of the current which the cathode can and probably does emit. This would seem to indicate that the flow of space charge from one region to another may be small. On the other hand, Warnecke's group have observed large components of

random velocities in a stream of electrons only a few Larmor periods after they were emitted from an electron gun in a linear magnetron.[1] From this it would appear that rather large changes in momentum and energy can take place in a short time.

If there is little probability of a significant change in energy or momentum due to these collisions or other variations from radial fields in a few Larmor periods, then the ideas of accessible regions of phase space are still useful. The energy E and the momenta P_θ and P_z which would remain constant with a purely radial field are now subject to changes which are small or infrequent. Under these conditions, an electron's state can change, and it may even move from an accessible region to the secular region, or vice versa. Electrons may be so near the boundary of two regions that an infinitesimal change in one of the constants E, P_θ, or P_z might place it in the other region. Indeed, the average energy of electrons emitted from the cathode is kT, where k is the Boltzmann constant and T the temperature of the cathode in degrees Kelvin. If an average emitted electron should lose a little more energy than kT in a collision, and if the momenta P_θ and P_z should not be affected, then the electron would fall into the secular region.

In these terms, the operation of a static magnetron can be described as follows: each electron starts from the cathode, and hence in the cathode-accessible region. It probably stays in the magnetron a few Larmor periods, and then returns to the cathode. A few of these emitted electrons, however, suffer large enough changes in their energy or momentum to place them in the secular region, or even the anode-accessible region. There are many electrons in the cathode-accessible region, although each electron leaves the cathode-accessible region after only a

---

[1] Guénard and Huber, Ref. 22.

few Larmor periods. The cathode emission supplies electrons as fast as they leave. There are many electrons in the secular region. Electrons enter the secular region at a slow rate, but the average electron spends many Larmor periods in the secular region. There are few electrons in the anode-accessible region. Electrons drift into the anode-accessible region at a slow rate and spend only a short time in it. The significant electron drift is from the cathode-accessible region to the secular region (and perhaps to the anode-accessible region), and from the secular region into both the anode- and cathode-accessible regions.

This qualitative theory explains the current to the anode at voltages below cutoff. If the anode voltage is far below cutoff, a large total change in energy or momentum is required before an electron can pass from the cathode-accessible region to the anode-accessible region. Only a very small fraction of the emitted electrons will reach the anode-accessible region. As the anode voltage is increased toward cutoff, a smaller total change in energy and momentum is required. Electrons which have passed into the secular region are more likely to go into the anode accessible region, and electrons are more likely to pass directly from the cathode-accessible region to the anode-accessible region. Thus the current to the anode will show a continuous rise in the neighborhood of cutoff. When the anode voltage is at or above cutoff, nearly all electrons are in both accessible regions, and a fairly large change in energy and momentum would be necessary to put an electron into the secular region. Also, the double-stream type of electron flow, which affords many opportunities for collisions does not occur. Thus, collisions and small variations in potential distribution probably play an important role only in the cutoff magnetron.

2.6.2 The Effect of Secular Space Charge on Electron Orbits in the DC Magnetron. If the collisions and small variations in the potential field have such a profound effect upon the operation of the static cutoff magnetron, then are the solutions obtained for the ideal case considered in the first part of this chapter of any interest? The answer is yes, but with limitations. Most of the electrons in the cathode-accessible region probably travel their entire orbit, little affected by the irregularities in the potential field. Their motion would be, except for two modifications, the same as that found in the ideal case. In the first place, electrons of the secular region contribute to the space-charge density ρ, so that ρ must be taken as

$$\rho = \frac{I}{2\pi r\dot{r}} + \rho_s \qquad (2.100)$$

where I is the sum of the magnitudes of the current flow inward and outward of the electrons of the cathode-accessible region, and ρ_s is the contribution of the secular electrons. This equation must replace (2.66). Also, when the Hull radius is calculated, it must be remembered that there are electrons, mostly secular electrons, outside this radius.

Unfortunately we have no way now to predict theoretically the space-charge distribution due to the secular electrons. Only a very crude estimate is possible--this will be discussed along with the other results of the trajectron study. Also, if an exact solution were desired for the ideal case modified by replacing equation (2.66) with (2.100), then it would be necessary to take into account the fact that the ρ_s would be affected by cathode-accessible electrons in some complicated way. Clearly, the best one could hope to do now would be to see how sensitive the solution is to the distribution ρ_s of secular electrons by obtaining solutions for several hypothetical distiibutions ρ_s. This was done with

the help of the electronic differential analyser at the University of Michigan.

If the secular space-charge density ρ_s is a simple function of r, the equation for the motion of electrons in the cathode-accessible region is hardly more complicated than in the case where ρ_s is assumed zero. The equations required for a solution in this case are those on page 37, with

$$\rho = \frac{I}{2\pi r\dot{r}} + \rho_s \qquad (2.100)$$

substituted for (2.66). Poissons equation (2.63) can be written

$$\frac{1}{r}\frac{d}{dt}(rF) = \frac{\rho}{\epsilon_o} \; . \qquad (2.71)$$

Multiplying both sides by $r\dot{r}$ and using (2.100) to eliminate ρ,

$$\dot{r}\frac{d}{dr}(rF) = \frac{d}{dt}(rF) = \frac{\rho r\dot{r}}{\epsilon_o} = \frac{I}{2\pi\epsilon_o} + \frac{\rho_s r\dot{r}}{\epsilon_o} \; . \qquad (2.101)$$

This equation can be integrated, since I is a constant, and

$$rF = \frac{It}{2\pi\epsilon_o} + \frac{1}{\epsilon_o}\int_a^r r\ \rho_s(r)\,dr \; . \qquad (1.102)$$

The constant of integration was chosen to make F zero on the cathode in accordance with (2.67). Equation (2.46a) can be written

$$\ddot{r} - r(\dot{\theta} - \omega_L)^2 + \omega_L^2 r = \frac{eF}{m} \qquad (2.74)$$

Equation (2.56) can be used to eliminate $\dot{\theta}$, and F can be eliminated by using (2.102).

$$\ddot{r} - \frac{\omega_L^2 a^4}{r^3} + \omega_L^2 r = \frac{eIt}{2\pi m\epsilon_o r} + \frac{1}{rm\epsilon_o}\int_a^r \rho_s r dr \qquad (2.103)$$

Introducing the dimensionless quantities

$$R = \frac{r}{a} ,$$

$$T = \omega_L t , \tag{2.76}$$

$$b = \frac{eI}{2\pi m \epsilon_o \omega_L^3 a^2} ,$$

and

$$Q(R) = \frac{1}{m \omega_L^2 \epsilon_o} \rho_s (aR) \tag{2.104}$$

equation (2.103) becomes

$$\frac{d^2R}{dT^2} + R - \frac{1}{R^3} = \frac{bT}{R} + \frac{1}{R} \int_1^R RQ (R) \, dR . \tag{2.105}$$

It is convenient to solve this equation on the differential analyser for the following four cases:

$$\begin{aligned} Q_1 (R) &= k_1 , \\ Q_2 (R) &= \frac{k_2}{R} , \\ Q_3 (R) &= \frac{k_3}{R^3} , \text{ and} \\ Q_4 (R) &= \frac{k_4}{R^4} . \end{aligned} \tag{2.106}$$

The answer can be found analytically for the case

$$Q_5 (r) = k_5 (1 + \frac{1}{R^4}) ; \tag{2.107}$$

i.e., space charge with a distribution proportional to the distribution in the single stream (B_o) solution. These five functions are plotted in Figure 2.11.

Consider the last case first. Equation (2.105) becomes

$$\frac{d^2R}{dT^2} + R - \frac{1}{R^3} = bT + \frac{1}{R} \int_1^R Rk_5 (1 + \frac{1}{R^4}) \, dR$$

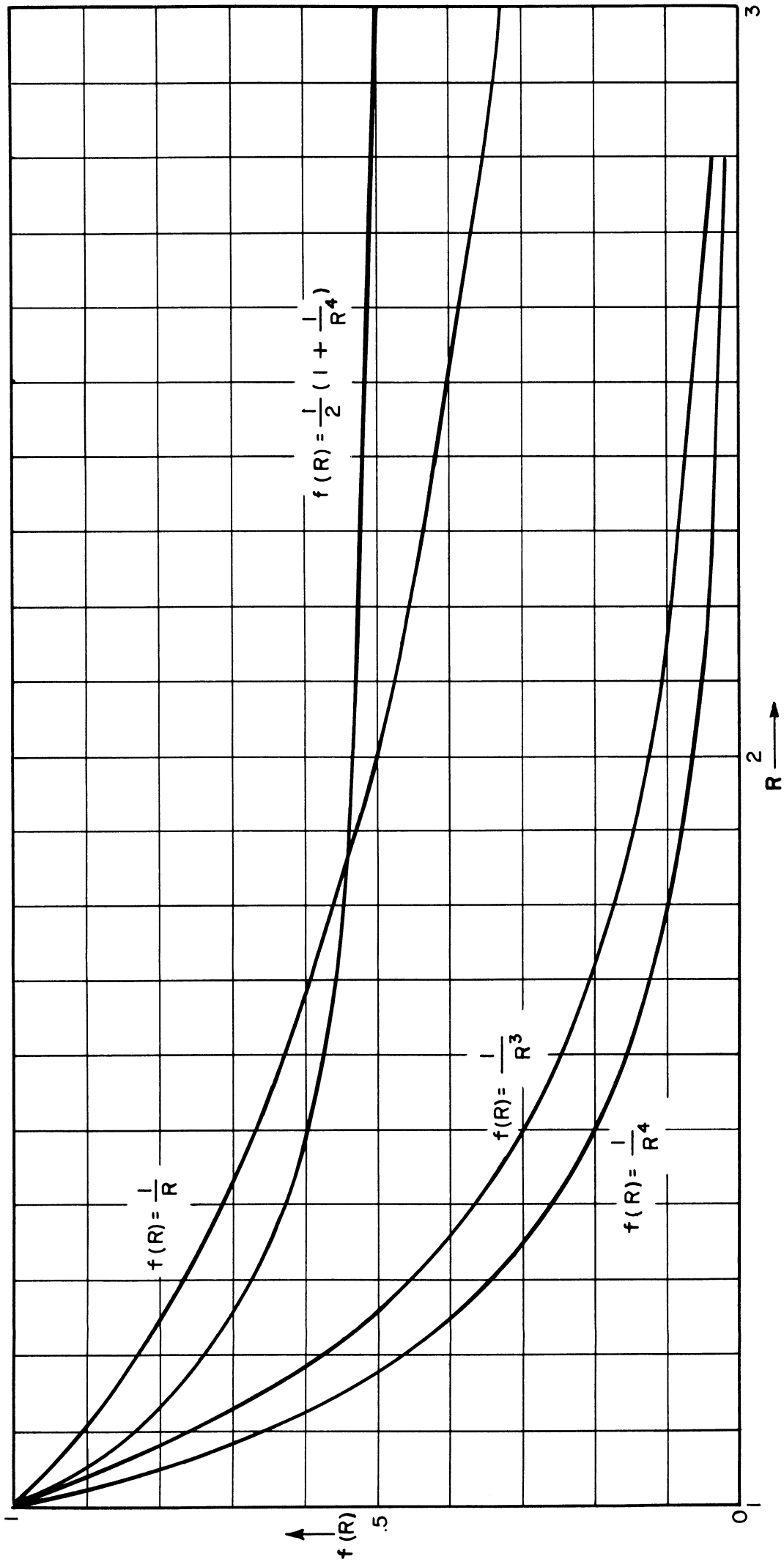

FIG. 2.11 HYPOTHETICAL SECULAR SPACE-CHARGE DISTRIBUTIONS

$$= bT + \frac{k_5}{R}\left(\frac{R^2}{2} - \frac{1}{2R^2}\right) , \text{ or}$$

$$\frac{d^2R}{dT^2} + \left(1 - \frac{k_5}{2}\right)\left(R - \frac{1}{R^3}\right) = bT . \qquad (2.108)$$

With the change of variables $T' = T\sqrt{1 - \frac{k_5}{2}}$, $b' = \frac{b}{\left(1 - \frac{k_5}{2}\right)^{\frac{3}{2}}}$

and with no change in R, this equation becomes

$$\frac{d^2R}{dT'^2} + R - \frac{1}{R^3} = b' T , \qquad (2.109)$$

which is the same equation as appeared in the case of the ideal cylindrical magnetron (equation (2.77)). The solutions have been studied in detail in Section 2.5. In particular, since the variable R was not changed in transforming equation (2.108) into equation (2.10), any type of solution can occur in the same range and only the same range of Hull radius R_h regardless of the value of the constant k_5 ($0 \leqq k_5 \leqq 2$), the same range as in the case of no secular space charge.

Since it would require too much space, the differential analyser solutions could not be included in this dissertation. The most important constants of those solutions are summarized in Appendix B, however. For each solution, the values of maximum radius, the transit time, and the type of solution are recorded as well as the parameter values for the solution. The solutions are all similar to those presented in Figures 2.5 and 2.6.

The most important information which can be obtained from these solutions is the range of maximum radius R_h possible with the various types of solutions. These data are summarized in Figure 2.12. The single

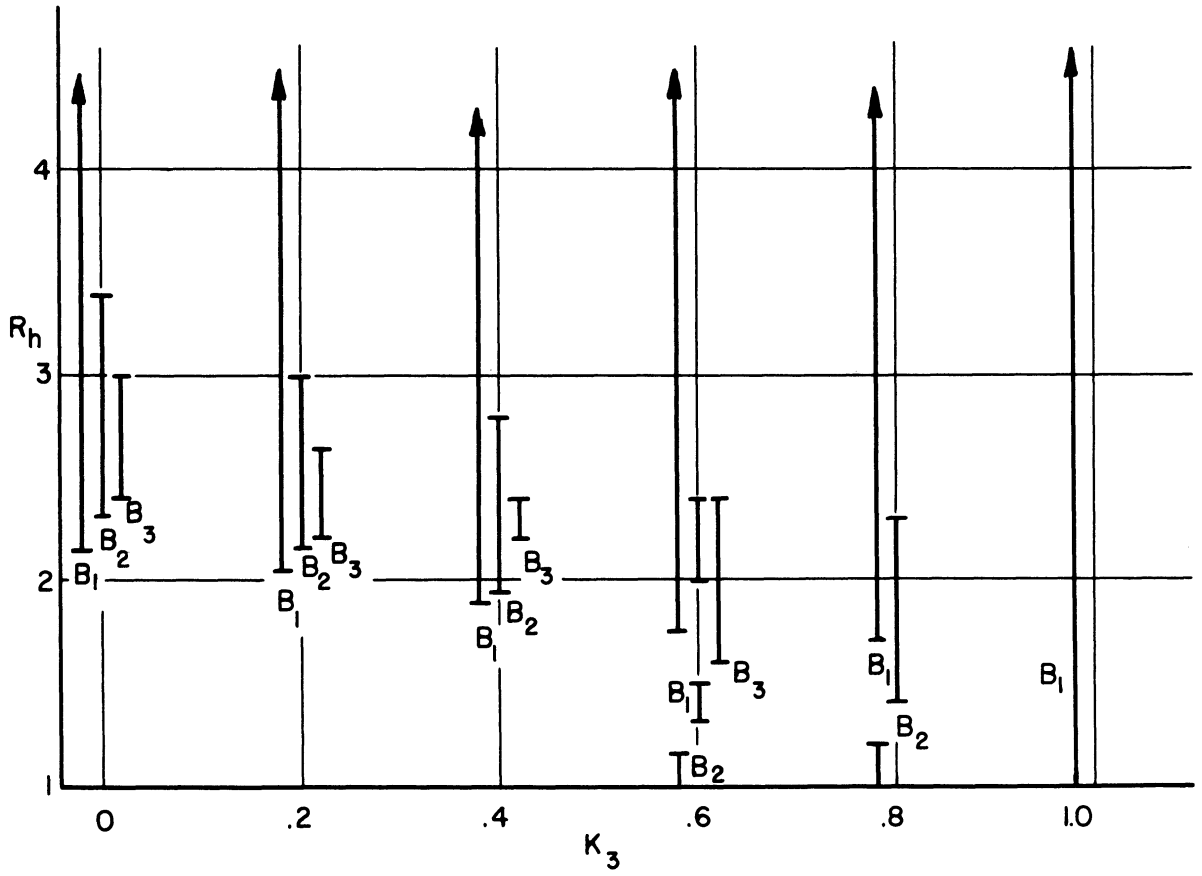

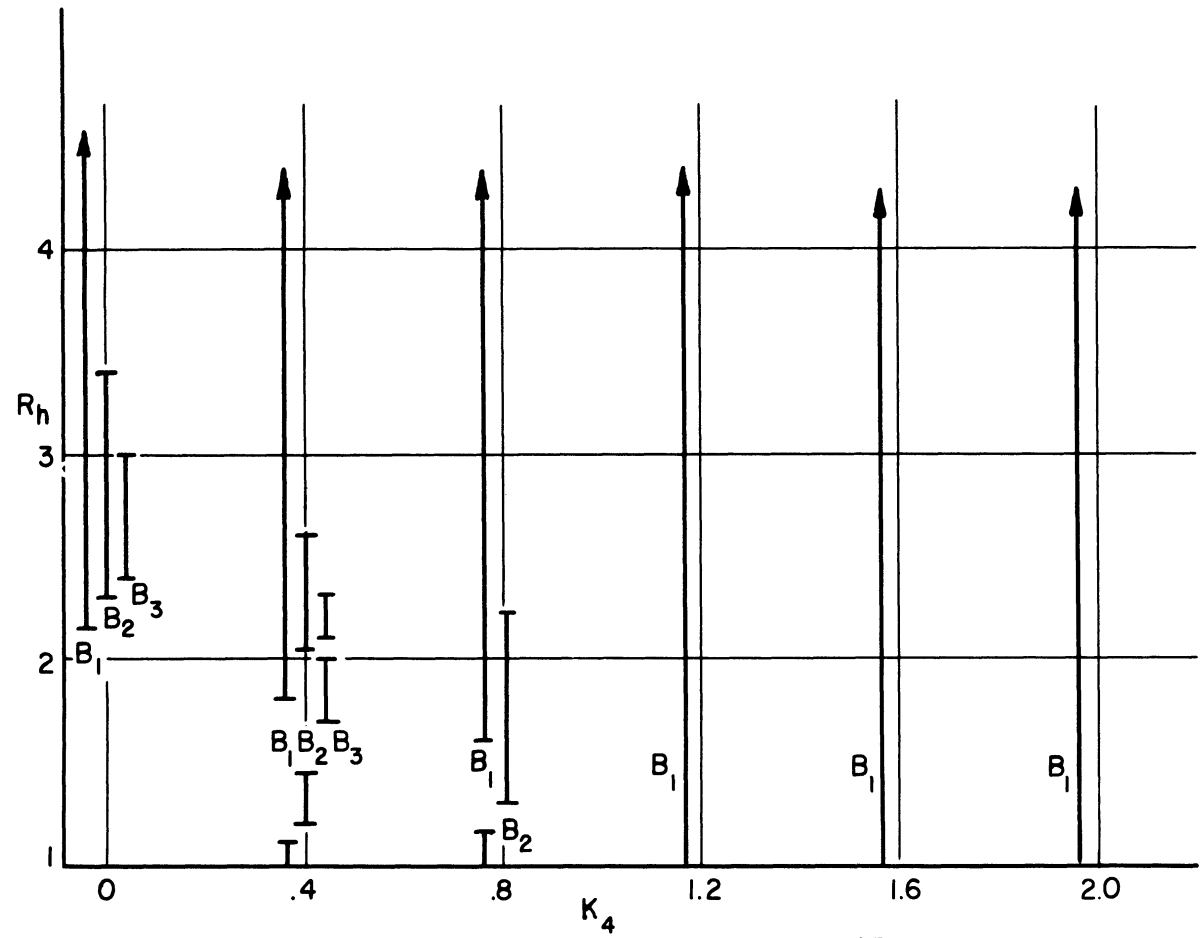

FIG.2.12a. RANGE OF RADIUS IN WHICH B_1, B_2, AND B_3 SOLUTIONS CAN OCCUR (DIFFERENTIAL ANALYSER DATA)

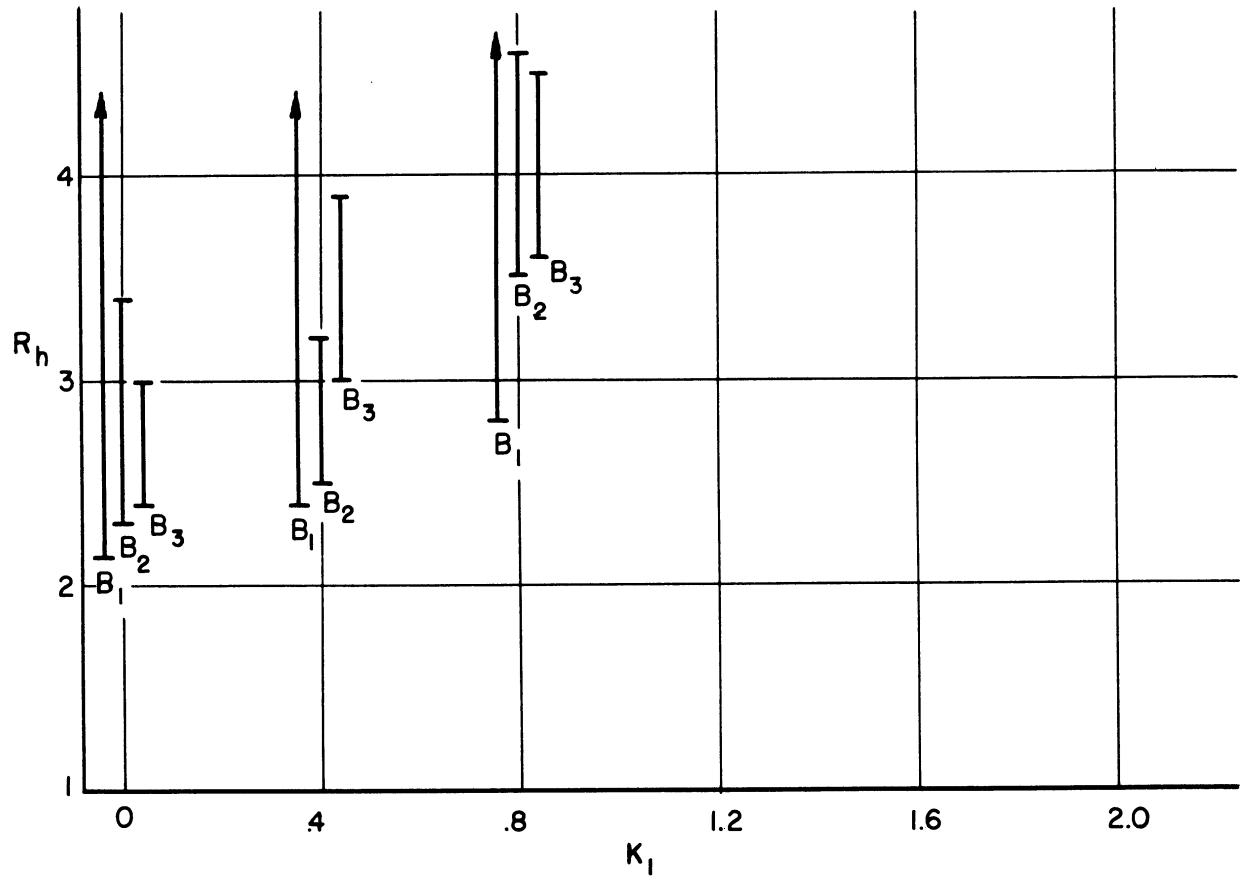

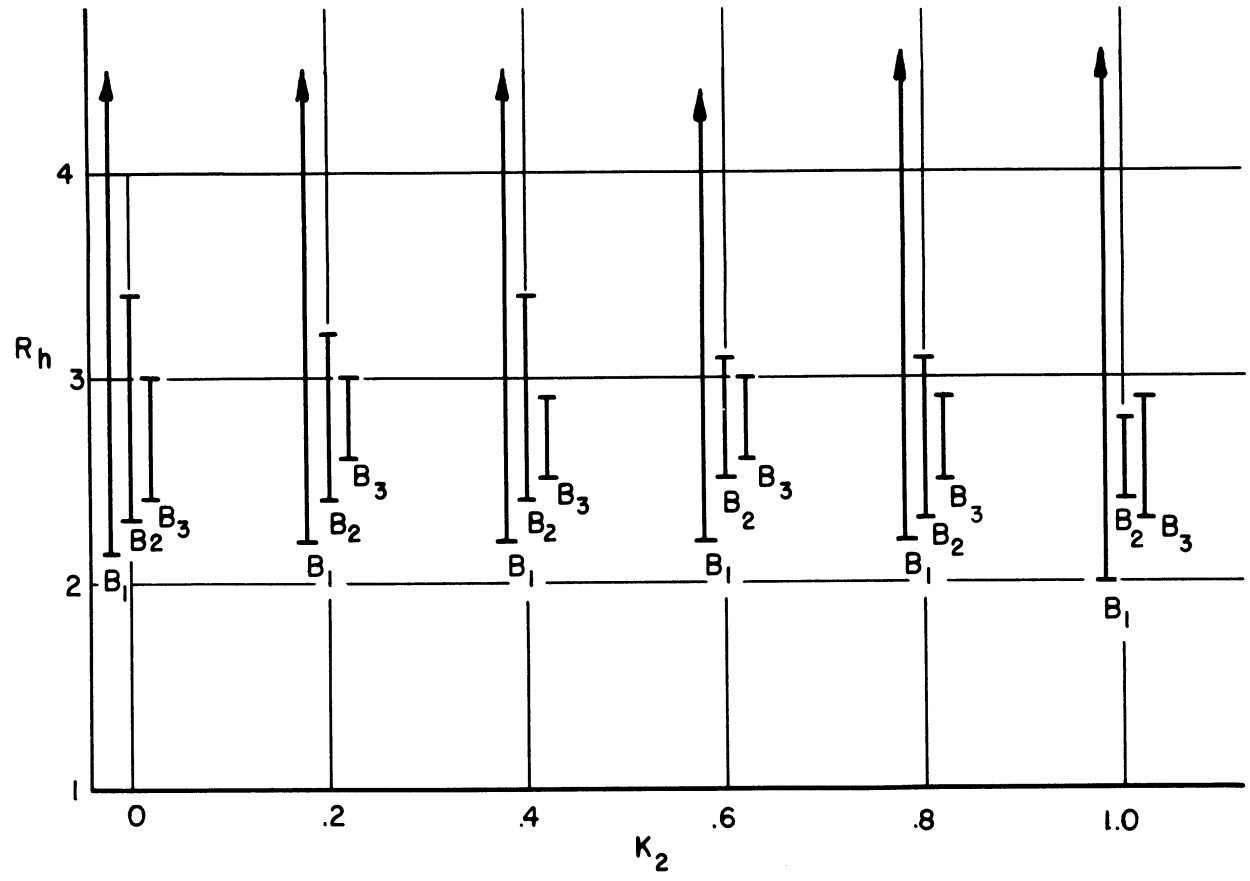

FIG.2.12b RANGE OF RADIUS IN WHICH B_1, B_2, AND B_3 SOLUTIONS CAN OCCUR (DIFFERENTIAL ANALYSER DATA)

stream (B_o) solution can always occur with any maximum radius. (The anode voltage determines R_h for any given possible type of solution.) Figure 2.12 gives the range of R_h possible for the B_1, B_2, and B_3 solutions. Where one of these solutions does not appear in the figure at some parameter value, this may be taken to mean it does not occur. All these data--even that for the case of no secular space charge--were taken from solutions on the University of Michigan differential analyser. There are slight discrepancies between these solutions and the more precise solutions obtained by Brillouin.

In the case of no secular space charge, the B_1 solution can occur with any value of R_h greater than 2.15. The B_2 solution occurs only in the range $2.2 \leqq R_h \leqq 3.1$, and the B_3 occurs in the range $2.25 \leqq R_h \leqq 2.9$. These would also be the ranges which would apply to the Q_5 distribution of secular space charge. For the distribution Q_1, the limits for R_h are increased, and the region in which only the single swarm solution is possible is widened. The increase is small for small values of k_1, large for large values of k_1. The Q_2 distribution has little effect on the range of maximum radius. For the Q_3 distribution, the limits are made smaller, and the B_1 solution can occur with R_h very small if k_3 is large enough. In fact only the B_1 and B_2 solutions occur when $k_3 \geqq 0.8$, and only the B_1 solution occurs when $k_3 = 1$. The Q_4 distribution has this same effect on the solutions, except that the effect is greater. Only the B_1 and B_2 solutions occur if $k_4 \geqq 0.4$, and only the B_1 solution occurs if $k_4 \geqq 0.6$.

This can be summarized as follows: For a distribution of secular space charge proportional to the space charge in the B_o solution (Q_5), the range of maximum radius for which any particular type of solution can occur is not affected. For secular space charge distributions

that do not decrease as fast as a function of radius as the Q_5 distribution, the limits are increased. For the distributions which decrease faster than the Q_5 distribution, the limits decrease. It may even happen that only the B_1 solution occurs, and it can occur with any maximum radius R_h.

2.6.3 Conclusions. In an infinite cylindrical magnetron it is possible for an electron to be in such a state that until its energy, angular momentum, or z-momentum is changed, it cannot reach the anode or cathode. Such electrons are said to be in the secular region of phase space, and they make up the secular space charge in the dc magnetron. On account of collisions of electrons with ions or other electrons, and on account of fluctuations in the potential field, electrons can experience changes in energy and momentum. No reliable estimate of the magnitude or frequency of occurrance of these changes, or of the rate of flow of electrons in and out of the secular region is available. There is evidence that the secular space charge is an important part of the space charge in the dc magnetron.[1]

The actual secular space charge distribution is unknown, and therefore it would be impossible to calculate the orbits for emitted electrons in the presence of the secular space charge. The most obvious effect of the presence of secular space charge would be to make the Hull radius smaller.

Calculations were made for electron orbits in the presence of hypothetical secular space charge distributions in order to learn what other effect the secular space charge might cause. The result of most interest concerned the range possible for the Hull radius for the

[1]See Section 5.4.

particular types of solutions. The B_1 solution could occur only with $R_h > 2$ (approximately) with no secular space charge. With the secular space-charge density constant or slowly decreasing as a function of radius, the lower limit for R_h was increased. If the secular space charge decreased rapidly as a function of radius, the lower limit for R_h was decreased, in some cases to unity. Thus the presence of secular space charge is enough to make possible the existence of the B_1 type solution with any Hull radius.[1]

[1]Twiss (in Ref. 44) suggests that the distribution of initial velocities may modify the electron motion in such a way that the B_1 solution is always possible. End effect in the tube may also affect this.

CHAPTER 3

DESIGN OF THE TRAJECTRON

3.1 Basic Design Parameters

The purpose of this chapter is to discuss the design of the trajectron and to describe the trajectron and associated equipment.

The principal parts of the trajectron and their functions are shown diagrammatically in Figure 3.1. The magnetron diode has concentric cylindrical cathode and anode surfaces and is operated as a dc magnetron. A beam of electrons is sent from the electron gun parallel to the axis of the magnetron entering the magnetron at the cathode surface. The trajectron was designed with the following mode of operation in mind: the initial radial and angular velocities and displacements were almost the same for beam electrons as for emitted electrons. Therefore beam electrons experienced nearly the same forces as emitted electrons, and their displacement in the radial and angular directions during the time they spent in the magnetron should have approximated the displacement which would be experienced by an emitted electron in the same time. The exit point of the beam showed on a fluorescent screen. By varying the beam voltage, the time the beam spent in the magnetron could be varied, and the spot on the fluorescent screen could be made to trace out paths which should correspond to trajectories of emitted electrons.

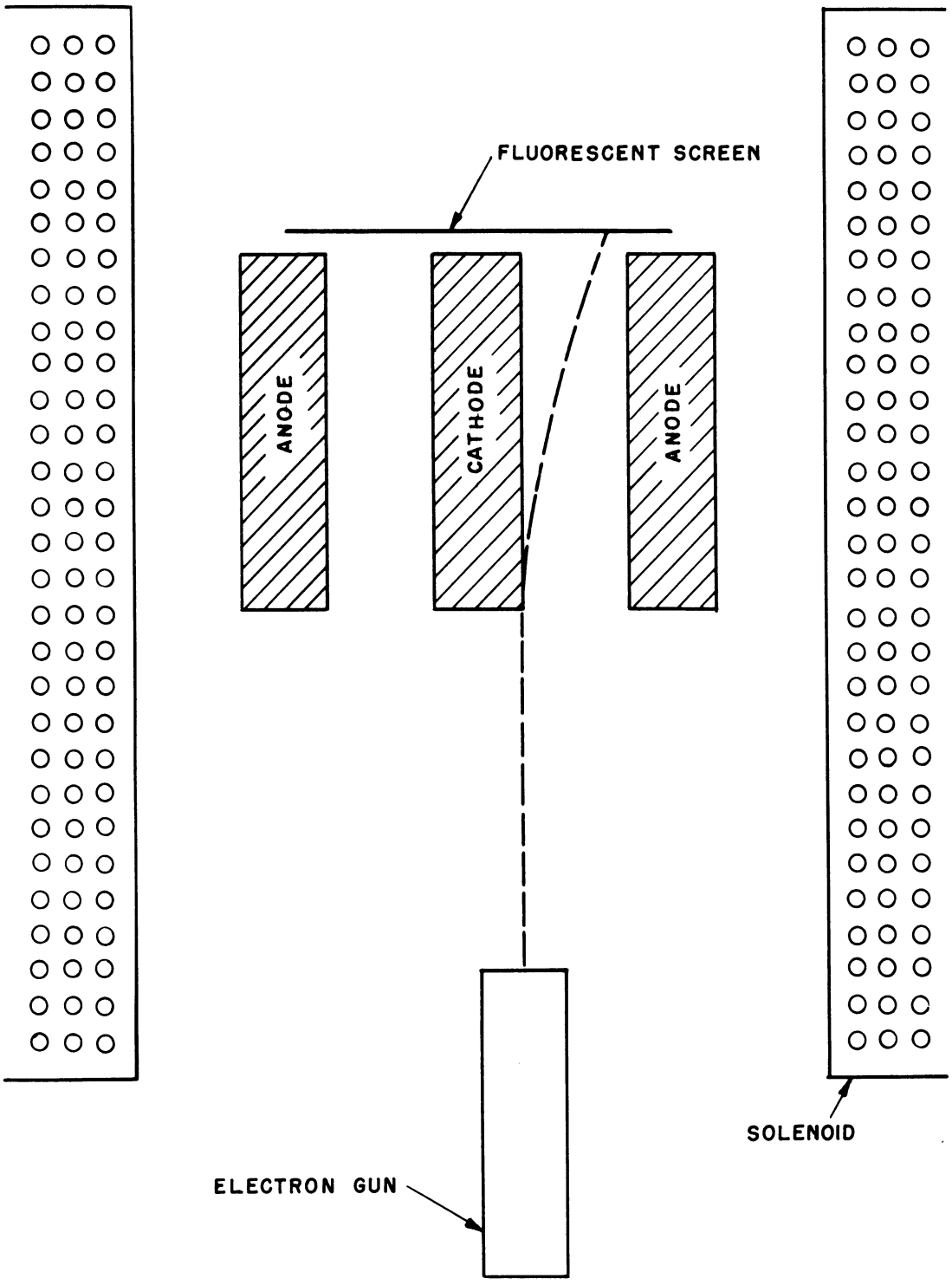

FIG. 3.1

SIMPLIFIED DRAWING OF THE TRAJECTRON

The first questions of design which had to be answered were (1) what should the dimensions of the magnetron diode be; and (2) in what range of anode voltage, magnetic field, and beam voltage should the trajectron be operated? In order to obtain results as accurate as possible, a large ratio of magnetron dimensions to beam diameter was desirable. Therefore, the magnetron diode had to be made as large as possible without incurring excessive anode voltages or difficult cathode heating and heat dissipation problems. The personnel of the tube laboratory recommended a cathode one-half inch in diameter and two inches long for the first model of the trajectron, and no change seemed advisable in later models. The cathode required approximately one-hundred watts heater power, and the heat dissipation presented no real difficulty.

The anode diameter was made about three and one-half times the cathode diameter. The theory of the static magnetron predicts transitions from one type of solution to another when the radius of the space charge cloud is in the range of twice to three times the cathode radius -- this range is easily observed when the anode radius is three and one-half times the cathode radius.

Conventional electron guns of the type used in oscillograph tubes were employed because they were readily available and inexpensive. P-1 phosphor (RCA No. 33-W-2A) was found to be the most satisfactory fluorescent screen coating. Then the approximate range of beam voltage was determined, since the phosphor is not satisfactory for beams of less than approximately 200 volts and the electron guns are rated to operate at no higher than 3000 volts (although they were found to work quite satisfactorily above 4000 volts).

An estimate of the required magnetic field is now possible. Suppose

we wish to have the beam deflected to its maximum radius when the beam voltage is 2000 volts. It can be seen from the differential analyser solutions given in Chapter II (Figure 2.5 and 2.6) that an electron will reach the maximum radial position in its orbit after a little more than one-half Larmor period; or π/ω_L seconds. Therefore we wish the 2000 volt beam to travel the length of the tube, two inches, in π/ω_L seconds. The velocity of the 2000 volt beam is

$$v = \frac{2e}{m} \phi \text{ beam} = 2.6 \times 10^7 \text{ meters per second.} \qquad (3.1)$$

The time it takes the beam electrons to travel the two inches through the magnetron is

$$t = \frac{\ell}{v} = 1.9 \times 10^{-9} \text{ seconds,} \qquad (3.2)$$

and this is to equal π/ω_L . Then

$$\omega_L = \frac{\pi}{t} = 1.65 \times 10^9 \text{ radians per second,} \qquad (3.3)$$

and since $\omega_L = eB/2m$,

$$B = \frac{2m\omega_L}{e} = 0.0185 \text{ webers per square meter,} \qquad (3.4)$$

or 185 gauss. Such a field can be obtained easily with a solenoid. The anode potential required to operate the tube with a given Hull radius can be found by referring to Figure 2.10 of Chapter II. For a Hull radius equal to twice the cathode radius, Figure 2.10 gives $\phi_a/B^2 = .067$, and hence if B = 185 gauss, $\phi_a = 2300$ volts. For cutoff conditions, $\phi_a/B^2 = .111$, and $\phi_a = 3800$ volts.

3.2 Details of the Tube Construction

Figure 3.2, an assembly drawing of the trajectron, shows most of the details in the design of the trajectron. A photograph of the assembled

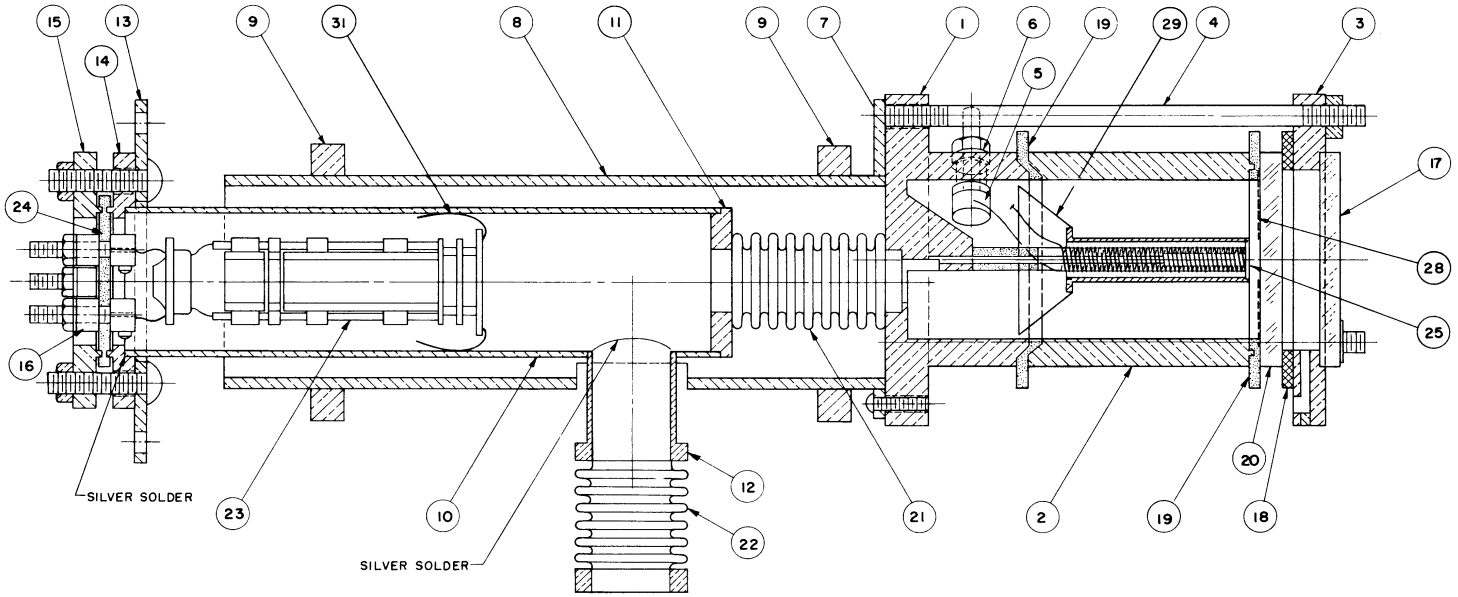

SECTION B-B

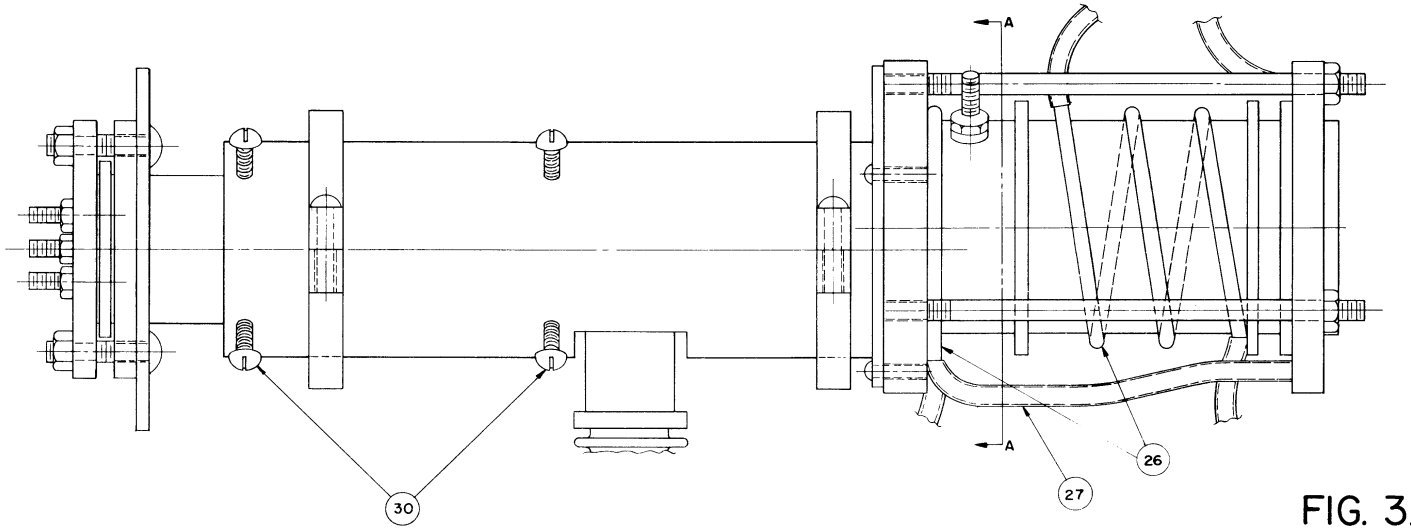

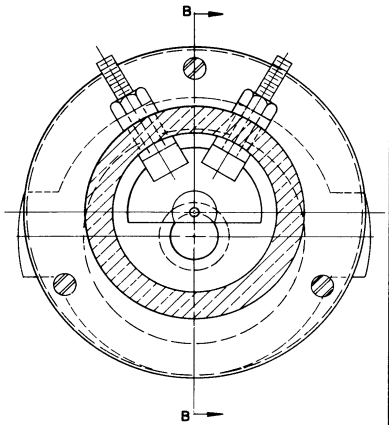

SECTION A-A

FIG. 3.2

ALL DIMENSIONS UNLESS OTHERWISE SPECIFIED MUST BE HELD TO A TOLERANCE - FRACTIONAL ± 1/64" DECIMAL ± .005" ANGULAR ± ½°

		ENGINEERING RESEARCH INSTITUTE UNIVERSITY OF MICHIGAN ANN ARBOR MICHIGAN	DESIGNED BY W.W. PETERSON	APPROVED BY
			DRAWN BY PLW	SCALE FULL
			CHECKED BY	DATE MARCH 19, 1953
		PROJECT 2009	TITLE TRAJECTRON	
6 ISSUE	5-19-53 DATE	CLASSIFICATION	DWG. NO. C-11008	

DWG. NO. C

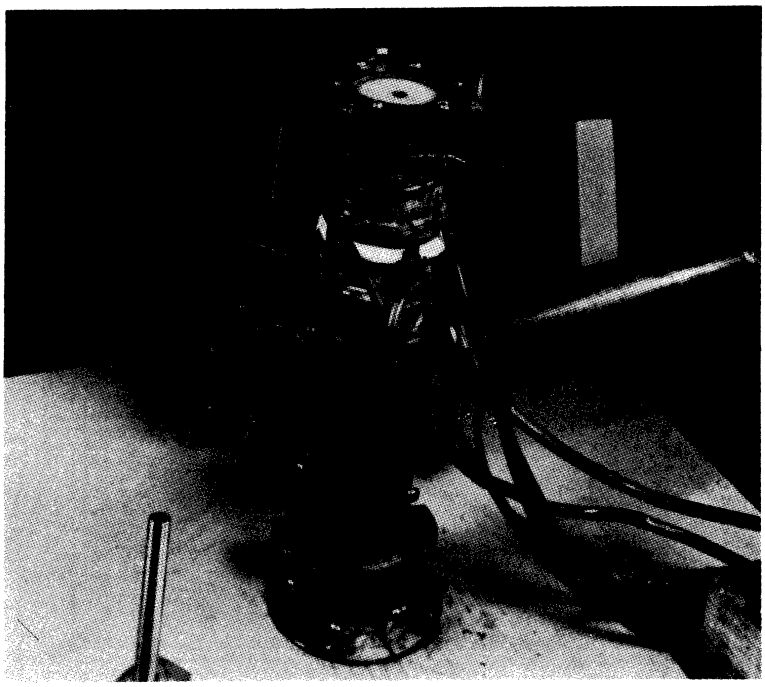

FIG. 3.3
ASSEMBLED TRAJECTRON

trajectron appears in Figure 3.3. The fluorescent screen was a coating of P-1 phosphor on the inside surface of the pyrex window (20).[1] This pyrex disk (20) was cut from an ordinary pyrex baking dish by using a "biscuit cutter".[2] The P-1 phosphor was suspended in acetone and sprayed onto the pyrex disk with a handmade glass spraygun. The phosphor was wiped off the outside edge of the disk where the glass contacts the teflon gasket (19), and a spot in the center of the disk was wiped so that the end of the cathode could be seen.

---

1 The numbers in the parentheses here and in the following paragraphs refer to the part numbers on the assembly drawing, Figure 3.2.

2 Strong, Ref. H, p. 36.

A little thought will make it clear that the fluorescent screen must be as near as possible to the magnetron diode. If it were not, the point where the beam leaves the magnetron space charge would have to be calculated from knowledge of where it hits the fluorescent screen. But such a beam path would be difficult curve to calculate because of the presence of the electric and magnetic fields in the region near the end of the diode. In the trajectron the spacing between the end of the cathode and the fluorescent screen was made one-eighth of an inch.

Placing the fluorescent screen near the magnetron cathode resulted in several problems. In the first place, the phosphor was subject to some heat and contamination from the cathode. P-1 phospor was recommended as the most rugged of the commonly used phosphors, and was found quite satisfactory. The efficiency of the fluorescent screen decreased with time as the trajectron was being used; therefore the fluorescent screen was recoated every time the tube was modified in any way and reassembled. In order to keep the fluorescent screen cool, cold water was run between the outside of the pyrex disk (20) and the transparent plastic disk (17). Holes in the clamping ring (3) were for water intake and outlet.

The most serious difficulty encountered with the fluorescent screen near the cathode was the lighting of the fluorescent screen by stray electrons from the magnetron space charge. The fluorescent screen was essentially the boundary of the magnetron space charge, and many electrons struck it because of initial z-components of velocity and because of z-components of velocity acquired in collisions. The only satisfactory way found to overcome this difficulty was to place a copper mesh (28) between the fluorescent screen and the magnetron diode. The mesh was connected to

ground (the cathode potential) through a narrow strip of .003 inch copper which was brought through the gasket seal. Glyptal was used at the point where the copper strip passed through the seal in order to make the seal vacuum-tight. Unfortunately, the presence of the copper mesh at ground potential at the end of the diode made end effects more serious.

Details of the cathode (25) are shown in Figure 3.4. The cathode was made of a Grade A nickel cylinder with a fine mesh of Grade A nickel sintered to its surface. The surface was coated with barium carbonate RCA No. 33-C-131. The coating was scraped so that the surface of the coating was flush with the outside of the mesh. The heater was a bifilar winding of .020 inch tungsten wire wound 20 turns per inch on a threaded piece of ceramic tubing. The ceramic tubing was found necessary to prevent the heater from sagging. The cathode and the ceramic were supported on a molybdenum rod. The electron beam entered the magnetron diode through a .063 inch hole in the flange at the bottom of the cathode. The flange served to support the shield (29) which was made of .003 inch molybdenum sheet. The shield was necessary to prevent any deflection of the electron beam by the electric field before it actually entered the magnetron space charge region.

Two .0035 inch wires were mounted on the cathode -- one on the center of the hole in the flange at the bottom of the cathode, and the other in exactly the same angular position at the other end of the cathode. These were used in aligning the beam.[1] A .025 inch hole was drilled in the end of the cathode centered in the axis of the cathode. This hole identified the center of the cathode on the data photographs. It was found to show up bes

---

[1] The beam alignment procedure is described in detail in Section 4.2.

DWG. NO. A

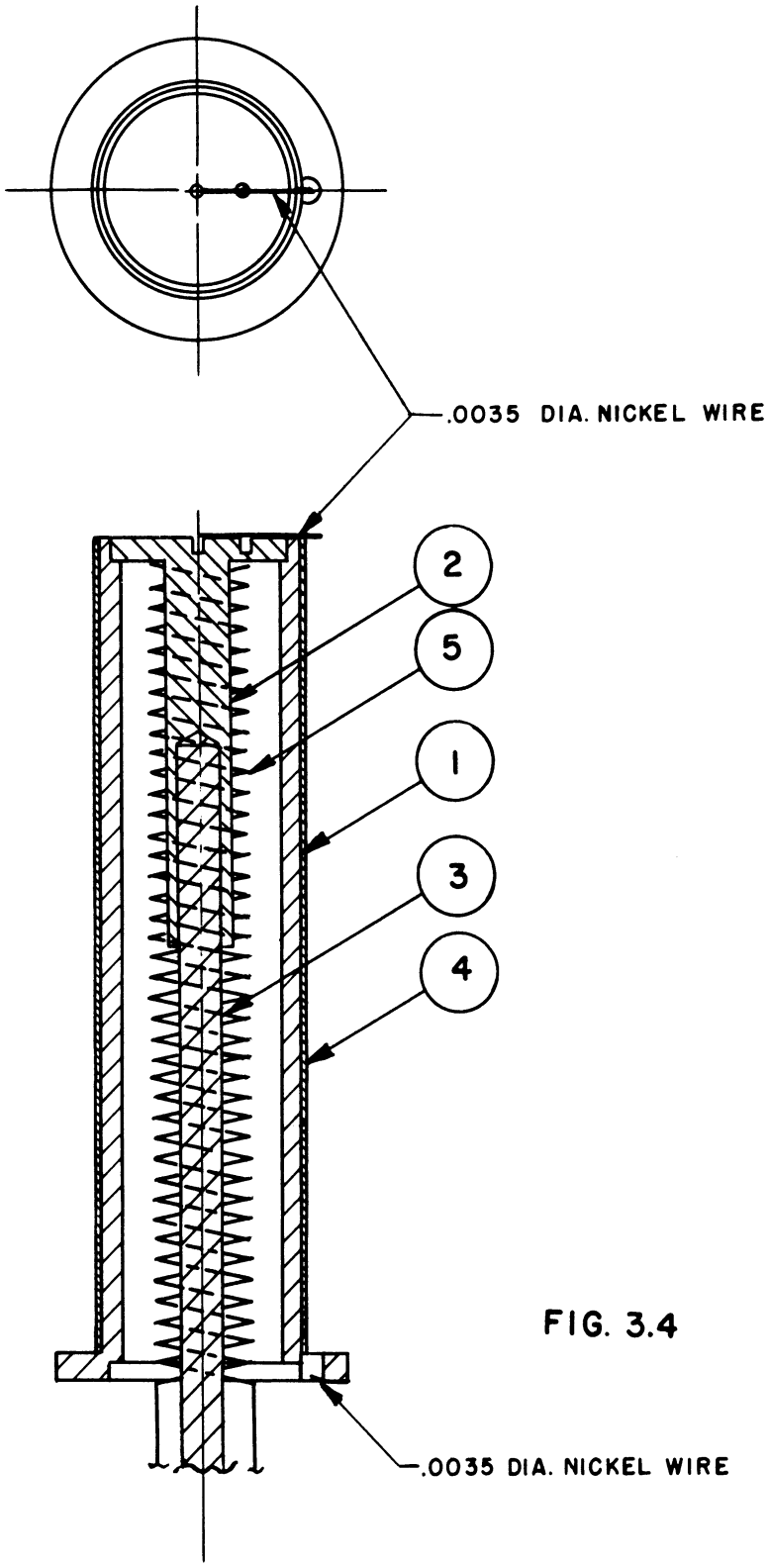

FIG. 3.4

ALL DIMENSIONS UNLESS OTHERWISE SPECIFIED MUST BE HELD TO A TOLERANCE - FRACTIONAL ± 1/64," DECIMAL ± .005," ANGULAR ± ½°

		ENGINEERING RESEARCH INSTITUTE UNIVERSITY OF MICHIGAN ANN ARBOR MICHIGAN	DESIGNED BY W. P.	APPROVED BY W.O.N.P.
			DRAWN BY PLW	SCALE 2 X
			CHECKED BY	DATE 2-2-54
		PROJECT 2009	TITLE MAGNETRON CATHODE FOR THE TRAJECTRON	
1	2-2-54	CLASSIFICATION	DWG. NO. A- 8047	
ISSUE	DATE			

on the photographs when aluminum oxide powder was put in the hole -- the aluminum oxide region appears dark on the photographs because it did not become as hot as the cathode and did not emit as much light.

All vacuum seals which could not be soldered were made with teflon gaskets, teflon being selected because of its low vapor pressure and good insulating qualities. The heater connections were made through two terminals (5) brought through the base of the diode and insulated with teflon gaskets. The three bolts (4) and the clamping ring (3) applied pressure to the water seal gasket (18), and to the two vacuum seals which were teflon gaskets (19). The anode (2) was thereby insulated from ground. Both gasket seals (19) were designed so that the pressure on the gasket was greatest on a narrow section in the middle of the seal. The bottom seal was given the beveled shape so that the anode would align itself concentrically with the base when the pressure was applied to the clamp.

Both the anode and the base were cooled by means of cold water running through copper tubes (26) soldered to the anode and the base. Water from the mains was run first through a 25-foot length of rubber tubing, then through the anode cooling tube, and through another 25-foot length of rubber tubing. From there it flowed through the base cooling tube, and finally through the chamber between the plastic window (17) and the pyrex window (20), and on into the drain. The water in the two rubber tubes formed a path to ground from the anode with a resistance of about eight megohms.

The electron gun chamber (10) was connected with the diode base (1) through a brass bellows (21). With this arrangement, the electron beam could be aligned after the tube was operating. The alignment was accomplished by adjusting the eight tangent screws (30) which control the relative position

of the electron gun chamber (10) and the diode support (8).[1] The diode support (8), which was outside the vacuum seal and served as mechanical support for the diode section of the trajectron, could be removed without opening any vacuum seals; this facilitated checking for leaks in the vacuum envelope of the tube.

The connections to the electron gun (23) were made through a teflon disk (24) at the base of the tube. The four terminals (16) brought through the insulator connected to [1] heater, [2] heater and cathode, [3] grid, and [4] focussing electrode.

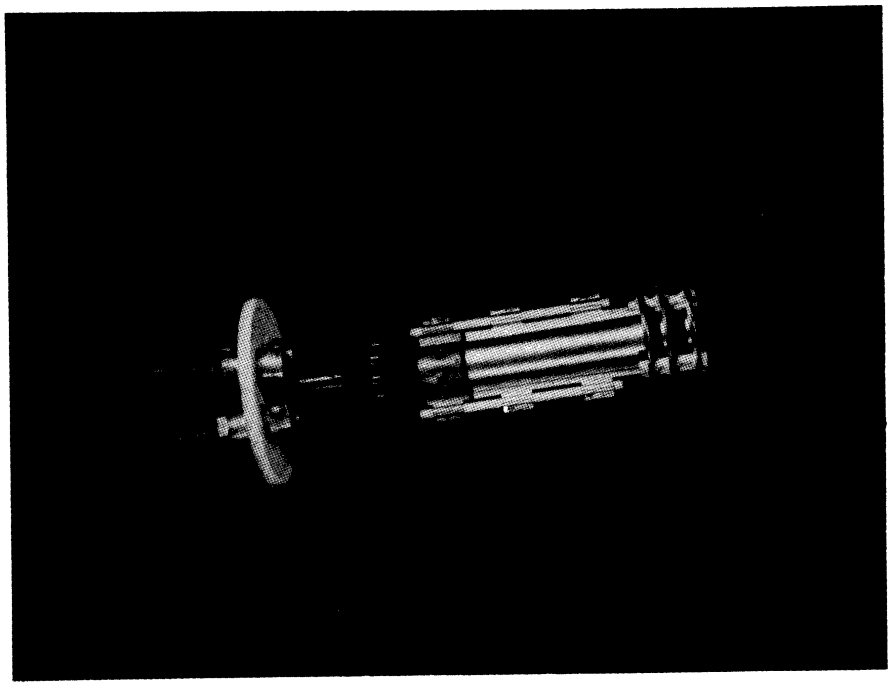

FIG. 3.5
ELECTRON GUN READY FOR INSTALLATION

---

1 The exact alignment procedure is described in detail in Section 4.2.

Figure 3.5 is a photograph of the electron gun and terminals ready for installation. The anode was connected to the grounded electron gun chamber through mounting springs (31). The terminals in the teflon also served as supports for the electron gun. The teflon insulating disk was clamped to the base of the electron gun chamber with two rings (14) and (15). The ring (14) and the base plate (13) were used to mount the tube to the bench on which it was operated. The vacuum seal between the ring (14) and the electron gun chamber (10) had to be silver soldered in order to give it sufficient strength to support the whole tube.

All parts of the tube were brass except for the insulators, gaskets, windows, copper cooling tubes, and parts associated with the cathode. All metal seals were soft soldered except the two noted on Figure 3.2 and the joints on the cathode itself. The molybdenum support was arc welded to the nickel cathode sleeve, the mesh was sintered to the cathode surface, and the two parts of the molybdenum cathode support were platinum-brazed together.

3.3 The Magnetic Field

The magnetic field was produced by a solenoid. The solenoid was wound on a brass spool 12-1/2 inches long with a 4-3/4 inch inside diameter. The winding itself consisted of about 925 turns of No. 14 double cotton covered wire.[1] The winding was 30.5 cm. long, 1.2 cm. thick, and had a 12.7 cm. inside diameter. The solenoid can be seen in Figure 3.6, page 86.

---

[1] There may be an error of as much as $\pm$ 1% in the estimate of the number of turns, and hence in the estimate of magnetic flux density.

The field of the solenoid could be calculated more accurately than it could be measured with available instruments. Calculations were made only for the field on the axis of the solenoid. The assumption is made that the current flow is uniformly distributed through the cross-section of the winding rather than being concentrated in the wires; this is a very good approximation in this case, since the distance from the axis to the winding is many times the spacing between wires. The magnetic field on the axis of a cylindrical sheet of current of zero thickness is[1]

$$H_{axis} = \frac{ni}{2s}\left[\frac{(\frac{s}{2} - b)}{\sqrt{R^2 + (\frac{s}{2} - b)^2}} + \frac{(\frac{s}{2} + b)}{\sqrt{R + (\frac{s}{2} + b)^2}}\right], \qquad (3.5)$$

where s is the length of the solenoid; n, the number of turns; i, the current; b, the distance along the axis to the point at which the field is being calculated; and R is the radius of the cylinder. The field of a solenoid of appreciable thickness can be found by integrating (3.5) with respect to R between the limits R_1, the radius of the inside of the coil, and R_2 the radius of the outside of the coil.

$$H_{axis} = \frac{n}{2s}\frac{i}{R_2 - R_1}\int_{R_1}^{R_2}\left[\frac{(\frac{s}{2} - b)}{\sqrt{R^2 + (\frac{s}{2} - b)^2}} + \frac{(\frac{s}{2} + b)}{\sqrt{R^2 + (\frac{s}{2} + b)^2}}\right]dR \qquad (3.6)$$

$$= \frac{ni}{2s}\left\{\frac{(\frac{s}{2} - b)}{2(R_2 - R_1)}\left[\sinh\text{-}1\ \frac{R_2}{(\frac{s}{2} - b)} - \sinh\text{-}1\ \frac{R_1}{(\frac{s}{2} - b)}\right] +\right.$$

---

[1] Attwood, Ref. A, p. 262.

$$\frac{(\frac{s}{2}+b)}{2(R_2-R_1)}\left[\sinh^{-1}\frac{R_2}{(\frac{s}{2}+b)}-\sinh^{-1}\frac{R_1}{(\frac{s}{2}+b)}\right]\Bigg\}$$

At the center of the coil b = 0, and this reduces to

$$H_{\text{axis center}} = \frac{ni}{s}\left[\frac{\sinh^{-1}\frac{R_2}{2s}-\sinh^{-1}\frac{R_1}{2s}}{\frac{R_2}{2s}-\frac{R_1}{2s}}\right] \tag{3.7}$$

As s approaches infinity, H_{axis} approaches ni/s, the field of an infinite solenoid. The expressions in the brackets can be considered the factors which correct for finite length. For the coil described above, the correction factor turns out to be 0.91 at the center of the coil (b = 0), and 0.895 at 10 cm. from the end of the coil (b = 5.25). The flux density is

$$B = \mu_o H \text{ webers per square meter}, \tag{3.8}$$

and since $\mu_o = 4\pi \times 10^{-7}$,

$$B = 4\pi \times 10^{-7} \times \frac{925}{0.305}$$

$$= 0.00381 \text{ webers per square meter per ampere}$$

$$= 38.1 \text{ gauss per ampere} \tag{3.9}$$

for an infinite solenoid. At the center of the coil described above,

$$\frac{B}{I_m} = 38.1 \times 0.910 = 34.6 \text{ gauss per ampere}, \tag{3.10}$$

and at 5.25 centimeters from the center,

$$\frac{B}{I_m} = 38.1 \times 0.885 = 33.7 \text{ gauss per ampere}, \tag{3.11}$$

or about two and three-quarters percent lower than at the center.

When the magnetron diode was placed in the solenoid, one end of the diode was at the center of the solenoid, placing the other end, was approximately 5 centimeters from the center of the solenoid. The beam path was placed on the axis of the solenoid.

It is not easy to calculate the field of a solenoid off the axis; however, relative field strength on the axis and off the axis can be measured easily by means of a search coil. Alternating voltage was applied to the solenoid, and the voltage induced in a search coil was then measured by means of an oscilloscope. The measurements indicated that the field inside the diode would be nowhere appreciably stronger than on the axis at the center of the solenoid and nowhere weaker than on the axis five centimeters from the center of the solenoid. The difference in field strength at these two points was approximately two and three quarters percent, as was indicated by the theoretical calculation.

As an average value for the magnetic field in the diode, the figure 34.3 gauss per ampere was used in all calculations.

3.4 Instruments and Recording of Data

Electron gun cathode potential was measured on a Simpson model 260 meter which was calibrated with a Weston model 45-300 volt voltmeter with a 3000 volt multiplier. The anode voltage was also usually measured with a Simpson model 260 meter, but some anode potential data were taken directly on the Weston model 45 voltmeter. The errors in these Simpson voltmeter readings should be less than one percent of the full scale voltage 5000, 1000, or 300 volts.

Magnet current was measured on a Weston model 45 ammeter usually with a five ampere shunt. Anode current was usually measured with the Simpson model 260 meter, and there may be errors as great as ten percent in some of the anode current figures given. The current data for the volt ampere curves of Figs. 1.1 and 5.10, however, were taken on a Weston model 45

ammeter with a one-ampere shunt, and those readings probably involve no errors greater than five milliamperes.

All data from the fluorescent screen were taken on photographs. The fluorescent screen was inaccessible for direct measurements, but convenient for photographing. In addition the photographs formed permanent records of the data which could be studied at any time.

The camera used was a Dumont model 296, 35mm. oscillograph type with an f2.8 lens. An adapter was made so that the camera could be mounted on the end of the solenoid. The camera is shown ready for use in Figure 3.6. When the cathode was heated a Kodak Series V Wratton Filter B was used to filter out as much of the light of the hot cathode as possible. This filter matches very closely the spectrum of the light emitted by P-1 phosphor. In addition Kodak Linagraph-Ortho film, which is a fast film insensitive to red light, was used. The aperture was usually set at about f4 to increase the resolution. The shadow of the copper mesh, on which the wires are spaced .010 inch, is resolved on the photographs except when the spot was over-exposed. This is certainly adequate resolution, since the spot was never less than .010 inch in diameter, and was usually much larger than this. A single photograph usually includes a number of spots. This was accomplished by making exposures with the spot in each of many positions. The exposure time was varied to make the spots appear more uniform on the photographs, the times ranging from as much as 20 seconds for a 300 volt spot to as little as 1/50 second for a 4000 volt spot. Many typical photographs are included in Chapters IV and V and Appendix E.

All the negatives were developed in the tube laboratory immediately after exposure so that they could be checked while the equipment was still

in operating condition. They were developed in tanks with Kodak Microdal fine grain developer for fifteen minutes. They were then placed in an acid fix for fifteen minutes, rinsed in cold water for fifteen minutes, and hung up to dry.

3.5 Auxiliary Equipment

The trajectron tube was mounted on a special bench, illustrated in Figures 3.6 and 3.7. The whole bench could be moved, since the pump-out tube had a bellows at each end. In addition, the surface (A) on which the tube was mounted could be tilted. These two degrees of freedom permitted adjusting the tube so that the electron beam traveled parallel to the earth's magnetic field. The solenoid was placed on surface (B), which could be adjusted relative to surface A by means of three bolts (C), which can be seen in Figure 3.7. By tilting the surface (B) and sliding the solenoid about on surface (B), the solenoid could be aligned with the electron beam. The complete alignment procedure is described in detail in Section 4.2.

The heater supply for the beam consisted of a well-insulated 10-volt transformer connected to a "Variac" auto-transformer. The auto-transformer was connected to the safety circuit of the vacuum station, so that it would be turned off in case of failure of the power or the vacuum station.

The beam anode voltage was supplied by a small power supply built especially for this application. It supplied 300-4500 volts, but less than one milliampere, and hence was not a hazard to the operator.

The circuit of this power supply appears in Figure 3.8. It is similar to that used in television receiver high voltage supplies, and

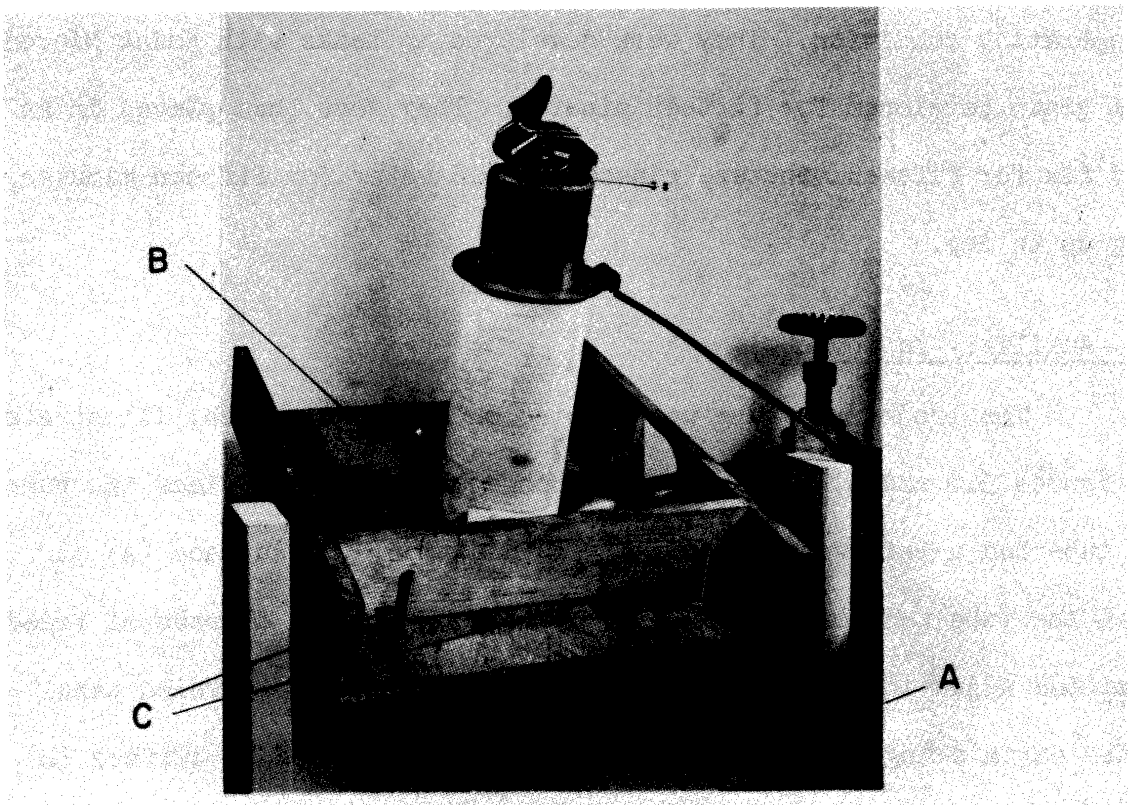

FIG. 3.6 THE TRAJECTRON READY FOR RECORDING OF DATA

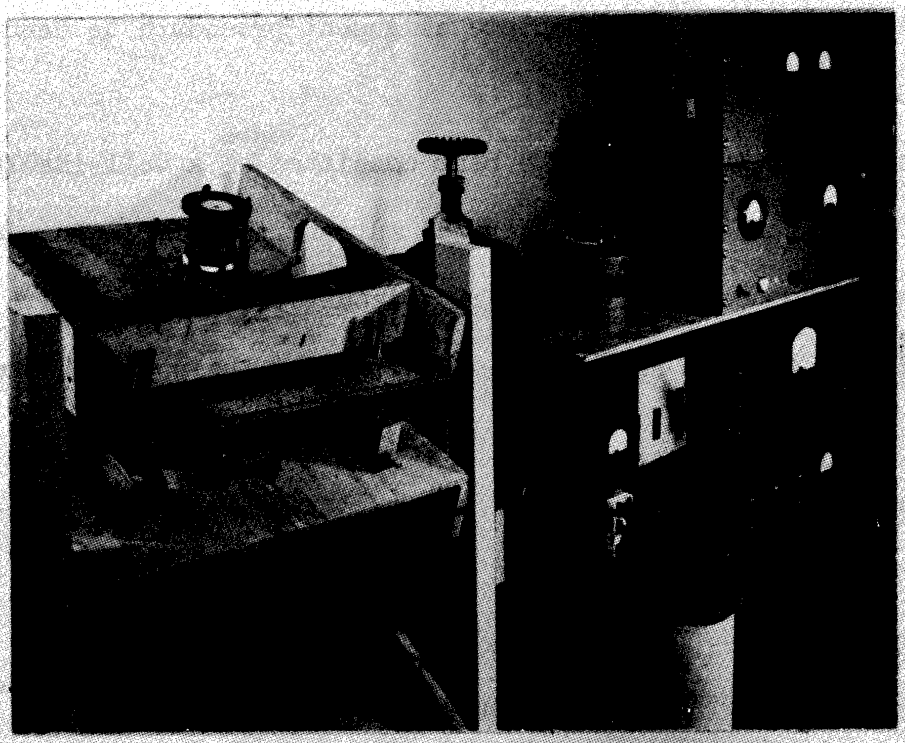

FIG. 3.7 THE TRAJECTRON, VACUUM STATION AND POWER SUPPLIES

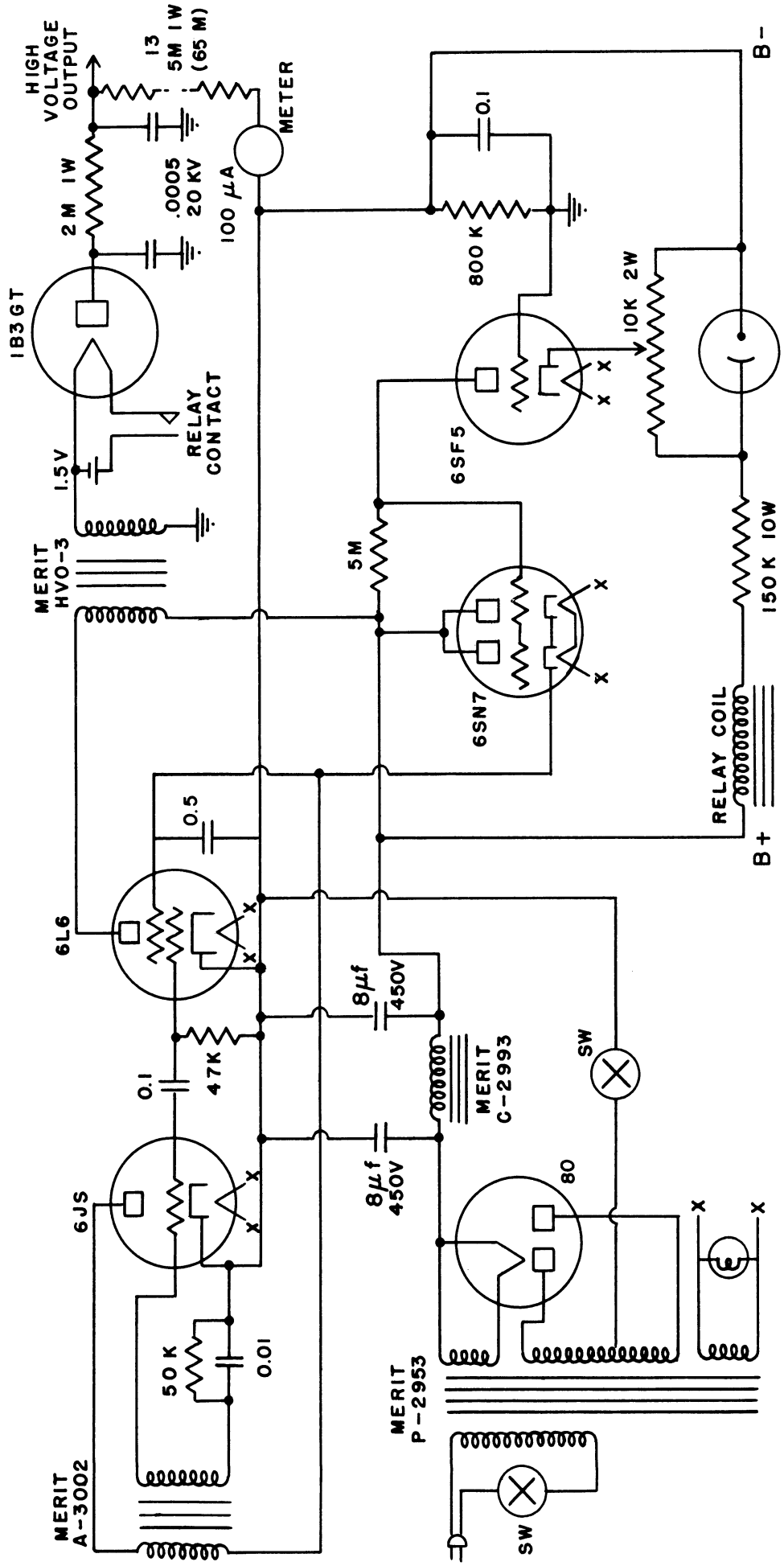

FIG. 3.8

CIRCUIT DIAGRAM OF BEAM VOLTAGE SUPPLY

standard television components were used. A voltage regulator circuit was incorporated in order to stabilize the voltage. The 6SN7 blocking oscillator, operating at about 15 kc, drives the 6L6 power amplifier. The output transformer in the 6L6 plate circuit steps up the voltage to about 5000 volts. It is rectified and filtered. The resistor R_1 is essentially part of the bleeder resistor on the output, and the voltage developed across it and applied to the grid of the 6SF5 is proportional to the output voltage. A constant regulated voltage is applied to the cathode of the 6SF5, and the difference voltage is amplified by the 6SF5 and 6SN7 to control the 6L6 screen grid voltage and 6SN7 oscillator plate voltage. The potentiometer P_1 controls the regulated voltage applied to the cathode of the 6SF5, and the output voltage is maintained by the regulator at approximately a constant multiple of this voltage. This potentiometer was used to adjust the output voltage to the desired value.

The electron gun grid and focussing electrode potentials were controlled by potentiometers mounted on the bench with the trajectron (on surface A, Figure 3.7). The circuit is shown in Figure 3.9.

The heater voltage for the diode was supplied by a small 24 volt transformer connected to a "Variac" auto-transformer. The auto-transformer was connected to the safety circuit of the vacuum station. It was found that the magnetic field of the heater current deflected the beam and affected slightly the operation of the magnetron diode, so that it was necessary to make observations when the heater was turned off. In order to accomplish this, a multivibrator with a relay in its plate circuit was built. It was adjusted so that the relay was closed ten seconds and then open ten seconds. The relay was inserted in the heater circuit. A

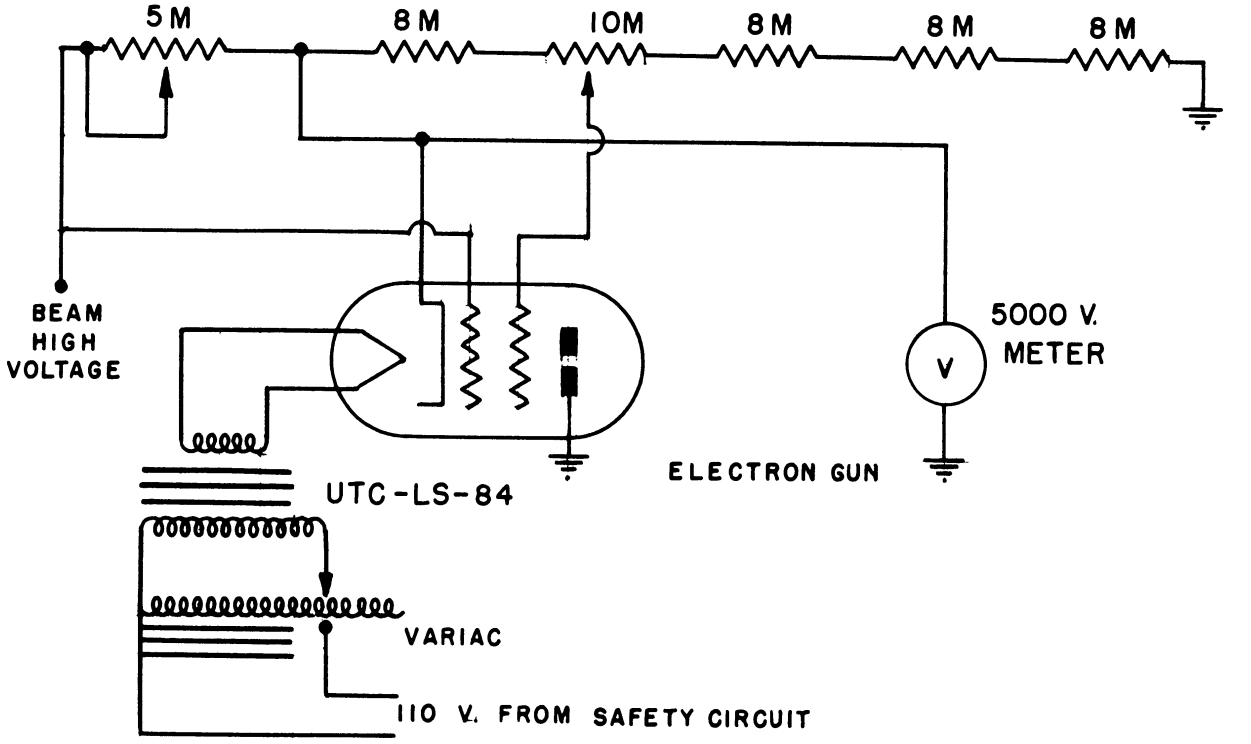

FIG. 3.9 CIRCUIT FOR ELECTRON GUN

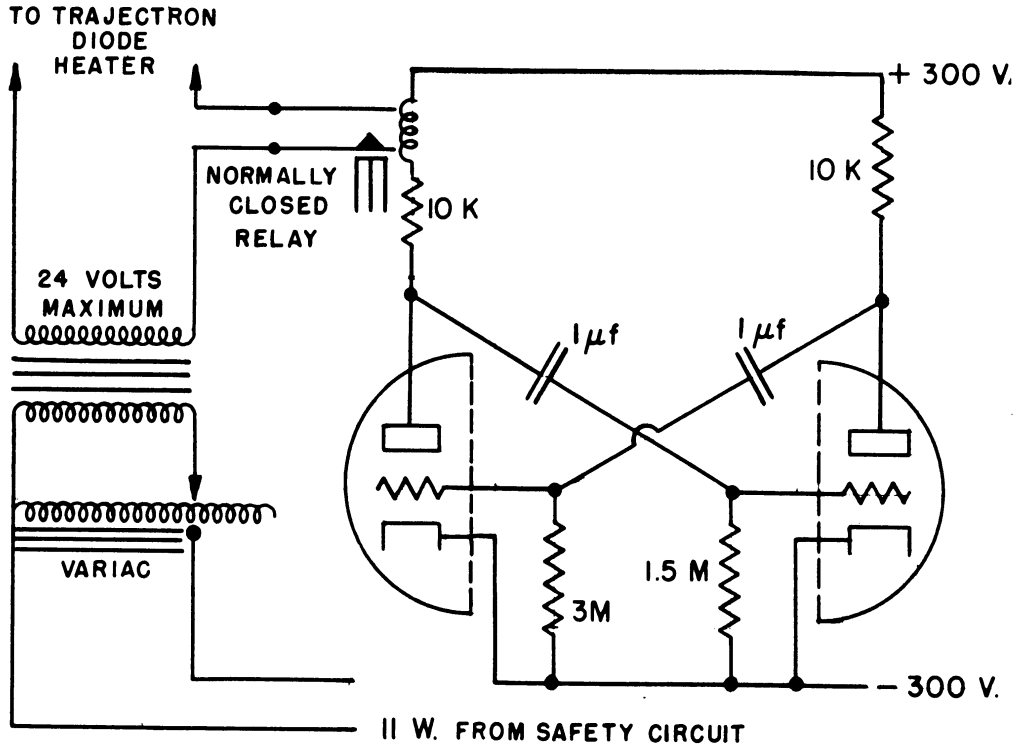

FIG. 3.10 CIRCUIT FOR HEATER INTERRUPTION

circuit diagram of this setup is shown in Figure 3.10.

The anode voltage for the diode was obtained from either one of two supplies. The first was rated at 1000 volts 100 ma, but would deliver up to 1400 volts with very light loads. It was a conventional, unregulated supply with a 3 section filter. When higher voltages and/or currents were required, a rebuilt Signal Corps RA-38 rectifier was used. It would deliver up to about 15,000 volts -- much more than was required for the trajectron -- and up to 800 ma.

Power was supplied to the solenoid by a small thirty volt motor-generator and controlled by a rheostat. The ripple in the supply voltage was approximately one and one-half percent. The ripple in magnetic field was undoubtedly less than this: the brass spool on which the solenoid was wound acts as a secondary winding. The magnetic field of the ac component of the solenoid current and the magnetic field of the current induced in the brass spool tend to cancel one another.

The vacuum pump used with the trajectron was a National Research Corporation type H-2-P oil diffusion pump, which is rated to have a blanked off ultimate vacuum of 2×10^{-7} mm of Hg., and a pumping speed unbaffled of 50 liters per second at 10^{-5} mm of Hg. The forepump was a Welch type 1400B. There was a valve in the pumpout tube so that the pump could be kept in operation while modifications were being made in the trajectron. The vacuum gauge, which was mounted near the diffusion pump, was a Distillation Products, Inc., type VG-1A, and the gauge control circuit was a DPA type 37.

The circuit diagram for the power control system for the vacuum station and the trajectron is shown in Figure 3.11. There is a Geissler

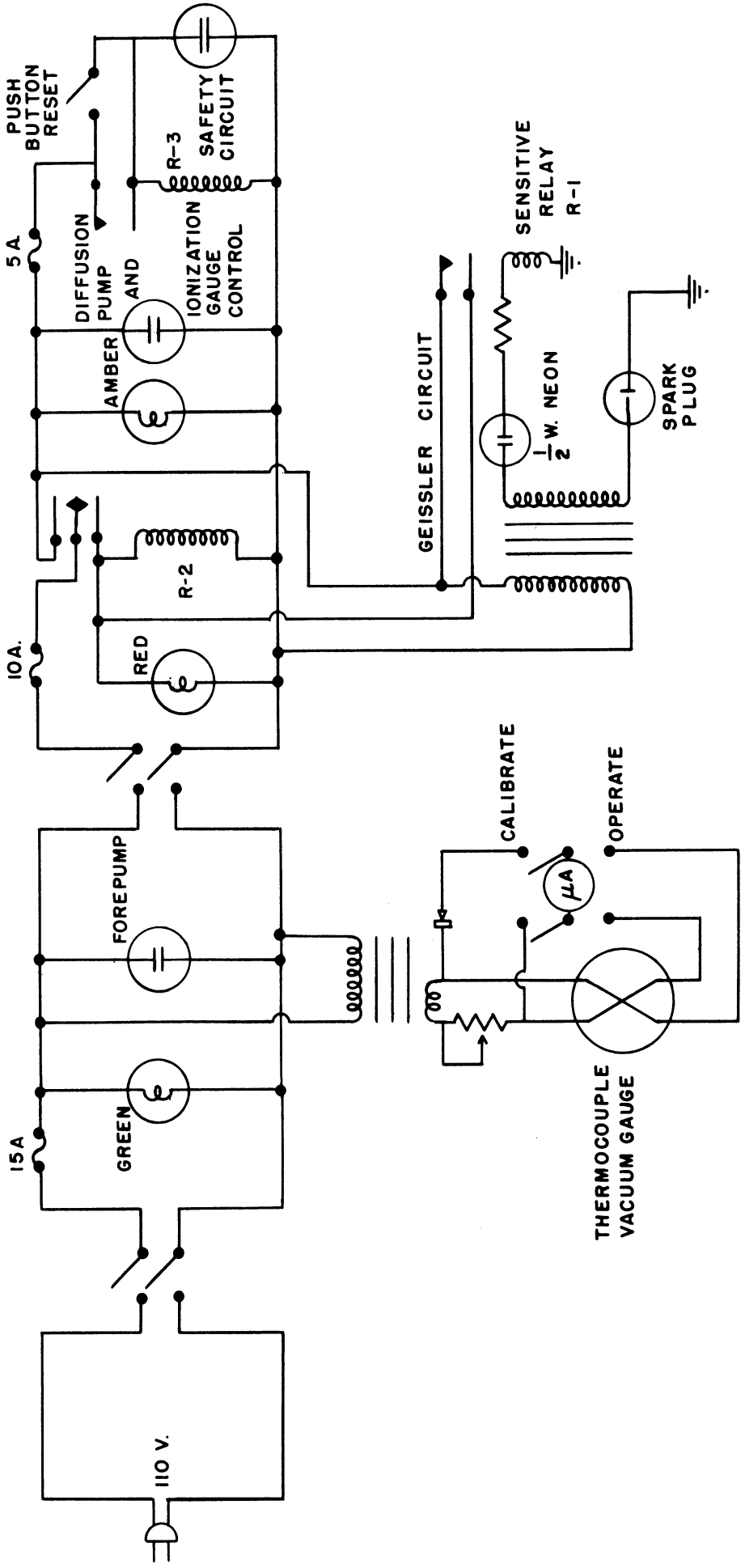

FIG. 3.11

DIAGRAM OF CONTROL CIRCUIT

circuit: if the pressure at the forepump rises above about 150 microns, there is a discharge in a spark gap mounted in the system, which closes the relays R-1 and R-2. The relay R-2 holds itself closed. Note that a brief power failure will not cause this relay to close and hence will not interrupt the operation of the diffusion pump, which is connected to this relay. There is also a safety circuit, controlled by relay R-3. This relay can be closed by the push-button switch at any time when the diffusion pump is turned on and receiving power. The relay then holds itself closed as long as there is no interruption of the power. However, if the power is even momentarily turned off either because of a power line failure or because of the Geissler circuit, the relay R-2 will open and remain open. The heater voltages for both cathodes were connected to this circuit.

3.6 Processing of the Cathodes.

In processing the diode cathode, about one volt was applied initially to the heater. The heater voltage was gradually increased as the cathode outgassed, the pressure in the system always being maintained at approximately 2×10^{-4} mm of Hg, until the cathode temperature reached about 875°C. The cathode temperature was measured by means of an optical pyrometer, the end of the cathode being viewed through the hole wiped in the center of the fluorescent screen. The cathode was kept at 875°C until the pressure in the system dropped to approximately 10^{-5} mm of Hg. This outgassing required about 30 hours. Then anode voltage was applied, starting at about ten volts. It was gradually increased to about 500 volts (with about 400 ma of anode current) over a period of several hours, and was operated at about 500 volts until the pressure in the system dropped

to 5×10^{-6} mm of Hg. During this time a record was kept of the anode current compared with the theoretical space-charge-limited current for a cylindrical diode of these dimensions, to show whether or not the cathode was operating with space-charge-limited current. When the cathode could deliver 400 ma of space-charge-limited current with the pressure in the system below 5×10^{-6} mm of Hg, the cathode was considered ready for operation.

The electron gun cathode was always processed after the diode cathode was activated. The voltage on the heater was increased gradually to about eight volts and held there until the pressure in the system dropped to 5×10^{-6} mm of Hg. This usually took an hour or two. Then the heater voltage was decreased to about six and one-half volts, and the electron gun was ready to use. Usually after several days of operation, the emission from the electron gun cathode dropped, and the gun cathode had to be heated somewhat more for satisfactory operation.

CHAPTER IV

CONTROL EXPERIMENTS

4.1 Introduction

This chapter consists of a description and discussion of control experiments and a discussion of the trajectron method based on the results of these experiments.

The trajectron could be operated under any one of four conditions: (1) Non-emitting cathode with no magnetic field,

(2) Non-emitting cathode with magnetic field,

(3) Emitting cathode with no magnetic field, or

(4) Emitting cathode with magnetic field.

The reason for building the trajectron was to obtain data for the fourth case, which is the magnetron case. The first two cases correspond to finding the trajectory of an electron in the field of concentric cylinders without space charge. The third case is that of finding the trajectory of an electron in a space-charge-limited cylindrical diode. These first three cases are well understood. Their study by means of the trajectron serves to demonstrate the possibilities and the limitations of the trajectron method and to give information about the trajectron useful in interpreting its data for the magnetron case. It is the purpose of this chapter to present and to discuss trajectron data for each of these first three cases.

In the first two cases the beam spots were found to trace out reasonably well the theoretical trajectrons of an electron starting from rest at the cathode. The discrepancies are shown to be largely due to end effects. When an emitting cathode was inserted and the current to the anode was space-charge-limited the situation was changed entirely. The electron beam entered the diode in a region of weak electric field and was deflected into a region of strong field. It is both shown theoretically and observed that the beam becomes defocussed under these circumstances. If the beam enters at the potential minimum, the spot extends back to the cathode. Such a spot cannot be interpreted as giving directly the displacement as a function of transit time for emitted electrons. Knowledge of the fields in the diode can be obtained only as a result of a more thorough study and indirect interpretation of the data.

In order to study the effects of the initial conditions of beam electrons, it is necessary to have a description of the beam. Therefore, the discussion of beam alignment and of size and position of the beam is included in this chapter. This information is important also in the discussion of the magnetron case.

4.2 Beam Alignment Procedure and Beam Description

The purpose of the beam alignment was to make the beam path as near to the cathode surface and as nearly parallel to the axis of the cathode as possible (when the anode voltage was zero) for all choices of beam voltage and magnetic field likely to be used in the experiment.

There are three steps in the alignment procedure. First, the electron beam must be aligned with the earth's magnetic field. Next,

the diode must be positioned correctly relative to the beam. Finally, the solenoid must be placed so that its axis is the path of the beam.

A simple calculation shows that if the electron beam is perpendicular to the earth's magnetic field (of 0.6 gauss), in travelling 9 inches, as in the trajectron, it will be deflected approximately 1 inch from a straight path if the beam voltage is 300 volts, 1/3 inch if the beam voltage is 4000. This makes clear the need for the beam to be parallel with the earth's field.

The first step in alignment was to loosen the tangent screws (Part [30] in Figure 3.2) which positioned the diode, turn on the electron beam, and move the diode until the beam came through the hole in the end shield of the cathode, showing a green spot on the fluorescent screen. Then the tangent screws were tightened. The spot was viewed through a 7 power magnifying glass while the beam voltage was varied. If the spot moved, the beam was not aligned with the earth's magnetic field, and the direction of the motion indicated which way the electron gun had to be tilted. For example, if the spot moved toward the south as the beam voltage was decreased, the electron gun had to be tilted toward the west. The angular position of the electron gun was adjusted by moving the bench on which the trajectron was mounted and by adjusting the angle of the plane surface (A) on which the trajectron was mounted on the bench. (See Figure 3.7.) It was adjusted until the deflection of the spot was unnoticeable (less than .005") when the beam voltage was varied from 300 to 4000 volts. This would require the beam to be within about 3° of parallelism with the earth's magnetic field.

For the next step, positioning the diode, the tangent screws were loosened again and the diode was brought to approximately its correct position. Then the tangent screws were tightened and final fine adjustments were made by moving pairs of tangent screws slightly. The spot was viewed through the magnifying glass, as before, and was alternately focused and defocused. When it was defocused, the shadows of the hole at the bottom end of the cathode and of the two .0035" wires mounted in this hole and at the other end of the cathode were visible. The shadow of the cathode surface showed also. The appearance of the spot is shown in Figure 4.1 for a slightly misaligned condition. The diode position was adjusted until the shadows of the two wire coincided, and until the beam path was as close as possible to the cathode surface at both ends of the cathode as indicated by the shadow of the cathode surface. Then the beam was focused, and the exact position of the beam spot relative to the wires and the cathode surface was noted. Typically the beam spot was placed about .010" to one side of the wires with its center about .015" from the cathode. It probably deviated no more than .020" in the two-inch length of the cathode from a line truly parallel with the axis of the cathode, or made an angle of less than two-thirds of a degree with the axis of the cathode. Its diameter was approximately .025".

The final step in the alignment procedure was to place the solenoid over the tube and apply a magnetic field typical of that which would be used in the experiments, 100 to 200 gauss. The spot was observed through the magnifying glass, and the magnet was adjusted until the spot position was, as nearly as possible, the same with all beam voltages and

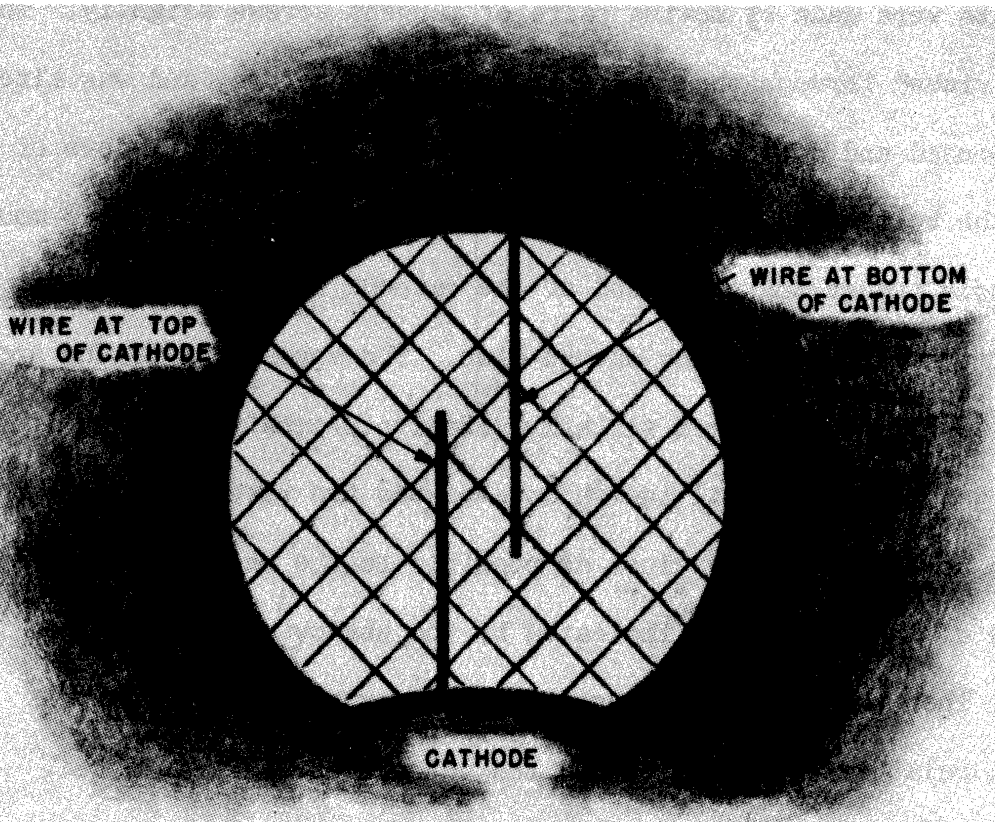

FIG. 4.1

APPEARANCE OF UNFOCUSED SPOT
DURING ALIGNMENT PROCEDURE
(B = 0)

magnetic fields as when there was no magnetic field. The adjustment was difficult for three reasons. First, the beam path was no longer nearly straight, but rather helical. The desired data at any stage in the adjustment were the radius and the position of the axis of the helix, and these data could be found only by varying the beam voltage continually during the alignment. Second, slight movements of the solenoid moved the beam so that is did not pass through the hole in the cathode end shield, and when the beam spot could not be seen, it was impossible to make a systematic adjustment. Finally, there were four degrees of freedom, two in the relative angle of the beam and the solenoid axis, and two in the relative position of their intersections with any fixed plane.

The first two degrees of freedom were adjusted in the trajectron by adjusting the relative angles of the plane surface (A) on which the tube was mounted and the surface (B) on which the solenoid was placed. (See Figure 3.7, page 86.) The adjustment was made with the three bolts (C). The other two degrees of freedom were adjusted by positioning the solenoid on the plane surface (B) on which the solenoid was placed.

The best procedure found for aligning the axis of the solenoid with the beam was hardly better than trial and error. Initially the surface (B) on which the solenoid rested was made parallel with the surface (A) on which the tube was mounted. (See Figure 3.7.) Then the solenoid was moved on this surface and the beam voltage was varied until the spot appeared. As the beam voltage was varied, the spot moved in approximately a circle. By trial and error, the solenoid position and

angle were adjusted until this circle was no larger than about one-eighth inch in diameter. From here on at each stage in the adjustment the center of this circle, which is the axis of the helical path of the beam, was placed at the point where the beam appeared with no magnetic field, by aligning the solenoid on its mounting surface. In this position the diameter of the circle was noted. The angular position of the solenoid was adjusted by trial and error in small steps, and the center of the circle readjusted at each step until satisfactory alignment was achieved.

TABLE 4.1

Description of Aligned Beam Spot
(Distances Measured in Inches)

Solenoid Current, amperes	1	2.5	4	5
Magnetic Field Strength, gauss	34.3	85.2	137.2	171.5
Maximum Diameter of Spot	.045	.040	.040	.025
Minimum Diameter of Spot	.040	.015	.015	.008
Distance from Center of Spot to Center of Rotation				
At Maximum Radius	.018	.013	.013	.008
At Minimum Radius	.015	0	0	0
Distance from Center of Rotation to Cathode Surface	.017"	.017"	.017"	.017"
Distance from Center of Rotation to Wires	.010"	.010"	.010"	.010"

When the beam was aligned as well as possible, at all beam voltages it exhibited approximately a circular cross section. As the beam voltage was increased, the diameter of the circle would oscillate between a minimum and a maximum value. Simultaneously it seemed to rotate around a point within the spot.[1] The approximate appearance of the outline of the spot for a series of beam voltages is shown in Figure 4.2. A typical data for the size and location of the spot are given in Table 4.1. These data were taken when much of the data on the magnetron case were taken. They cannot easily be duplicated because they are affected by even the slightest movement of the solenoid and also by the condition of the electron gun cathode and the setting of the electron gun grid voltage.

It is desirable to know the initial conditions of beam electrons in order to permit studying the effects of their initial conditions on the motion of the beam. The different beam electrons have different initial velocities, and it is possible to give only the approximate range of initial velocity and position. This approximate range can be calculated from the above description of the beam.

The case of no magnetic field is simple because the electrons must travel in straight lines from the limiting aperture of the electron gun to the fluorescent screen, a distance of 8.8 inches. The aperture of the electron gun was round, with a diameter of .063". The spot diameter was approximately .025". A sketch of the beam, gun aperture, and cathode with the width of the beam exaggerated is shown in Figure 4.3. It can be seen from the figure that the largest angle a

---

[1] This is consistent with the behavior predicted in Appendix A for the motion of an electron beam in an axially symmetric magnetic field.

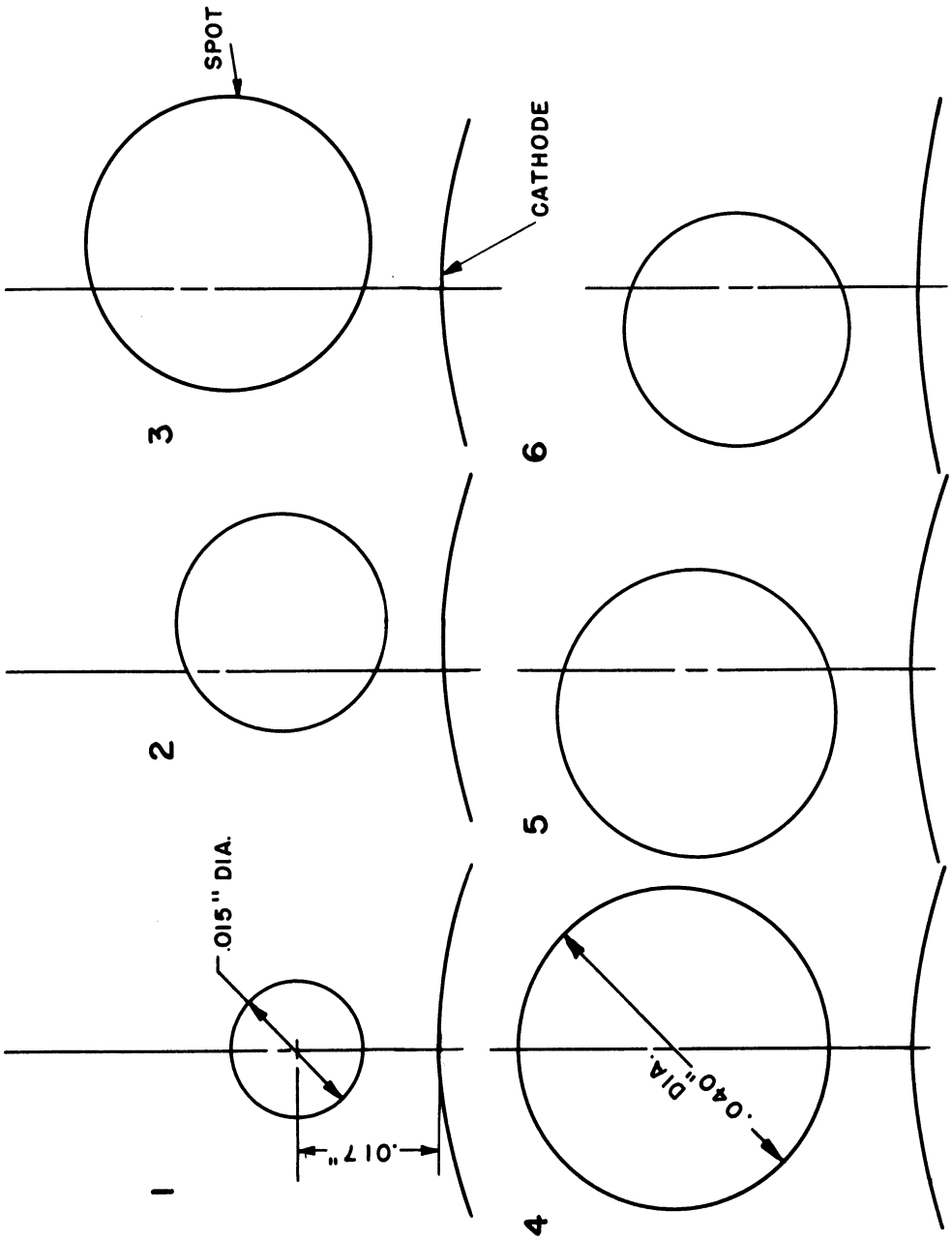

FIG. 4.2 VARIATION OF UNDEFLECTED SPOT POSITION WITH BEAM VOLTAGE

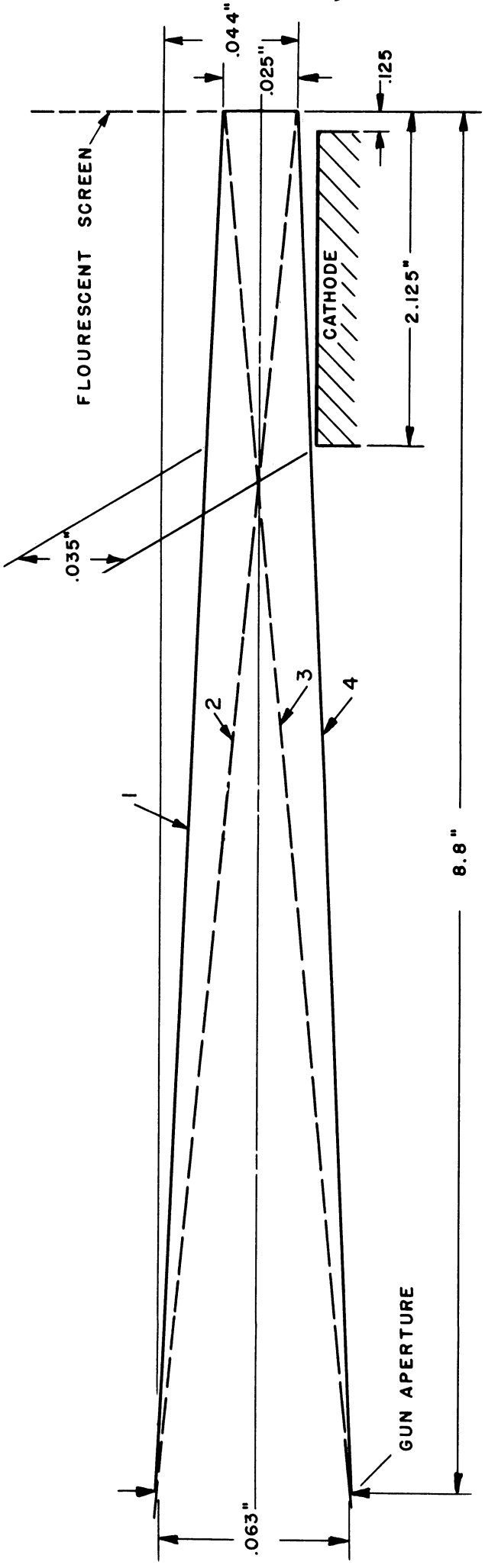

FIG. 4.3 ELECTRON BEAM WITH NO MAGNETIC FIELD

beam electron could make with the axis of the beam was arc sin $\frac{.044}{8.8}$, or about one-third degree. Since the axis of the beam deviated less than two-thirds of a degree from parallel with the axis of the cathode, a beam electron could make an angle of no more than one degree with the axis. The initial velocity was thus no greater than the beam velocity times the sine of one degree, or 0.018. It could be in any direction. The radial displacement of beam electrons as they entered the diode is seen from Figure 4.3 to be between 0 and approximately .035 inches from the cathode.

When there was a magnetic field, the field was essentially uniform in the diode and very near to the diode. Until the electrons entered the diode they experienced no electric fields. Therefore, each beam electron had a helical trajectory as it entered the diode. The parameters of the helix can be estimated from the data given in Table 4.1. Figure 4.4 shows a convenient set of parameters for describing the helix. The parameter h is the distance from the cathode to the center of the helix, s is the radius of the helix, and δ is the initial angular displacement. The angular velocity of the electron in the helix is the cyclotron angular velocity $2\omega_L$. Therefore, the beam electron displacement as a function of time is

$$
\begin{aligned}
z &= \dot{z}_o t, \\
r &= \sqrt{(a+h)^2 + s^2 + 2(a+h)s\cos(2\omega_L t + \delta)} \approx a + h + s\cos(2\omega_L t + \delta) \\
\tan\theta &= \frac{s\sin(2\omega_L t + \delta)}{a + h + s\cos(2\omega_L t + \delta)},
\end{aligned}
\tag{4.1}
$$

where $\dot{z}_o$ is the initial z velocity and a is the cathode radius. The angular momentum of a beam electron can be found in terms of h, s, and

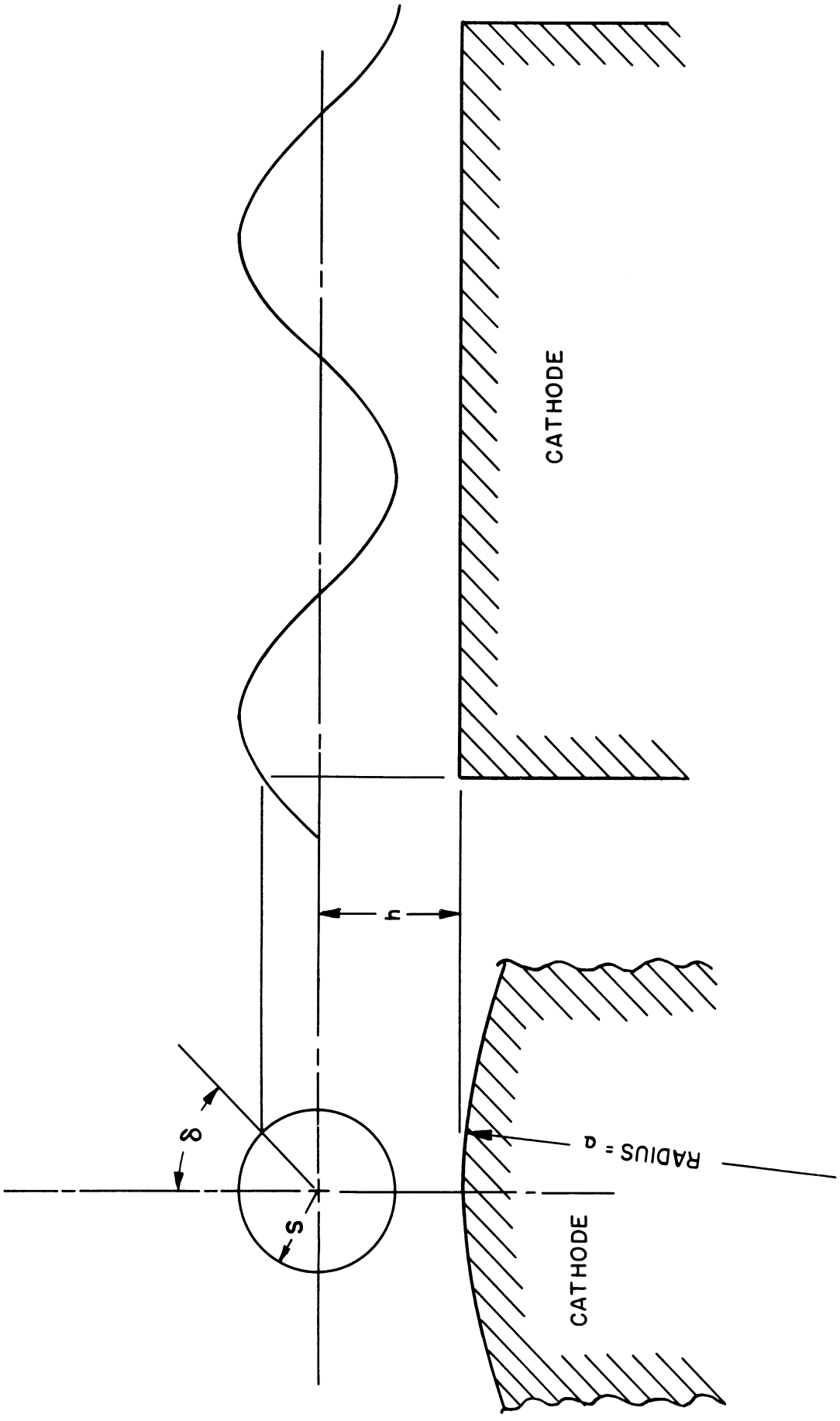

FIG.4.4 PARAMETERS FOR DESCRIBING HELICAL PATH OF BEAM ELECTRONS

δ by noting that $\dot{\theta}$ is 0 when $r = \sqrt{(a + h)^2 - s^2}$, and therefore by equation (2.48) of Chapter II,

$$P_\theta = -m\omega_L \left[(a + h)^2 - s^2 \right], \qquad (4.2)$$

at the instant when $\dot{\theta} = 0$. But P_θ is a constant, and therefore equation (4.2) is true at any time.

It seems reasonable to assume that at the fluorescent screen the variation in beam cross section as the beam voltage was varied is approximately the same as would be observed if the beam voltage were held constant and the position of the fluorescent screen were varied. Figure 4.5 shows the shape of the beam. The beam is made up of electrons all traversing helical paths. Possible paths for two such electrons are shown in Figure 4.5. The dimensions chosen for the beam in Figures 4.5 and 4.2 are typical of the beam of the trajectron when it was aligned well.

It is not possible to give the exact range of s and h for electrons in the beam, but some estimates of the range of s and h can be obtained by imagining what possible helices could fit into the beam. Clearly s could not be greater than .020 inch, because the whole beam could be fitted into a cylinder of radius .020 inch. If s = .020 inch. then h = .028 inch for the beam shown in Figure 4.5. It appears that s could be as small as 0. An electron with s = 0 would travel a straight line parallel to the z axis. Such lines could be fitted into the beam of Figure 4.5 with h anywhere in the range from .008 inch to .023 inch. The parameter s could take on any value between 0 and .020 inch, and the h could be anywhere between .008 inch and .028 inch. The possible values for h depend somewhat upon s.

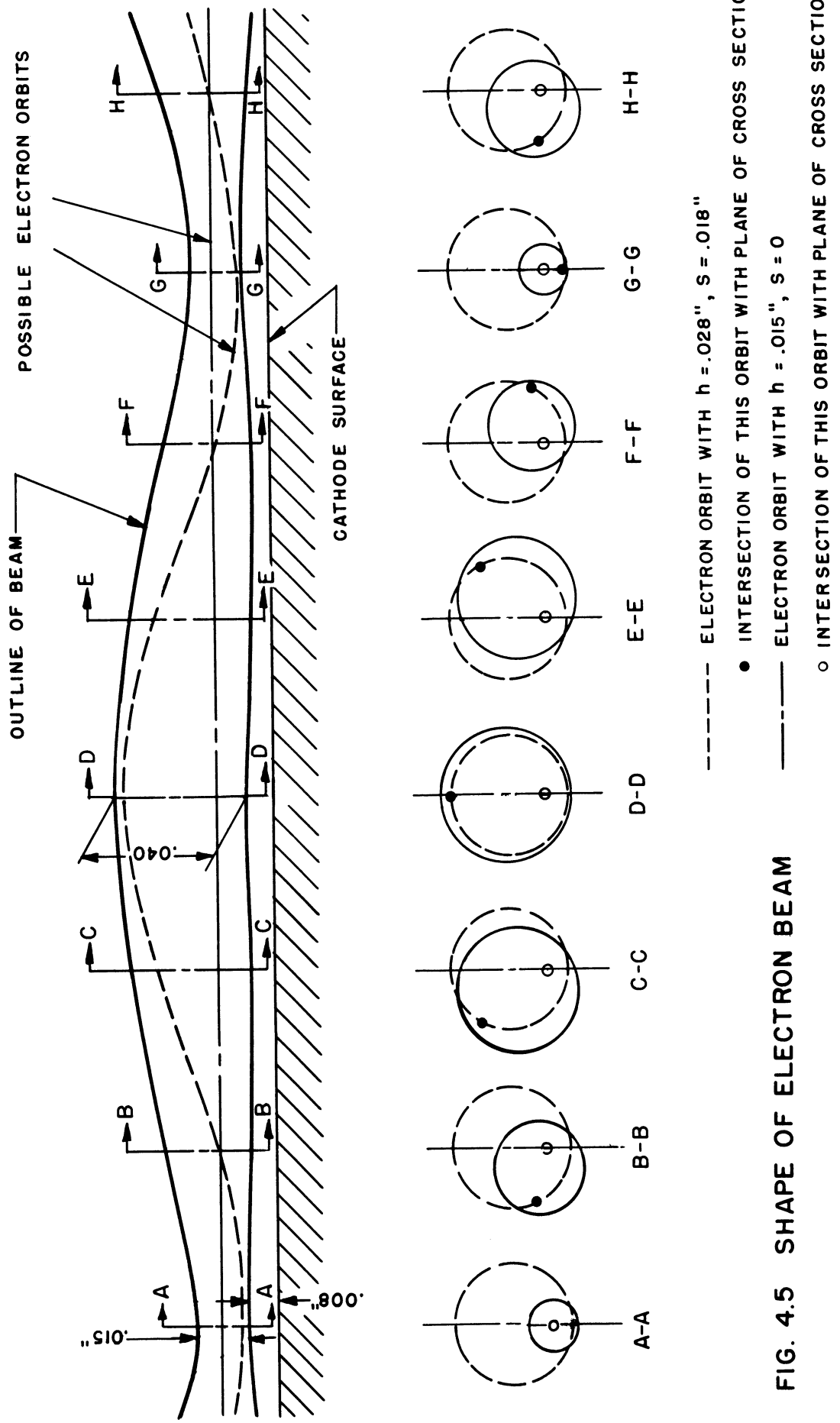

FIG. 4.5 SHAPE OF ELECTRON BEAM

4.3 The Case of a Non-Emitting Cathode and No Magnetic Field

Figure 4.6 shows data taken from the trajectron with no magnetic field and with a brass "dummy" cathode. The photograph was taken with the copper mesh shield[1] over the fluorescent screen, and the data from this photograph are replotted on the graph. The other experimental points on the graph were taken with mesh removed. The curve on the graph is the theoretical displacement as a function of time, neglecting end effects and initial velocities. The following discussion of the theoretical curve, the effects of initial velocities, and the end effects shows that the discrepancy between the theoretical curve and the experimental data can be explained by end effects and beam initial conditions.

First the theoretical curve is derived, neglecting initial angular velocities but not neglecting initial radial displacement or velocity. The field is logarithmic; this assumes no space charge and neglects end effects. The potential is

$$\phi = \phi_a \frac{\ell n\left(\frac{r}{a}\right)}{\ell n\left(\frac{r_a}{a}\right)} \tag{4.3}$$

where ϕ_a is the anode potential, r_a the anode radius, and a the cathode radius. Then the electric field is

$$F = -\frac{d\phi}{dr} = \frac{-\phi_a}{r\,\ell n\left(\frac{r_a}{a}\right)}, \tag{4.4}$$

and the equation of motion is

$$m\frac{d^2r}{dt^2} = -eF = \frac{e\phi_a}{r\,\ell n\left(\frac{r_a}{a}\right)}, \text{ or} \tag{4.5}$$

[1] Part 28 in Figure 3.2.

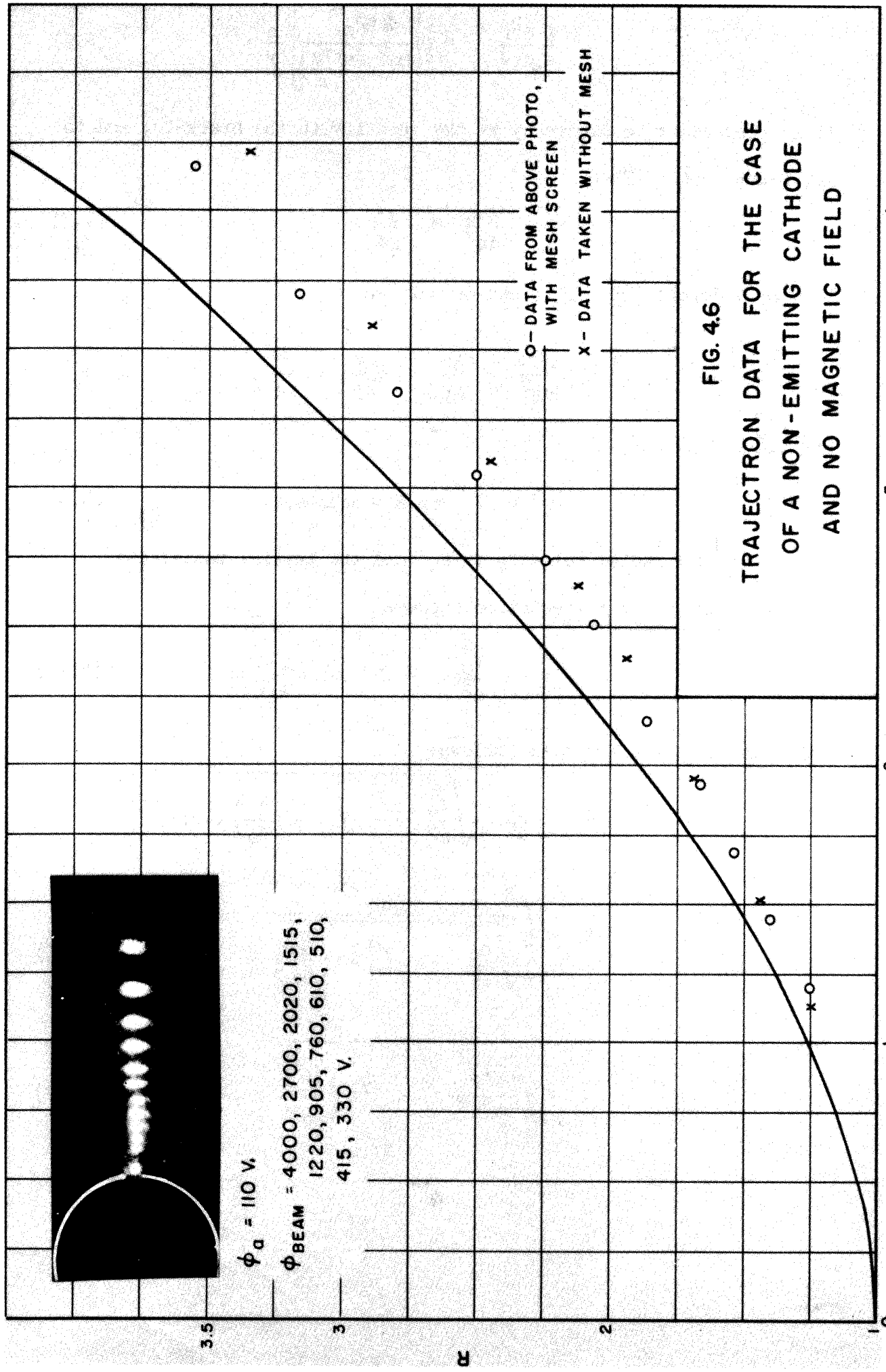
FIG. 4.6
TRAJECTRON DATA FOR THE CASE
OF A NON-EMITTING CATHODE
AND NO MAGNETIC FIELD
O- DATA FROM ABOVE PHOTO, WITH MESH SCREEN
X- DATA TAKEN WITHOUT MESH
ϕ_a = 110 V.
ϕ_{BEAM} = 4000, 2700, 2020, 1515, 1220, 905, 760, 610, 510, 415, 330 V.
α
γt
0
1
2
3
3.5
4

$$\frac{1}{a}\frac{d^2r}{dt^2} = \frac{1}{2}\left[\frac{2e\phi_a}{ma^2 \ell n\left(\frac{r_a}{a}\right)}\right]\frac{a}{r} . \qquad (4.6)$$

It is convenient to denote by γ^2 the quantity in the brackets, and to let R denote $\frac{r}{a}$. Then

$$\frac{d^2R}{dt^2} = \frac{\gamma^2}{2R} . \qquad (4.7)$$

Letting V denote $\frac{dR}{dt}$, this can be written

$$\frac{d^2R}{dt^2} = \frac{dV}{dt} = V\frac{dV}{dR} = \frac{\gamma^2}{2R} , \qquad (4.8)$$

and integrated to

$$V^2 = \gamma^2 \ell n\, R + \text{constant.} \qquad (4.9)$$

If the initial radial velocity is $\dot{r}_o$ and the initial radial displacement aR_o, then the equation becomes

$$V^2 - \frac{\dot{r}_o^2}{a^2} = \gamma^2 \ell n\left(\frac{R}{R_o}\right) . \qquad (4.10)$$

This can be solved for t as follows:

$$V = \frac{dR}{dt} = \sqrt{\frac{\dot{r}_o^2}{a^2} + \gamma^2 \ell n\left(\frac{R}{R_o}\right)}, \text{ or}$$

$$t = \int_{R_o}^{R} \frac{dR}{\sqrt{\frac{\dot{r}_o^2}{a^2} + \gamma^2 \ell n\left(\frac{R}{R_o}\right)}} . \qquad (4.11)$$

Let

$$u = \sqrt{\frac{\dot{r}_o^2}{\gamma^2 a^2} + \ell n\left(\frac{R}{R_o}\right)} . \qquad (4.12)$$

Then

$$R = R_o \exp\left[u^2 - \frac{\dot{r}_o^2}{\gamma^2 a^2} \right],$$

$$dR = 2uR_o \exp\left[u^2 - \frac{\dot{r}_o^2}{\gamma^2 a^2} \right] du, \text{ and}$$

$$t = \int_{\frac{\dot{r}_o}{\gamma a}}^{\sqrt{\frac{\dot{r}_o^2}{\gamma^2 a^2} + \ell n \frac{R}{R_o}}} \frac{2R_o}{\gamma} \exp\left[u^2 - \frac{\dot{r}_o^2}{\gamma^2 a^2} \right] du \quad , \text{ or} \qquad (4.13)$$

$$\gamma t = 2R_o \exp\left[- \frac{\dot{r}_o^2}{\gamma^2 a^2} \right] \int_{\frac{\dot{r}_o}{\gamma a}}^{\sqrt{\frac{\dot{r}_o^2}{\gamma^2 a^2} + \ell n \frac{R}{R_o}}} \exp\left[u^2 \right] du \quad . \qquad (4.14)$$

The integral is tabulated.[1] For the case of zero initial displacement and velocity, $R_o = 1$ and $\dot{r}_o = 0$, and

$$\gamma t = 2 \int_0^{\sqrt{\ell nR}} \exp\left[u^2 \right] du. \qquad (4.15)$$

This is the function which is plotted in Figure 4.6.

The effects of initial radial velocity and displacement of beam electrons for this case can be found by substituting typical initial conditions for beam electrons in equation (4.12). The quantity $\frac{\dot{r}_o^2}{\gamma a}$ can conveniently be found by noting that

$$t = \frac{\ell}{\dot{z}_o} \quad , \text{ or } \gamma = \frac{(\gamma t)\dot{z}_o}{\ell} \quad , \qquad (4.16)$$

1 Jahnke and Emde, Ref. E, p. 32.

where ℓ is the length of the tube and $\dot{z}_o$ is the beam velocity. Then

$$\frac{\dot{r}_o}{\gamma a} = \frac{\ell}{a} \cdot \frac{\dot{r}_o}{\dot{z}_o} \cdot \frac{1}{\gamma t} \quad . \tag{4.17}$$

The quantity γt can be found roughly from Figure 4.6; it is 3.2 when R = 3. Typical values for $\dot{r}_o/\dot{z}_o$ can be estimated from the dimensions of the beam given in Figure 4.3; $\dot{r}_o/\dot{z}_o$ is equal to the ratio of radial to z-displacement.

In Figure 4.3 the lines marked (1) and (4) represent the electron paths of extreme initial displacement. The lines (2) and (3) represent paths of extreme initial velocity. The values of γt calculated from the above formula for these four sets of initial conditions are summarized in Table 4.2.

TABLE 4.2

Calculated Time for an Electron to Reach the Radius R = 3. (B = 0, non-emitting Cathode.)

Electron Path (See Figure 4.3)	R_o	$\dot{r}_o/\dot{z}_o$	γt
1	1.13	-0.0022	3.24
2	1.08	-0.005	3.24
3	1.08	+0.005	3.19
4	1.00	+0.0022	3.20

The slow electrons should reach the anode $\frac{3.24 - 3.19}{\gamma} = \frac{.05}{\gamma}$ seconds later than the fast electrons. Since the curve of R versus γt has a slope of approximately unity at R = 3, at time $\gamma t = 3.2$ the fastest electrons should reach a radius .05a greater than that reached by the slow electrons, and the radial width of the beam should be

approximately .05a or .014", which is less than the initial width of the beam. This is plausible because the electric field is inversely proportional to the radius, and therefore the electrons which are nearer to the cathode are accelerated more than those farther out, and the distance between electrons will become smaller.

The observed spots at a radius of approximately three times the cathode radius had a width of approximately .030", or roughly twice that predicted. The explanation lies in end effects. An approximate mapping of the space charge free field of the diode is shown in Figure 4.7. It can be seen that the field near the cathode surface where the beam enters the diode is not inversely proportional to the radius, but instead does not change much with radius. Thus the focussing action described in the preceeding paragraph would not occur.

The increased width of the deflected spot in the angular direction is due to the fact that the field is radial, and an electrons displacement should be radial. Thus each spot has an angular width of approximately 4^{o}.

The beam axis might have made an angle as great as $2/3^{o}$ with the axis of the cathode. This would approximately triple the range of possible values of $\frac{V_o}{\gamma a}$, and approximately triple the discrepancy in theoretical and observed values of γt. Consequently one might expect to find γt increased by as much as 0.15. The observed values of γt, as indicated on Figure 4.6, differ from the theoretical curve at R = 3 by about 0.35. Hence the initial velocities of the beam account for less than a half of the difference between observed and theoretical values of γt.

The remainder of the difference can be explained by end effects. The electric field which the beam experiences in the first one-fifth of its path through the diode probably averages little more than half of what is would in the absence of end effects (See Figure 4.7). The displacement should be approximately the same as if the full field were applied and the tube were applied and the tube were shortened by one-half of one-fifth, or ten percent. If the tube were considered ten percent shorter, the calculated γt would be ten percent less, and would agree with the theoretical value.

4.4 The Case of the Non-Emitting Cathode with Magnetic Field

The deflection of the trajectron beam was studied with a brass "dummy" cathode in the diode and with the magnetic field applied. Typical data photographs are presented in Figures 4.8, 4.10, 4.12, and 4.14. In each photograph there are many exposures of the spot. In each case there is an exposure with no anode voltage. Then there are exposures with anode voltage applied and held constant at each of several beam potentials. At each beam potential an exposure was made, the magnetic field was reversed, and another exposure was made. A circle showing the projection of the cathode surface was drawn on each photograph. There was also a curve drawn on each photograph to represent the theoretical electron orbit neglecting end effects and initial velocities. The theoretical curves and the data from the photographs are replotted in Figures 4.9, 4.11, 4.13, and 4.15 to show R and Θ as functions of time. The time was calculated by dividing the length of the diode (two and one-eighth inches) by the velocity of the beam, calculated from the potential of the cathode of the electron gun.

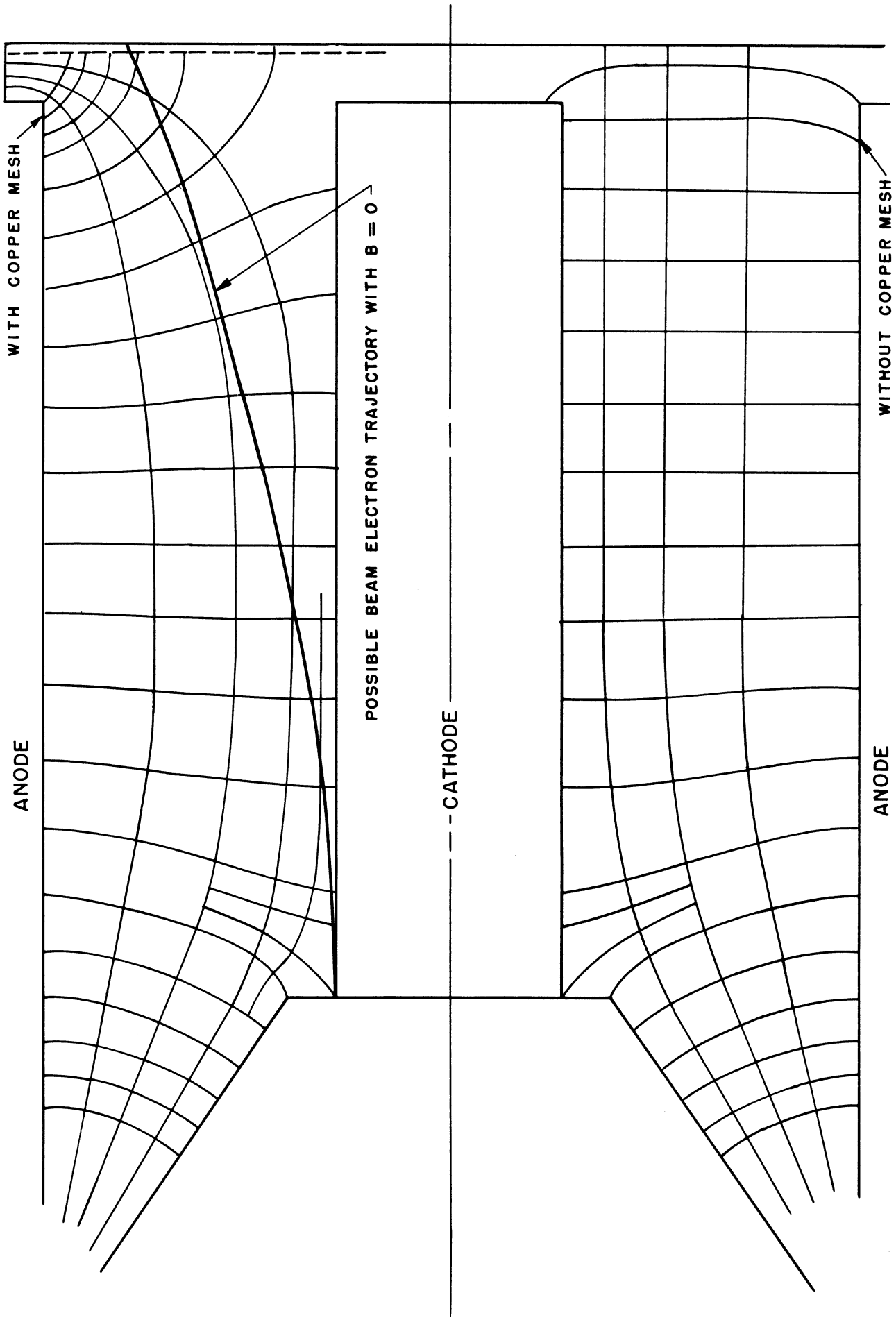

FIG. 4.7 FIELD MAP OF TRAJECTRON DIODE WITH NO SPACE CHARGE

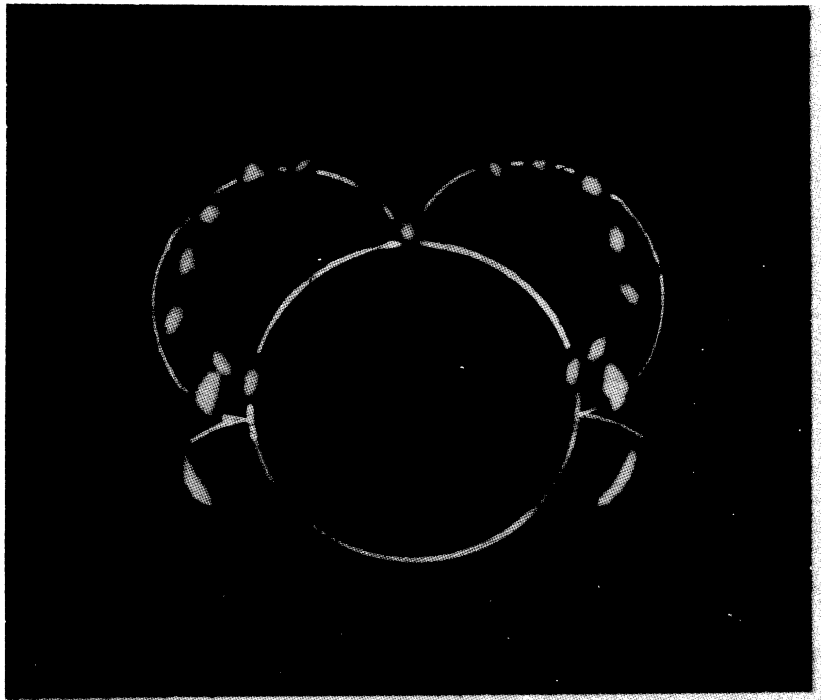

WITHOUT MESH SHIELD

ϕ_a = 640 VOLTS

I_m = 4.0 AMPS

ϕ_{BEAM} = 4020, 3220, 2500, 1980, 1580, 1220, 1000, 605, 400, 280 VOLTS

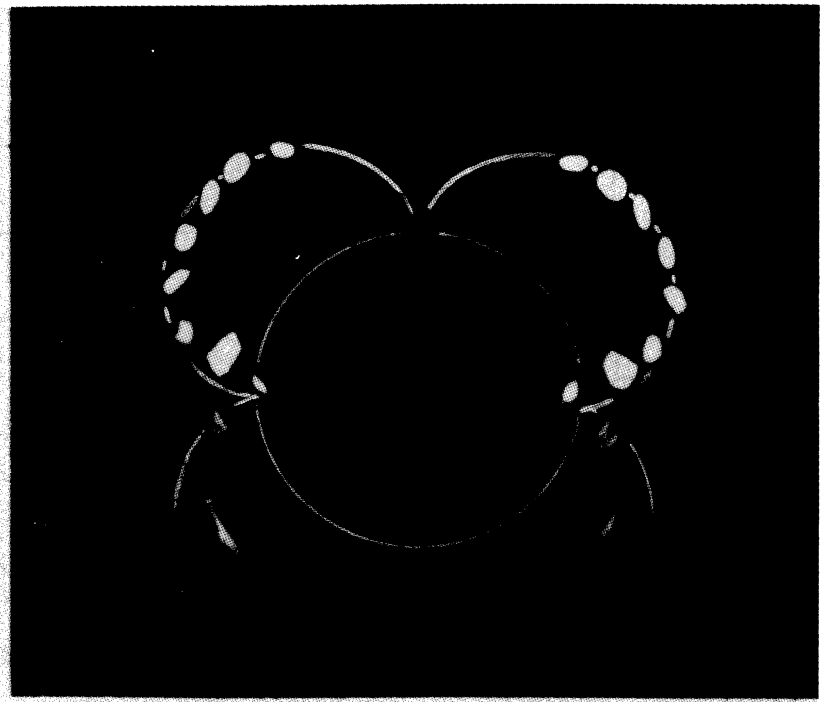

WITH MESH SHIELD

ϕ_a = 410 VOLTS

I_m = 3.2 AMPS

ϕ_{BEAM} = 4000, 2800, 2020, 1420, 1010, 760, 460, 310, 210 VOLTS

FIG. 4.8

TRAJECTRON DATA FOR THE CASE OF NON-EMITTING CATHODE WITH MAGNETIC FIELD (a = 1.27)

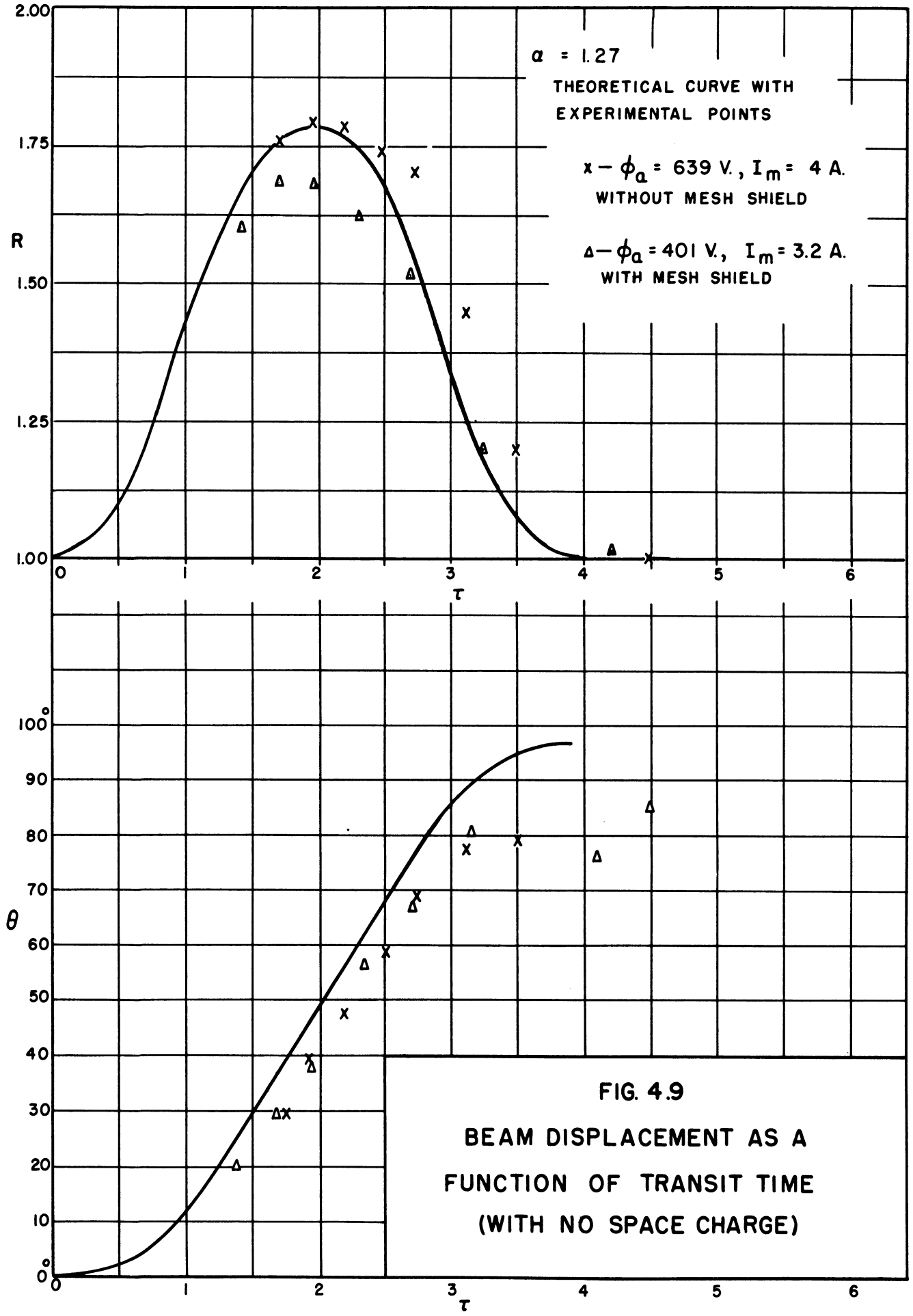

FIG. 4.9

BEAM DISPLACEMENT AS A FUNCTION OF TRANSIT TIME (WITH NO SPACE CHARGE)

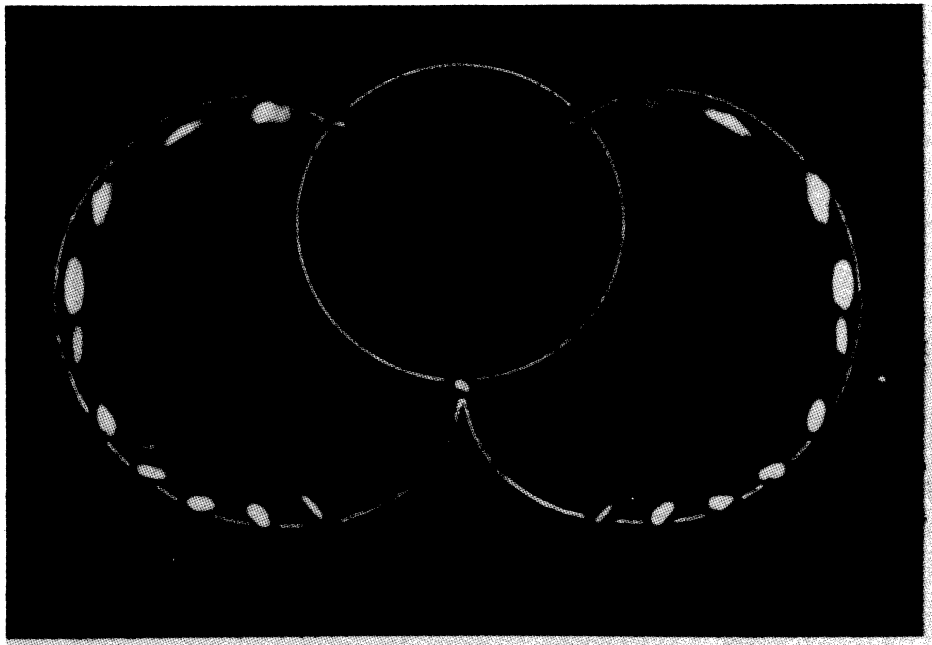

WITHOUT MESH SHIELD

ϕ_a = 700 V.

I_m = 3.0 AMPS

ϕ_{BEAM} = 4390, 3220, 2500, 1980, 1580, 1220, 1000, 810, 605, 450, 280, 195 VOLTS.

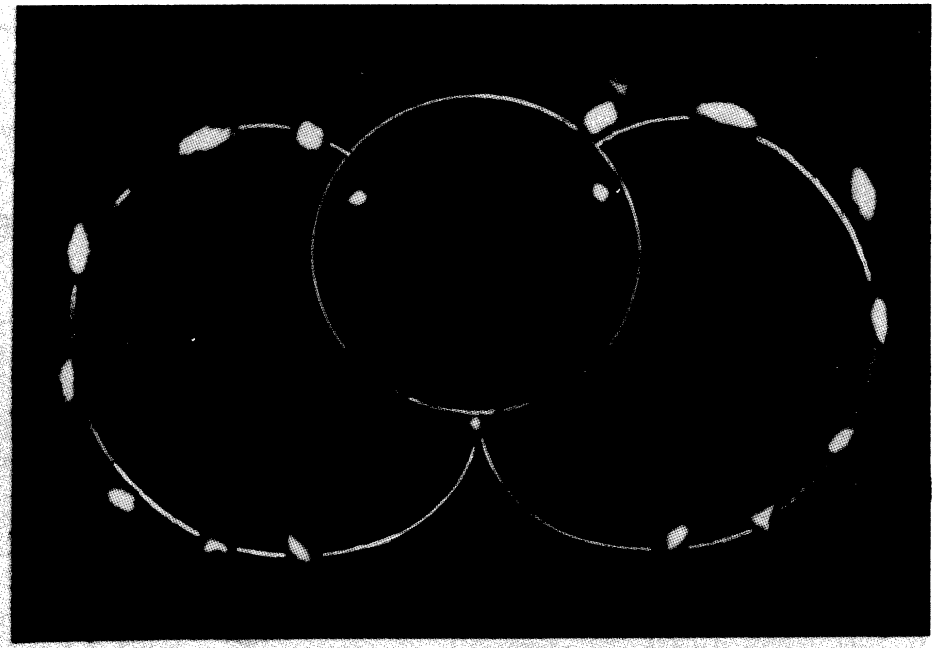

WITH MESH SHIELD

ϕ_a = 798 VOLTS

I_m = 3.2 AMPS

ϕ_{BEAM} = 4000, 2800, 2020, 1420, 1010, 760, 510, 330, 185 VOLTS

FIG. 4.10

TRAJECTRON DATA FOR THE CASE OF NON-EMITTING CATHODE WITH MAGNETIC FIELD (a = 2.48)

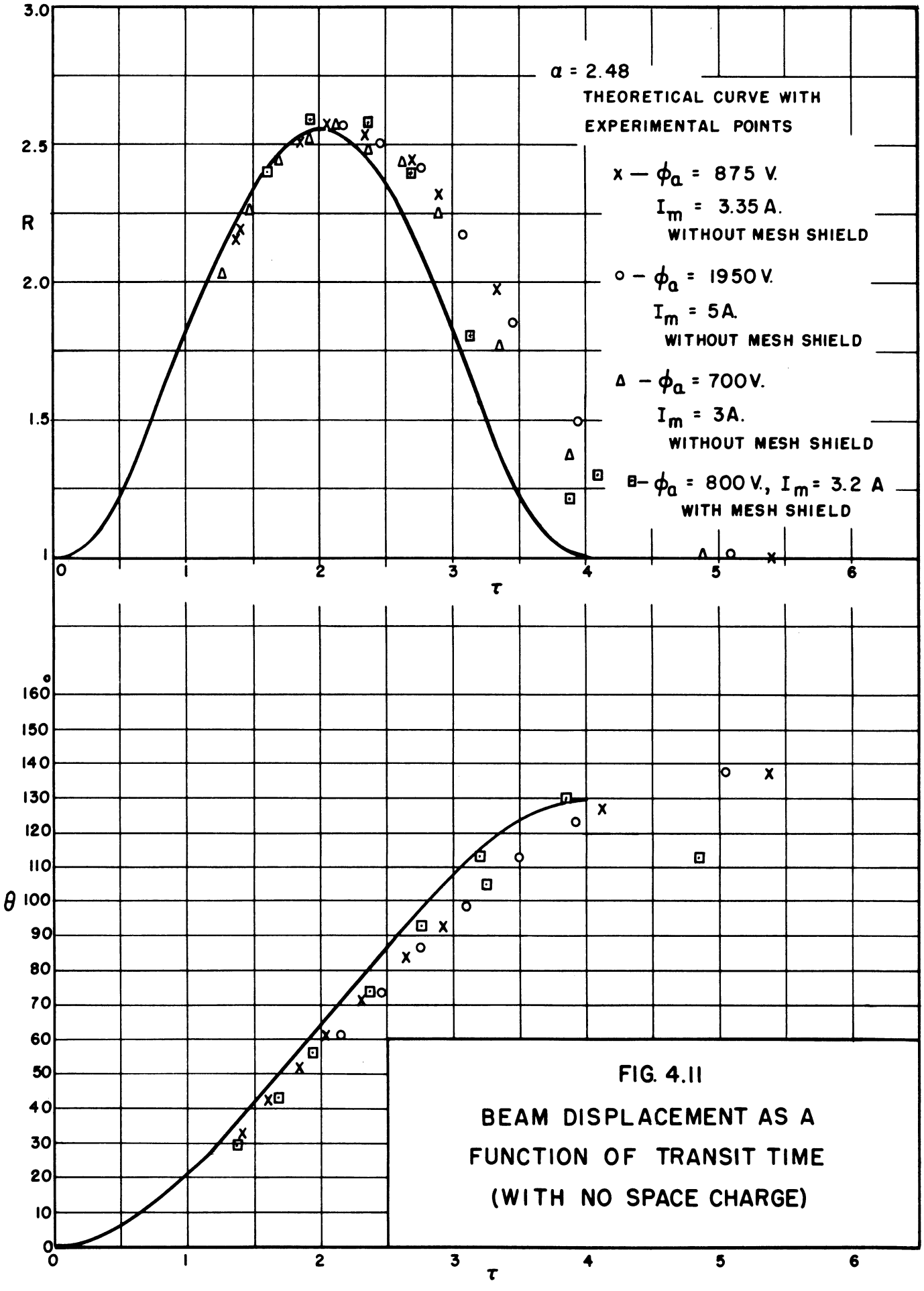

FIG. 4.11

BEAM DISPLACEMENT AS A FUNCTION OF TRANSIT TIME (WITH NO SPACE CHARGE)

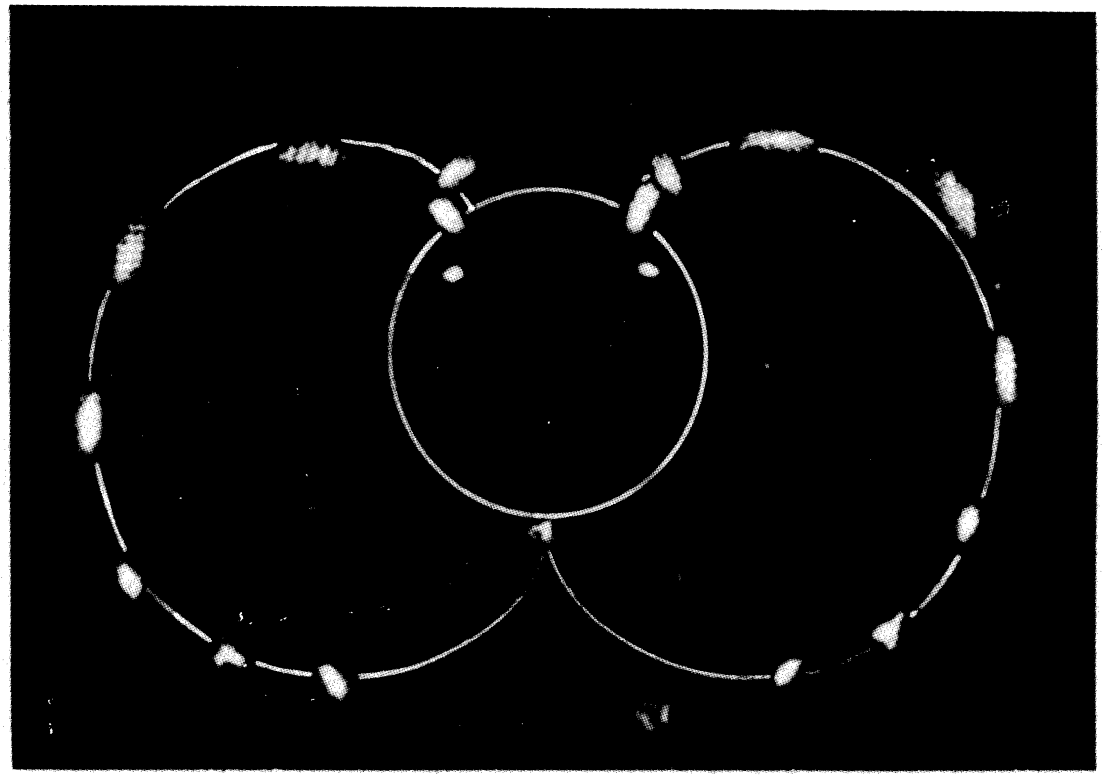

WITH MESH SHIELD

ϕ_a = 1000 VOLTS

I_m = 3.2 AMPS.

ϕ_{BEAM} = 4000, 2800, 2020, 1420, 1010, 760, 510, 330,

185 VOLTS

FIG. 4.12

TRAJECTRON DATA FOR THE CASE OF NON-EMITTING CATHODE WITH MAGNETIC FIELD (a = 3.11)

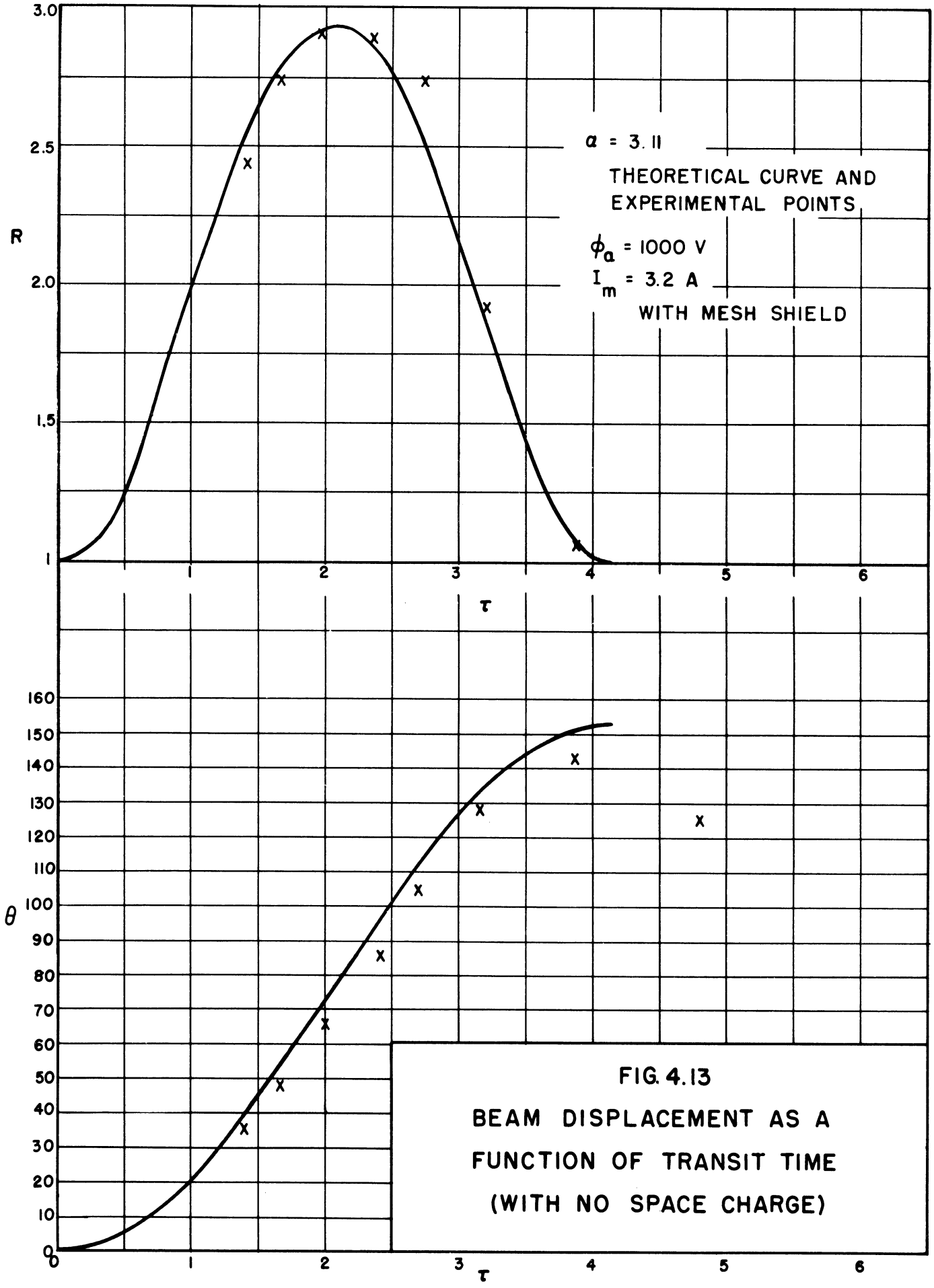

FIG. 4.13

BEAM DISPLACEMENT AS A FUNCTION OF TRANSIT TIME (WITH NO SPACE CHARGE)

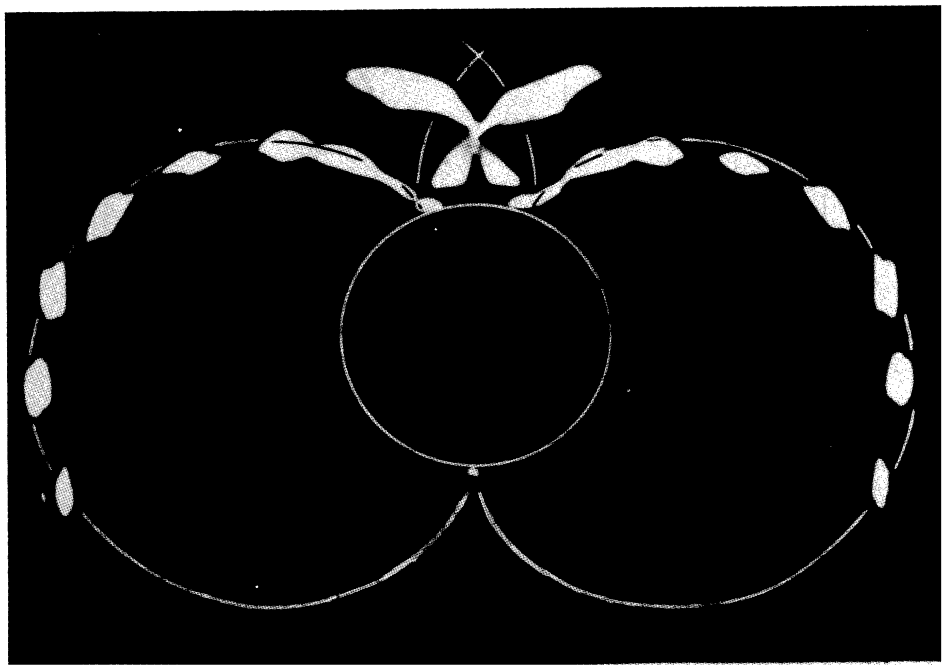

WITHOUT MESH SHIELD

ϕ_a = 2955 VOLTS

I_m = 5.0 AMPS.

ϕ_{BEAM} = 4220, 3220, 2500, 1980, 1580, 1225, 1005, 810, 605, 400, 195 VOLTS

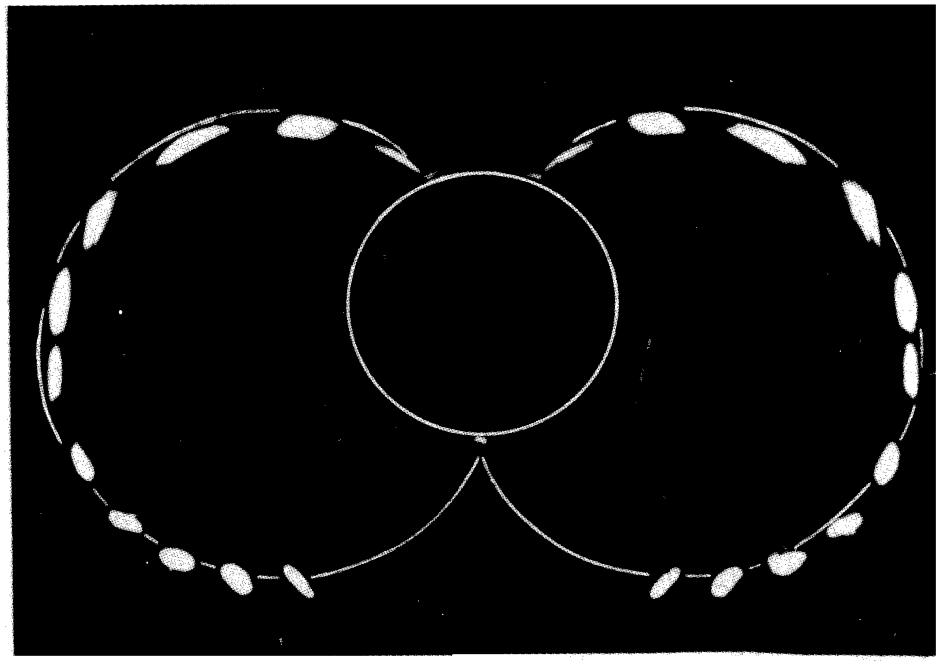

WITHOUT MESH SHIELD

ϕ_a = 106 VOLTS

I_m = 3.0 AMPS.

ϕ_{BEAM} = 4320, 3220, 2550, 1980, 1580, 1220, 1000, 810, 605, 450, 280 VOLTS

FIG. 4.14

TRAJECTRON DATA FOR THE CASE OF NON-EMITTING CATHODE WITH MAGNETIC FIELD (α = 3.76)

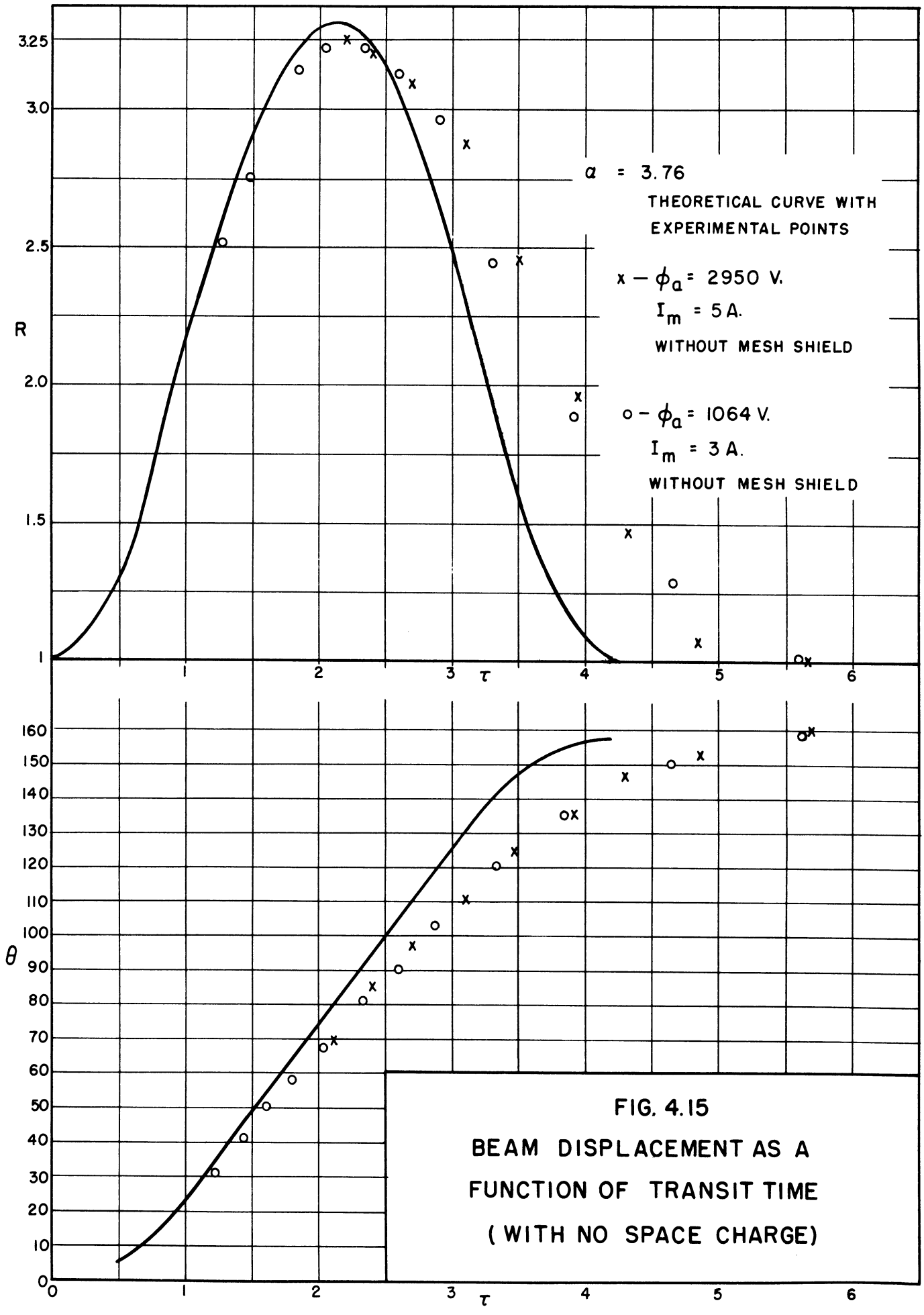

FIG. 4.15
BEAM DISPLACEMENT AS A
FUNCTION OF TRANSIT TIME
(WITH NO SPACE CHARGE)

Half of the data presented were taken with the copper mesh shield placed in front of the fluorescent screen, and the other half were taken without the shield.[1]

In the photographs of Figure 4.16 an exposure was made with no anode voltage. Then an anode voltage was applied, the beam voltage adjusted until the spot was at its cusp or minimum radius, and an exposure made with each orientation of magnetic field. This was done for several anode potentials, in order to show the locus of these minimum points in the orbit. On the graph the observed angular deflection and the theoretical angular deflection are plotted as functions of α, which is $40.45 \frac{\phi_a}{B^2}$.[2]

Without the copper mesh the observed orbits matched the theoretical orbits very closely. The angle to the first cusp was slightly smaller than the theoretical value. The calculated times were longer, especially near the first cusp. The cusps were well formed and occured very near the cathode radius. With the mesh the maximum radius of the orbit was approximately the theoretical maximum radius. The orbits did not have a good cusp, but rather had a loop at the minimum radius, and the minimum radius was observed to be as small as 0.7 times the cathode radius. The calculated time appeared to agree more closely with the theoretical time required for a given displacement. The time required for an electron to reach the minimum radius appeared to be somewhat longer than the

---

[1] The shield referred to is part number (28) in the assembly drawing, Figure 3.2.

[2] α is defined on page 126.

FIG. 4.16

ANGLE TO CUSP OF TRAJECTORY

(WITH NON-EMITTING CATHODE)

NOTE: THE THEORETICAL CURVE IS TAKEN FROM DIFFERENTIAL ANALYSER DATA.

Δ — I_m = 3.2 A. WITH MESH SHIELD

○ — I_m = 5.0 A. WITHOUT MESH SHIELD.

x — I_m = 4.85 A. WITHOUT MESH SHIELD

ANGLE TO CUSP (DEGREES)

150
125
100
75
50
25
0

0 1 2 3 4 5

a

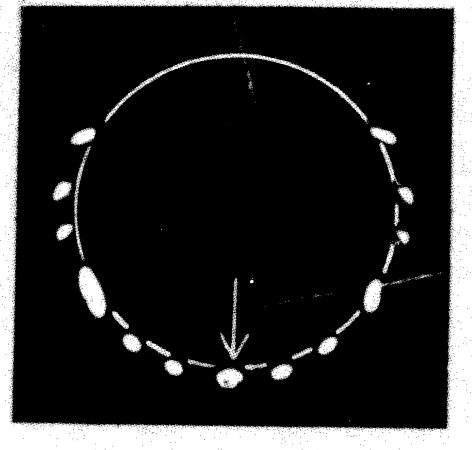

I_m = 4.85 AMPS

ϕ_a = 0, 205, 420, 630, 830, 1010, 1440 VOLTS

WITHOUT MESH SHIELD

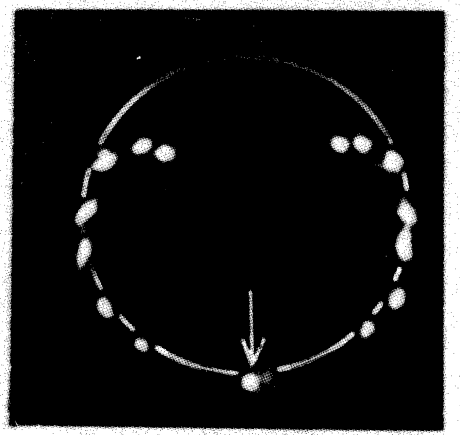

I_m = 3.2 AMPS

ϕ_a = 0, 200, 300, 400, 500, 700, 900, 1100 VOLTS

WITH MESH SHIELD

theoretical time required for an electron to complete one loop of its trajectory.

The theoretical curves in Figures 4.8 to 4.15 are based on the assumptions that the beam electrons have zero initial velocity, and that the electric field is that of infinite concentric cylinders, i.e. purely radial with a logarithmic potential. The potential assumed is

$$\phi = \frac{\phi_a}{\ell n \frac{r_a}{a}} \ell n \left(\frac{r}{a}\right) \tag{4.18}$$

and the equations of motion can be taken from Chapter II, page 32. From equation (2.46a),

$$m\ddot{r} - mr\dot{\theta}^2 + eBr\dot{\theta} - e\frac{\partial \phi}{\partial r} = 0 \tag{2.46a}$$

and from equation (2.49) and the fact that $\dot{\theta}$ is initially zero, it follows that

$$\theta = \omega_L\left(1 - \frac{a^2}{r^2}\right) \quad . \tag{4.19}$$

Eliminating $\dot{\theta}$ from (2.46a) and using (4.18) to eliminate ϕ yields

$$m\ddot{r} = \omega_L{}^2 r - \frac{\omega_L{}^2 a^4}{r3} + \frac{e\phi_a}{m \ell n \frac{r_a}{a}} \cdot \frac{1}{r} \quad . \tag{4.20}$$

Letting

$$R = \frac{r}{a}, \qquad T = \omega_L t \text{ , and } \quad \alpha = \frac{e\phi_a}{m\omega_L{}^2 a^2 \ell n R_a} \tag{4.21}$$

this becomes

$$\frac{d^2R}{dT^2} = \frac{\alpha}{R} - R + \frac{1}{R^3} \quad . \tag{4.22}$$

Solutions were obtained for this equation by means of the electronic differential analyser, as described in Appendix B, and the data for the theoretical curves in the figures of this section were taken from these solutions. An equation in closed form for the maximum radius of the orbits is possible; it is simply the cutoff equation, number (2.60) of Chapter II.

The parameter α is proportional to $\frac{\phi_a}{B^2}$, since ω_L is proportional to B. All other factors in α are either physical constants or are related to the geometry of the trajectron. Substituting these constants in (4.22) yields

$$\alpha = 40.45 \frac{\phi_a}{B^2} = 0.0344 \frac{\phi_a}{I_m^2} , \qquad (4.23)$$

where B is given in gauss, and the magnet current I_m is given in amperes. The magnetic field is taken as 34.3 gauss per ampere of solenoid current to obtain the second equation.

The discussion of the effect of initial velocities and end effects will be limited to the effect on the maximum radius of the orbit and on the radial width of the spot at the maximum radius of the orbit. This can be discussed rather simply through the use of the energy integral, while any further discussion would require some sort of numerical integration of the equations of motion. In the next three paragraphs the potential distribution is assumed to be an arbitrary function of r and z, and hence this discussion, and in particular equation (4.28), apply to the magnetron case, discussed in Chapter V, as well as to the case with the non-emitting cathode.

The energy integral for the motion of an electron is equation (2.51) of Chapter II:

$$\frac{m\dot{r}^2}{2} + \frac{mr^2\dot{\theta}^2}{2} + \frac{m\dot{z}^2}{2} - e\phi(r,z) = E \qquad (2.51)$$

where E is a constant, called the total energy of the electron. The canonical angular momentum

$$P_\theta = mr^2 (\dot{\theta} - \omega_L) \qquad (2.49)$$

is a constant, and it is convenient to use this equation to eliminate $\dot{\theta}$ in favor of P_θ as follows:

$$\frac{m\dot{r}^2}{2} + \frac{mr^2}{2}\left(\frac{P_\theta}{mr^2} + \omega_L\right)^2 + \frac{m\dot{z}^2}{2} - e\phi = E. \qquad (4.24)$$

The value of the constant E can be obtained from the initial conditions of the electron, since it is a constant of the motion. For an electron starting with no radial or angular velocity and with initial position at the cathode surface, $E = \frac{m\dot{z}_o^2}{2}$, and equation (4.24) can be solved for $\dot{r}^2$, which is a function of r, z, and $\dot{z}$.

It is convenient to introduce the function

$$\psi(r,z,\dot{z}) = \frac{2e\phi(r,z)}{m\omega_L^2 a^2} - \frac{r^2}{a^2}\left(1 - \frac{a^2}{r^2}\right)^2 - \frac{\dot{z}^2}{\omega_L^2 a^2} \qquad (4.25)$$

which is called the effective potential.[1] The effective potential $\psi(r,z,\dot{z})$ is the electric potential modified in two ways: (1) it is normalized, and (2) the energy of the θ and z motion of an electron initially at rest on the cathode is subtracted from it. The effective potential is a measure of the radial motion, and for an electron starting at rest from the cathode,

$$\frac{\dot{r}^2}{\omega_L^2 a^2} = \psi(r,z,\dot{z}) \qquad (4.26)$$

The initial conditions of any electron can be described by giving r_o, θ_o, $\dot{r}_o$, P_θ, and $\dot{z}_o$. In terms of these constants, E for an arbitrary electron is

$$E = \frac{mr_o^2}{2} + \frac{mr_o^2}{2}\left[\frac{P_\theta}{mr_o^2} + \omega_L\right]^2 + \frac{m\dot{z}_o^2}{2} - e\phi(r_o, z_o). \qquad (2.52)$$

Equation (4.24) can be solved for $\dot{r}^2$ in terms of the potential, r, z,

---

[1] The ideal of an effective potential appears to have originated in connection with the central force problem. For example, Webster, Ref. I, p. 181, describes an apparent potential, and Goldstein, Ref. D, p. 64, describes a fictitious potential. It has been used in connection with the cylindrical magnetron by Allis, Ref. 1.

$\dot{z}$, and the initial conditions, yielding

$$\frac{\dot{r}^2}{\omega_L^2 a^2} = \frac{\dot{r}_o^2}{\omega_L^2 a^2} + \frac{2e\phi(r,z)}{m\omega_L^2 a^2} - \frac{2e\phi(r_o,z_o)}{m\omega_L^2 a^2} - \frac{r^2}{\omega_L^2 a^2}\left[\frac{P_\theta}{mr^2} + \omega_L\right]^2 + \frac{r_o^2}{\omega_L^2 a^2}\left[\frac{P_\theta}{mr_o^2} + \omega_L\right]^2 - \frac{\dot{z}^2 - z_o^2}{\omega_L^2 a^2} \qquad (4.27)$$

By using (4.24), this can be put in the form

$$\frac{\dot{r}^2}{\omega_L^2 a^2} = \psi(r,z,\dot{z}) - \psi(r_o,z_o,\dot{z}_o) + \frac{\dot{r}_o^2}{\omega_L^2 a^2} + \frac{a^2}{r_o^2}\left(1 - \frac{r_o^2}{a^2}\right)\left[\frac{P_\theta^2}{m^2\omega_L^2 a^4} - 1\right]. \qquad (4.28)$$

At the maximum radius of the orbit, the radial velocity is zero. Thus if the potential field and the electron initial conditions are known, the maximum radius can be found by setting $\dot{r} = 0$ in (4.28) and solving for r. Solutions of adequate accuracy may be obtained simply if, in the last term, r is approximated by the maximum radius of the orbit of an electron with zero initial velocity and initial position at the cathode. Then the only term involving r is the first, $\psi(r, z, \dot{z})$.

If the electric field is assumed to be purely radial, i.e., end effects neglected, $\dot{z}$ is constant and the potential is independent of z. Then the effective potential ψ is a function of r only. The potential in the case of no space charge is

$$\phi = \frac{\phi_a}{\ell n\left(\frac{r_a}{a}\right)}\, \ell n\left(\frac{r}{a}\right), \qquad (4.18)$$

and the expression for effective potential becomes

$$\psi(r) = \frac{2e\phi_a}{m\omega_L^2 a^2} \frac{\ell n\left(\frac{r}{a}\right)}{\ell n\left(\frac{r_a}{a}\right)} - \frac{r^2}{a^2}\left(1 - \frac{a^2}{r^2}\right)^2$$

$$= 2\alpha\ \ell nR - R^2\left(1 - \frac{1}{R^2}\right)^2 , \qquad (4.29)$$

where α is defined by equation (4.21). This function is plotted in Figure 4.17. Solutions for the radius R at which $\dot{r} = 0$ can be obtained easily from equation (4.28) with the aid of the graph of $\psi(r)$. Solutions for the values of α appearing in Figures 4.8 to 4.15 were obtained in this manner, and they are summarized in Table 4.3.

TABLE 4.3

Maximum Radius Reached by Beam
Electrons with Various Initial Conditions

Initial Conditions (distances in inches)								
h =	0	.0075	.015	.030	.030	.030	.030	.030
s =	0	0	0	.020	.020	.020	.020	.020
δ =	-	-	-	0°	45°	90°	135°	180°
Maximum Normalized Radius								
(For α = 1.27)	1.78	1.78	1.77	1.70	1.74	1.80	1.87	1.90
(For α = 2.48)	2.55	2.53	2.52	2.41	2.42	2.50	2.58	2.62
(For α = 3.11)	2.92	2.90	2.88	2.74	2.78	2.86	2.95	2.98
(For α = 3.76)	3.32	3.30	3.27	3.12	3.15	3.24	3.33	3.36

The difference between the largest and the smallest radii for a given value of α is an estimate of the expected beam width. For example, for α = 2.48, the expected beam width would be 2.62-2.41 = 0.21 times the cathode radius. In Figure 4.10 the observed beam

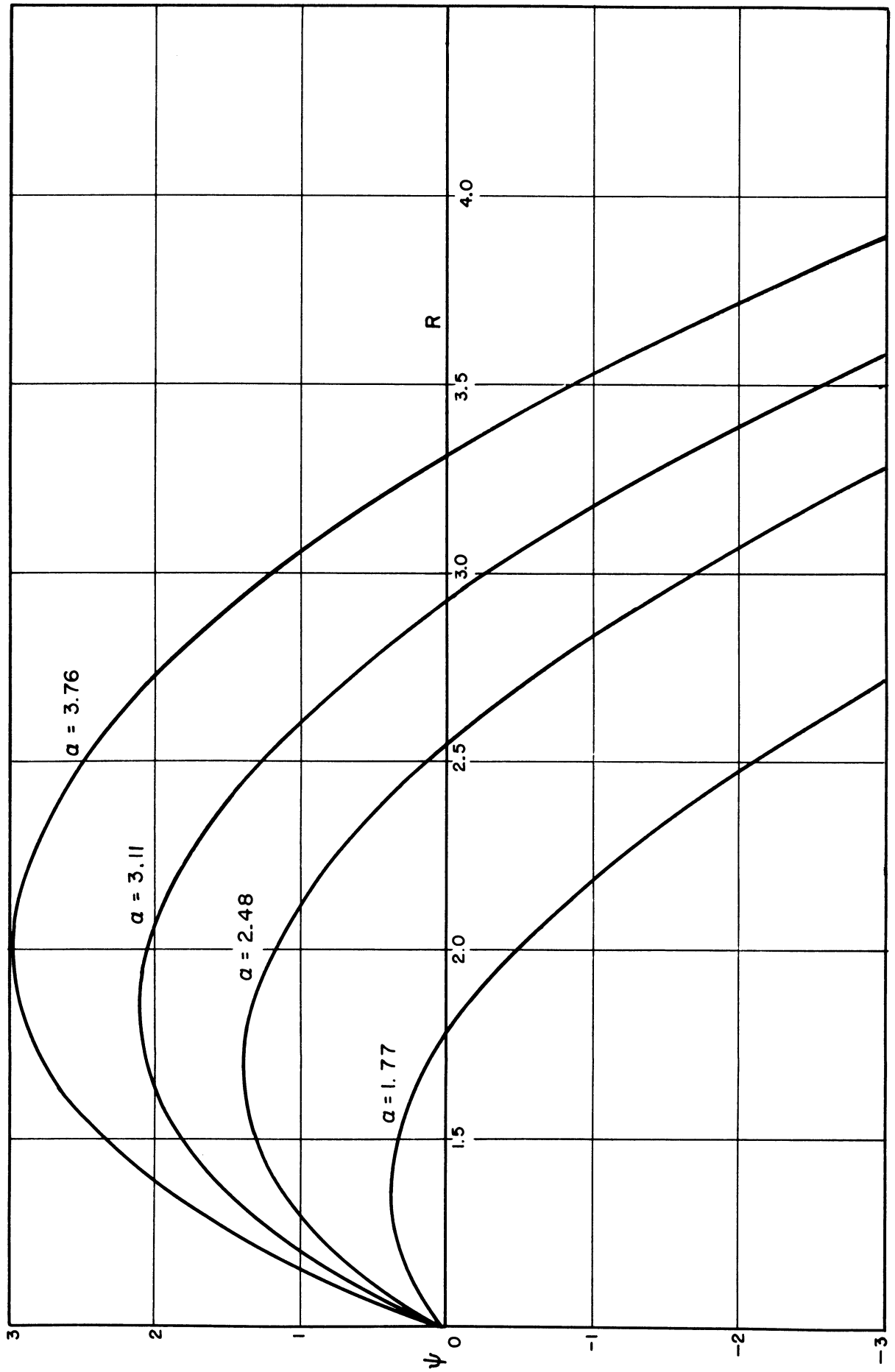

FIG. 4.17 EFFECTIVE POTENTIAL FOR THE CASE OF NON-EMITTING CATHODE

width at the maximum radius is approximately 0.13 times the cathode radius both with and without the mesh shield.

Table 4.3 also indicates that if end effects are negligible, the maximum radius of the electrons starting at the cathode with zero initial velocity would be somewhere between the maximum radius of the outside edge of the spot and the maximum radius of the inside edge of the spot; i.e., the spot would lie on the theoretical curve at the maximum radius.

End effects are the results of the fact that the electric potential is not independent of distance along the axis.[1] These effects on maximum radius of the orbit can be understood if the variation of the potential with z in equation (4.27) is taken into account. For simplicity assume that the electrons are initially at the cathode surface with zero velocity. Then

$$\frac{\dot{r}^2}{\omega_L^2 a^2} = \psi(r,z,\dot{z}) = \frac{2e\phi(r,z)}{m\omega_L^2 a^2} - \frac{r^2}{a^2}\left(1 - \frac{a^2}{r^2}\right)^2 - \frac{\dot{z}^2}{\omega_L^2 a^2} . \qquad (4.25)$$

At the maximum radius, $\dot{r} = 0$, and the maximum radius could be found by solving the equation

$$\psi(r, z, \dot{z}) = 0 . \qquad (4.30)$$

To solve this equation would require that the orbit be essentially known, since the variation of r and $\dot{z}$ with z would have to be given. This is out of the question. However, the orbit, neglecting end effects, can be used as a first order approximation. An estimate can be made of how $\dot{z}$ varies with z, and a second approximation to maximum radius can be made.

[1] The magnetic field is so nearly uniform that it does not contribute appreciably to end effects in this experiment.

By equation (2.46b) of Chapter II,

$$m\ddot{z} = eF_z = e\frac{\partial\phi(r,z)}{\partial z}, \text{ or}$$
$$\dot{m}\dot{z}\dot{z} = eF_z\dot{z} \quad . \tag{4.31}$$

This equation can be integrated to

$$\frac{m\dot{z}^2}{2} - \frac{m\dot{z}_o^2}{2} = e\int_{z_o}^{z} F_z \, dz \tag{4.32}$$

The integral of F along the path gives the potential; i.e.

$$\phi(r_2,z_2) - \phi(r_1,z_1) = \int_{z_1,r_1}^{z_2,r_2} F\cdot ds = \int_{r_1}^{r_2} F_r dr + \int_{z_1}^{z_2} F_z dz \quad . \tag{4.33}$$

This can be considered as

$$\phi(r_2,z_2) - \phi(r_1,z_1) = \bar{F}_r \cdot (r_2-r_1) + \bar{F}_z \cdot (z_2-z_1) \tag{4.34}$$

where $\bar{F}_r$ is the average radial field and $\bar{F}_z$ is the average axial field along the path from (r_1, z_1) to (r_2, z_2). If the path from one equipotential to the next is considered, then $\phi(r_2, z_2) - \phi(r_1,z_1)$ is known. The ratio of $\bar{F}_r$ to $\bar{F}_z$ can be estimated from the direction of the field along the path. The distances r_2-r_1 and z_2-z_1 can be measured from the field map. Thus the ratio of the two terms on the right of equation (4.34) can be found. Since the left side is known also, the term $\bar{F}_z\ (z_2-z_1)$ is easily obtained. But this is $\frac{m}{2e}(\dot{z}^2 - z_o^2)$, by equation (4.32).

An approximate map of the electric field in the trajectron is shown in Figure 4.18. The equipotential lines are placed at 0.125 ϕ_a, 0.25 ϕ_a, 0.5 ϕ_a, and 0.75 ϕ_a. The curves are the trajectories for

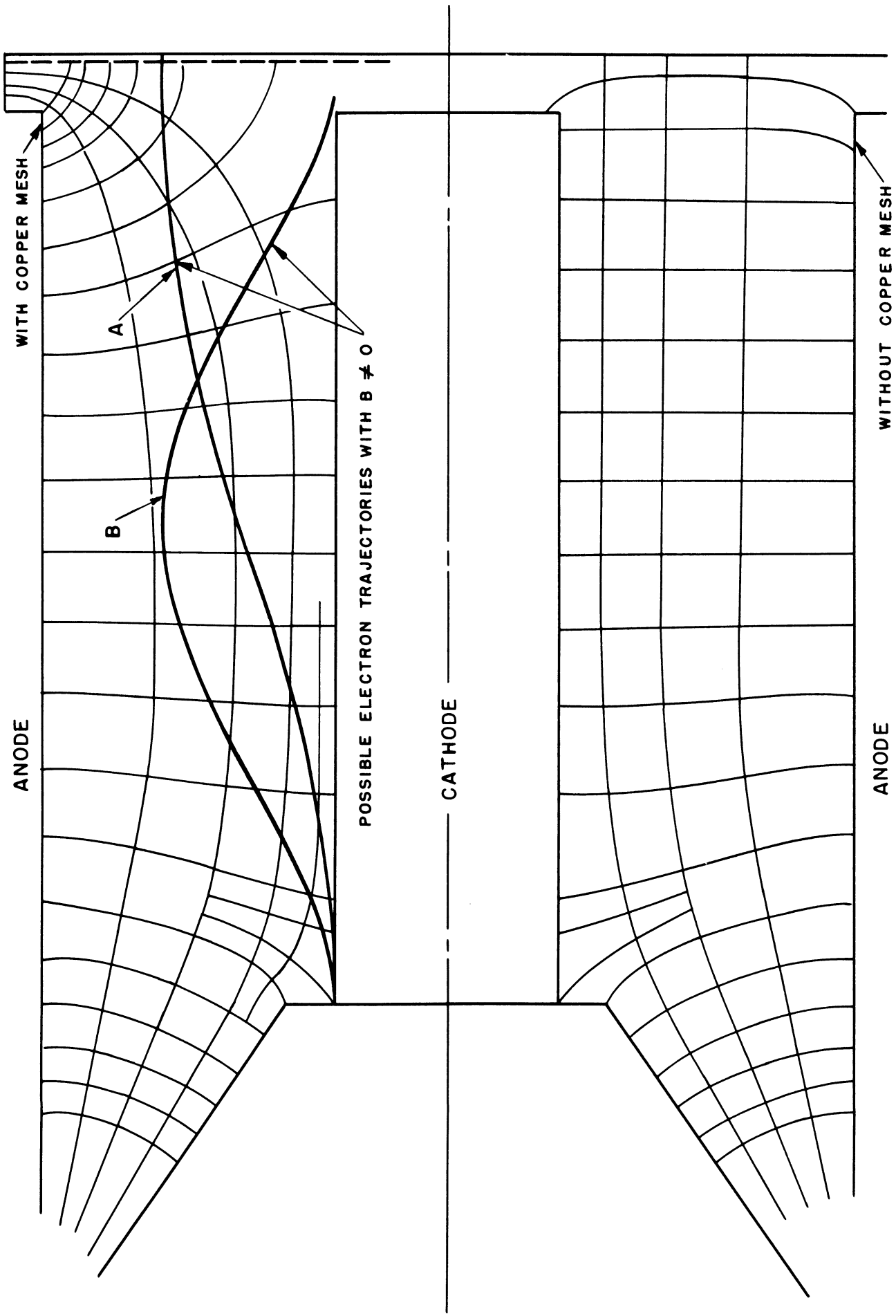

FIG.4.18 FIELD MAP OF TRAJECTRON DIODE WITH NO SPACE CHARGE

$\alpha = 2.48$ of electrons starting at the cathode with zero initial velocities and with end effects neglected. Curve A represents an electron reaching the fluorescent screen at the maximum radius of its orbit.

For the section of the trajectory A between the entry point of the beam and the 0.125 ϕ_a equipotential line, the ratio of axial to radial displacement is

$$\frac{z_2 - z_1}{r_2 - r_1} \approx 11, \tag{4.35}$$

and the electric field on the average makes an angle of approximately 78° with the axis of the cathode, so that

$$\frac{\bar{F}_z}{\bar{F}} = \cot 78^\circ = .21. \tag{4.36}$$

$$\frac{(z_2-z_1)}{(r_2-r_1)} \frac{\bar{F}_z}{\bar{F}_r} = 2.3, \tag{4.37}$$

and since $\phi(z_2,r_2) - \phi(z_1 r_1)$ is $0.125\phi_a$,

$$(z_2-z_1)\bar{E}_z = \frac{m(z_2^2-\dot{z}_1^2)}{2e} = 0.125\ \phi_a \frac{2.3}{2.3+1} = 0.087\ \phi_a. \tag{4.38}$$

For the next section of the trajectory, that between the 0.125 ϕ_a and the 0.25 ϕ_a equipotentials, the ratio of axial to radial displacement is roughly four, and the angle the field makes with the axis is about 87°. Hence for this section $\frac{m(\dot{z}_2^2-\dot{z}_1^2)}{2e}$ is approximately 0.021 ϕ_a. When the copper mesh was not placed in front of the fluorescent screen, the change in $\dot{z}^2$ is probably negligible for the rest of the path, and $\frac{m(\dot{z}^2-\dot{z}_o^2)}{2e}$ at the fluorescent screen is approximately $0.087\ \phi_a + 0.021\ \phi_a = 0.108\ \phi_a$. Also in this case the potential can be considered logarithmic at the fluorescent screen, so that at the fluorescent screen

$$\phi(r) = \frac{\phi_a}{\ell nR_a} \ell nR \quad , \tag{4.3}$$

and the equation $\psi(r,z,\dot{z}) = 0$ becomes

$$0 = \frac{2e\phi_a}{m\omega_L^2 a^2 \ell nR_a} \ell nR - R^2\left(1 - \frac{1}{R^2}\right)^2 - 0.108 \frac{2e\phi_a}{m\omega_L^2 a^2} \quad , \text{ or} \tag{4.39}$$

$$2\alpha \ell nR - R^2\left(1 - \frac{1}{R^2}\right)^2 = 0.108 \cdot 2\alpha \ell nR_a = 0.28\alpha \tag{4.40}$$

The function on the left is plotted in Figure 4.17, and this function for $\alpha = 2.48$ equals 0.28α, or 0.69 at $R = 2.28$. Neglecting end effects a maximum radius $R = 2.55$ is predicted. Thus end effects should reduce the maximum radius reached by the spot by $2.55 - 2.28 = 0.27$ times the cathode radius. The observed orbits shown in Figure 4.10 reach a maximum radius of approximately 2.55. The other observed orbits in Figures 4.8 through 4.15 are quite close to the theoretical orbits, and although they are generally smaller where there is an appreciable difference, they are not this much smaller. The discrepancy is only one or two times the width of the spot.

With the copper mesh in front of the fluorescent screen, the problem is more difficult to analyze. The only difference would be in the neighborhood of the fluorescent screen. The potential $\phi(r,z)$ is zero at the fluorescent screen, of course. The difficult question is: what is $\dot{z}^2 - \dot{z}_o^2$? Certainly $\dot{z}^2$ is less with the mesh than without; probably most of the energy the electron gives the field in moving to fluorescent screen, which is at zero potential, comes from the z-momentum. If

$$\frac{m(\dot{z}^2 - \dot{z}_o^2)}{2} = \frac{e\phi_a \ell nR}{\ell n\, R_a} \quad , \tag{4.41}$$

which is the potential that would appear at the fluorescent screen in the absence of the mesh, then the maximum radius would be the same as in the absence of the mesh. Apparently equation (4.40) holds approximately, for the maximum radius observed with the mesh in the diode is about the same as without the mesh.

The fact that the calculated times are longer for the experimental data than the theoretical analysis predicts can be accounted for by end effects. The calculated times were obtained by dividing the length of the diode by the beam velocity, calculated from the beam potential. Actually the z-velocity of the beam within the diode is greater than the velocity of the beam as it enters the diode, and the actual transit time of the beam is less than that calculated by dividing tube length by initial beam velocity.

A rough quantitative estimate of this effect can be made by estimating the increase in $\dot{z}$ by the method used in the preceding paragraphs. Consider, for example, the case in which $\alpha = 2.48$, and the beam spot is at the cusp of the trajectron. The theoretical orbit, neglecting end effects and initial velocities, is shown as Curve B, Figure 4.18. This curve can be used as a first approximation to the orbit, and the increase in $\dot{z}^2$ can be calculated. The calculation is summarized in the following table.

TABLE 4.3

Increase in Beam z-Velocity Due to End Effects for Trajectory B of Figure 4.18.

Section of Beam Path Between Equipotentials Corresponding to	$\frac{\bar{F}_z}{\bar{F}_r}$	$\frac{z_2-z_1}{r_2-r_1}$	$\frac{m(\dot{z}_2^2 - z_1^2)}{2e}$
0 and 0.125 ϕ	0.28	4.2	0.068 ϕ_a
0.125 ϕ_a and 0.25 ϕ_a	0.20	2.0	.036 ϕ_a
0.25 ϕ_a and 0.50 ϕ_a	0.09	1.8	.033 ϕ_a
0.50 ϕ_a and ϕ_a	0		0
Total			.137 ϕ_a

Thus the z-component of velocity corresponds to a potential of approximately $\phi_{beam} + 0.137\ \phi_a$, rather than ϕ_{beam} alone.

For the data presented in Figure 4.10a, $\phi_a = 700$ volts and $\phi_{beam} = 280$ volts for the spot corresponding to the cusp. The actual z-velocity in the diode was

$$\dot{z} = \sqrt{\frac{2e(\phi_{beam} + 0.137\ \phi_a)}{m}} \qquad (4.42)$$

while the value used in the calculation was

$$V_{beam} = \sqrt{\frac{2e\phi_{beam}}{m}} \ . \qquad (4.43)$$

The actual velocity was $\frac{\phi_{beam} + 0.137\phi_a}{\phi_{beam}}$, or 1.16, times the value used in the calculation of the beam transit time. Thus the actual time was approximately 0.86 times the calculated time. This accounts for the discrepancy between the experimental points and theoretical curves of Figure 4.11.

On one occasion when the anode voltage was set at a high value (2500 volts) a beam spot was observed when the beam potential

was zero! Evidently the emission velocities of the beam electrons carried them into the diode, where they received enough energy and z-momentum from the electric field in the diode to light the fluorescent screen.

4.5 The Case of an Emitting Cathode with No Magnetic Field

Photographs of the trajectron spot taken with an emitting cathode and no magnetic field are shown in Figures 4.19 and 4.20. The arrows at each spot in this figure indicate the theoretical deflection of a beam electron neglecting end effects and initial velocities of both emitted and beam electrons.

The striking thing about these photographs is the radial length of the spots. The reason the spots are long is that the beam enters the tube in a region of weak electric field and is deflected into a region of strong electric field. A simple example will show how this effect takes place. Suppose the electric field is proportional to the distance from the cathode of a planar device. Consider the motion of a beam electron which enters parallel to the cathode surface at a distance h from the cathode surface. If the field is in the y-direction, the differential equation for the y-displacement of the beam electron is

$$m \frac{d^2y}{dt^2} = eF = eky, \tag{4.44}$$

with the boundary conditions $y = h$, and $\dot{y} = 0$ when $t = 0$. The solution is easily found to be

$$y = h \cosh t\sqrt{\frac{ek}{m}} . \tag{4.45}$$

Considered as a function of initial conditions, the displacement of the beam electron is proportional to its initial displacement from the cathode.

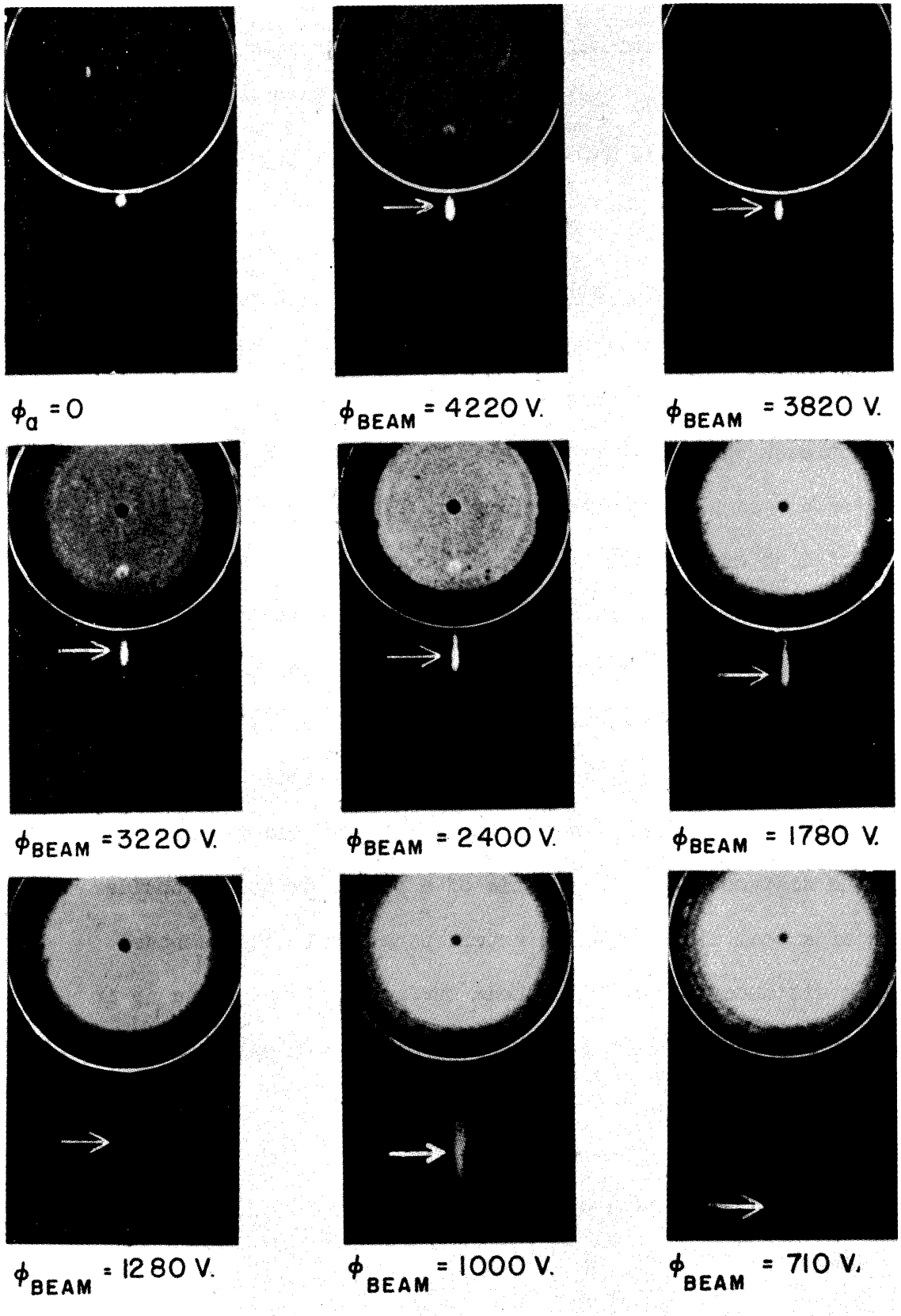

FIG. 4.19

TRAJECTRON DATA FOR THE CYLINDRICAL DIODE

($\phi_a = 217$ V., $I_a = 120$ ma., $I_m = 0$)

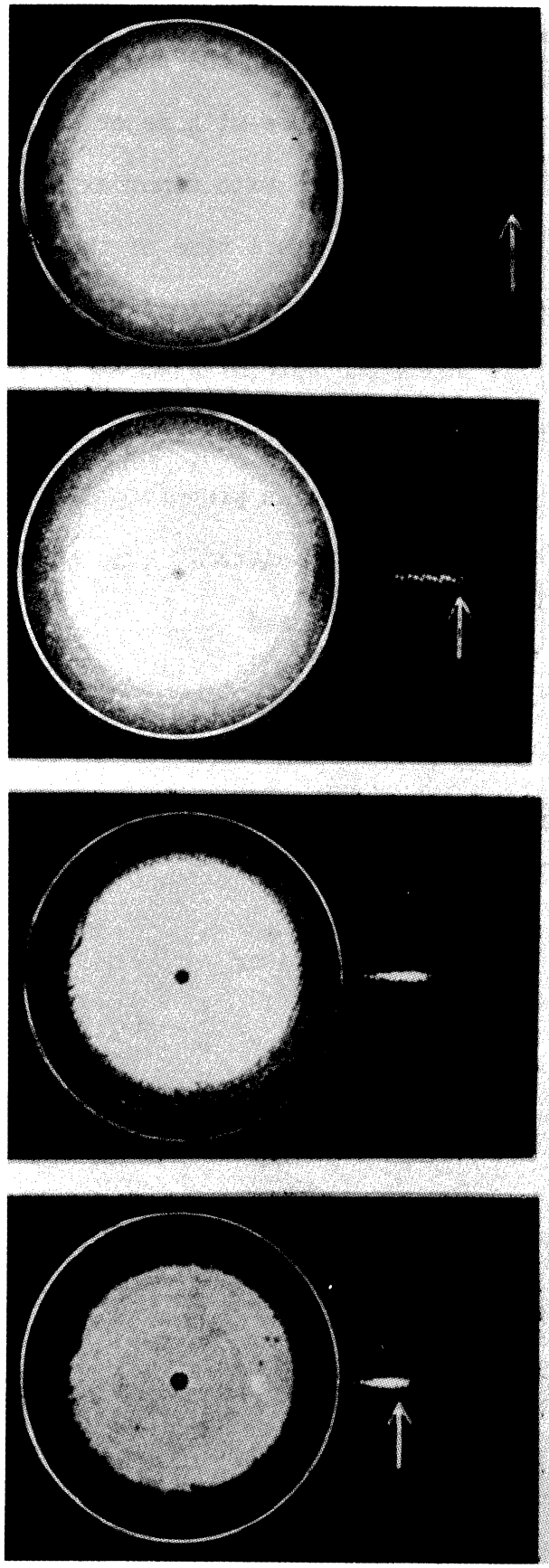

FIG. 4.20

TRAJECTRON DATA FOR THE CYLINDRICAL DIODE

(ϕ_a = 500 V , I_a = 500 MA, I_m = 0)

Suppose the beam consists of electrons whose paths are all parallel with each other and with the cathode, and that the cross-section of the undeflected beam is a circle of diameter d. Then the cross-section of the beam after transit time t would be an ellipse with major axis d cosh $t\sqrt{\frac{ek}{m}}$ (parallel with the electric field) and with minor axis d (perpendicular to the field). The longer the transit time of the beam, the greater the elongation of the spot is. If the spot initially touches the cathode, the ellipse will touch the cathode also.

If the initial velocities of emitted electrons are neglected, the potential distribution in a cylindrical diode is proportional to $(r\beta^2)^{2/3}$, where β^2 is a function of r which is tabulated.[1] The constant of proportionality can be evaluated at the anode, and

$$\phi = \phi_a \left[\frac{R\beta^2}{R_a\beta_a{}^2} \right]^{2/3} . \tag{4.46}$$

Since electrons start at the cathode with zero initital velocity, the velocity of electrons at any given radius is given by

$$\frac{m\dot{r}^2}{2} = e\phi = e\phi_a \left[\frac{R\beta^2}{R_a\beta_a{}^2} \right]^{2/3} , \text{ or} \tag{4.47}$$

$$\dot{r} = \frac{2e\phi_a}{m} \left[\frac{R\beta^2}{R_a\beta_a{}^2} \right]^{1/3} = \frac{dr}{dt} . \tag{4.48}$$

The relation between time and displacement is then

$$\gamma t = \int_1^R \frac{dR}{(R\beta^2)^{1/3}} , \text{ where} \tag{4.49}$$

---

[1] Spangenberg, Ref. G, pp. 176-178.

$$\gamma = \frac{1}{a}\left[\frac{2e\phi_a}{m}\right]^{1/2}\left(R_a\beta_a{}^2\right)^{-1/3} \tag{4.50}$$

The curve of R as a function of γt, found by integrating (4.49) numerically, is plotted in Figure 4.21.

For a given beam potential, the velocity of beam electrons is

$$v = \sqrt{\frac{2e\phi_{beam}}{m}} \tag{4.51}$$

and hence the transit time is

$$t = \frac{\ell}{v} = \ell\sqrt{\frac{m}{2e\phi_{beam}}} \tag{4.52}$$

where ℓ is the length of the diode. For these electrons

$$t = \frac{1}{a}\left(\frac{2e\phi_a}{m}\right)^{1/2}\left(R_a\beta_a{}^2\right)^{-1/3}\cdot\left(\frac{m}{2e\phi_{beam}}\right)^{1/2}, \text{ or}$$

$$t = \frac{\ell}{a}\left(R_a\beta_a{}^2\right)^{-1/3}\sqrt{\frac{\phi_a}{\phi_{beam}}} = 6.17\sqrt{\frac{\phi_a}{\phi_{beam}}} \tag{4.53}$$

for the trajectron. The radial displacement corresponding with these values of γt are indicated on the photographs of Figures (4.19) and (4.20), by arrows. This would be the displacement of the beam if it corresponded exactly with emitted electrons, and if the initial velocities of emitted electrons could be neglected.

The actual potential differs near the cathode from that given by equation (4.46) because of the initial velocities of emitted electrons. There is actually a potential minimum near the cathode. An exact theoretical determination of the potential distribution for this case has been carried out only for the parallel-plane diode case.[1] Consider an area on the

[1]Dow, Ref. C, pp. 242-246.

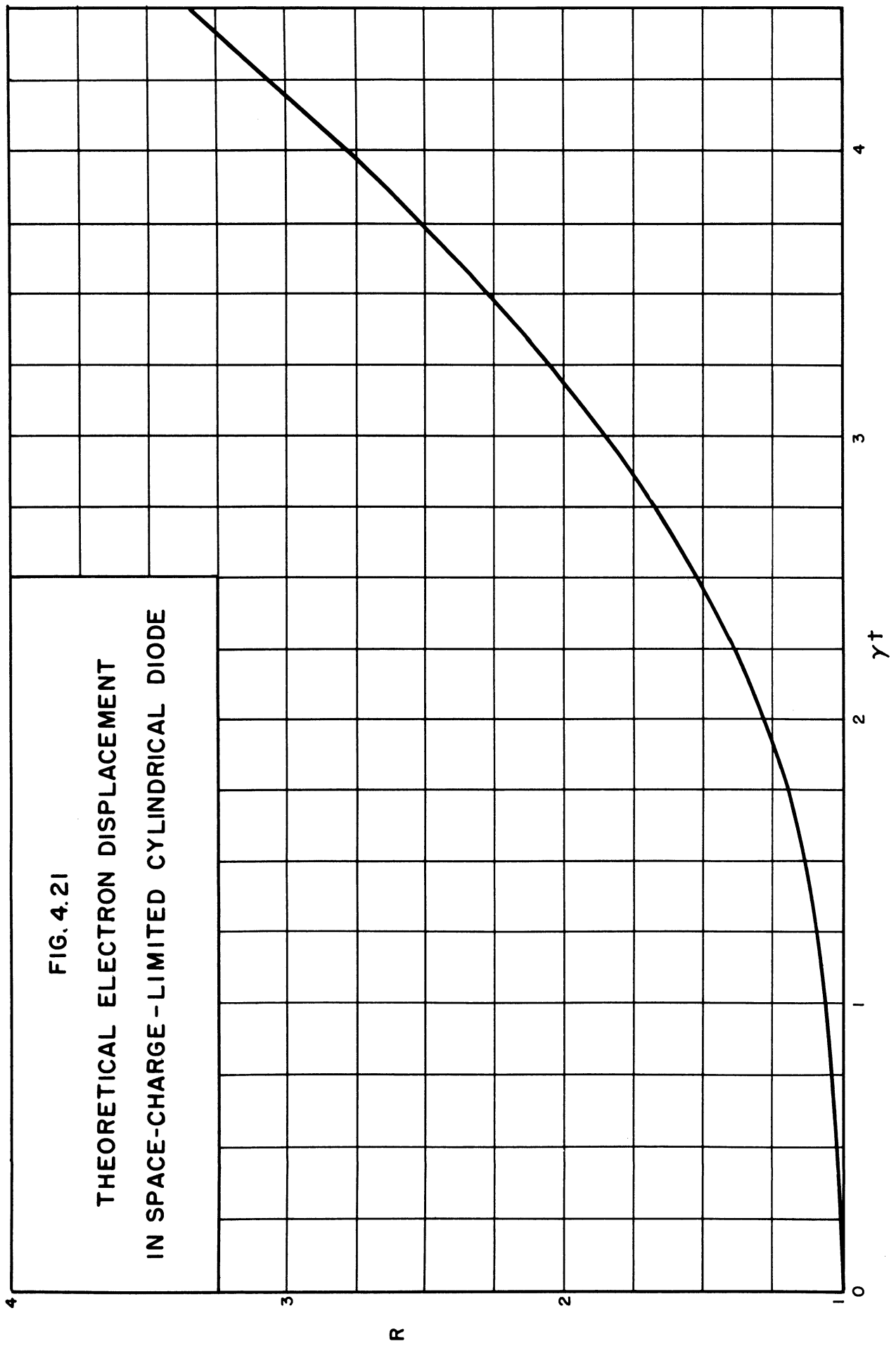

FIG. 4.21
THEORETICAL ELECTRON DISPLACEMENT
IN SPACE-CHARGE-LIMITED CYLINDRICAL DIODE

trajectron cathode about 0.10" square, and the region from this area on the cathode out about .020". This area is probably near enough so that the potential in this region could be approximated by considering it to be a planar diode. This approximation to the potential is plotted in Figure 4.22 for the conditions under which the photographs of Figure 4.19 were taken.[1] The distance from the cathode to the potential minimum is roughly inversely proportional to the square root of the anode current. For an anode current of 500 ma, the distance is only about .001", while for an anode current of 20 ma, the distance is about .006".

The modification of the potential distribution indicated in Figure 4.22 has an important effect on the deflection of beam electrons. A few trajectories of beam electrons were calculated numerically for the potential field which would occur if there were no initial velocities. The calculations were made for a transit time the same as for the 1880 volt beam spot of Figure 4.19. They indicated that the initial position, i.e., entry point, of beam electrons was a much more important factor than initial velocity in determining displacement of a beam electron. The beam deflections were found to range from approximately the theoretical value for emitted electrons, indicated by the arrow in Figure 4.19, to a radius of about three times the cathode radius, which is well beyond the maximum deflection observed for beam electrons.

---

[1] The cathode temperature was approximately 900° C., or 1173° K. The cathode area was approximately 20 square centimeters. The largest current which the cathode delivered was 800 ma., but it certainly was capable of deliverying more. One hundred milliamperes per square centimeter, or two amperes, would be a conservative estimate for the maximum emission. This information together with the data on Figure 4.19 is sufficient for finding the potential distribution from the formulas given by Dow (Ibid., pp. 242-246). Note that

$$E_m = E_T \ell n \frac{J_{emission}}{J_{anode}} .$$

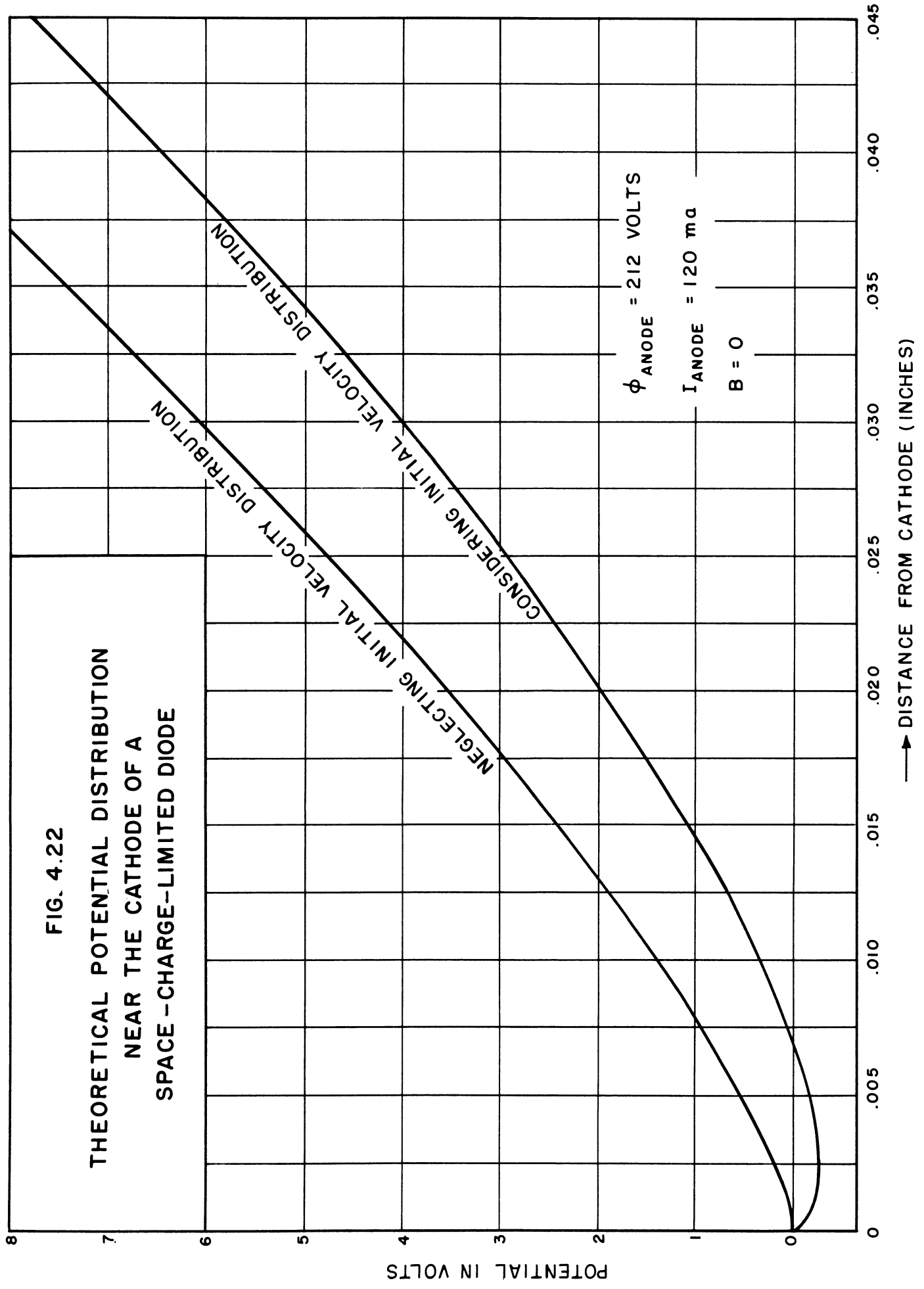

FIG. 4.22
THEORETICAL POTENTIAL DISTRIBUTION NEAR THE CATHODE OF A SPACE-CHARGE-LIMITED DIODE

When the potential minimum is taken into account, the field in the neighborhood of the potential minimum is approximately parabolic. (The space charge density, and hence the second derivative of the potential curve, is finite and not zero for this case.) The undeflected spot is approximately .025" in diameter and is no more than a few thousands of an inch from the cathode. Thus the edge of the beam nearest the cathode is very near the potential minimum. The potential minimum may even lie within the beam at the entry point. The deflected beam spot should resemble the spots calculated for a parabolic potential field more closely than a spot calculated for the field which would occur if emitted electrons had zero initial velocity. This resemblance is apparent in Figures 4.19 and 4.20. The spots are not elliptical, but they are very long and they extend nearly back to the cathode, as would be expected if the spot were initially very near the potential minimum.

4.6 A Discussion of the Trajectron Method.

The trajectron method, i.e., the interpretation of beam deflection as equal to the deflection of emitted electrons in the same transit time[1], would seem at first glance to be a very powerful method for studying electronic devices. The beam spot deflection agreed reasonably well with the theoretical deflection of an electron starting at rest from the cathode when a non-emitting cathode was used in the trajectron diode. With an emitting cathode delivering space-charge-limited current in the diode, however, the situation is entirely different.

---

[1] See page 2.

A beam starting in a region of weak field and moving into a region of strong field will tend to defocus. The extreme case occurs when the beam enters in the neighborhood of the potential minimum, as near the cathode of a tube operating in a space-charge-limited condition. The part of the beam entering at the surface of zero field will not be deflected, while the displacement of other electrons will depend in a continuous manner upon their initial distance from the point of zero field. As a result, the beam spot will extend from the surface of zero field out to some maximum displacement which will depend strongly upon the relationship between the beam and the point of zero field. Thus the trajectron method cannot be used to obtain displacement as a function of time if the beam must enter at a point of zero field.

While the direct interpretation of beam deflection as equal displacement of emitted electrons is not possible in a large class of problems, the use of an electron beam as a probe may still serve as a valuable technique. Indeed, some important knowledge about the fields in the dc magnetron was obtained by studying the trajectron beam spots. (See Chapter V.)

CHAPTER V

THE MAGNETRON CASE

5.1 Introduction

The purpose of this chapter is to present data taken from the trajectron for the magnetron case, to discuss these data, and to present whatever conclusions can be made on the behavior of electrons in a dc magnetron. Most of the chapter is concerned with the magnetron in the cutoff condition. Some data with the anode voltage slightly above cutoff are presented and discussed in Section 5.7. Additional data for the magnetron both above and below cutoff is included in Appendix E.

The discussion of the trajectron data consists of two parts: in the first part only the maximum radius of beam electron orbits is studied, while in the second the entire orbits, and especially the configuration of beam spot, are considered. The maximum radii of beam electron orbits were observed to be smaller than would be expected if there were no secular space charge in the magnetron and hence no space charge outside the Hull radius. From this it can be concluded that there is space charge outside the Hull radius. Estimates of the amount of this secular space charge indicate that it is far from negligible, and probably more important than the cathode-accessible space charge. The maximum radius of beam electron orbits is observed to have a much greater range than predicted by the calculations in which secular space charge is neglected. Calculations of beam electron orbits indicate that the explanation probably lies in the presence of secular

space charge and fluctuations in the electric field.

Inflections in anode current as a function of anode voltage were observed in the trajectron magnetron diode. These inflections were associated by Delcroix[1] with changes in the character of the (cathode-accessible) space charge from one type of orbit to another. As the trajectron anode voltage was varied in the neighborhood of these inflections, the beam spot was observed to move only a few thousandths of an inch and to change shape only slightly. There appear to be two possible explanations. The anode current inflections may not be associated with changes in space-charge type. The second possible explanation is that the inflections in anode current are associated with changes in the type of orbits of cathode-accessible electrons, but these electrons contribute so little and the secular space charge so much to the total space that changes in the orbits of cathode-accessible electrons have a negligible effect upon the beam spots.

5.2 The Magnetron in the Cutoff Region

Typical data photographs for the cutoff magnetron are shown in Fig. 5.1. Each photograph includes several exposures of the spot. There is an exposure with the anode voltage removed showing the undeflected, or initial, position of the spot. The other exposures are made with various beam potentials. The two photographs differ only in the orientation of the magnetic field. On each photograph a circle showing the position of the cathode surface is drawn. (The anode radius is 3.65 times the cathode radius.)

Clearly the beam does not trace out the orbits of the emitted

---

[1] Refs. 14, 15, and 16.

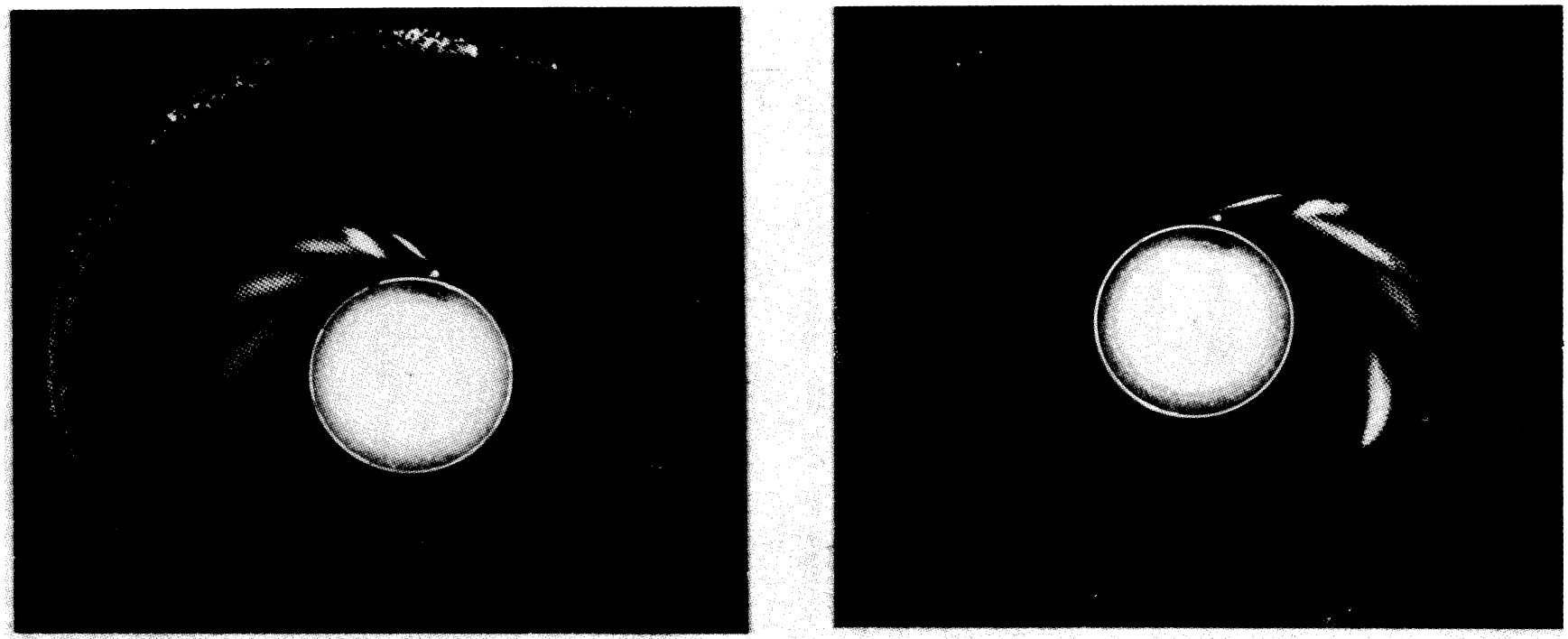

ϕ_a = 1550 VOLTS ; I_a = 10 MA ; I_m = 4 AMPS

ϕ_{BEAM} = 710, 1000, 1480, 2500, 4020 VOLTS

FIG. 5.1 TYPICAL DATA PHOTOGRAPHS FOR CUTOFF MAGNETRON CASE

electrons. However, significant information concerning the space charge and potential distributions can be obtained from the trajectron data since the motion of the beam electrons depends upon the potential distribution in the diode. The following sections discuss the effects of various conditions or phenomena which may occur in the trajectron on the motion of beam electrons. The purpose of these discussions is to achieve an understanding of how the spot should appear under various conditions, and to draw conclusions on what conditions prevailed in the trajectron magnetron diode.

5.3 End Effects

End effects result from the fact that the electric field in the diode is not independent of distance in the axial direction[1]. They are not as easily discussed for the magnetron case as for the space-charge-free case[2], since the potential distribution in the magnetron diode is not known. Even an approximate plot of the field with a hypothetical space-charge distribution would be more difficult to obtain than in the case of no space charge. Some idea of the magnitude of the effect can be obtained, however, by a comparison of the magnetron case with the space-charge-free case.

The variation of electric field with axial distance can be considered the result of placing in the infinite diode the shields which are at each end of the diode[3]. These shields were both at the cathode potential;

---

[1] The magnetic field is so nearly uniform that it does not contribute appreciably to end effects in this experiment.

[2] See Section 4.6.

[3] The copper mesh shield (Part No. 28 of Figure 3.2) was used in obtaining all data presented in this chapter.

they had the effect of lowering the potential where they were placed to the potential of the cathode. The presence of space charge had the effect of depressing the potential, as illustrated in Figure 5.2. The points at which the shields were placed were more nearly at ground potential with the space charge present than without. Therefore the changes in the field resulting from the shields in the ends of the diode were smaller with space charge present than in the case with no space charge.

Since the field was disturbed less in the magnetron case than in the space-charge-free case, it seems reasonable to assume that end effects were smaller also. The end efffects for the space charge free case are discussed in Section 4.4. Typical results were that the maximum radius of the orbits were changed by a negligible amount and the beam acted as if the beam potential were increased by approximately one-seventh of the anode voltage.

5.4 The Effect of Initial Velocities of Beam Electrons on the Maximum Radius of the Beam Electron Orbit

For any given potential distribution in the magnetron the maximum radius of the orbit of a beam electron can be found through the energy integral just as in the space-charge-free case. The initial part of the discussion of this problem in Chapter IV assumed the electric potential to be an arbitrary function of r, and hence equation (4.26) can be used in the magnetron case as well as in the space-charge-free case[1]. At the maximum radius of a beam electron's orbit, its radial velocity $\dot{r}$ is zero, and by (4.26),

---

[1] See page 127.

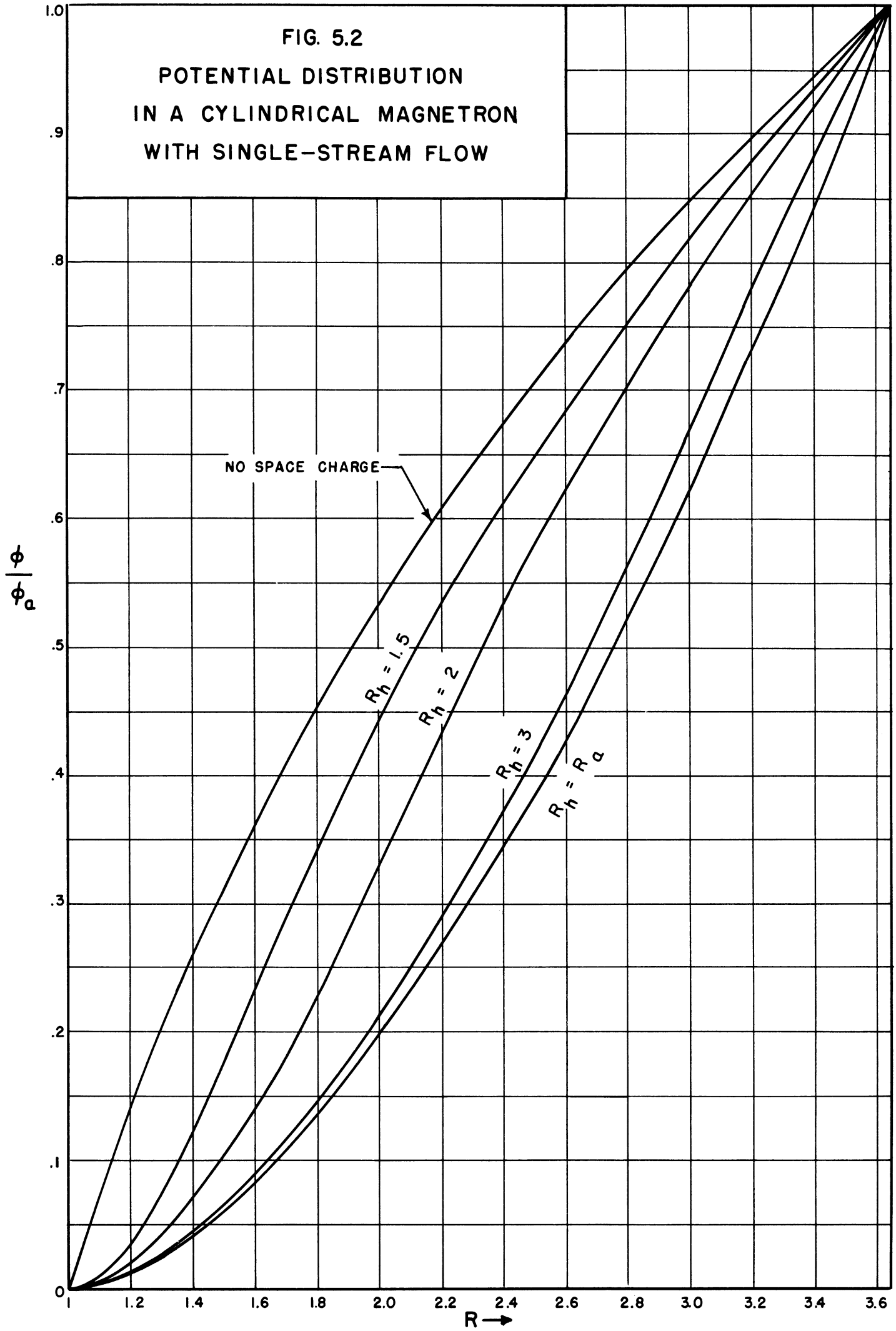
FIG. 5.2
POTENTIAL DISTRIBUTION
IN A CYLINDRICAL MAGNETRON
WITH SINGLE-STREAM FLOW
NO SPACE CHARGE
$R_h = 1.5$
$R_h = 2$
$R_h = 3$
$R_h = R_a$
$\frac{\phi}{\phi_a}$
R
1.0
.9
.8
.7
.6
.5
.4
.3
.2
.1
0
1
1.2
1.4
1.6
1.8
2.0
2.2
2.4
2.6
2.8
3.0
3.2
3.4
3.6

$$\psi(r) = \psi(r_o) - \frac{\dot{r}_o^2}{\omega_L^2 a^2} - \left(\frac{a^2}{r_o^2} - \frac{a^2}{r^2}\right)\left(\frac{P_\theta^2}{m^2 \omega_L^2 a^4} - 1\right) \quad (5.1)$$

The effective potential $\psi(r)$ is the electric potential modified in two ways: (1) it is normalized, and (2) the energy of angular motion of an electron initially at rest on the cathode is subtracted from it:

$$\psi(r) = \frac{2e\phi(r)}{m \omega_L^2 a^2} - \frac{r^2}{a^2}\left(1 - \frac{a^2}{r^2}\right)^2 \quad (5.2)$$

The effective potential is a measure of the energy of the radial motion, and in a region of the magnetron containing cathode-accessible space charge, electrons starting at rest from the cathode have a radial velocity given by

$$\psi(r) = \frac{\dot{r}^2}{\omega_L^2 a^2} \quad . \quad (5.3)$$

Using this fact, the function $\psi(r)$ can be calculated easily for the B_o, B_1, and B_2 solutions if the secular space charge is neglected. Within the space-charge region $\psi(r) = 0$ for the B_o solution, since $\dot{r} = 0$ for all emitted electrons. For the B_1 and B_2 solutions $\dot{r}$ can be taken from differential analyser data. Outside the space charge region the space charge distribution is assumed zero, and $\psi(r)$ is calculated from equation 5.2 above and equation (2.84) of Chapter II. Curves of $\psi(r)$ are shown in Figure 5.3 for $R_h = 2.5$.

With $\psi(r)$ and the beam initial conditions known, equation (5.1) can be solved for the maximum radius. Graphical solutions of equation (5.1) obtained for a number of cases typical of beam electrons in the trajectron

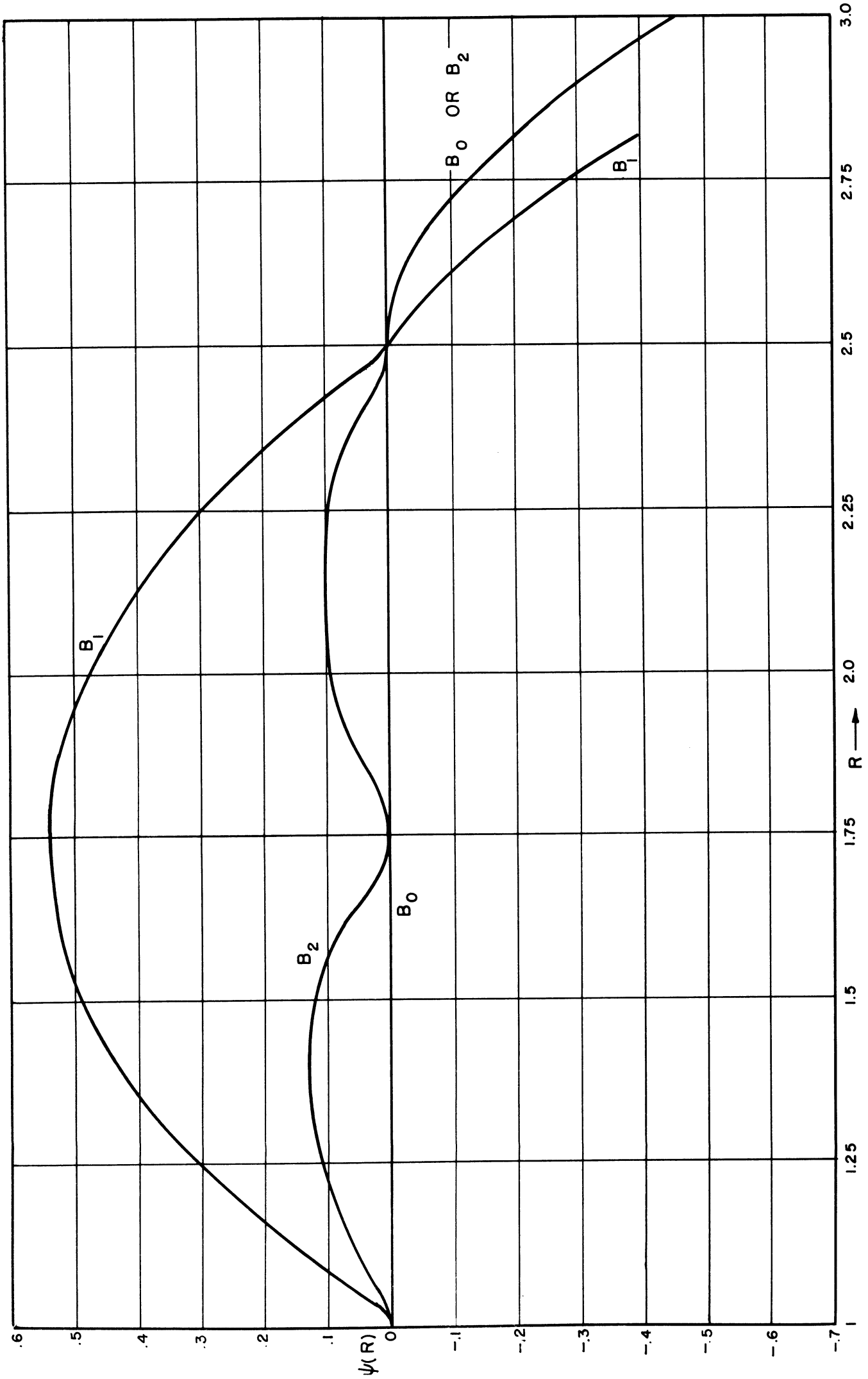
B0 OR B2
B1
B1
B2
B0
ψ(R)
R
.6
.5
.4
.3
.2
.1
0
-.1
-.2
-.3
-.4
-.5
-.6
-.7
1
1.25
1.5
1.75
2.0
2.25
2.5
2.75
3.0

are summarized in Table 5.1[1].

TABLE 5.1

CALCULATED MAXIMUM RADIUS OF THE ORBIT
OF BEAM ELECTRONS IN MAGNETRON SPACE CHARGE

Initial Conditions of Beam Electrons (See Figure 4.4)						
h		.030"	.030"	.030"	.0151	.0075"
s		.020"	.020"	.020"	0	0
δ		0°	± 90°	180°	-	-
Space Charge Type	R_h	Maximum Normalized Radius of Beam Electron Orbit				
B_1	1.75	1.88	2.05	2.17	1.97	1.91
B_2	1.75	2.03	2.07	2.085	2.01	1.94
B_0	1.75	2.05	2.08	2.09	2.01	1.94
B_1	2.5	2.6	2.72	2.82	2.63	2.58
B_2	2.5	2.82	2.92	2.97	2.79	2.70
B_0	2.5	2.90	2.96	2.98	2.81	2.71
B_1	3.58	3.54	3.69	3.77	3.65	3.62

In the previous chapter the effect of the potential minimum at the cathode of a space-charge-limited diode was found to have a profound effect on the motion of the beam. The potential minimum was not taken into account in the present discussion. Up to this point only the maximum radius of beam electron orbits has been discussed. The maximum radius was calculated from the effective potential. The effective potential curve would differ a negligible amount if the potential minimum were considered: it

[1] The B_1 and B_2 solutions in the ideal cylindrical magnetron do not exist with $R_h = 1.75$, so that the effective potential curves could not be taken from the differential analyser for these cases. The B_1 and B_2 solutions can occur if the conditions in the magnetron are not the ideal conditions described in Section 2.2. The presence of secular space charge can make this possible, for example. (See Section 2.6) The approximation taken for potential distribution in this case was the potential distribution in an ideal planar magnetron with a space charge region of the same thickness.

would be a fraction of a volt lower and would have appreciably different slope only within a few thousandths of an inch of the cathode. Thus the potential minimum should have little effect upon the maximum radius of the beam electron orbits.

In comparing the calculations summarized in Table 5.1 with the data photographs, the first question which arises is, how can the range of maximum radius for the beam electron orbits be found from the photographs? The maximum radius of the largest beam electron orbit is obviously the largest radius reached by any beam electron. This might be found by considering the outside edge of the area swept through by the beam spot as the beam voltage is varied, as illustrated by R_M in Fig. 5.4. It might seem that the maximum radius R_m of the inside edge of this area would be the maximum radius of the smallest beam electron orbit. Actually it may not not be. All that can be said definitely is that the maximum radius of the smallest beam electron orbit is at least this large. However, comparing the range of maximum y-displacement[1] for beam electrons for the planar magnetron case and the calculated "spots" which are shown in Fig. 5.6 in the next section we see that the maximum y-displacement of the smallest beam electron orbit for these cases differs very little from the maximum y-displacement of the inside edge of the area swept through by the beam. Thus it is reasonable to estimate the maximum radius of the smallest beam electron orbit by R_m.

For the case presented in Figure 5.1a, $R_M = 2.2$ and $R_m = 1.4$ approximately. For Figure 5.1b, $R_M = 2.5$ and $R_m = 1.7$. These two cases differ only in the orientation of the magnetic field, and if the alignment

---

[1] The y-displacement in the planar case corresponds to radial displacement in the cylindrical case.

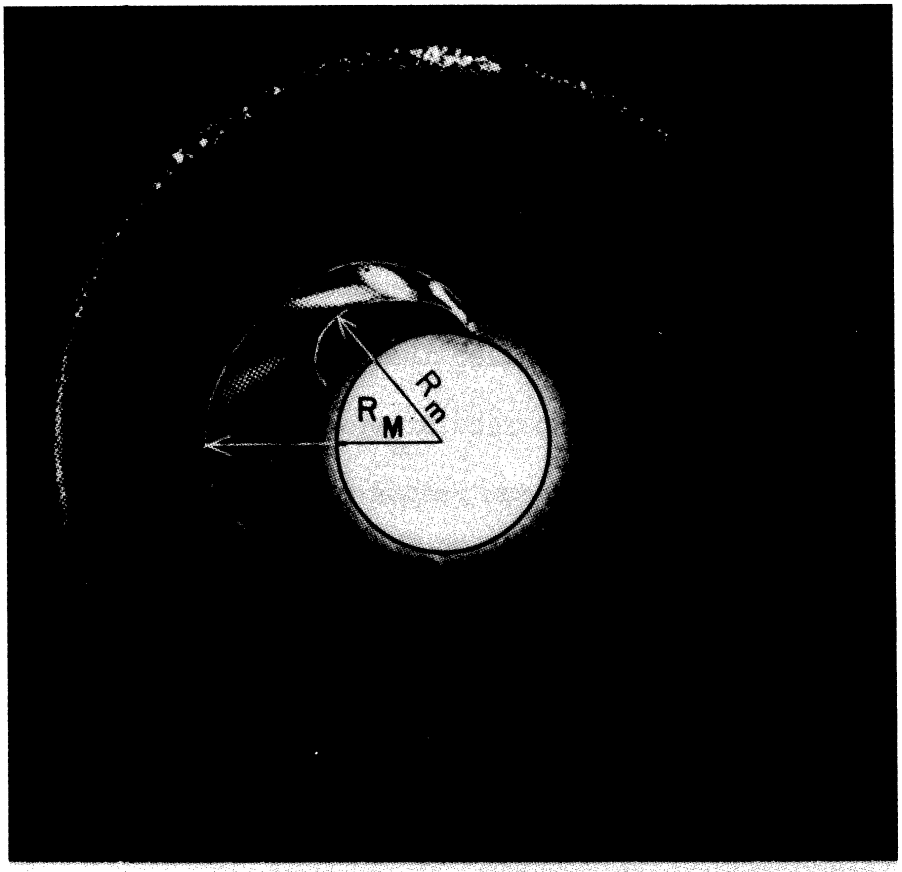

ϕ_a = 1185 V., I_a = 2.5 ma, I_m = 3.5 A.

ϕ_{BEAM} = 500, 710, 1000, 1980, 3020, 4020 VOLTS

FIG. 5.4

TRAJECTRON DATA SHOWING PARAMETERS R_M AND R_m

were perfect, the photographs would be mirror images of each other. The Hull radius R_h calculated on the assumption of no space charge outside the space charge cloud is 2.23 for the B_0 solution, 2.25 for the B_2 solution, and 2.33 for the B_1 solution[1]. There are several facts which must be discussed. First, judging from the calculations summarized in Table 5.1, one would expect the maximum radius of the smallest beam electron orbit, and hence R_m, to be either approximately equal to or somewhat greater than the Hull radius R_h. It is observed to be smaller than the Hull radius calculated on the assumption that there is no secular space charge. In the second place, the observed range of maximum radius (R_M - R_m) is much greater than that predicted by the calculations summarized in Table 5.1. In the third place, the difference between Figures 5.1a and 5.1b is great enough to be conspicuous. These data are typical in all three respects, of the trajectron data taken for the cutoff magnetron. The first point mentioned above is examined in the next paragraph. The second and third points are discussed in Sections 5.6 and 5.7.

The beam was not deflected as far as calculations neglecting space charge outside the Hull radius indicated it should be. The obvious conclusion is that the space charge outside the Hull radius is not negligible. This conclusion is shown more rigorously to be true in Appendix F. A consequence of this fact is that the Hull radius cannot be calculated from knowledge of the anode potential and magnetic field alone. In this experiment it must be estimated from the data photographs. With the spots as large as they are on the data photographs, an accurate estimate of R_h is impossible.

---

[1] See Figure 2.10.

Even if R_h were known, the amount of secular space charge or its distribution could not be found from the trajectron data. If the Hull radius and the form of the secular space charge distribution were known, however, the amount of secular space charge could be calculated. For the purpose of estimating very roughly the amount of secular space charge, the space charge distribution might be assumed the same as the distribution for the B_o solution, and the Hull radius could be estimated from the data photograph. In Figure 5.1a, the Hull radius might reasonably be taken as 1.4a since all the beam electrons would be expected to reach at least the Hull radius.(See Table 5.1.) Because Poisson's equation is linear, the field can be thought of as being the sum of two components, one associated with the secular space charge and the other the difference between the entire field and the component associated with the secular space charge. If the secular space charge is assumed to have a distribution proportional to that of the B_o solution for the magnetron, the secular component of the potential can be taken as a fraction, say f, of the potential associated with the B_o solution. It is shown in Appendix D[1] that with this particular choice for the secular space-charge distribution, the distribution of the remaining space charge is that which would occur if there were no secular space charge and the Hull radius were the same, reduced by a factor 1-f. In terms of the potential, this means that

$$\phi(r) = f\,\phi_1(r) + (1-f)\,\phi_2(r) \qquad (5.4)$$

where ϕ_1 is the potential of the B_o solution with space charge reaching the anode, and ϕ_2 is the potential which would occur with no secular space

---

[1] See pp. 229-231. Equation (5.4) is obtained from equation (D.3) by letting $f = \frac{1}{2} k_5$.

charge. At the anode, ϕ_1 is the same as the cutoff potential, .111 B^2, and ϕ_2 can be found from Figure 2.10 to be .030 B^2. The anode potential for Figure 5.1a was .077 B^2. From equation (5.4) f is found to be 0.58.

With the same assumptions the total space charge inside the Hull radius, and the total space charge outside the Hull radius, can be calculated. For simplicity the calculation will be made assuming the B_o type solution for cathode accessible electrons[1]. The result will hold approximately for other types of solutions since the boundary conditions at the Hull radius are approximately the same for different type solutions of the same Hull radius. Then, by equation (2.70), the space charge distribution between the cathode and the Hull radius is

$$\rho = C\left(1 + \frac{1}{R^4}\right) \tag{5.5}$$

where C is a constant depending on the magnetic field and physical constants. Outside the Hull radius the space charge density is assumed to be of the same form as (5.5) but reduced by the factor f, i.e., outside R_h

$$\rho = fC\left(1 + \frac{1}{R^4}\right) \tag{5.6}$$

---

[1] According to the definition of secular space charge given in Chapter II, the B_o type space charge is secular space charge, not cathode-accessible space charge. It is a limiting case, however. The electrons in the B_o type space charge have the same total energy and canonical angular momentum as electrons at rest on the cathode, and an infinitesimal change in energy or momentum would make them cathode-accessible. Furthermore, the B_o type space charge is in a sense the limit approached by B_n type space charge as n becomes infinite, and because of its simplicity it is often convenient to consider it an approximation to B_n type cathode-accessible space charge.

The space charge Q between any two radii can be found by integrating:

$$Q = \int_{r_1}^{r_2} \rho(R)\, 2\pi r dr$$

$$= a^2 \int_{r_1}^{r_2} \rho(R)\, 2\pi R dR \qquad (5.7)$$

For the case in the preceding paragraph, R_h was taken to be 1.4 and f was found to be 0.58. By equations (5.5) and (5.7) the charge between the cathode and the Hull radius can be found to be $1.45 \cdot 2\pi a^2 C$. By equations (5.6) and (5.7), the charge between the Hull radius and the anode is $6.8 \cdot 2\pi a^2 C$. There is more than four times as much space charge outside the Hull radius as inside.

The estimate of R_h is rather crude. Probably R_h was less than 1.4. Certainly it was no larger than 1.7. If R_h is taken as 1.7, f is found to be 35%. The total amount of space charge between the cathode and the Hull radius turns out to be $2.54 \cdot 2\pi a^2 C$. The total charge between the Hull radius and the anode is $3.76 \cdot 2\pi a^2 C$, about half again as much as inside the Hull radius.

For a given Hull radius, the amount of space charge required between the Hull radius and the anode to produce a given anode potential depends upon how the space charge is distributed. Space charge near the Hull radius has a greater effect than space charge near the anode. If all the space charge were concentrated at the Hull radius, the amount of space charge required would be reduced by a factor of less than three[1].

---

[1] See Appendix F, p. 247.

The data apparently cannot give an accurate estimate of the space charge outside the Hull radius, but even a very conservative estimate indicates that the space charge outside the Hull radius is far from negligible. Indications are that this secular space charge is in reality the most important portion of the space charge.

5.5 Calculated Beam Electron Orbits

Calculations were made of the orbits of beam electrons neglecting end effects but considering initial conditions. The calculations were made for the planar magnetron for simplicity. Even so, a considerable amount of numerical work was required; much of this was done with the electronic differential analyser. The method of calculation is simply to assume the B_1, B_2, and B_0 type of space charge occurs in the magnetron, with the space charge region of given width. This determines the potential distribution. Then the trajectories in this potential field of electrons with initial conditions typical of beam electrons in the trajectron were calculated. The method of calculation is described in Appendix C. The results of these calculations are given in Figures 5.5, C.3, C.4, C.5, and C.6. For each figure the beam initial conditions and the thickness of the space charge cloud are fixed. The three solid curves give the beam electrons' radius as a function of time for the potential distributions of the B_0, B_1, and B_2 solutions. The dashed curves are the radial displacement as a function of time for electrons starting at the cathode with zero velocity with the potential distributions of the B_1 and B_2 solutions. They are given for comparison; they represent the motion of beam electrons in an ideal trajectron.

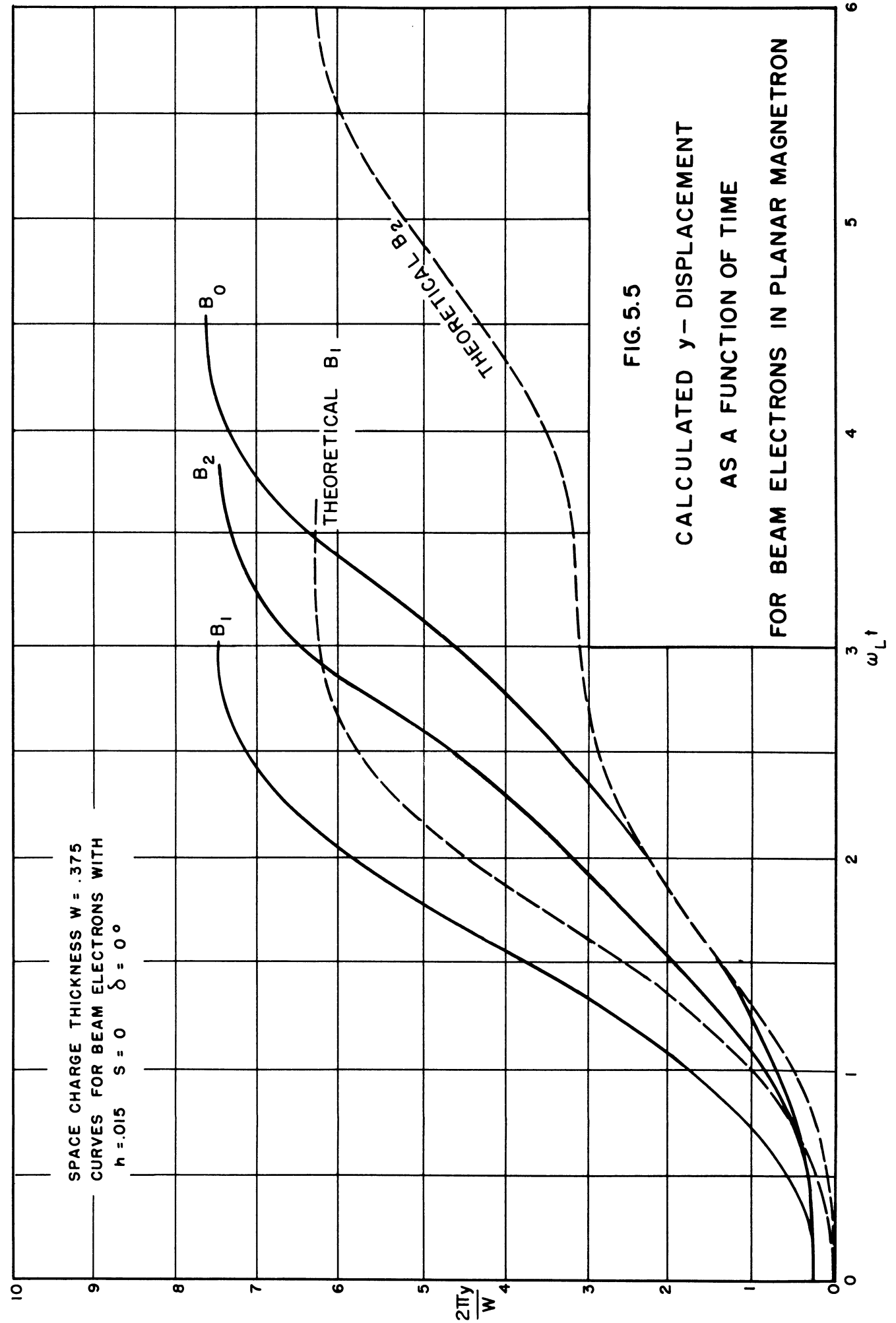
FIG. 5.5
CALCULATED y- DISPLACEMENT
AS A FUNCTION OF TIME
FOR BEAM ELECTRONS IN PLANAR MAGNETRON
SPACE CHARGE THICKNESS W = .375
CURVES FOR BEAM ELECTRONS WITH
h = .015 S = 0 δ = 0°
THEORETICAL B2
THEORETICAL B1
B0
B2
B1
2πy/W
ωLt
0
1
2
3
4
5
6
7
8
9
10

The x-displacement for beam electrons can be found from Figures 5.5, C.3, C.4, C.5, and C.6 by applying equation (2.8) of Chapter II.

$$\dot{m}x + eBy = P_x \text{ , or} \tag{2.8}$$

$$\dot{x} = -2\omega_L y + \frac{P_x}{m} \text{ .} \tag{5.8}$$

The constant P_x can be evaluated at any point in the motion. At a point where $y = h$, $\dot{x} = 0$, and $P_x = 2m\omega_L h$. Thus

$$\dot{x} = -2\omega_L (y - h) \text{ , or}$$

$$x = -2\omega_L \int_o^t (y - h)\, dt \text{ .} \tag{5.9}$$

Thus $x(t_o)$ can be obtained as an area on the graphs of y as a function of time, the area bounded by the line $y = h$, the line $\omega_L t = 0$, the line $\omega_L t = \omega_L t_o$, and the curve of y as a function of $\omega_L t$. These x-displacements were calculated from the curves in Fig. 5.5 and those in Appendix C for $2\omega_L t = 4$, 6, 8, and 10. For each of the three potential fields considered, the points corresponding to each of the initial conditions are plotted in Figure 5.6. The points corresponding to a particular $\omega_L t$ are encircled by a dashed curve; they give a rough idea what sort of a beam spot might be expected in the trajectron under the corresponding conditions.

The calculated "beam spots" shown in Figure 5.6 differ markedly for the three cases, the B_o, B_1, and B_2 solutions. The differences are great enough so that if the space charge in the magnetron were known to be of one of these types, it would be quite obvious from the trajectron data which one occurred. For the B_o or B_2 type space charge, the calculated spots deflected beyond the maximum radius portion of the orbit have

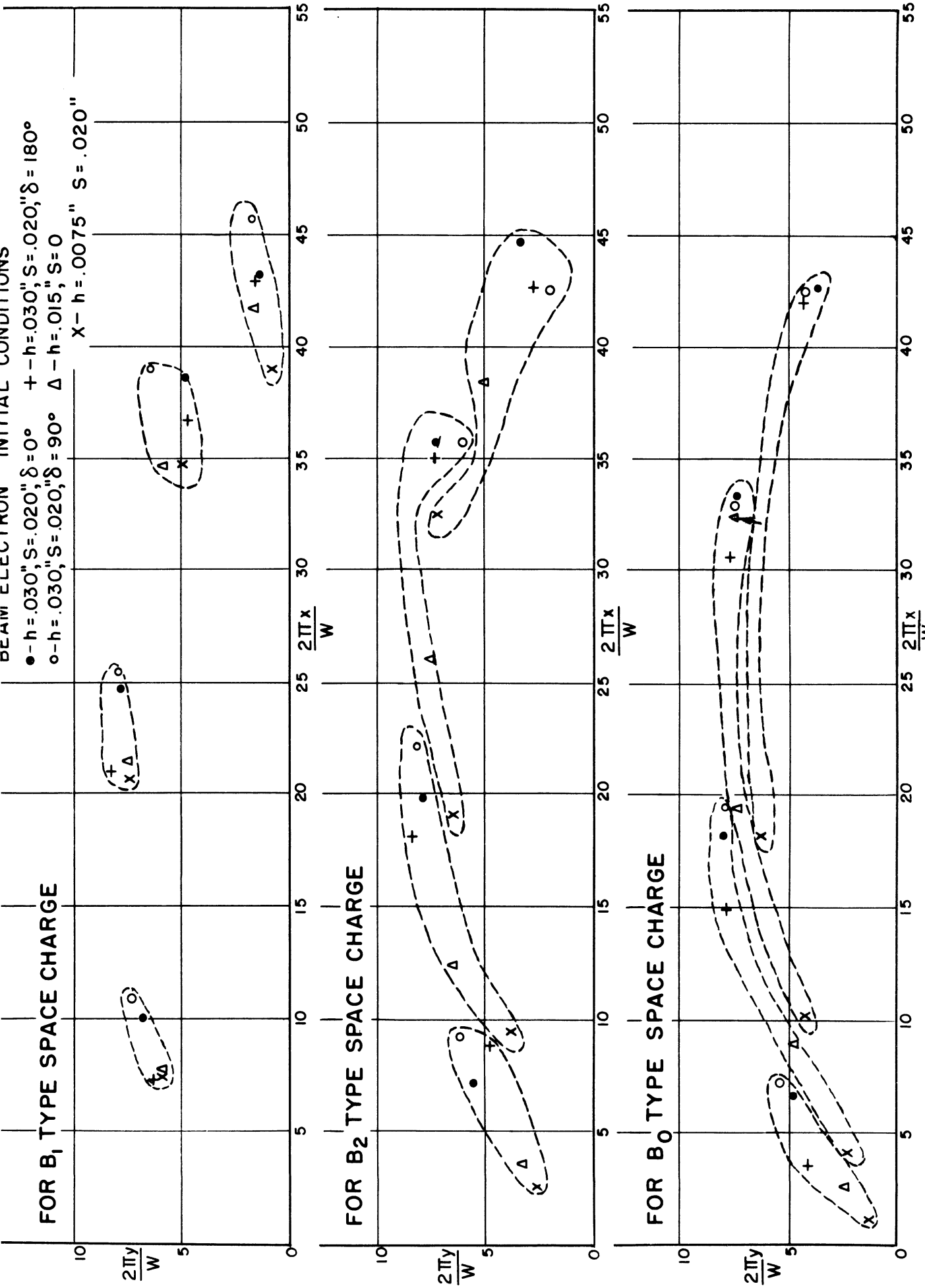

FIG. 5.6 CALCULATED BEAM SPOTS FOR PLANAR MAGNETRON
($2\omega_L t$ = 4, 6, 8, AND 10)

their leading ends nearer the cathode than their trailing ends, in the manner illustrated in Figure 5.7a. The opposite is true for the B_1 type space charge; the spots for the B_1 case resemble Figure 5.7b. In this respect the trajectron data definitely resembles the "spots" calculated for the B_1 solution. The difference between the observed spots in the trajectron data and the calculated "spots" for the B_0 and B_2 solutions is great enough for us to conclude that these solutions do not occur. Even for the B_1 solution there are differences, however, between the calculated "spots" and the spots observed on the trajectron. In the first place, the spots in the trajectron data are somewhat longer than the calculated spots. In the second place, in the trajectron data for all spots the trailing end is closer to the cathode than the leading end, while the calculated "spot" for the B_1 solution which is roughly at the maximum radius of the orbit is nearly parallel to the cathode. The potential minimum certainly accounts for some lengthening of the spot, but it cannot account for the increase in radial width of the spots, and hence it cannot account for the fact that the leading end of the spot always has a considerably greater radial displacement than the trailing end. The explanation of this latter observation seems to lie in the presence of secular space charge and electric field fluctuations in the diode.

The two photographs in Figure 5.1 differ only in the orientation of the magnetic field. Physically the only important difference is in the initial conditions of the beam. When the magnetic field was reversed with no anode voltage applied to the magnetron diode, the beam was observed to shift only .010 to .020 inches; i.e., an amount somewhat smaller than the initial displacement of the beam. This difference in initial conditions

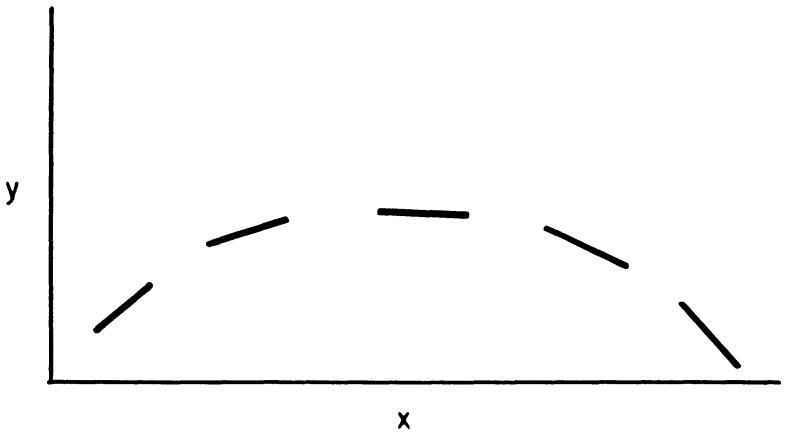

(a.)

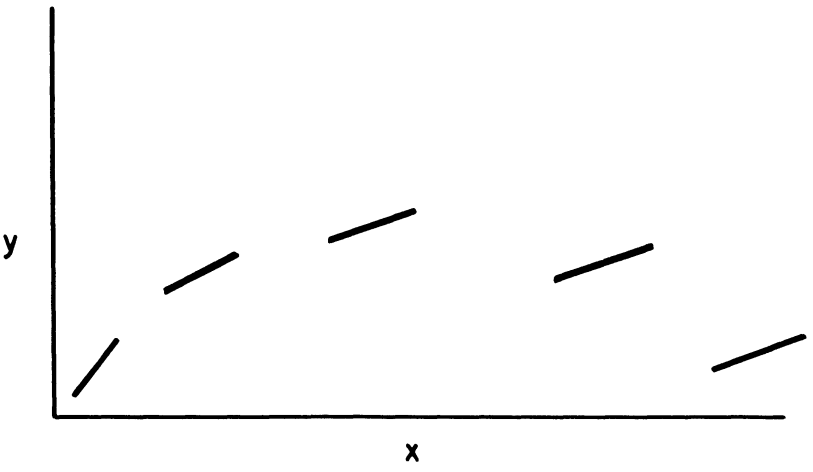

(b.)

FIG. 5.7
IDEALIZED BEAM SPOTS

resulted in a difference in spot displacement between the two photographs in Figure 5.1 which are of the order of magnitude of the spot width itself. This difference between the two photographs is another indication of the strong dependence of displacement of beam electrons on their initial conditions.

5.6 The Effects of Secular Space Charge

Calculations similar to those described in Sections 5.3 and 5.4 were carried out assuming the presence of secular space charge. For both sets of calculations the secular space charge was assumed to be proportional to the space charge density of the B_0 solution, i.e., the space charge density given by equations (2.104) and (2.107). Thus

$$\rho_s (aR) = m\omega_L^2 \epsilon_0 Q(R) = m\omega_L^2 \epsilon_0 k_5 \left(1 + \frac{1}{R^4}\right). \qquad (5.10)$$

The calculations of maximum radius of beam electron orbits are summarized in Table 5.2[1]. In the description of the aligned electron beam in the trajectron, it appears that h could not be less than about .008". The values .004", .002", and .001" were included in this calculation for two reasons. In the first place, for the purpose of calculations h should be measured from the potential minimum near the cathode (i.e., the virtual cathode) rather than from the cathode itself. The difference may be several thousandths of an inch, especially since the presence of the secular space charge reduces the amount of current of the cathode accessible electrons. The second reason for considering the small values of h is that

---

[1] The method of finding effective potential for this case is described in Appendix D. Otherwise the method is the same as that of Section 5.3. Only the B_1 type of solution was considered.

there is a greater dependence of maximum radius upon h where there is secular space charge.

It can be seen from Table 5.2 that the range of maximum radius of beam electrons increases from .39a without secular space charge to .75a with secular space charge equal to 75% of the B_o solution[1]. Thus the presence of secular space charge can account for the observed range of maximem radius (i.e., 75% of the B_o space charge) agrees reasonably with the amount of secular space charge estimated from the observed reduction in maximum radius of orbits (i.e., 58% of the B_o space charge).

TABLE 5.2

MAXIMUM RADIUS OF BEAM ELECTRON ORBITS WITH SECULAR SPACE CHARGE ($R_h = 1.75$),

$$\rho_s = m\omega_L^2 \epsilon_o k_5 \left(1 + \frac{1}{R^4}\right)$$

Initial Conditions								
h	.030"	.030"	.030"	.015"	.0075"	.004"	.002"	.001"
S	.020"	.020"	.020"	0	0	0	0	0
δ	0°	± 90°	180°	-	-	-	-	-
Maximum Radius of Beam Electron Orbit								
$k_5 = 0$	1.88	2.05	2.17	1.97	1.91	1.86	1.83	1.78
$k_5 = 1.0$	2.13	2.28	2.38	2.12	1.99	1.93	1.87	1.83
$k_5 = 1.5$	2.45	2.53	2. 2	2.30	2.12	2.03	1.93	1.87

Calculations were made of orbits of beam electrons in a planar diode with varying amounts of secular space charge[2]. The results are presented in Figure 5.8 in the form of calculated beam "spots" similar to those of Figure 5.6. Only the B_1 type solution was considered and in order

---

1 Equation (5.7) with $K_5 = 2$ is the expression for space charge density for the B_o solutions.

2 The details of the calculation are described in Appendix D.

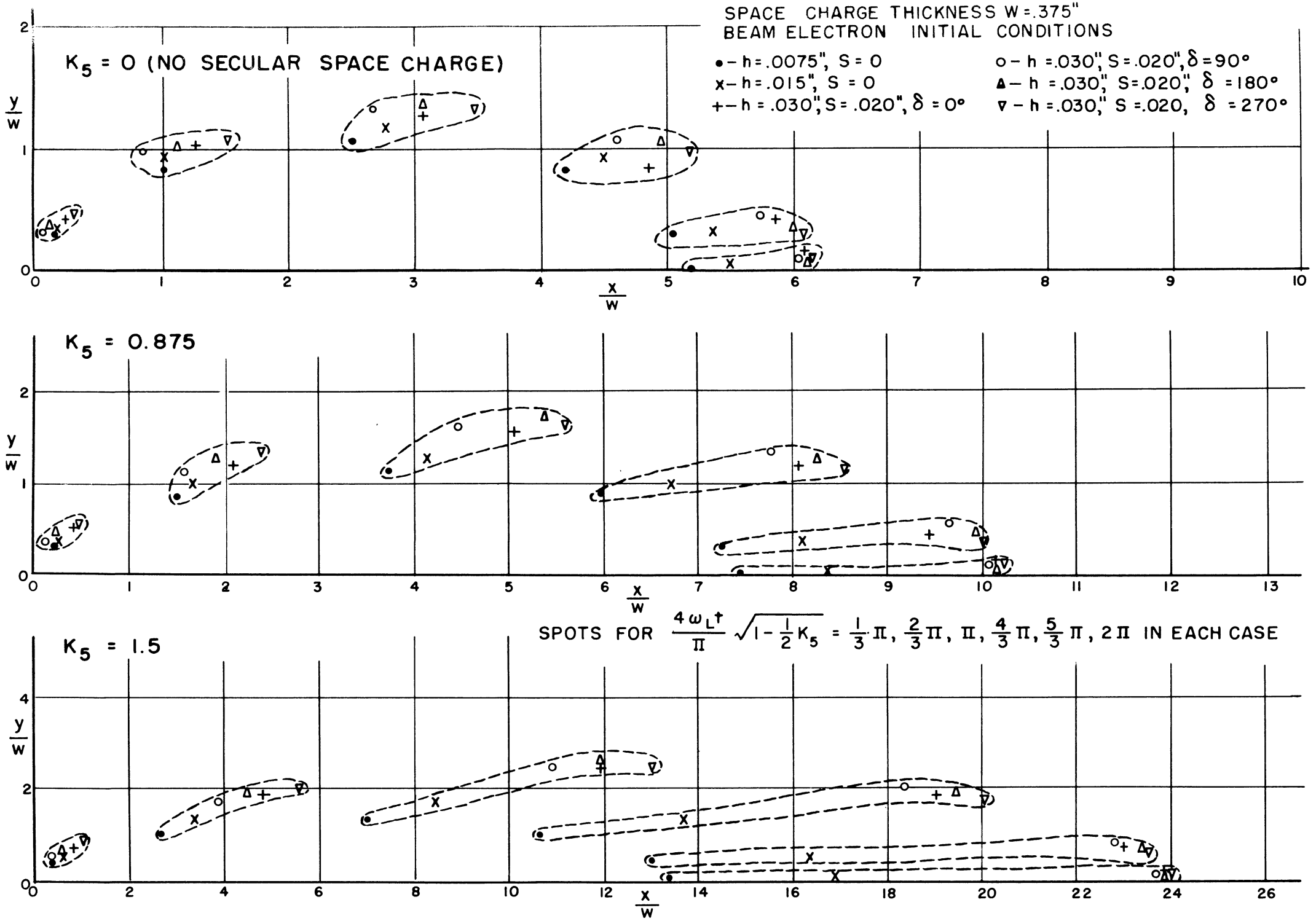
SPACE CHARGE THICKNESS W=.375"
BEAM ELECTRON INITIAL CONDITIONS
●– h=.0075", S = 0
x– h=.015", S = 0
+– h = .030", S=.020", δ = 0°
o – h =.030", S=.020", δ=90°
Δ– h =.030", S=.020", δ =180°
▽ – h =.030," S =.020, δ =270°
K5 = 0 (NO SECULAR SPACE CHARGE)
K5 = 0.875
K5 = 1.5
y/w
x/w
SPOTS FOR 4ωLt/π √(1 − ½K5) = ⅓π, ⅔π, π, 4/3π, 5/3π, 2π IN EACH CASE

to simplify the calculations, the effective potential was approximated by a parabola. The results for the case of no secular space charge compare well with those presented in Figure 5.6. The radial spread and the length of the spots increases with the amount of secular space charge. (Note that the scales are different for each case in Figure 5.8.) The spots become very similar to those observed in the trajectron.

5.7 The Effect of Field Fluctuations on the Shape of the Beam Spot

Another possible cause for the increased size of the beam spot is fluctuations of the electric field in the magnetron diode. Some idea of what effect might be expected is given by the following very simple example. Consider an ideal planar magnetron in an ideal trajectron (i.e., one which actually traces out electron orbits). Fluctuations in the field are introduced by applying to the anode a voltage which fluctuates between a minimum and a maximum value, the fluctuations being slow enough so that the anode voltage is essentially constant during the transit time of an electron, but fast enough so that it appears to spread out the spot. Now consider the shape of the resulting spot. The orbits for the anode voltage at its minimum and maximum appear in Figure 5.9 as dashed curves. At fixed beam voltage, or fixed transit time, the x and y deflections increase in the same proportion when the anode voltage increases. Thus the spot would be a straight line between the maximum and minimum orbits, which would intersect the origin if extended. Several such spots are drawn in Figure 5.9. They are of the type illustrated in Figure 5.7b, the type which was found to occur in the trajectron. For the cylindrical case the transit time is somewhat greater for the larger orbits so that the leading end would be expected to be a small distance from the cathode when the

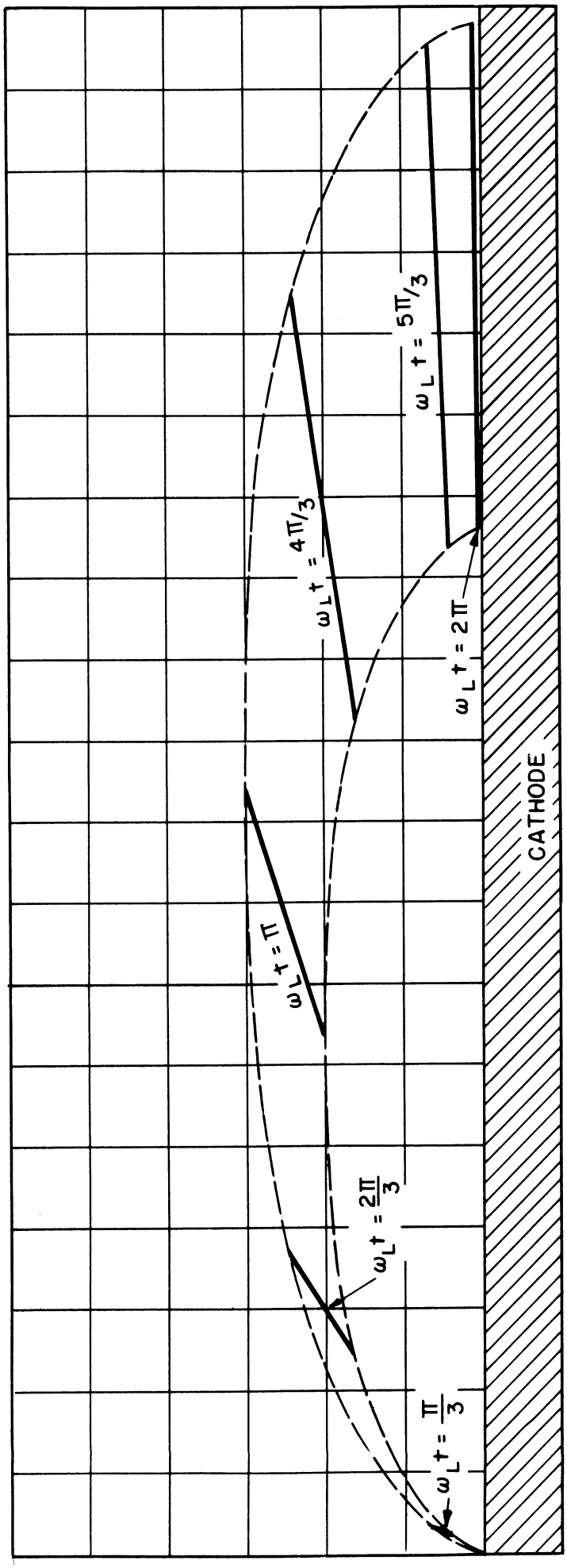

FIG. 5.9
BEAM SPOTS IN AN IDEAL TRAJECTRON
WITH FLUCTUATING ANODE VOLTAGE
(PLANAR MAGNETRON)

trailing end meets the cathode. The spots have this appearance in the trajectron data. Field fluctuations would have to be very great, however, to make the spot as large as it is observed to be.

Three possible causes for the large size of the observed spots have been suggested. The first, the potential minimum, undoubtedly contributes to the length of the spots, but cannot have much effect on the radial dimensions of the spot. The other two, secular space charge and electric field fluctuations are expected to result in a spot configuration similar to that observed in the trajectron data. On the basis of the evidence at hand there appears to be no way to determine to what extent each contributes to the size of the spot.

5.8 The Magnetron at Approximately the Cutoff Voltage

When the anode voltage is a small fraction of the cutoff voltage, the anode current is extremely small. As the anode voltage is increased, the anode current increases. It increases rapidly near the cutoff voltage, and above the cutoff voltage the anode current is nearly as great as it would be with no magnetic field. Several curves of anode current versus anode voltage for the trajectron diode are shown in Figure 1.1. These data are replotted in normalized form in Figure 5.10.

The anode current at cutoff can be found from equation (2.76) of Chapter II.

$$b = \frac{eJ}{m2\pi \epsilon_o \omega_L^3 a^2} \qquad (2.76)$$

where J is the cathode current density. If numbers are substituted for the physical constants and the trajectron dimensions, this becomes

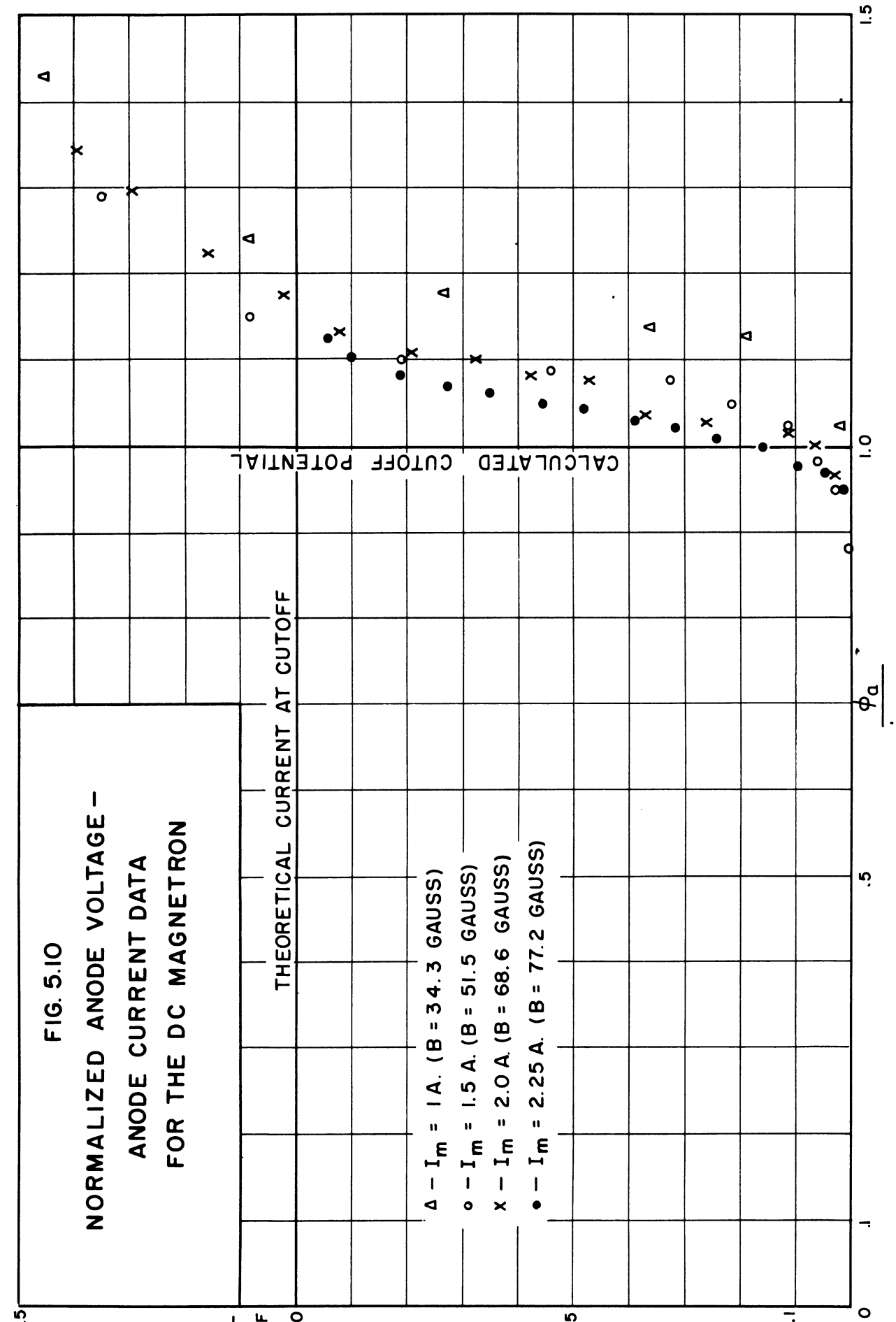
FIG. 5.10
NORMALIZED ANODE VOLTAGE – ANODE CURRENT DATA FOR THE DC MAGNETRON
THEORETICAL CURRENT AT CUTOFF
CALCULATED CUTOFF POTENTIAL
Δ – Im = 1 A. (B = 34.3 GAUSS)
o – Im = 1.5 A. (B = 51.5 GAUSS)
x – Im = 2.0 A. (B = 68.6 GAUSS)
• – Im = 2.25 A. (B = 77.2 GAUSS)
Ia / ICUTOFF
φa
1.5
1.0
.5
.1
0
.5
1.0
1.5

$$I_a = 4.75 \cdot 10^{-7} B^3 b \text{ ma} \quad (B \text{ in gauss})$$
$$= 0.0192 I_m^3 b \text{ ma} . \qquad (5.11)$$

At cutoff, $R_h = R_a = 3.65$, and b is found from differential analyser solutions to be approximately 2.7. For the values of magnet current appearing in Figure 1.1, the anode current calculated from equation (5.11) is indicated on the figure. At the calculated cutoff potential the actual current was always considerably less than the theoretical current. It does not appear that the discrepancy can be attributed to errors in the measurement of anode potential magnetic field, or anode current. Probably it results from the fact that this diode was not an infinite cylindrical magnetron, but on the contrary had rather severe end effects.

Two photographs of trajectron data for the magnetron diode approximately at cutoff are shown in Figure 5.11. The theoretical orbits obtained from the differential analyser solution and circles representing the cathode surface have been drawn on the photographs. The data and theoretical curves are replotted in Figure 5.12 to show displacement as a function of time. The parameter b was calculated from equation (2.76) using the observed value of anode current and taking B as 34.3 gauss per ampere of magnet current.

The beam spots are farther from the cathode than the theoretical orbit, and they obviously would reach the maximum radius portion of the orbit sooner and with a smaller angular displacement. The maximum radial displacement of the beam spot clearly would be greater than the maximum radius of the theoretical orbit, but since the last beam spot appearing on the photograph is not at the maximum radius, a quantitative comparison of the

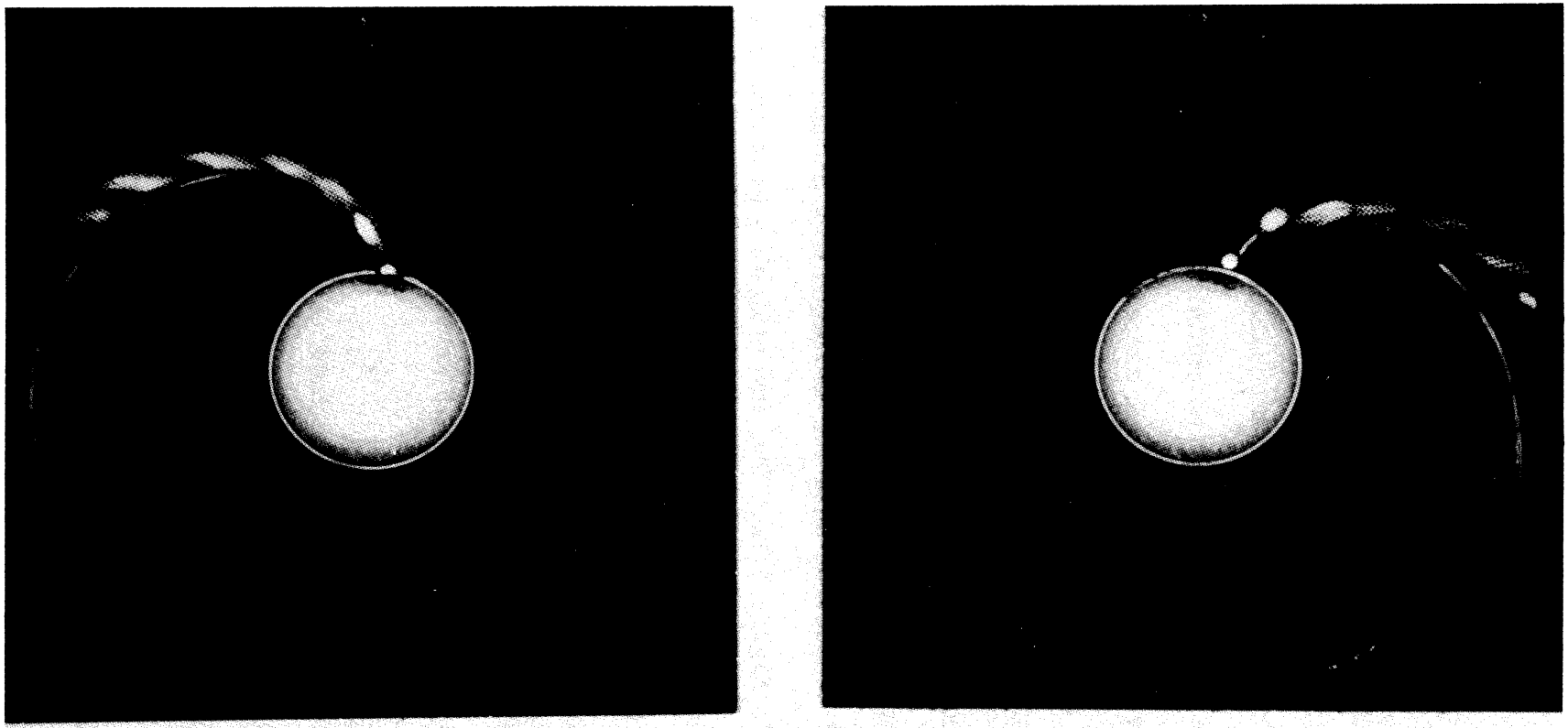

ϕ_a = 475 V., I_m = 1.75 A., I_a = 280 ma.

ϕ_{BEAM} = 500, 600, 750, 1000, 1500, 3000 VOLTS

(THEORETICAL CURVE IS FROM DIFFERENTIAL ANALYSER DATA WITH b = 2.7)

FIG. 5.11 TRAJECTRON DATA FOR THE DC MAGNETRON AT APPROXIMATELY CUTOFF

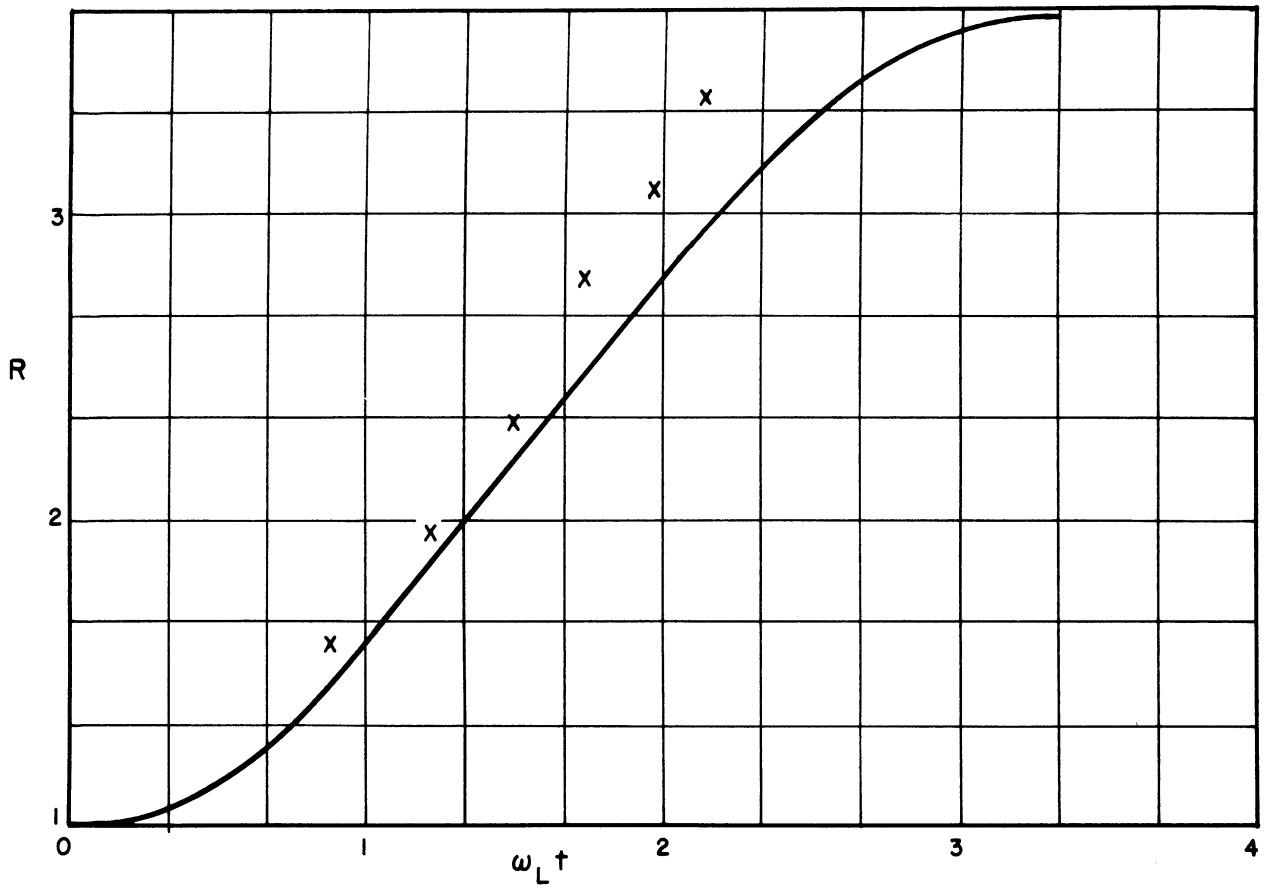

THE THEORETICAL CURVES ARE FROM DIFFERENTIAL ANALYSER SOLUTIONS WITH b = 2.7

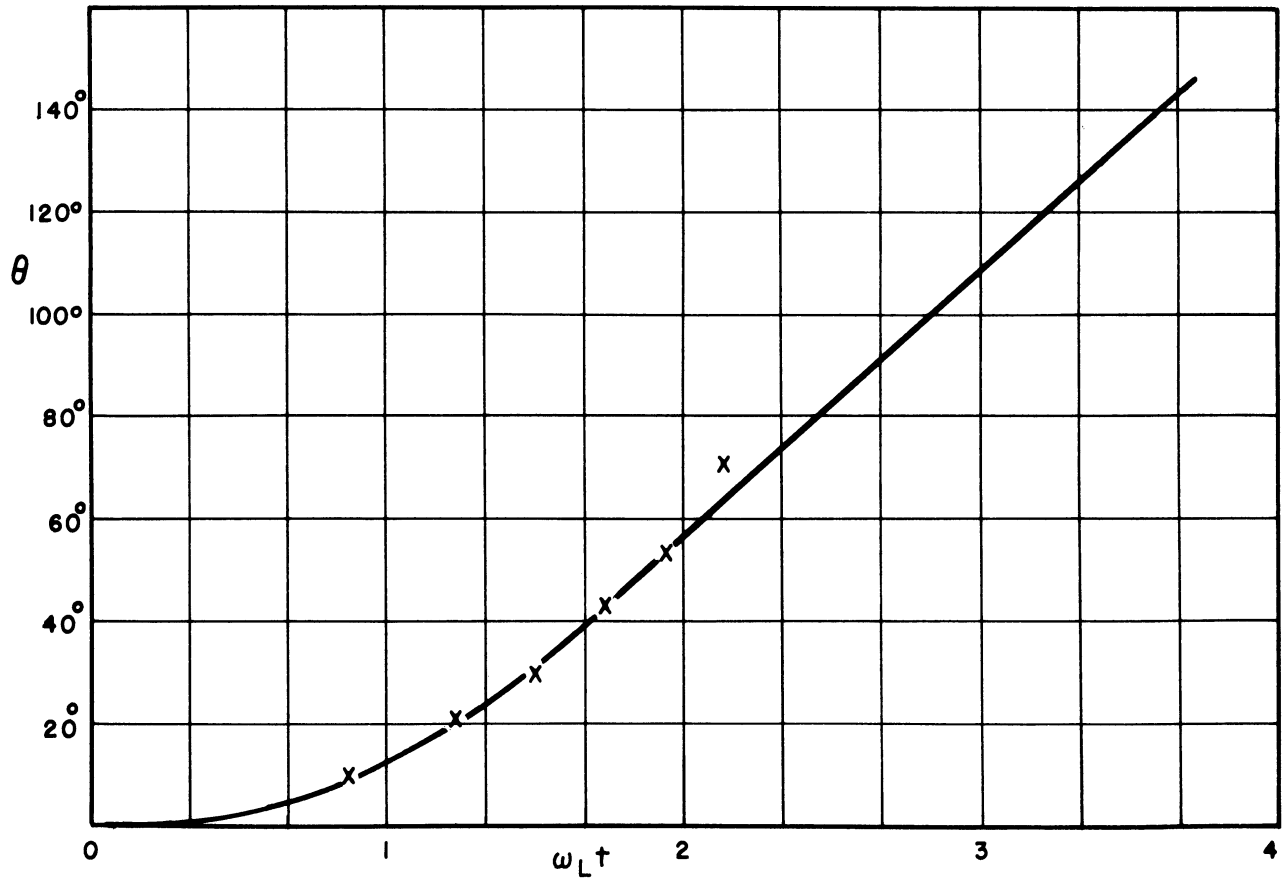

FIG. 5.12 BEAM DISPLACEMENT AS A FUNCTION OF TRANSIT TIME FOR THE MAGNETRON APPROXIMATELY AT CUTOFF

maximum radius of the beam spots and of the theoretical orbit cannot be made.

The initial spot in these photographs appears to be well aligned, and yet the spots do not spread out as far in this case as in the case with emitting cathode and no magnetic field (Section 4.5). The diode cathode was certainly capable of emitting more than the anode current of 280 ma measured when these data were taken, and hence the diode was certainly space-charge limited. With so much anode current, however, the potential minimum was probably very near the cathode. The beam was not as close to the cathode in this case as when data were taken with no magnetic field. Furthermore, the beam electrons are traveling in helical paths and have greater initial radial and angular components of velocity with the magnetic field present than in the case of no magnetic field, and in this sense are not so near the potential minimum as beam electrons were with B = 0.

5.9 Irregularities in the Volt-Ampere Characteristics of the DC Magnetron

The low current region of a volt-ampere curve like those of Figure 5.10 is plotted in Figure 5.13 to show the details of the variation of anode current with anode voltage in this region. The curves show some inflection points, and even regions of negative resistance or discontinuities. It was found that these regions always occur in the same range of values of ϕ_a/B^2 as the anode voltage and magnetic field are varied. Some data showing this are presented in Figure 5.14, where the vertical lines represent observed regions of negative resistance and dots represent inflection points observed in the anode current as the anode voltage was varied. The data were taken on an early model of the trajectron diode.

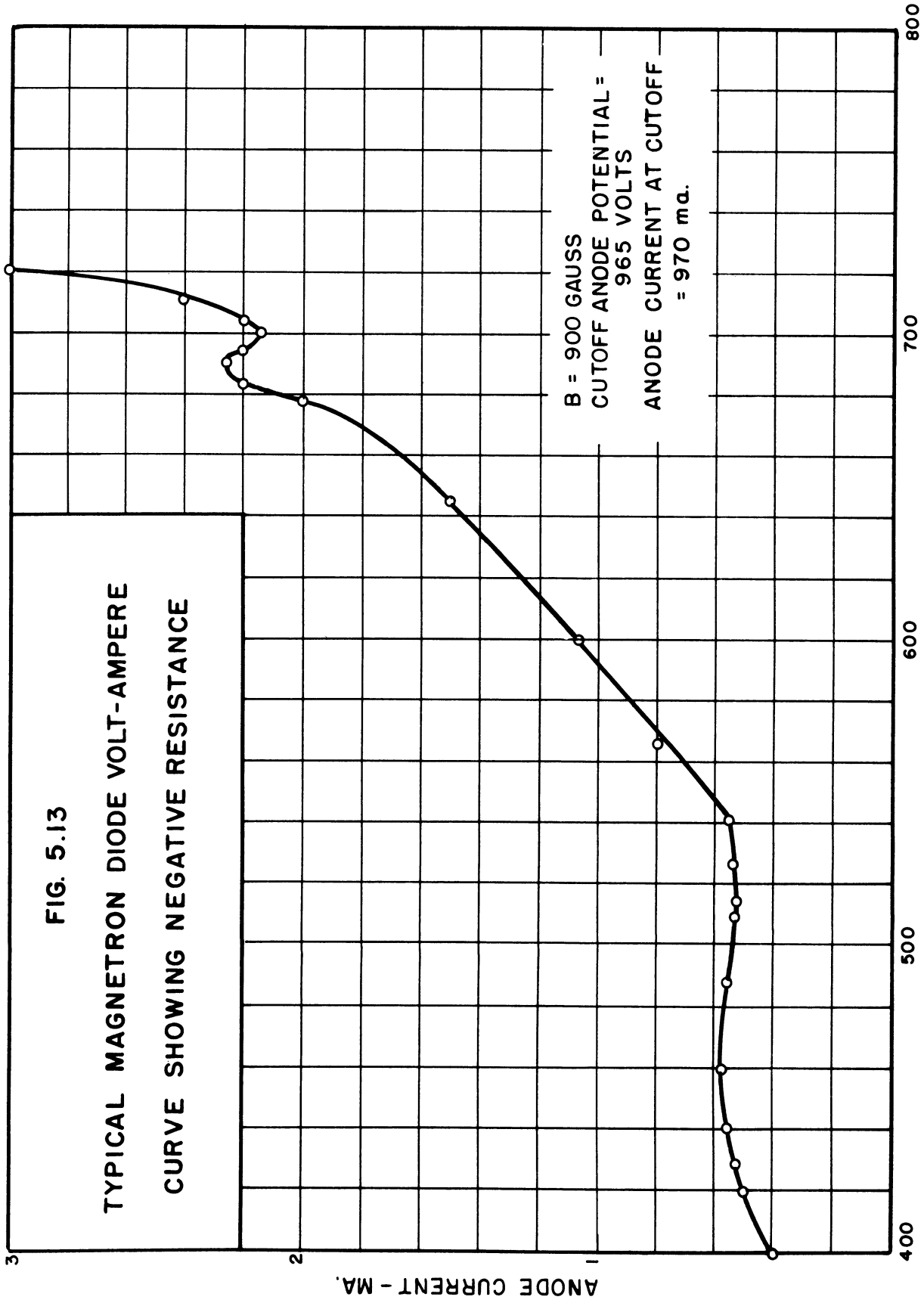

FIG. 5.13

TYPICAL MAGNETRON DIODE VOLT-AMPERE CURVE SHOWING NEGATIVE RESISTANCE

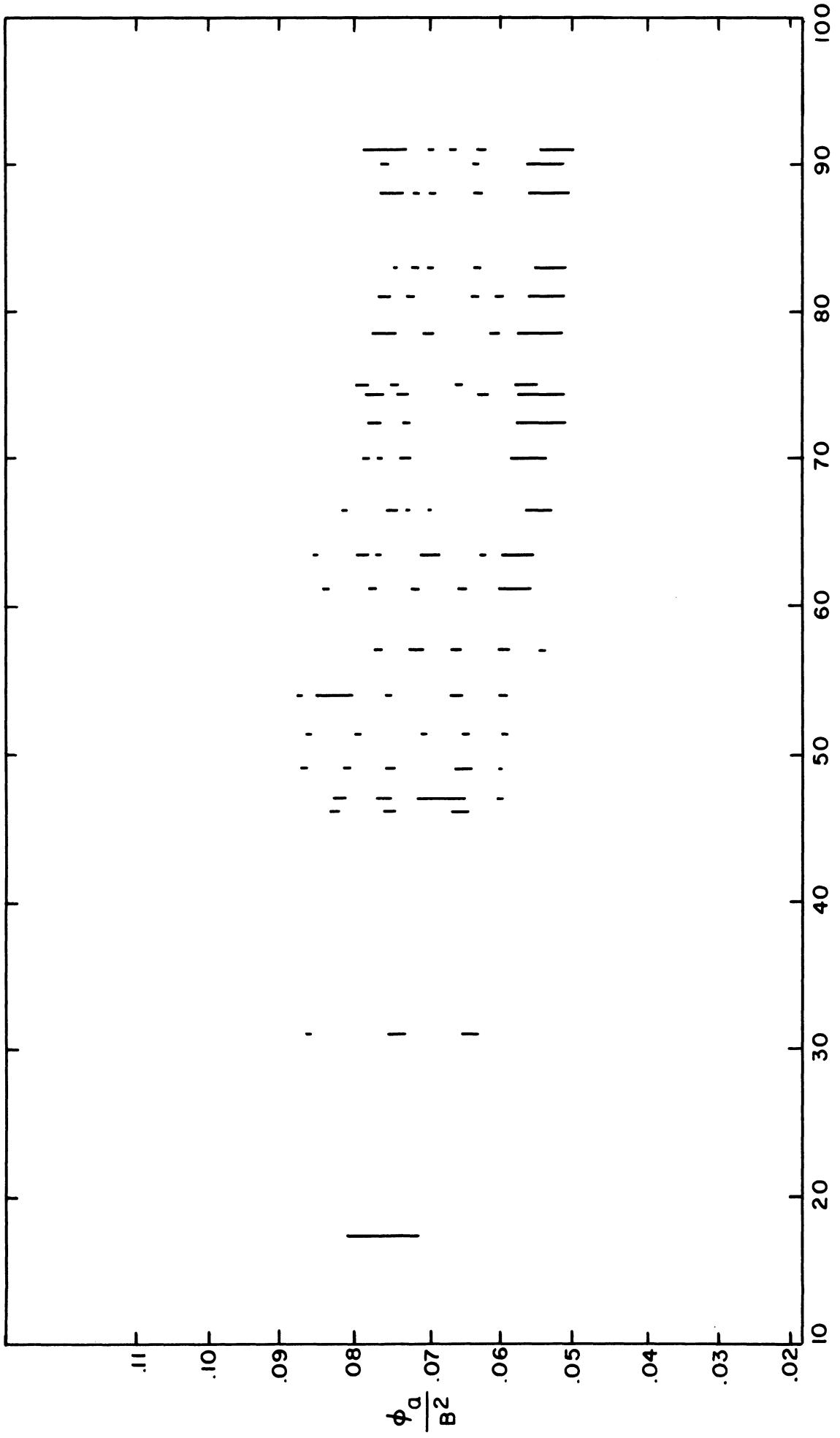

FIG. 5.14

POINTS WHERE NEGATIVE OR ZERO RESISTANCE HAS

This phenomenon was observed also by Delcroix[1], who built a series of cylindrical dc magnetrons with the ratio of anode radius to cathode radius ranging from 1.25 to 7.5. He interpreted these regions of irregularity in anode current as regions in which the space charge changes from one to another of the solution types found theoretically possible in the theory of the dc cylindrical magnetron presented in Chapter II. The same explanation occurred to the author when he observed this phenomenon. Indeed the irregularities occur in very nearly the range of ϕ_a/B^2 predicted by the theory. Any discrepancy between the location of observed regions of irregularity and theoretical region of possible transitions for the case of no secular space charge could certainly be attributed to the presence of secular space charge.

With the trajectron there was additional information available. The changes in the beam spot resulting as the anode voltage was varied could be observed. Such observations are described in the following paragraphs. They do not appear to substantiate the hypothesis that the irregularities in the anode current-anode voltage curve associated with transitions from orbits of one type to orbits of another type.

A series of experiments were run in which the anode current, the beam spot, and the low frequency components of noise in the anode current were observed simultaneously as the anode voltage was increased from zero through the cutoff voltage. The noise was observed on a Techtronix 514D oscilloscope, which was connected to the anode circuit of the trajectron in the manner shown in Figure 5.16. The following data were taken with a magnet current of 3.5A, and with a beam voltage of 1300 V.

---

[1] Refs. 14, 15, and 16,

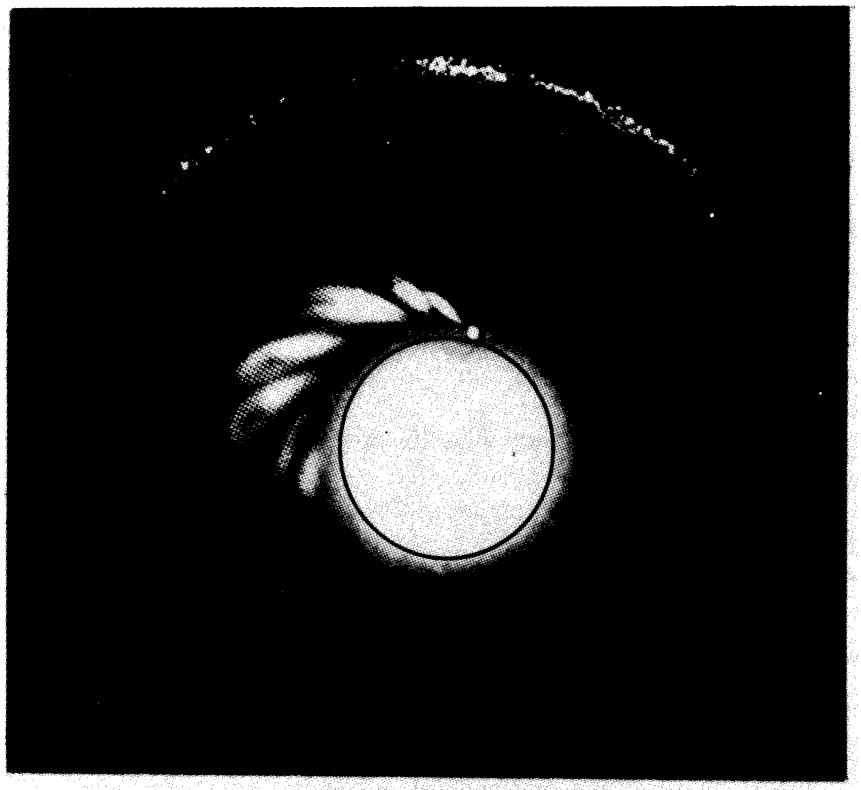

ϕ_a = 1233 V. , I_a = 2.5 ma., I_m = 4 A.

I_{BEAM} = 550, 710, 910, 1070, 1480, 1980, 3020, 4020

FIG. 5.15

TRAJECTRON DATA INDICATING
THE PRESENCE OF OSCILLATION

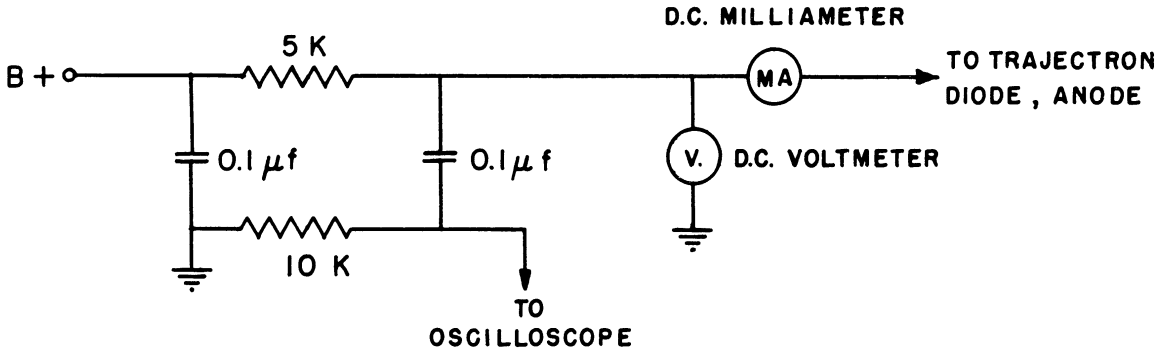

FIG. 5.16 CIRCUIT FOR OBSERVING NOISE IN ANODE CURRENT

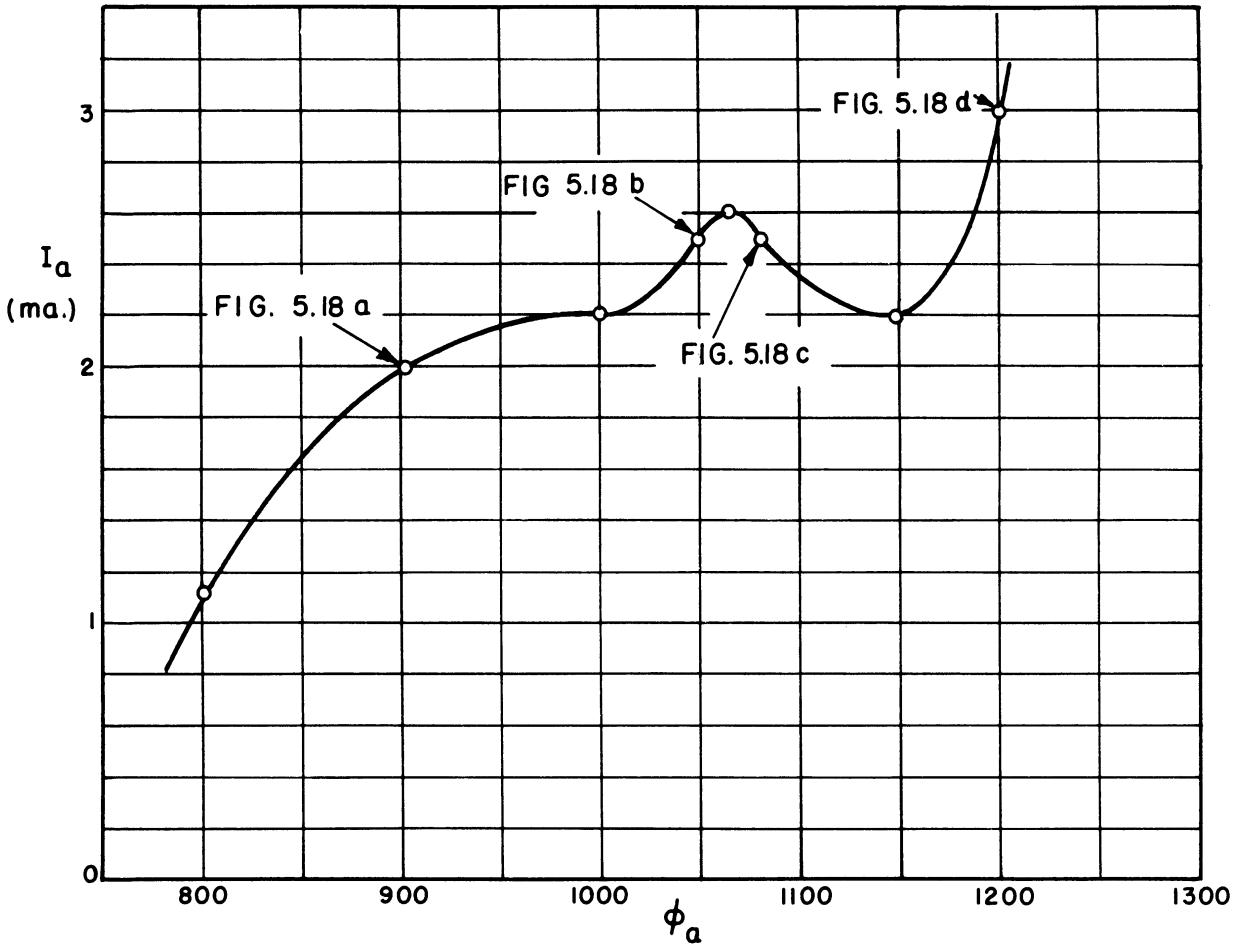

FIG. 5.17 ANODE VOLT-AMPERE CURVE, SHOWING POINTS AT WHICH DATA PHOTOGRAPHS WERE TAKEN.

When the anode voltage reached 260 V., a small voltage appeared on the oscillosxope. It was an oscillation at approximately 8 mc. It also appeared at ϕ_a = 370 V., I_a = 0.05 ma. Noise appeared with an amplitude of .03 V. at ϕ_a = 500 V., I_a = 1 ma. The noise had components as high in frequency as the oscilloscope could amplify (10 mc). The noise became jumpy at about ϕ_a = 800 V., I_a = 1.1 ma. (There were fluctuations in noise amplitude with frequencies of a few cycles per second.) The noise built up to approximately 0.33 volt amplitude at ϕ_a = 850 V., I_a = 2 ma. The maximum frequency of this noise was approximately 0.5 mc. There was a relative maximum in anode current at ϕ_a = 930 V., I_a = 2.1 ma, and a relative minimum at ϕ_a = 960 V., I_a = 2.0 ma. The noise disappeared at the relative minimum, and the beam spot jumped at .025" toward its undeflected position. There was no observed change in the spot size or shape.

An unsteady oscillation at approximately 0.5 mc appeared at ϕ_a = 1000 V., I_a = 2.5 ma. There was a relative maximum in anode current at ϕ_a = 1050 V., I_a = 2.6 ma. The oscillation stopped at this point. There was a relative minimum at ϕ_a = 1090 V., I_a = 2.3 ma, and the spot jumped back .010" at this point. Beyond this relative minimum, noise appeared which had frequency components in the entire range of the oscilloscope. The noise increased in amplitude continuously as the anode voltage was increased toward the cutoff voltage, where it reached an amplitude of approximately five volts.

On several occasions the spot took on the shape of a loop, suggesting that some sort of oscillation occurred. Such data are shown in Figure 5.15. This was observed only with relatively strong magnetic fields ($I_m \geq 3.5A$) and with the anode voltage a little below the voltage at

which the first inflection point in the graph of anode current occurred. It was not found to occur consistently. Oscillations were not observed on the oscilloscope in this range of anode voltage. No further search for oscillations was made.

Photographs of beam spots in this range appear in Figure 5.18. Figure 5.17 is a graph of the anode current versus anode voltage, showing the points at which photographs were taken. Figure 5.18a was taken just below the inflection point. Figure 5.18b was taken between the inflection point and the relative maximum. Figure 5.18c was taken between the relative maximum and the relative minimum. Figure 5.18d was taken just above the relative minimum. Another set of photographs of this type is included in Appendix E.

There is one striking thing about these data. The spot does not change much as the anode voltage is increased through the region in which inflections occur in the anode current. Judging from the calculated "spots" of Figure 5.6, one would expect that if the space charge changed from that of one solution to that of another (as B_o to B_1 or B_1 to B_2), there would be a conspicuous change in the configuration of the spot at the same time as the spot is observed to jump back. This did not occur in any observed situation. The series of photographs shown in Figure 5.17 show no sign of the change in spot configuration which would be expected to occur if the space charge changed character from one solution to another. The spots in these photographs are very similar from one photograph to the next -- corresponding spots even have the same general shape. The transition in spot configuration through this series of photographs appears to be smooth and uniform -- there is no sign of the change in spot configuration which one would expect to accompany a change in the type of space charge.

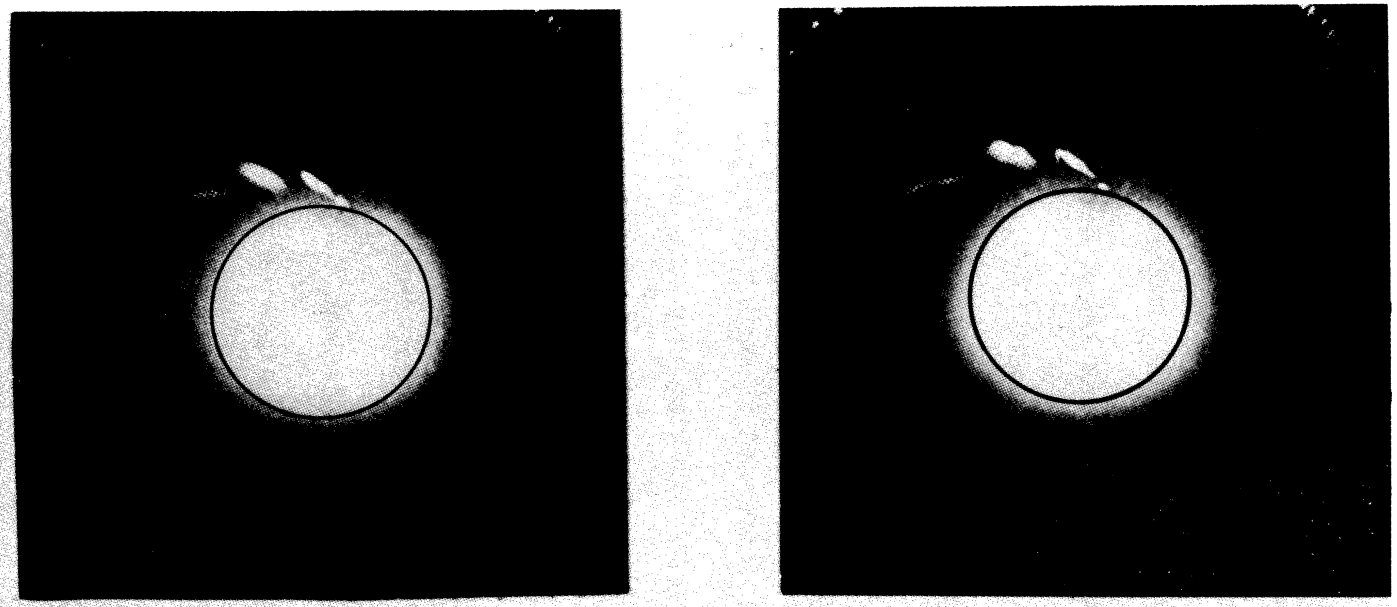

(a.) ϕ_a = 920 VOLTS, I_a = 2 ma (b.) ϕ_a = 1080 VOLTS, I_a = 2.5 ma.

I_m = 3.5 A.

ϕ_{BEAM} = 500, 1000, 1980, 4020 VOLTS

FIG. 5.18

TRAJECTRON DATA NEAR ANODE CURRENT INFLECTIONS

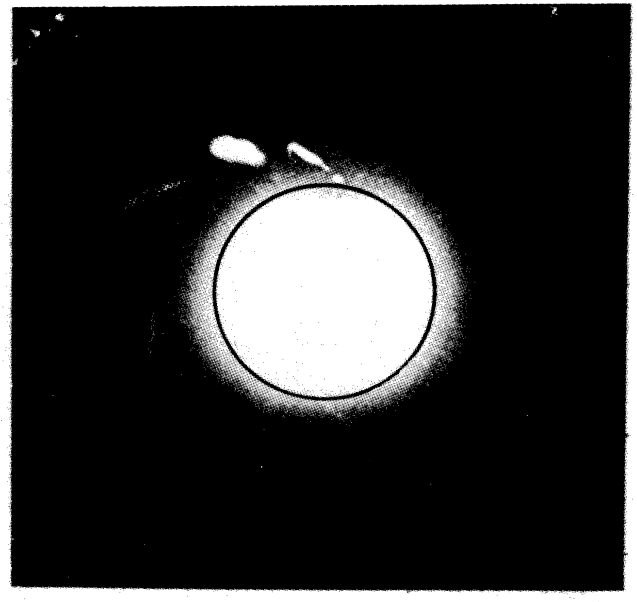

(c.) ϕ_a = 1115 VOLTS, I_a = 2.5 ma.

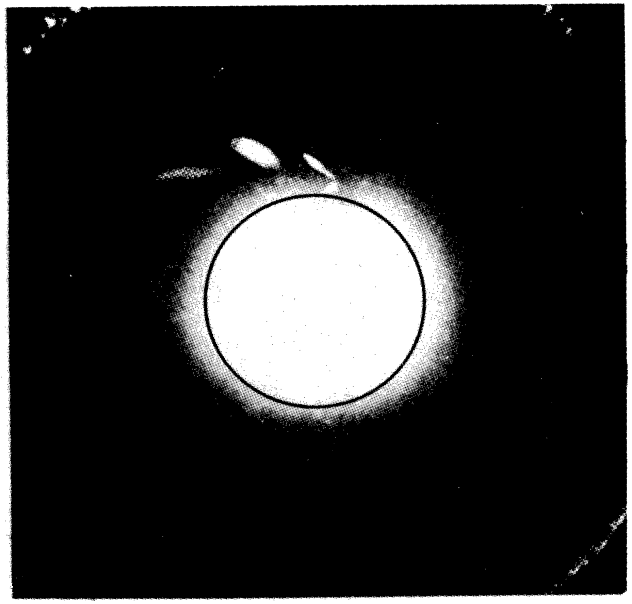

(d.) ϕ_a = 1240 VOLTS, I_a = 3 ma.

I_m = 3.5 A.

ϕ_{BEAM} = 500, 1000, 1980, 4020 VOLTS

FIG. 5.18

TRAJECTRON DATA NEAR ANODE CURRENT INFLECTIONS

Certainly, if the space charge in the dc magnetron were closely approximated by the solutions described in Chapter II for the case of no secular space charge, and if the inflection in anode current did accompany changes in the space charge from one type of solution to another, then changes in the shape of the spot of the order of magnitude indicated by the calculated beam spots of Figure 5.6 would have occurred. The changes would have been observed easily. It follows that at least one of these conditions is contrary to fact. It was concluded in Section 5.3 that a substantial portion of the space charge in the dc magnetron under cutoff conditions is secular space charge. The presence of the secular space charge would decrease the amount of cathode-accessible space charge, and the effect on the beam spot of changes in the character of this cathode-accessible space charge would be lessened. It is possible that the changes from one type of solution to another do occur in the cathode accessible space charge, but that the amount of cathode accessible space charge is so small that the effect on the beam is unnoticeable. On the other hand, the trajectron data does not support the theory that the inflections in anode current are indications of changes in the solution type of the cathode accessible space charge. A possible alternative theory to account for the inflections in anode current is discussed below in connection with noise in the dc magnetron.

The observations of noise in the anode current of the trajectron are probably not significant because they cover such a small portion of the spectrum. A measurement of noise could not be considered complete unless it covered the spectrum from zero frequency to beyond the cyclotron frequency, which for the trajectron would range between 140 and 450 mc. Some measurements in the high frequency range have been made on the dc magnetron

by Warnecke and his coworkers[1]. They observed what they described as oscillation in the microwave region. They gave the following explanation for the presence of these oscillations. It is apparently possible to have waves propagate around the cathode and be amplified at the same time. In the cylindrical magnetron the path of propagation closes on itself. At any frequency for which the phase shift is an integral multiple of 2π for the complete path, oscillation is possible. Warnecke[2] analyzed the propagation of waves in the space charge of the B_0 solution, and his analysis indicates that there is a mode with a different frequency possible for each integral multiple of 2π in phase shift. The experimental data correlated quite well with the predicted mode frequencies, and the third mode seemed to predominate.

The space charge in the magnetron appears not to be the B_0 type, but is more likely a combination of the B_1 type and secular space charge. Certainly the theory based upon B_0 type space charge cannot be expected to furnish details of the behavior of the magnetron. It is entirely possible that certain modes predominate in the actual dc magnetron only in certain ranges of anode voltage, and that the inflections which are observed in the anode current as the anode voltage is increased reflect changes in the space charge accompanying a change in mode in the space charge oscillations. In more general terms, it appears that the space charge in the magnetron has certain resonances, and that the space charge is unstable in such a way that oscillations can be sustained at these resonances. These resonances undoubtedly depend upon the space charge configuration, and hence upon the

---

1 Guénard and Huber, Ref. 23.

2 Refs. 46 and 47.

anode voltage. It is quite possible that as the anode voltage is increased the oscillation changes discontinuously from one mode to another, and the accompanying change in space charge results in the inflections noted in the anode current.

CHAPTER VI

CONCLUSIONS

6.1 The DC Magnetron

In the trajectron, an electron beam is sent through a dc magnetron diode and its exit point shows on a fluorescent screen. The beam is deflected by the fields in the magnetron, and through the study of the deflected spot, significant information can be obtained about the space charge distribution and potential distribution in a dc magnetron.

According to the most widely used theory of the dc magnetron in the cutoff condition, the space charge is confined to a region between the cathode and a maximum radius commonly called the Hull radius. One observed fact about the trajectron data is that the beam electrons' radial deflection was not as great as that predicted by calculations assuming no space charge outside the Hull radius. From this it can be shown that the space charge outside the Hull radius is not negligible. In fact, rough calculations based on the trajectron experiment, for a typical situation in which the Hull radius was located approximately one-fifth of the distance from the cathode to the anode, show the quantity of space charge outside the Hull radius to be several times the amount inside. The space charge outside the Hull radius must consist of electrons whose energy and

momentum have been changed from initial values by collisions or irregularities in the fields. Nearly all of these electrons have had their energy and momentum affected in such a manner that these electrons are trapped within the magnetron. Such space charge is called secular space charge.[1]

A second observed fact is that the spots in the trajectron data at the maximum radius part of their orbit have a much greater radial width than predicted by calculations in which secular space charge was neglected. Two factors which might contribute to this have been discussed. The first is the modification of the potential distribution due to the presence of secular space charge. The second is fluctuations of the electric field, which are known to occur in the dc magnetron. Calculations indicate that both of these should have essentially the same effect on the beam spot, to make it take on the shape and size which it is observed to have. Probably both factors contribute to the enlarging of the spot, but it does not appear possible to tell their relative importance.

A third observation on the cutoff magnetron concerns regions of negative resistance and inflections observed in the anode current-anode voltage curves in the cutoff region. These inflections in anode current were associated by Delcroix[2] with changes in the character of the space charge from one type of electron orbits to another. Some calculations neglecting secular space charge were made showing roughly the expected spot configuration for a beam entering space charge of the B_0, B_1, and B_2 types. The calculated beam spots indicated that changes from one type space charge to another should have resulted in a

---

[1] See Section 2.5, or Hok, Refs. 28 and 29.

[2] Refs. 14, 15, and 16.

conspicuous change in the spot configuration. No such changes were observed in the spot configuration. There appear to be two possible explanations. The inflections may not be associated with changes in space change type, but rather with some other phenomenon. (A possible alternative theory is suggested in Section 5.9.) The second possible explanation is that the inflections are associated with changes in the type of orbits of the electrons as they leave the cathode (i.e., the cathode accessible electrons), but that these electrons contribute so little and the secular space charge contributes so much to the total space charge that changes in the orbits of the cathode accessible space charge have a negligible effect on the beam spots.

6.2 The Trajectron Method

If the beam initial conditions could be made to match the initial conditions of emitted electrons closely enough and if end effects could be made negligible, the beam displacement as a function of transit time would be the same as the displacement of emitted electrons in the same time, making possible a very simple interpretation of the data. In spite of rather serious end effects the trajectron data for the cases with non-emitting cathode agreed reasonably well with the theoretical trajectories. It appears that end effects could be reduced in many problems to the point where fairly accurate trajectories could be traced out by the trajectron method.

A different situation arises in the important case in which the electric field is zero near the cathode, as it is at the potential minimum in any space-charge-limited electronic device. The deflected beam spreads out so much because of a defocussing effect of the

electric field, that the spot extends back to the potential minimum. This is shown both theoretically and by experimental results. In this case the beam spots do not represent displacement as a function of time for emitted electrons. The shape of the orbits of emitted electrons may or may not be given by the spots. Of course the electric field may still be studied through its effects on the electron beam, but the spot position cannot be interpreted as the displacement of emitted electrons as a function of transit time.

APPENDIX A

The purposes of this appendix are: (1) to show that the electron beam in the trajectron must be on an axis of symmetry of the field if its path is to be a straight line, and (2) to explain the observed variation in the beam spot in the trajectron as the anode voltage is varied. The magnetic field is assumed cylindrically symmetric, and the paths of electrons as they move from a region of zero magnetic field to a region of high magnetic field will be discussed. This was approximately the situation in the trajectron, since the electron gun was placed outside the solenoid.

The equations of motion can be obtained from the Lagrangian

$$L = \frac{m}{2}(\dot{r}^2 + r^2\dot{\theta}^2 + \dot{z}^2) - er\dot{\theta}A_\theta \qquad (A.1)$$

just as in Section 2.4. Here, however, ϕ is zero, and A_θ is a function of r and z. The equations of motion are, from (2.45),

$$m\ddot{r} - mr\dot{\theta}^2 + e\dot{\theta}\frac{\partial}{\partial r}(rA_\theta) = 0, \qquad (A.2)$$

$$m\ddot{z} - er\dot{\theta}\frac{\partial A_\theta}{\partial z} = 0, \text{ and} \qquad (A.3)$$

$$\frac{d}{dt}(mr^2\dot{\theta} - erA_\theta) = 0. \qquad (A.4)$$

The last equation can be integrated to give

$$P_\theta = mr^2\dot{\theta} - erA_\theta, \qquad (A.5)$$

where P_θ is a constant of integration.

The electrons for which $P_\theta = 0$ are relatively simple to study, and a discussion of their motion will indicate the answers to the two problems posed for this appendix. If $P_\theta = 0$,

$$\dot{\theta} = \frac{eA_\theta}{mr} , \tag{A.6}$$

and equation (A.2) becomes

$$\ddot{mr} - \frac{e^2A_\theta^2}{mr} + \frac{e^2A_\theta}{mr} \frac{\partial}{\partial r} (rA_\theta) = 0, \text{ or}$$

$$\ddot{r} + \frac{e^2A_\theta}{m^2} \frac{\partial A_\theta}{\partial r} = 0. \tag{A.7}$$

Since B = curl A, the z-component of B is

$$B_z = \frac{1}{R} \frac{\partial}{\partial r} (rA_\theta) = \frac{\partial A_\theta}{\partial r} + \frac{A_\theta}{r} , \text{ or} \tag{A.8}$$

$$A_\theta = \frac{1}{R} \int_0^r rB_z dr . \tag{A.9}$$

It can be shown that an axially-symmetric magnetic field in a region where there is no current flow is determined completely by its value on the axis of symmetry.[1] If cylindrical coordinates with the z-axis along the axis of symmetry are used, the components of the magnetic field B are

$$B_r(r,z) = - \frac{rB_o'}{2} + \frac{r^3B_o'''}{4\cdot 2^2} - \frac{r^5B_o(5)}{6\cdot 2^2\cdot 4^2} + \ldots ,$$

$$B_\theta(r,z) = 0 \quad , \text{ and} \tag{A.10}$$

$$B_z(r,z) = B_o - \frac{r^2B_o''}{2^2} + \frac{r^4B_o(4)}{2^2\cdot 4^2} - \ldots .$$

where B_o, a function of z, is the field strength on the axis.

---

[1] Spangenberg, Ref. G, p. 396.

This field can be derived from a vector potential A with the following components:

$$A_r = A_z = 0 ,$$

$$A_\theta = \frac{rB_o}{2} - \frac{r^3 B_o''}{4 \cdot 2^2} + \frac{r^5 B_o(4)}{6 \cdot 2^2 \cdot 4^2} - \ldots . \qquad (A.11)$$

To show this, it is necessary to verify only that the equation

$$B = \text{curl } A \qquad (A.12)$$

is satisfied.

By differentiating equation (A.11) with respect to r, it can be seen that $\partial A_\theta / \partial r$ will have the same sign as B_z near the axis. Consider a region which includes the axis and in which B_z and $\partial A_\theta / \partial r$ are either both positive or both negative. Then by (A.9) A_θ has that same sign. Thus in that region A_θ and $\frac{\partial A_\theta}{\partial r}$ have the same sign, and $A_\theta \frac{\partial A_\theta}{\partial r}$ is positive or zero. Thus if B_z is not zero, and if an electron has $P_\theta = 0$, $\ddot{r}$ will be negative,[1] and the electron will bend towards the axis of symmetry. Given time enough the electron will go through the axis. An electron with $P_\theta = 0$ outside the region of magnetic field ($A_\theta = 0$) will travel in a straight line (since $\ddot{r} = 0$) parallel to or intersecting the axis (since $\dot{\theta} = 0$).

Conversely, any electron whose path is parallel to the axis in the region of no magnetic field must have $P_\theta = 0$, and so does any electron which goes through the axis of symmetry at any time.

[1] From (A.9) it follows that $A_\theta = 0$ only if $B = 0$. If $\frac{\partial A_\theta}{\partial r} = 0$ and $B_z \neq 0$, equation (A.8) becomes $A_\theta = rB_z$, or $\frac{\partial A_\theta}{\partial r} = 0 = \frac{\partial}{\partial r}(rB_z)$. Then rB_z is independent of r, or B_z is inversely proportional to r. Such a field can not satisfy Laplace's equation. (See Spangenberg, Ref. G, p. 396.) Therefore $A_\theta \frac{\partial A_\theta}{\partial r} \neq 0$.

Clearly, an electron beam cannot be sent into an axially symmetric magnetic field parallel to but not on the axis of the field. If an electron beam is started outside the magnetic field parallel to but not on the axis of the field, it bends toward the axis upon entering the field and travels a helix-like path which goes through the axis. There are other possibilities; the electron need not be started parallel with the axis of the field. However, in a situation where the beam velocity and the magnetic field must be varied, the only hope for a straight beam is for a beam sent along the axis of the field.

If the electron paths are close enough to the axis of the magnetic field, all terms except the first are negligible in each of the above expansions. Then equation (A.7) becomes

$$\ddot{r} + \frac{e^2}{4m^2} B_o^2 r = 0. \qquad \text{(A.13)}$$

B_o is a function of z, but it can be thought of as a function of time as the electrons move along the z-axis. This is the equation of a harmonic oscillator with varying frequency $\frac{eB_o}{2m}$. The nature of the solution can be seen from the approximate solution.[1]

$$r = c\left(\frac{eB_o}{2m}\right)^{-1} \cos \int^t \frac{eB_o}{2m}\, dt \quad ,$$

where c is a constant of integration. The distance from the axis oscillates between zero and a maximum distance. The maximum distance is smaller in the region where the magnetic field is greater. The approximation is only good enough to show qualitatively the nature of the solution. A numberical solution was carried out for conditions typical in the trajectron, and it indicated that the maximum distance

[1]Schiff, Ref. F, p. 179.

from the axis would be reduced by a factor of about three. This in agreement with the observed convergence of the beam when the magnetic field was strong.

Suppose that a beam of electrons parallel with the axis of the magnetic field enters the region of magnetic field. Each electron path satisfies equations (A.6) and (A.13). Since (A.13) is homogeneous, all solutions with $\frac{dR}{dt}$ initially zero are the same except for a constant factor; the electrons move toward and away from the axis together. With the approximation that the distance from the axis is small, equation (A.6) becomes

$$\dot{\theta} = \frac{eB_o}{2m} \quad , \qquad (A.15)$$

and thus all electrons are moving around the axis at the same angular velocity. It follows that the beam cross-section will always have the same shape it had initially, but the size will vary between zero and a maximum, and it rotates around the axis of the field.

This phenomenon was observed by varying the voltage on the electron gun and hence the beam velocity. Of course, the spot size actually observed did not become zero, because the electrons were not initially parallel with the axis. The spot was observed to rotate around a point, to keep its shape approximately circular, and to vary in size typically over a range of about three to one.

APPENDIX B

This appendix describes the method of obtaining solutions to several equations for the motion of electrons in a cylindrical diode by means of the differential analyser. The first is the equation for the motion of electrons in the magnetron, taking into account the space charge of the moving electrons but neglecting secular space charge. It is, from page ,

$$\frac{d^2R}{dT^2} + R - \frac{1}{R^3} = \frac{bT}{R}, \qquad (2.77)$$

$$R = 1, \quad \frac{dR}{dT} = 0 \text{ when } T = 0. \qquad (2.78)$$

The second equation, that for the motion of an electron in the cylindrical diode with no space charge, is, from page ,

$$\frac{d^2R}{dT^2} + R - \frac{1}{R^3} = \frac{\alpha}{R}, \qquad (4.22)$$

with the same initial conditions as above. The third is the equation for the motion of electrons in a cylindrical magnetron taking into account the space charge of the moving electrons and assuming a distribution for secular space charge. This is, from page ,

$$\frac{d^2R}{dT^2} + R - \frac{1}{R^3} = \frac{bT}{R} + \frac{1}{R}\int_1^R RQ(R)dR \qquad (2.105)$$

with the same initial conditions as above and for the following functions Q(R):

$$Q_1(R) = k_1,$$

$$Q_2(R) = \frac{k_2}{R},$$

$$Q_3(R) = \frac{k_3}{R^3}, \text{ and} \qquad (2.106)$$

$$Q_4(R) = \frac{k_4}{R^4}.$$

The second and third equations are slight modifications of the first. The solution of the first equation will be described in detail and then the modifications in the setup and the method for the other cases will be discussed.

The electronic differential analyzer is an analogue machine employing voltages as the dependent variables and time as the independent variable. It consists of a number of high-gain amplifiers which, through suitable feedback connections, can be made to perform the operations of addition and integration of these variables. The differential analyser is designed to handle voltages up to 100 volts. The variable R ranges from one to about four. Therefore, it was appropriate to let the machine voltage E equal 25R. The equations (2.77) and (2.78) in terms of E become

$$\frac{d^2E}{dT^2} = \frac{625\ bT}{E} - E + \frac{25^4}{E^3}, \quad E = 25, \quad \frac{dE}{dT} = 0 \text{ when } T = 0. \qquad (B.1)$$

It is convenient to let the machine time equal T.

The circuit diagram for the differential analyser setup is shown in Figure B.1. Let the voltage at point A in the figure be

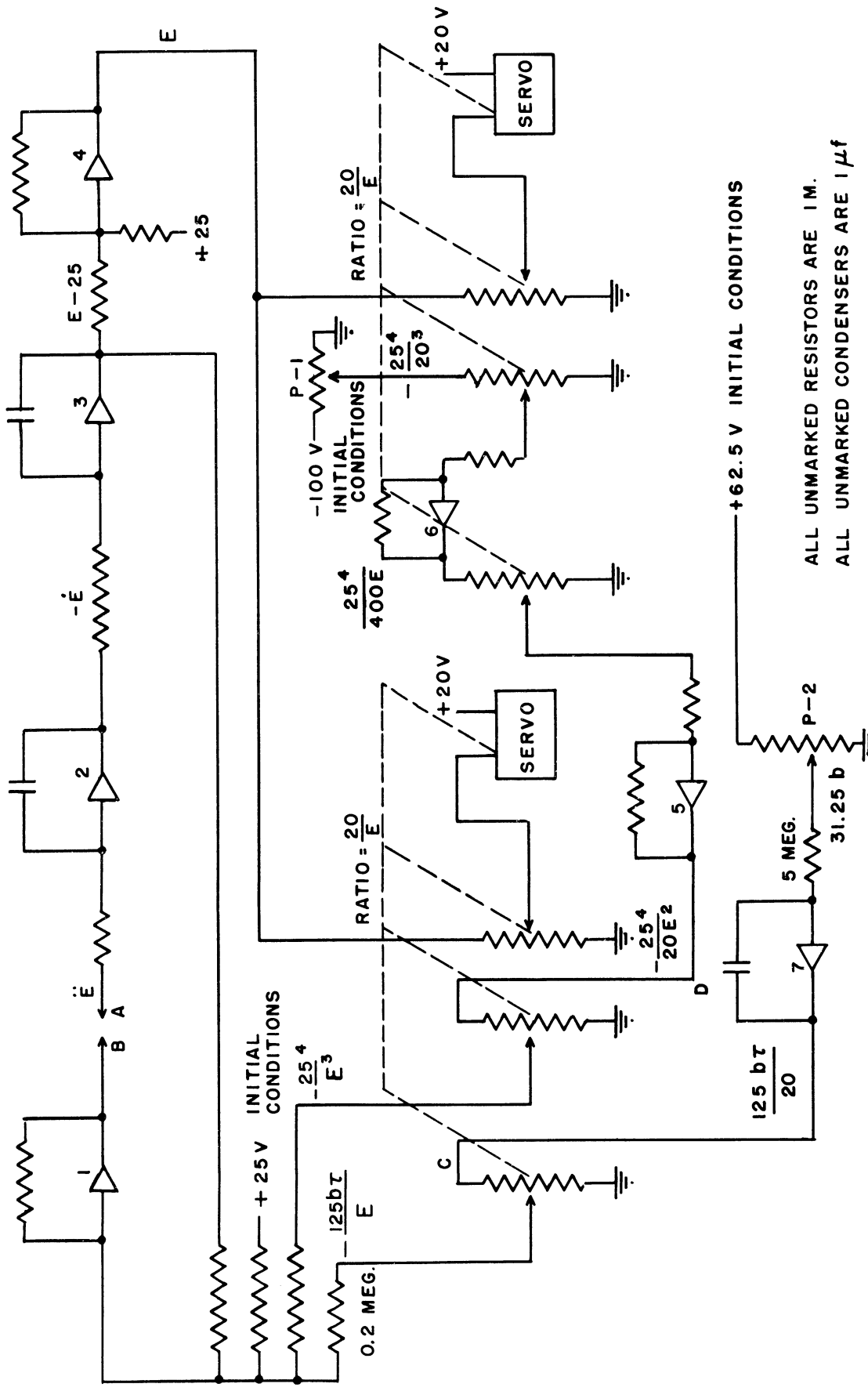

FIG. B.1 DIFFERENTIAL ANALYSER SETUP FOR SOLVING CYLINDRICAL MAGNETRON EQUATION

d^2E/dT^2. Then the voltage -E can be found by integrating twice and adding the constant of integration. A voltage proportional to bT is obtained by integrating a constant voltage proportional to b. Two servo-multipliers are used as dividers to make available four potentiometers with the ratio 20/E. The voltage proportional to bT is applied to one to obtain the term 625bT/E in equation (B.1). The other three are connected in cascade and a constant voltage is applied to the first in order to obtain the term $25^4/E^3$. The voltage E is already available, and a voltage equal to the right side of the equation is formed by adding, in amplifier (1), these three terms. This voltage appears at point (B). The equation states that this voltage should equal d^2E/dT^2, and hence that the voltage at points A and B should be equal; i.e., that these points should be connected together in the circuit.

When the machine is ready to start a solution, the condensers in the integrating circuits are disconnected and discharged, and the voltages marked initial conditions are disconnected. The solution is started by simultaneously connecting into the circuit these condensers and voltages. It is desirable to have the servo-mechanisms in their initial positions when the solution is started; their being out of position momentarily as the solution starts may seriously affect the accuracy of the solution. Therefore, the circuit is arranged so that the initial voltages applied to the servo-amplifiers are constant voltages not removed when the machine is ready to start a solution.

Equation (B.1) states that d^2E/dT^2 is zero initially, since T = 0 and E = 25 initially. Thus the voltage at point B should be

zero initially. It would be if P-1 were set at $25^4/20^3 \approx 43.8$ volts, and all potentiometers on the servomechanisms were perfectly accurate. In practice, a small voltage appears at point B initially when P-1 is set at 43.8 volts. The solutions can be improved by adjusting P-1 until no voltage appears at point B initially. This can be accomplished by setting P-2 to zero, starting a solution, and adjusting P-1 to give the minimum initial slope in dE/dT, which was connected to a recorder.

The voltages E and $\dot{E}$ were recorded. In addition a voltage proportional to θ was recorded. Equation (2.79) of Chapter II gives

$$\theta = \int_0^T (1 - \frac{1}{R^2})\, dT \quad . \tag{2.79}$$

In terms of E this becomes

$$20\,\theta = \int_0^T \left(20 - \frac{1250}{E^2}\right)\, dT. \tag{B.2}$$

The voltage $25^4/20E^2$ is available as the output of amplifier (5) in Figure B.1. The circuit used to calculate (B.2) is shown in Figure B.2 A resistor was substituted for the condenser on amplifier (8), making it an adder, and the potentiometer P-3 was adjusted to make the output zero initially. Then the condenser was replaced.

Typical solutions taken from the differential analyser are shown in Figures 2.5 and 2.6 on pages 41 and 42.

When $\frac{E}{25}$ is substituted for R, equation (4.22) becomes

$$\frac{d^2E}{dT^2} = \frac{625\alpha}{E} - E + \frac{25^4}{E^3} \quad . \tag{B.3}$$

Solutions for this equation can be obtained by eliminating the integrator (7) in Figure B.1, and replacing its output by a voltage (from the

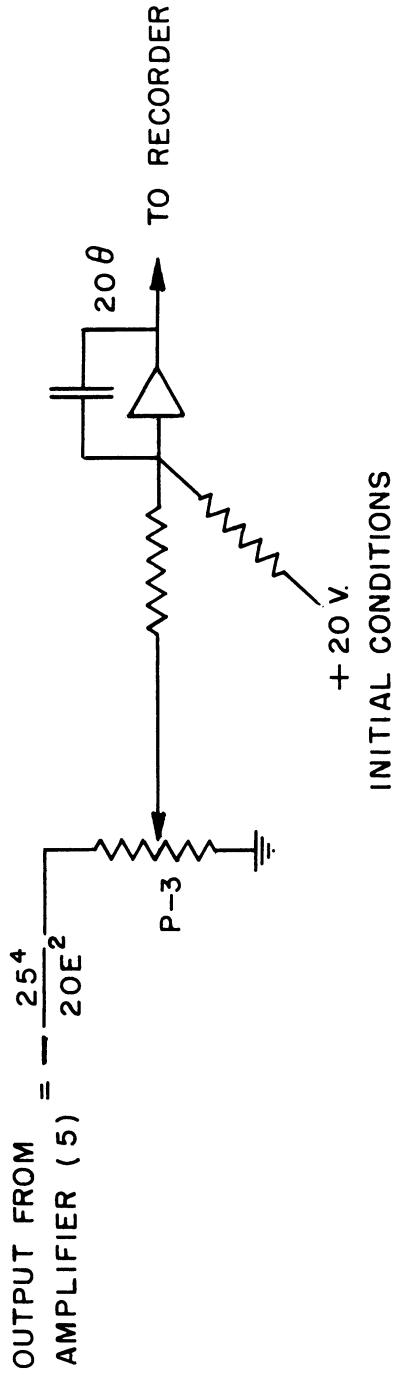

FIG. B.2 DIFFERENTIAL ANALYSER CIRCUIT FOR CALCULATING θ.

initial conditions) equal to $\frac{125\alpha}{20}$.

The differential analyser setup for equation (2.95) in each case is only a slight modification of the setup shown in Figure B.1. Consider first the case in which $Q(R) = Q_1(R) = k_1$.

$$\frac{1}{R}\int_1^R RQ(R)dR = \frac{k_1 R}{2} - \frac{k_1}{2R} \quad , \tag{B.4}$$

and equation (2.95) becomes

$$\frac{d^2R}{dT^2} = \frac{bT - \frac{1}{2}k_1}{R} - \left(1 - \frac{1}{2}k_1\right)R + \frac{1}{R^3} \quad . \tag{B.5}$$

If the machine voltage E is equal to 25R, this becomes

$$\frac{d^2E}{dT^2} = \frac{625bT - 312.5k_1}{E} - \left(1 - \frac{1}{2}k_1\right)E + \frac{25^4}{E^3} \quad . \tag{B.6}$$

The necessary modification of the setup in Figure B.1 is quite obvious. The voltages E-25 and 25 applied to the adder, amplifier (1), must be reduced by using potentiometers, in the ratio $1-\frac{1}{2}k_1$, and a constant voltage $-3.125k_1$ must be added to the output $125bT/20$ of the integrator (7) before it is applied to the potentiometer at point (C) in Figure B.1. The best results are achieved by adjusting this latter voltage to return d^2E/dT^2 to zero rather than by setting it to $-3.125k_1$.

In the case $Q(R) = Q_2(R) = k_2/R$,

$$\frac{1}{R}\int_1^R Q(R)dR = k_2 - \frac{k_2}{R} \quad , \tag{B.7}$$

and equation (2.95) becomes

$$\frac{d^2R}{dT^2} = \frac{bT + k_2}{R} - R + \frac{1}{R^3} + k_2 \quad . \tag{B.8}$$

With the machine voltage equal to 25R, this becomes

$$\frac{d^2E}{dT^2} = \frac{625bT - 625k_2}{E} - E + \frac{25^4}{E^3} + 25k_2 \quad . \tag{B.9}$$

The modification of the setup in Figure B.1 required for this case consists of adding a constant voltage $-25k_2$ to the input of the adder amplifier (1), and adding a voltage $-6.25k_2$ to the output $6.25bT$ of the integrator (7) and applying the sum to the potentiometer at point (C).

For the case $Q(R) = Q_3(R) = \frac{k_3}{R^3}$,

$$\frac{1}{R}\int_1^R RQ(R)dR = \frac{k_3}{R} - \frac{k_3}{R^2} \quad , \tag{B.10}$$

and equation (2.95) becomes

$$\frac{d^2R}{dT^2} = \frac{bT + k_3}{R} - R + \frac{1}{R^3} - \frac{k_3}{R^2} \quad . \tag{B.11}$$

With the machine voltage E equal to 25R, this becomes

$$\frac{d^2E}{dT^2} = \frac{625bT + 625k_3}{R} - E + \frac{25^4}{E^3} - \frac{25^3k_3}{E^2} \quad . \tag{B.12}$$

For this case the modification of the setup shown in Figure B.1 consists of connecting the voltage $25^4/20E^2$ obtained at point (D) to a potentiometer to reduce it in the ratio $4k_3/5$, and then adding the result, $25^3k_3/E^2$, into the adding amplifier (1). Again a constant

voltage $6.25k_3$ must be added to the output $6.25bT$ of the integrator (7) and the sum applied to the potentiometer at point (D) on the circuit diagram.

For the last case, $Q(R) = Q_4(R) = \frac{k_4}{R^4}$,

$$\frac{1}{R}\int_1^R RQ(R)dR = \frac{k_4}{2R} - \frac{k_4}{2R^3} \quad , \tag{B.13}$$

and equation (2.95) becomes

$$\frac{d^2R}{dT^2} = \frac{bT + \frac{1}{2}k_4}{R} - R + \left(1 - \frac{1}{2}k_4\right)\frac{1}{R^3} \quad . \tag{B.14}$$

The substitution $E = 25R$ in this equation results in

$$\frac{d^2E}{dT^2} = \frac{625bT + 312.5k_4}{E} - E + \left(1 - \frac{1}{2}k_4\right)\frac{25^4}{E^3} \quad . \tag{B.15}$$

The simplest way of achieving a modification of the setup shown in Figure B.1 to solve this equation is to add a constant voltage $3.125k_4$ to the output $6.25bT$ of the integrator (7), apply the sum to the potentiometer at point (C), and reduce the potentiometer P-1 in the ratio $1-\frac{1}{2}k_4$. This last step is best accomplished by readjusting P-1 to make d^2E/dT^2 zero initially with the voltage $3.125k_4$ added at point (C).

A total of 215 solutions of equation (2.105) and 2.106) for various cases were run on the differential analyser. It would not be practical to include them.. They are all very similar to those shown in Figures 2.5 and 2.6 on pages 40 and 41. The most important data from the solutions are summarized in Table B. The first two columns in the

table give the values of the parameters b and k. The other columns give data taken from the solutions. The data included are the solution type, the maximum radius of the orbit, and the transit time. It is possible to calculate from these data the potential at the Hull radius, the potential gradient at the Hull radius, the total space charge, and the acceleration of an electron at the Hull radius. The potential is obtained from equation (2.58) by noting that $\dot{r} = 0$ at the Hull radius.

$$e\phi(r) = \frac{m\dot{r}^2}{2} + \frac{mr^2\omega_L^2}{2}\left(1 - \frac{a^2}{r^2}\right)^2 \quad . \qquad (2.58)$$

The potential gradient at the Hull radius can be calculated from equation (2.102),

$$rF = \frac{It}{2\pi\epsilon_o} + \frac{1}{\epsilon_o}\int_a^r r_s(r)dr. \qquad (2.102)$$

The total space charge follows from (2.102), and the acceleration at the Hull radius from the differential equation (2.105).

TABLE B

	k	b	R_h	T_h	Solution Type
k =	0	0.4	2.28	11.8	3
	0	0.5	2.60	12.1	3
	0	0.6	2.88	12.1	3
	0	0.7	2.48	7.7	2
	0	0.8	2.67	7.6	2
	0	0.9	2.87	7.8	2
	0	1.0	3.04	7.8	2
	0	1.1	2.2	3.7	1
	0	1.2	2.3	3.6	1
	0	1.4	2.5	3.5	1
	0	1.6	2.7	3.5	1
	0	1.8	2.9	3.4	1
	0	2.0	3.08	3.4	1
k_1 =	0.4	0.2	2.12	17.0	4
	0.4	0.4	3.20	18.6	4
	0.4	0.6	3.41	13.8	3
	0.4	0.8	3.20	9.1	2
	0.4	1.0	3.65	8.7	2
	0.4	1.0	2.43	4.7	1
	0.4	1.2	2.73	4.3	1
	0.4	1.4	3.00	4.1	1
	0.4	1.6	3.28	4.0	1
	0.4	1.8	3.50	4.0	1
	0.4	2.0	3.71	4.0	1
k_1 =	0.8	0.2	2.80	25.7	6
	0.8	0.4	4.50	27.6	5
	0.8	0.6	4.28	16.1	3
	0.8	0.8	4.03	10.5	2
	0.8	1.0	3.06	4.9	1
	0.8	1.2	3.44	4.8	1
	0.8	1.4	3.78	4.6	1
	0.8	1.6	4.10	4.5	1
	0.8	1.8	4.39	4.5	1
	0.8	2.0	4.67	4.5	1
k_1 =	1.2	0.8	3.68	6.3	1

	k	b	R_h	T_h	Solution* Type
k_2 =	0.2	0.2	1.92	16.2	4
	0.2	0.4	2.80	16.5	4
	0.2	0.6	3.00	12.4	3
	0.2	0.6	2.40	8.4	2
	0.2	0.8	2.81	8.3	2
	0.2	1.0	3.20	8.0	2
	0.2	1.0	2.18	4.2	1
	0.2	1.2	2.40	3.8	1
	0.2	1.4	2.63	3.7	1
	0.2	1.6	2.85	3.6	1
	0.2	1.8	3.03	3.6	1
	0.2	2.0	3.26	3.6	1
k_2 =	0.4	0.2	2.30	21.2	5
	0.4	0.4	2.50	13.1	3
	0.4	0.6	2.52	8.6	2
	0.4	0.8	2.97	8.5	2
	0.4	1.0	2.30	4.1	1
	0.4	1.2	2.54	3.8	1
	0.4	1.4	2.79	3.8	1
	0.4	1.6	3.00	3.7	1
	0.4	1.8	3.20	3.7	1
	0.4	2.0	3.40	3.6	1
k_2 =	0.6	0.2	2.38	21.5	6
	0.6	0.4	3.06	17.7	4
	0.6	0.6	2.63	8.7	2
	0.6	0.8	3.10	8.5	2
	0.6	0.8	2.14	4.2	1
	0.6	1.0	2.40	4.0	1
	0.6	1.2	2.68	3.9	1
	0.6	1.4	2.92	3.8	1
	0.6	1.6	3.16	3.8	1
	0.6	1.8	3.36	3.7	1
	0.6	2.0	3.55	3.6	1
k_2 =	0.8	0.2	2.75	27.1	6
	0.8	0.4	2.78	13.3	3
	0.8	0.6	2.80	8.9	2
	0.8	0.8	2.28	4.1	1
	0.8	1.0	2.54	4.0	1
	0.8	1.2	2.82	3.9	1
	0.8	1.4	3.10	3.9	1
	0.8	1.6	3.31	3.8	1
	0.8	1.8	3.54	3.7	1
	0.8	2.0	3.73	3.7	1

*An n in this column indicates the B_n type solution.

TABLE B (cont.)

	k	b	R_h	T_h	Solution Type
k_2 =	1.0	0.2	2.38	18.5	4
	1.0	0.4	2.91	13.9	3
	1.0	0.4	2.38	9.4	2
	1.0	0.6	2.08	4.5	1
	1.0	0.8	2.40	4.3	1
	1.0	1.0	2.71	4.0	1
	1.0	1.2	3.00	3.9	1
	1.0	1.4	3.23	3.9	1
	1.0	1.6	3.48	3.9	1
	1.0	1.8	3.70	3.8	1
	1.0	2.0	3.90	3.8	1
k_3 =	0.2	0.2	1.45	7.3	2
	0.2	0.2	1.7	11.3	3
	0.2	0.3	2.35	16.0	4
	0.2	0.4	2.35	12.6	3
	0.2	0.5	2.65	13.0	3
	0.2	0.5	2.13	8.1	2
	0.2	0.6	2.35	8.2	2
	0.2	0.7	2.55	7.8	2
	0.2	0.8	2.75	7.8	2
	0.2	0.9	2.93	7.8	2
	0.2	1.0	2.13	3.9	1
	0.2	1.2	2.35	3.6	1
	0.2	1.4	2.55	3.5	1
	0.2	1.6	2.78	3.5	1
	0.2	1.8	2.99	3.5	1
	0.2	2.0	3.15	3.5	1
k_3 =	0.4	0.2	1.45	7.5	2
	0.4	0.2	1.73	11.2	3
	0.4	0.3	2.40	16.7	4
	0.4	0.4	2.40	11.8	3
	0.4	0.4	1.95	8.2	2
	0.4	0.5	2.20	8.0	2
	0.4	0.6	2.40	7.9	2
	0.4	0.7	2.60	7.9	2
	0.4	0.8	2.80	7.8	2
	0.4	0.8	1.95	4.0	1
	0.4	1.0	2.20	3.8	1
	0.4	1.2	2.40	3.7	1
	0.4	1.4	2.60	3.7	1
	0.4	1.6	2.80	3.6	1
	0.4	1.8	3.00	3.5	1
	0.4	2.0	3.20	3.4	1
k_3 =	0.6	0.2	1.73	11.6	3
	0.6	0.3	2.10	12.0	3
	0.6	0.4	1.98	7.9	2
	0.6	0.5	2.20	7,8	2
	0.6	0.6	2.45	7.8	2
	0.6	0.6	1.73	4.1	1
	0.6	0.7	1.88	3.8	1
	0.6	0.8	2.00	3.8	1
	0.6	1.0	2.22	3.7	1
	0.6	1.2	2.44	3.6	1
	0.6	1.4	2.66	3.6	1
	0.6	1.6	2.88	3.5	1
	0.6	1.8	3.08	3.4	1
	0.6	2.0	3.25	3.4	1
k_3 =	0.8	0.2	1.53	7.9	2
	0.8	0.3	1.8	7.9	2
	0.8	0.4	2.03	7.8	2
	0.8	0.5	2.28	7.8	2
	0.8	0.5	1.68	4.0	1
	0.8	0.6	1.8	3.7	1
	0.8	0.7	1.9	3.7	1
	0.8	0.8	2.03	3.6	1
	0.8	1.0	2.28	3.6	1
	0.8	1.2	2.5	3.5	1
	0.8	1.4	2.7	3.5	1
	0.8	1.6	2.9	3.5	1
	0.8	1.8	3.1	3.4	1
	0.8	2.0	3.3	3.4	1
k_3 =	1.0	0.2	1.30	3.8	1
	1.0	0.3	1.42	3.8	1
	1.0	0.4	1.58	3.8	1
	1.0	0.5	1.70	3.7	1
	1.0	0.6	1.83	3.7	1
	1.0	0.8	2.08	3.6	1
	1.0	1.0	2.30	3.6	1
	1.0	1.2	2.55	3.5	1
	1.0	1.4	2.75	3.5	1
	1.0	1.6	2.98	3.5	1
	1.0	1.8	3.18	3.4	1
	1.0	2.0	3.35	3.4	1

TABLE B (cont.)

	k	b	R_h	T_h	Solution Type
k_4 =	0.4	0.1	1.1	3.0	1
	0.4	0.2	1.44	7.3	2
	0.4	0.2	1.70	11.2	3
	0.4	0.3	2.37	16.0	4
	0.4	0.4	1.82	7.6	2
	0.4	0.5	2.23	7.7	2
	0.4	0.6	2.35	7.8	2
	0.4	0.7	2.55	7.7	2
	0.4	0.8	1.82	3.8	1
	0.4	0.9	2.03	3.8	1
	0.4	1.0	2.14	3.8	1
	0.4	1.2	2.37	3.7	1
	0.4	1.4	2.58	3.7	1
	0.4	1.6	2.79	3.6	1
	0.4	1.8	2.99	3.5	1
	0.4	2.0	3.17	3.5	1
k_4 =	0.8	0.1	1.22	3.3	1
	0.8	0.2	1.50	7.8	2
	0.8	0.2	1.75	11.6	3
	0.8	0.3	1.73	7.7	2
	0.8	0.4	1.97	7.7	2
	0.8	0.5	2.20	7.9	2
	0.8	0.5	1.60	4.0	1
	0.8	0.6	1.72	3.8	1
	0.8	0.7	1.85	3.7	1
	0.8	0.8	1.98	3.7	1
	0.8	1.0	2.20	3.6	1
	0.8	1.2	2.42	3.6	1
	0.8	1.4	2.65	3.5	1
	0.8	1.6	2.85	3.5	1
	0.8	1.8	3.02	3.5	1
	0.8	2.0	3.22	3.4	1
k_4 =	1.2	0.1	1.14	3.6	1
	1.2	0.2	1.28	3.8	1
	1.2	0.3	1.42	3.8	1
	1.2	0.4	1.55	3.7	1
	1.2	0.5	1.67	3.7	1
	1.2	0.6	1.80	3.7	1
	1.2	0.8	2.04	3.7	1
	1.2	1.0	2.30	3.6	1
	1.2	1.2	2.52	3.5	1
	1.2	1.4	2.73	3.5	1
	1.2	1.6	2.91	3.4	1
	1.2	1.8	3.10	3.4	1
	1.2	2.0	3.30	3.4	1
k_4 =	1.6	0.1	1.17	3.6	1
	1.6	0.2	1.31	3.6	1
	1.6	0.3	1.48	3.6	1
	1.6	0.4	1.60	3.7	1
	1.6	0.6	1.88	3.6	1
	1.6	0.8	2.13	3.5	1
	1.6	1.0	2.37	3.5	1
	1.6	1.2	2.58	3.4	1
	1.6	1.4	2.80	3.4	1
	1.6	1.6	3.00	3.4	1
	1.6	1.8	3.20	3.4	1
	1.6	2.0	3.38	3.3	1
k_4 =	2.0	0.1	1.19	3.8	1
	2.0	0.2	1.38	3.8	1
	2.0	0.3	1.54	3.8	1
	2.0	0.4	1.67	3.7	1
	2.0	0.6	1.94	3.6	1
	2.0	0.8	2.20	3.5	1
	2.0	1.0	2.45	3.5	1
	2.0	1.2	2.67	3.5	1
	2.0	1.4	2.88	3.4	1
	2.0	1.6	3.07	3.4	1
	2.0	1.8	3.26	3.4	1
	2.0	2.0	3.43	3.3	1

APPENDIX C

This appendix describes the calculation of y-displacement as a function of time for beam electrons in an ideal planar magnetron with the B_o, B_1, and B_2 types of space charge, and neglecting secular space charge.

Consider first the case for which the solution which occurs is the B_o, or single-stream, solution. Then the potential field is, from Chapter II,

$$\phi = \frac{2m}{e}\omega_L{}^2 y^2 . \tag{2.25}$$

The equations of motion for beam electrons can also be taken from Chapter II,

$$m\ddot{x} + eB\dot{y} = 0, \text{ and} \tag{2.6a}$$

$$m\ddot{y} - eB\dot{x} + e\frac{d\phi}{dy} = 0. \tag{2.6b}$$

Again the z motion can be disregarded: the z-velocity is constant. From equation (2.8)

$$x = \frac{P_x}{m} - 2\omega_L y. \tag{C.1}$$

where P_x is the canonical x-momentum of the beam electron. This equation can be used to eliminate $\dot{x}$ from (2.6b):

$$\begin{aligned} m\ddot{y} - eB\left(\frac{P_x}{m} - 2\omega_L y\right) - e\frac{d\phi}{dy} &= 0, \text{ or} \\ \ddot{y} = \frac{e}{m}\frac{d\phi}{dy} - 4\omega_L{}^2 y + \frac{2\omega_L P_x}{m} & \end{aligned} \tag{C.2}$$

Substituting (2.25) in (C.2) to eliminate ϕ yields

$$\ddot{y} = \frac{2\omega_L P_x}{m} . \tag{C.3}$$

This equation can be integrated immediately to give

$$y = \frac{\omega_L P_x}{m} t^2 + \dot{y}_o t + y_o . \tag{C.4}$$

Where y_o and $\dot{y}_o$ are the initial y-displacement and y-velocity of the beam electron. This is the y-displacement as a function of time valid for $y \leqq y_h$.

The solution for the double-stream case is not nearly so simple. The electric potential cannot even be expressed explicitly as a function of y. The following equations from Chapter II describe the potential field quantitatively:

$$\phi = \frac{m}{2e} (\omega_L^2 y^2 + \dot{y}^2) , \tag{2.17}$$

$$y = \frac{W}{2\pi} (2\omega_L t - \sin 2\omega_L t), \text{ and} \tag{2.34}$$

$$\dot{y} = \frac{W}{2\pi} (1 - \cos 2\omega_L t) , \tag{2.35}$$

where t is the transit time of an emitted electron. These equations can be used to describe the potential parametrically. It is convenient to change the notation t to p, since t will be used to denote the transit time of a beam electron. Then eliminating $\dot{y}$ from (2.17) yields

$$\phi = \frac{2m\omega_L^2 y^2}{e} = \frac{m\omega_L^2 W^2}{2e\pi^2} (1 - \cos 2\omega_L p)^2 \tag{C.5}$$

$$y = \frac{W}{2\pi} (2\omega_L p - \sin 2\omega_L p) . \tag{C.6}$$

The equations of motion are the same as in the previous case except for the potential, and equation (C.2) can be used:

$$\ddot{y} = \frac{e}{m}\frac{d\phi}{dy} - 4\omega_L^2 y + \frac{2\omega_L P_x}{m} \quad . \tag{C.2}$$

Multiplying both sides by $\dot{y}$ and integrating yields

$$\frac{\dot{y}^2}{2} = \frac{e}{m}\phi(y) - \phi(y_o) + \frac{2\omega_L P_x}{m}(y - y_o) - 2\omega_L^2(y^2 - y_o^2) + \frac{\dot{y}_o^2}{2} \quad . \tag{C.7}$$

Now (C.5) can be used to eliminate ϕ and (C.6) to eliminate y.

$$\frac{\dot{y}^2}{2} = \frac{\omega_L^2 W^2}{2\pi^2}(1 - \cos 2\omega_L p)^2 - \frac{e\phi(y_o)}{m} + \frac{2\omega_L P_x W}{2\pi m}(2\omega_L p - \sin 2\omega_L p) -$$

$$- \frac{2\omega_L P_x y_o}{m} + 2\omega_L y_o^2 + \frac{\dot{y}_o^2}{2} \quad , \text{ or}$$

$$\dot{y}^2 \equiv \left(\frac{dy}{dt}\right)^2$$

$$= \frac{\omega_L^2 W^2}{\pi^2}\left[(1 - \cos 2\omega_L p)^2 + a(2\omega_L p - \sin 2\omega_L p) + k\right] \tag{C.8}$$

where

$$a = \frac{2\pi P_x}{m\omega_L W} \quad , \text{ and}$$

$$k = \frac{\pi^2}{\omega_L^2 W^2}\left[\dot{y}_o^2 + 4\omega_L^2 y_o^2 - \frac{4\omega_L P_x y_o}{m} - \frac{2e\phi(y_o)}{m}\right]. \tag{C.9}$$

Then the transit time of a beam electron is

$$t = \int_{y_o}^{y} \frac{dy}{\frac{\omega_L W}{\pi}\sqrt{(1 - \cos 2\omega_L p)^2 + a(2\omega_L p - \sin 2\omega_L p) + k}} \quad . \tag{C.10}$$

Equation (C.6) can be used to eliminate y:

$$t = \int_{p_o}^{p} \frac{(1 - \cos 2\omega_L p)\, dp}{(1 - \cos 2\omega_L p)^2 + a(2\omega_L p - \sin 2\omega_L p) + k} \quad ,(C.11)$$

where p_o corresponds to the starting position y_o, and p corresponds to y in (C.6).

Equation (C.11) cannot be evaluated in terms of tabulated functions, but is is in fairly convenient form for numerical computation.

The integral was evaluated with the aid of the electronic differential analyser; answers could be obtained quickly and with sufficient accuracy in that way.

In the differential analyser setup, machine time was made to correspond to the parameter $2\omega_L p$. The function $f = (1-\cos 2\omega_L p)$ was generated as the solution of the differential equation

$$\frac{d^2 f}{dp^2} + 4\omega_L{}^2 f = 4\omega_L{}^2 \qquad (C.12)$$

with the initial conditions

$$f = \frac{df}{dp} = 0 \text{ when } p = 0. \qquad (C.13)$$

The function $2\omega_L p - \sin 2\omega_L p$ was obtained as $2\omega_L \int f\, dp$. These two functions then were combined to form the integrand by means of adding circuits and servo-multipliers. (Note the use of a servo- multiplier for taking square root.) The integral was obtained by applying the integrand to an integrating circuit. The circuit for the differential analyser setup is shown in Figure C.1.

One difficulty which arises in setting up this problem is that the integrand becomes infinite at a point p near zero. The integration should be carried out from this point to as large a value

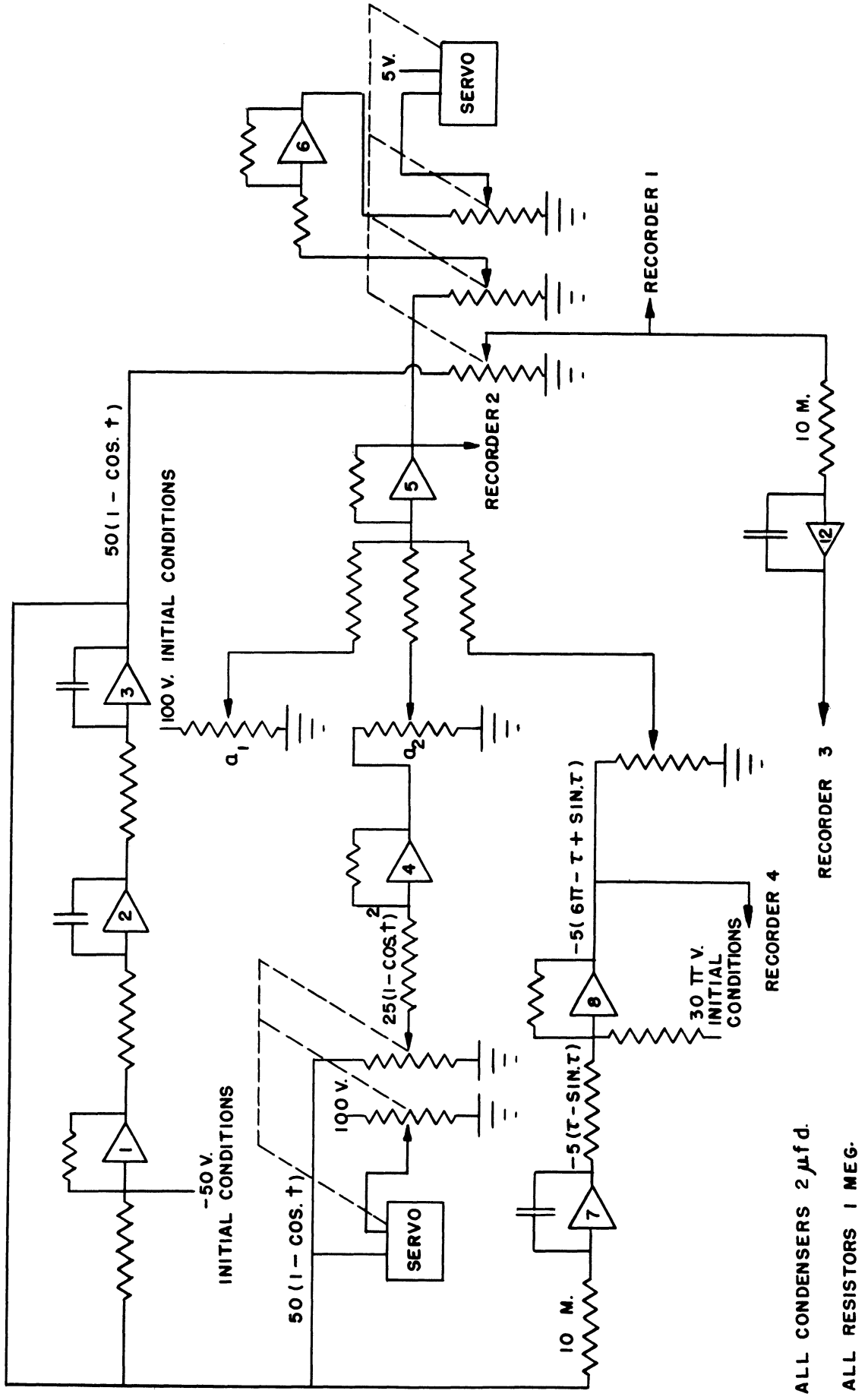

FIG. C·1

DIFFERENTIAL ANALYSER SETUP FOR EVALUATING THE INTEGRAL

of p as one expects to encounter. (The singularity occurs when the beam electron has no radial velocity initially: the integrand becomes infinite whenever $\dot{r}$ becomes zero. If the beam electron has an initial radial velocity, its motion can be found from the same data as a part of the integral.) The integral was evaluated for the beam electron's motion to $\omega_L p = 3\pi$. The problem was simplified by integrating from the upper limit towards the singularity; this was accomplished by letting the machine time equal $(6\pi - 2\omega_L p)$. The point in the approach to the singularity at which the servo-mechanisms became inoperative showed clearly as a discontinuity in the derivative of the integrand. The integral, the integrand, the expression under the square root sign, and

$$y = \frac{W}{2\pi}(2\omega_L p - \sin 2\omega_L p) \qquad (C.6)$$

were all recorded. The value of the integral from the point where the servo-multiplier becomes inoperative to the point of discontinuity in the integrand was found approximately by assuming that the expression under the square root sign to be linear in the interval in question. It is zero at the discontinuity. Then the integral is approximately

$$\Delta I = \int_0^{p_1} \frac{dp}{\sqrt{kp}} = 2\sqrt{\frac{p_1}{k}} = \frac{2p_1}{\sqrt{kp_1}} \qquad (C.14)$$

where ΔI is the contribution to the integral of this interval, p_1 is t the length of the interval, and k is a constant. Since $1/\sqrt{kp_1}$ is the value of the integrand where the servo becomes inoperative, ΔI can be obtained simply as twice the product of the value of the integrand where the servo becomes inoperative and the length of the interval between there and the point where the integrand becomes infinite. The point

at which the integrand becomes infinite shows on the differential analyser tapes as the point where the expression under the radical becomes zero.

Examples of the differential analyser solutions and the calculation of the integral in the interval near the discontinuity in the integrand are shown in Figure C.2. These data, like equation (C.4), are valid only for $y = y_h$.

In Figure 4.4, the beam initial conditions are described in terms of the parameters of the helical path the electron would follow with no electric field. The convenient parameters are h, the distance from the cathode to the axis of the helis; s, the radius of the helix; and δ, the initial angular position of the electron with respect to the axis of the helix. In these terms, the coordinates of an electron can be written

$$\begin{aligned} x &= -s \sin (\delta + 2\omega_L t) \\ y &= h + s \cos (\delta + 2\omega_L t); \end{aligned} \tag{C.15}$$

and the initial conditions are

$$\begin{aligned} \dot{x}_o &= -2\omega_L s \cos \delta , \\ \dot{y}_o &= -2\omega_L s \sin \delta , \\ y_o &= h + s \cos \delta , \text{ and} \\ P_x &= 2m\omega_L h. \end{aligned} \tag{C.16}$$

Substituting these expressions in (C.4) yields

$$y = 2h\omega_L{}^2 t^2 - (2s \sin \delta)\omega_L t + h + s \cos \delta , \tag{C.17}$$

for the single-stream case.

In terms of these constants, equations (C.9) become

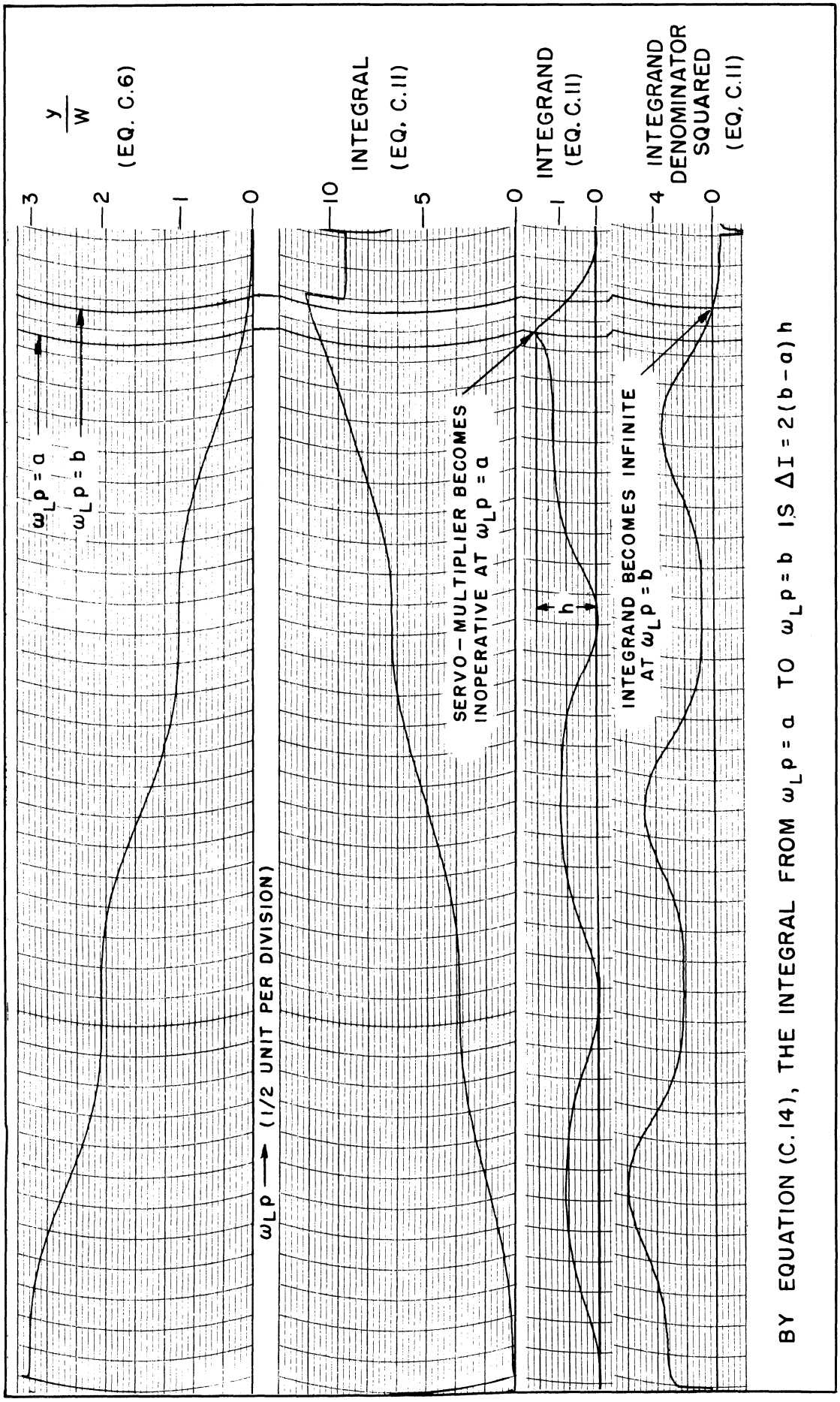

FIG. C.2 DIFFERENTIAL ANALYSER SOLUTIONS FOR EQUATION (C.11)

$$a = \frac{4\pi h}{W}$$

$$k = \frac{\pi^2}{W^2}\left[4s^2 - 4h^2 - \frac{2e\phi(y_o)}{m\omega_L^2}\right]. \qquad (C.18)$$

Note that if $s < h$, $k < 0$. In fact equation (2.17) shows that

$$\phi(y) \geq \frac{2m\omega_L^2 y^2}{e} \qquad (C.19)$$

and hence

$$k < -4\pi^2\frac{2y_o^2}{W^2} \quad . \qquad (C.20)$$

Beam electrons are generally not at their maximum y-displacement when they reach the edge of the space charge cloud, y_h. If the y-displacement curve is continued to its maximum displacement (turning point), then the y-displacement for all times can be found simply: the electron returns to the cathode on the mirror image of its outward path and the y-displacement as a function of time for the return path is the mirror image of the first portion of the curve.

The y-displacement as a function of time for the remainder of the orbit can be found from the equation of motion (C.2)

$$\ddot{y} + 4\omega_L^2 y^2 = \frac{e}{m}\frac{d\phi}{dy} + \frac{2\omega_L P_x}{m} \quad . \qquad (C.2)$$

From equation (2.40) of Chapter II,

$$\frac{d\phi}{dy} = \frac{m}{e}(4\omega_L^2 y_h) \qquad (2.40)$$

at $y = y_h$. But the potential gradient is constant because there is no space charge. Then equation (C.2) becomes

$$\ddot{y} + 4\omega_L^2 y = 4\omega_L^2\left(y_h + \frac{P_x}{2m\omega_L}\right) \quad . \qquad (C.21)$$

The solution of this linear differential equation is

$$y = C \cos(2\omega_L t + \lambda) + y_h + \frac{P_x}{2m\omega_L} \qquad (C.22)$$

where C and λ are constants of integration. The maximum displacement is

$$y_m = C + y_h + \frac{P_x}{2m\omega_L} , \qquad (C.23)$$

$$C = y_m - y_h - \frac{P_x}{2m\omega_L} . \qquad (C.24)$$

The maximum displacement y_m can be calculated from the energy integral, as was done for the cylindrical case in Sections 4.4 and 5.4. The Hull displacement y_h is known, and P_x can be evaluated from the initial conditions of the electrons. Then if λ can be determined, this portion of the curve can be calculated. Changing λ simply translates the curve along the time axis, so choosing λ amounts to simply starting this portion of the curve where the previous portion ended.

The data which are required are the graphs of y as a function of t. These are given parametrically by the differential analyser tapes, since both y and t, which is the integral, were recorded as functions of p. The data were plotted and appear in Figures 5.5 and C.3 through C.6 for values of y_h and beam initial conditions typical of conditions met in the trajectron. The calculated y-displacement as a function of time for the B_o solution (Equation C.4)), the B_1 solution, and the B_2 solution are plotted together. The curves have been extended to their maxima by the method described above.

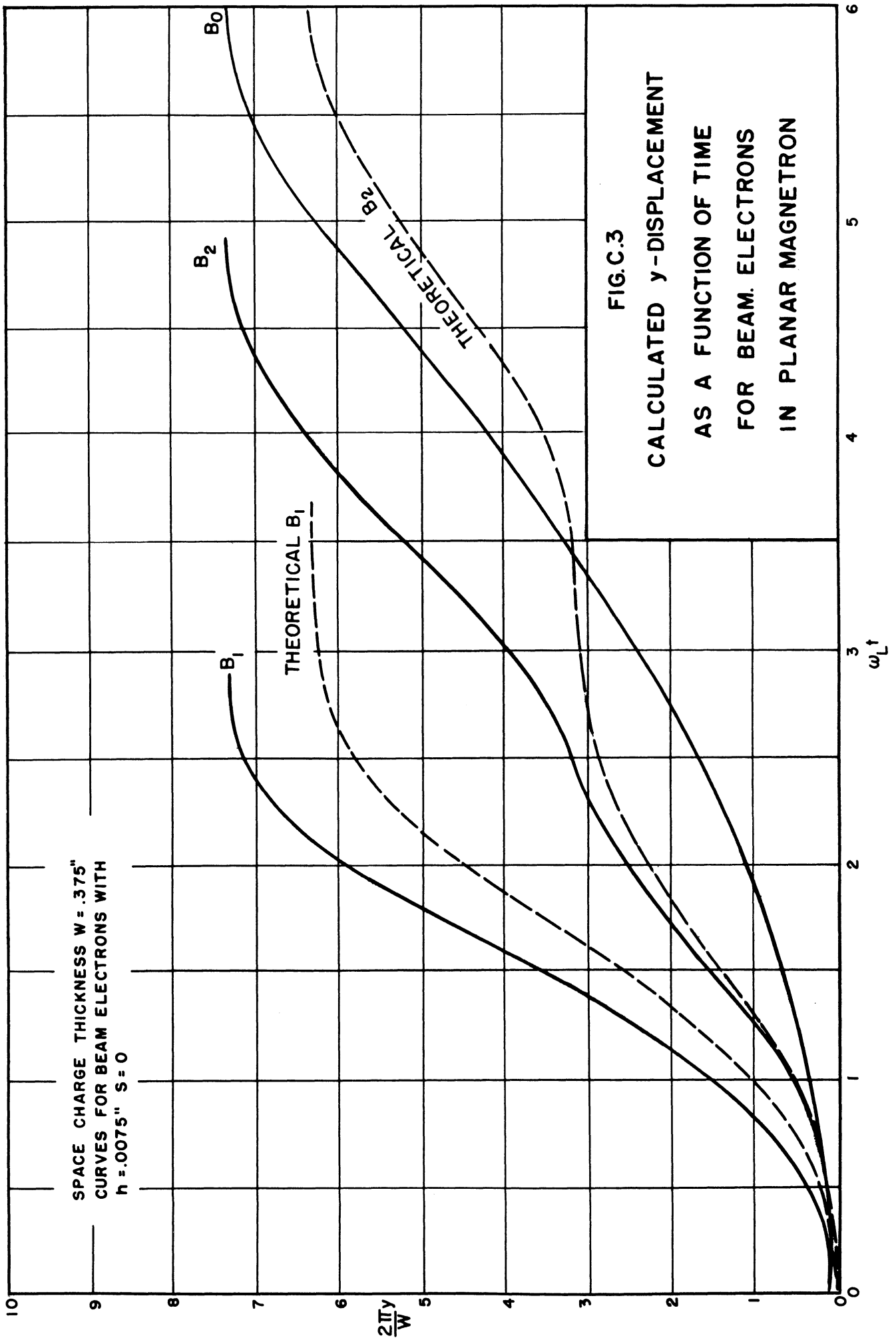
FIG.C.3
CALCULATED y-DISPLACEMENT
AS A FUNCTION OF TIME
FOR BEAM. ELECTRONS
IN PLANAR MAGNETRON
SPACE CHARGE THICKNESS W = .375"
CURVES FOR BEAM ELECTRONS WITH
h = .0075" S = 0
B_0
B_2
B_1
THEORETICAL B_2
THEORETICAL B_1
$\frac{2\pi y}{W}$
$\omega_L t$
0
1
2
3
4
5
6
7
8
9
10

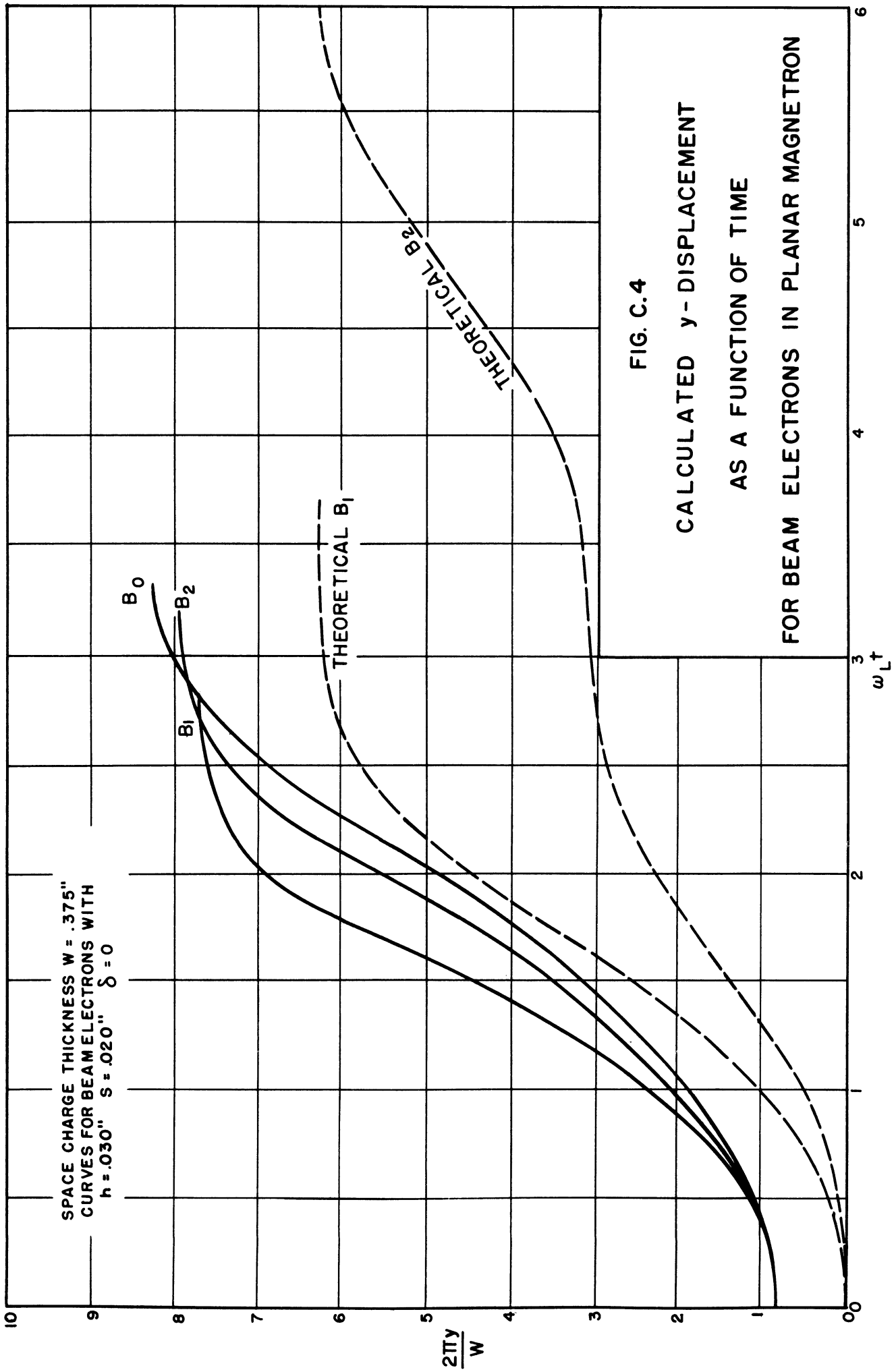
FIG. C.4
CALCULATED y-DISPLACEMENT
AS A FUNCTION OF TIME
FOR BEAM ELECTRONS IN PLANAR MAGNETRON
SPACE CHARGE THICKNESS W = .375"
CURVES FOR BEAM ELECTRONS WITH
h = .030" S = .020" δ = 0
THEORETICAL B2
THEORETICAL B1
B0
B2
B1
2πy/W
ωLt
0
1
2
3
4
5
6
7
8
9
10

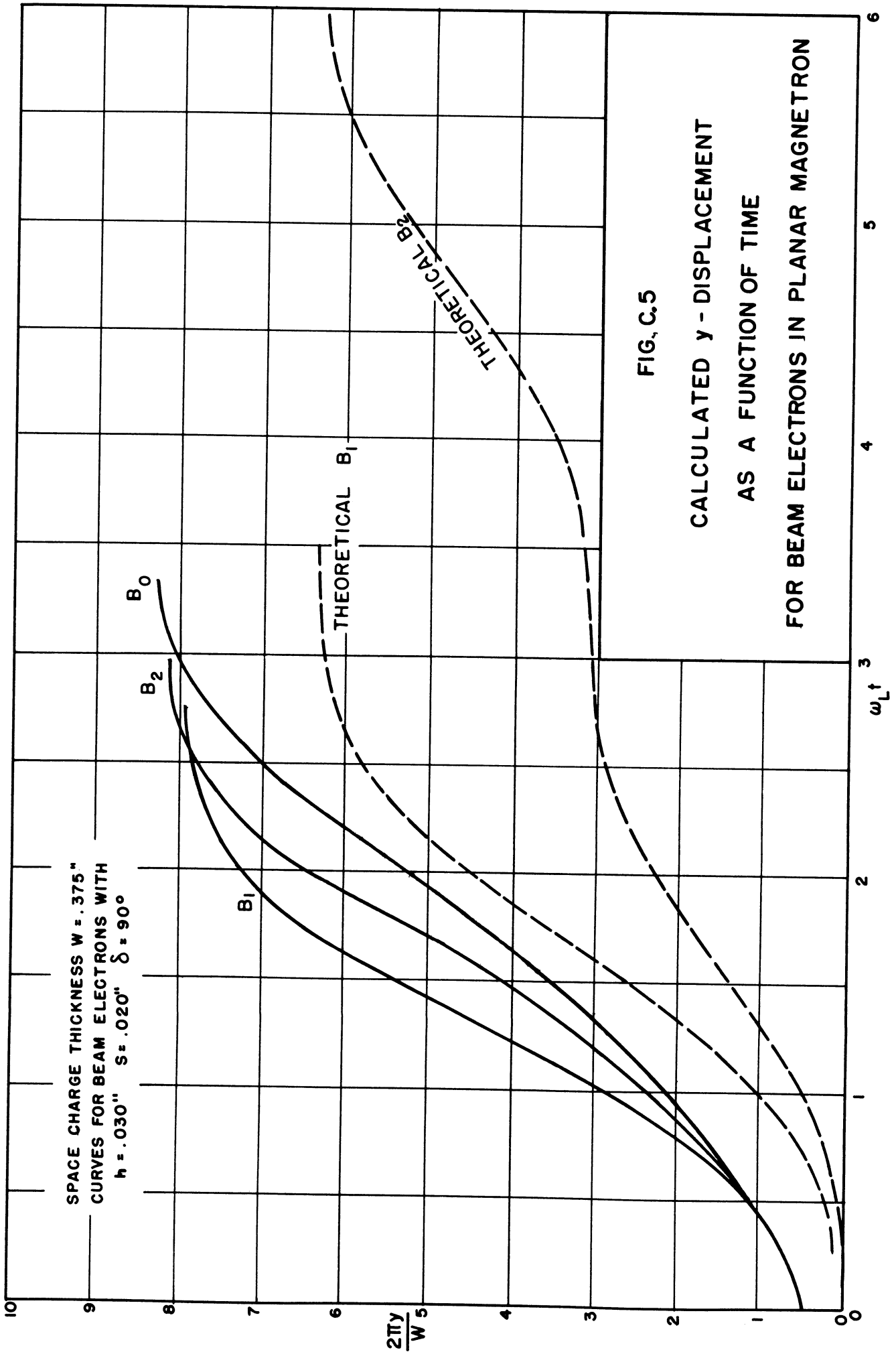
FIG. C.5
CALCULATED y - DISPLACEMENT
AS A FUNCTION OF TIME
FOR BEAM ELECTRONS IN PLANAR MAGNETRON
SPACE CHARGE THICKNESS W = .375"
CURVES FOR BEAM ELECTRONS WITH
h = .030" S = .020" δ = 90°
THEORETICAL B2
THEORETICAL B1
B0
B2
B1
2πy/W
ωLt
0
1
2
3
4
5
6
7
8
9
10

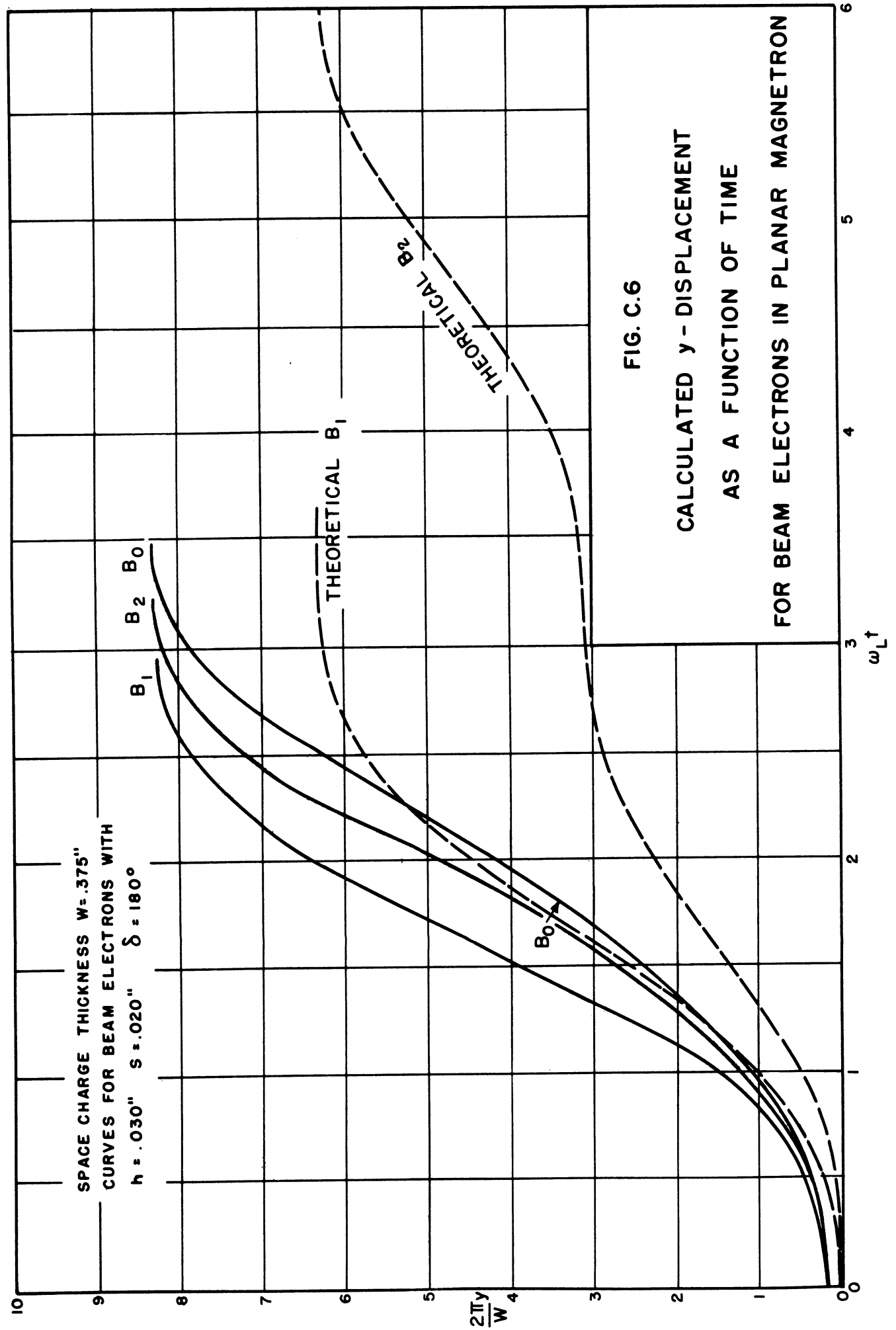
FIG. C.6
CALCULATED y - DISPLACEMENT
AS A FUNCTION OF TIME
FOR BEAM ELECTRONS IN PLANAR MAGNETRON
THEORETICAL B_1
THEORETICAL B_0
B_0
B_2
B_1
SPACE CHARGE THICKNESS W=.375"
CURVES FOR BEAM ELECTRONS WITH
h = .030" S = .020" δ = 180°
$\frac{2\pi y}{W}$
$\omega_L t$
0
1
2
3
4
5
6
7
8
9
10

APPENDIX D

In this appendix, the effect of the presence of secular space charge on the motion of beam electrons is discussed. First the change in the effective potential is considered. Then the motion of beam electrons in a planar magnetron with secular space charge is derived with the effective potential approximated by a parabola. For both problems the secular space charge is assumed to have a distribution proportional to that of the B_o solution.

Because Poisson's equation is linear, the potential in the magnetron can be thought of as the sum of two components, one associated with the secular space charge ρ_s, and the other associated with the cathode accessible space charge ρ_c. These two components of the potential are uniquely defined if it is required that each be zero and have zero gradient at the cathode. They can be found by integrating Poisson's equation. Let ρ_s be the fraction $\frac{1}{2}k_5$ of the space charge of the B_o solution.[1] Then the potential associated with ρ_s is

$$\phi_s(r) = \tfrac{1}{2}k_5 \frac{m\omega_L^2 a^2}{2e} R^2\left(1 - \frac{1}{R^2}\right)^2 , \qquad (D.1)$$

i.e., the fraction $\frac{1}{2}k_5$ of the potential of the B_o solution. (See equation [2.69] .)

[1] The notation $\frac{1}{2}k_5$ is used in order to make this notation correspond to that used in Chapter II.

The differential equation for the motion of the cathode accessible electrons for this case was discussed in Chapter II. It was found to have the same form, after a simple change of variables, as the equation for the case of no secular space charge; i.e.,

$$\frac{d^2R}{dT'^2} + R - \frac{1}{R^3} = \frac{b'T'}{R} \tag{2.109}$$

where $b' = b(1 - \frac{1}{2}k_5)^{-3/2}$ and $T' = T(1 - \frac{1}{2}k_5)^{-1/2}$. Compare the solution taking into account secular space charge with the solution of the same type and same Hull radius neglecting secular space charge. Because of the change in scale in time in the equation, the r-velocity is reduced by a factor $(1 - \frac{1}{2}k_5)^{1/2}$ if there is secular space charge. In order to have the parameter b' for the case with secular space charge equal the b without, the current, and hence the current density, would have to be reduced by a factor $(1 - \frac{1}{2}k_5)^{3/2}$. This is the only change in the space charge distribution, and hence ρ_c is equal to the space charge density for the corresponding solution with no secular space charge and the same Hull radius r_h, reduced by a factor $(1 - \frac{1}{2}k_5)$. The same is true of the associated component ϕ_c of the potential. If the potential for the solution with no secular space charge is denoted by $\phi_o(r)$, then

$$\phi_c(r) = (1 - \frac{1}{2}k_5)\phi_o(r), \tag{D.2}$$

and the potential with secular space charge is,

$$\phi(r) = \phi_c + \phi_s = (1 - \frac{1}{2}k_5)\phi_o(r) + \frac{1}{2}k_5\frac{m\omega_L^2a^2}{2e}R^2(1 - \frac{1}{R^2})^2. \tag{D.3}$$

The effective potential is defined as

$$\psi(r) = \frac{2e\phi(r)}{m\omega_L{}^2a^2} - R^2\left(1 - \frac{1}{R^2}\right)^2. \qquad (5.2)$$

Substituting from equation (D.3), this becomes

$$\psi(r) = \left(1 - \tfrac{1}{2}k_5\right)\frac{2e\phi_o(r)}{m\omega_L{}^2a^2} + \tfrac{1}{2}k_5R^2\left(1 - \frac{1}{R^2}\right)^2 - R^2\left(1 - \frac{1}{R^2}\right)^2$$

$$= \left(1 - \tfrac{1}{2}k_5\right)\left[\frac{2e\phi_o(r)}{m\omega_L{}^2a^2} - R^2\left(1 - \frac{1}{R^2}\right)^2\right] . \qquad (D.4)$$

The expression in the brackets is the effective potential for the solution with the same Hull radius but with no secular space charge. Thus the presence of secular space charge with a distribution equal to $\frac{1}{2}k_5$ times the space charge of the B_o solution simply reduces the effective potential by the fraction $\left(1 - \frac{1}{2}k_5\right)$. (This statement is true also for the planar case.)

The equations for the displacement of beam electrons in a planar magnetron can be made to come out in closed form if the effective potential is approximated by a parabola. This facilitates greatly the calculations required for a plot of "calculated beam spots". The effective potential for the B_1 solution can be fitted quite well by a parabola made to meet the effective potential curve at the cathode, at the Hull displacement, which is W, and half way between these points. It turns out that the two curves meet again at approximately 2W.

The convenient definition of $\psi(y)$ for the planar case is

$$\psi(y) = \frac{2e\phi(y)}{m\omega_L{}^2W^2} - \frac{4y^2}{W^2} . \qquad (D.5)$$

This leads to

$$\psi(y) = \frac{\dot{y}^2}{\omega_L{}^2W^2} \qquad (D.6)$$

in the space charge region for emitted electrons. Then

$$\psi(0) = \psi(W) = 0 \quad , \tag{D.7}$$

and from equations (2.34), (2.35), and (D.6), it follows that the maximum of ψ occurs at W/2 and

$$\psi(\tfrac{W}{2}) = \frac{4}{\pi^2} \quad . \tag{D.8}$$

Thus the approximate effective potential for the case of no secular space charge is the parabola

$$\psi(y) = \frac{16y(W - y)}{W^2\pi^2} \quad . \tag{D.9}$$

If there is secular space charge with a density $\frac{1}{2}k_5$ times that of the B_o solution, this becomes

$$\psi(y) = (1 - \tfrac{1}{2}k_5)\frac{16y(W - y)}{W^2\pi^2} \quad . \tag{D.10}$$

From equation (D.5), the potential is

$$\frac{2e\phi(y)}{m} = 4\omega_L{}^2y^2 + \omega_L{}^2W^2\,\psi(y). \tag{D.11}$$

Then the potential gradient is

$$\frac{e}{m}\frac{d\phi}{dy} = 4\omega_L{}^2y + \frac{1}{2}\,\omega_L{}^2W^2\,\frac{d}{dy}\,\psi(y) \quad . \tag{D.12}$$

From Chapter II, the necessary equations for the motion of beam electrons are

$$m\ddot{y} - eB\dot{x} - e\frac{d\phi}{dy} = 0, \text{ and} \tag{2.6b}$$

$$m\dot{x} + eBy = P_x \text{ , or}$$

$$\dot{x} = \frac{P_x}{m} - 2\omega_L y \quad . \tag{2.8}$$

When (D.10) and (D.12) are used to eliminate $\frac{d\phi}{dy}$, and (2.8) to eliminate $\dot{x}$ from (2.6b), it becomes

$$\ddot{y} - \frac{2\omega_L P_x}{m} + (1 - \tfrac{1}{2}k_5)\left(\frac{16\omega_L^2}{\pi^2} - \frac{8W\omega_L^2}{\pi^2}\right) = 0 \quad , \text{ or}$$

$$\ddot{y} + \lambda^2 y = \lambda^2 \mu \quad , \text{ where} \tag{D.13}$$

$$\lambda = \frac{4\omega_L}{\pi}\sqrt{(1 - \tfrac{1}{2}k_5)} \quad , \text{ and}$$

$$\mu = \frac{W}{2} + \frac{\pi^2 P_x}{8\omega_L m(1 - \frac{1}{2}k_5)} \quad . \tag{D.14}$$

The sol tion of this linear differential equation is

$$y = C_1 \cos \lambda t + C_2 \sin \lambda t + \mu \quad , \tag{D.15}$$

where C_1 and C_2 are constants of integration. The values of C_1 and C_2 can be found from the initial conditions of the beam electron, and

$$C_1 = y_o - \mu, \qquad C_2 = \frac{\dot{y}_o}{\lambda} \quad . \tag{D.16}$$

the x-displacement can be found by substituting (D.15) in (2.8),, and integrating.

$$x = x_o + \frac{P_x t}{m} - \frac{2\omega_L C_1}{\lambda} \sin \lambda t + \frac{2\omega_L C_2}{\lambda}(1 - \cos \lambda t) + 2\omega_L \mu t \tag{D.17}$$

Figure 5.7 was plotted from calculations based on equations (D.14), (D.15), (D.16), and (D.17).

APPENDIX E

The purpose of this appendix is to include data for the magnetron case to supplement that presented in Chapter V.

The series of Figures E.1, E.2, E.3, and E.4 present typical data with ϕ_a/B^2 ranging from above cutoff to well below cutoff.

Figure E.5 presents data in the region of anode voltage in which inflection points were observed in curves of anode current as a function of anode voltage. These data are similar to that presented in Figure 5.18. The relationship between the anode current--anode voltage curve and the data is illustrated in Figure E.6.

In Figure E.7 a series of photographs in which the beam voltage was fixed and the anode voltage was varied are shown. There is only one spot in each photograph. It corresponds to a beam potential of 810 volts; at this potential the radial deflection of the spot is near its maximum. The spot for which the anode potential was 850 volts has an odd, loop-like configuration which is suggestive of oscillation. This phenomenon was not observed to occur consistently. (See also Figure 5.15.)

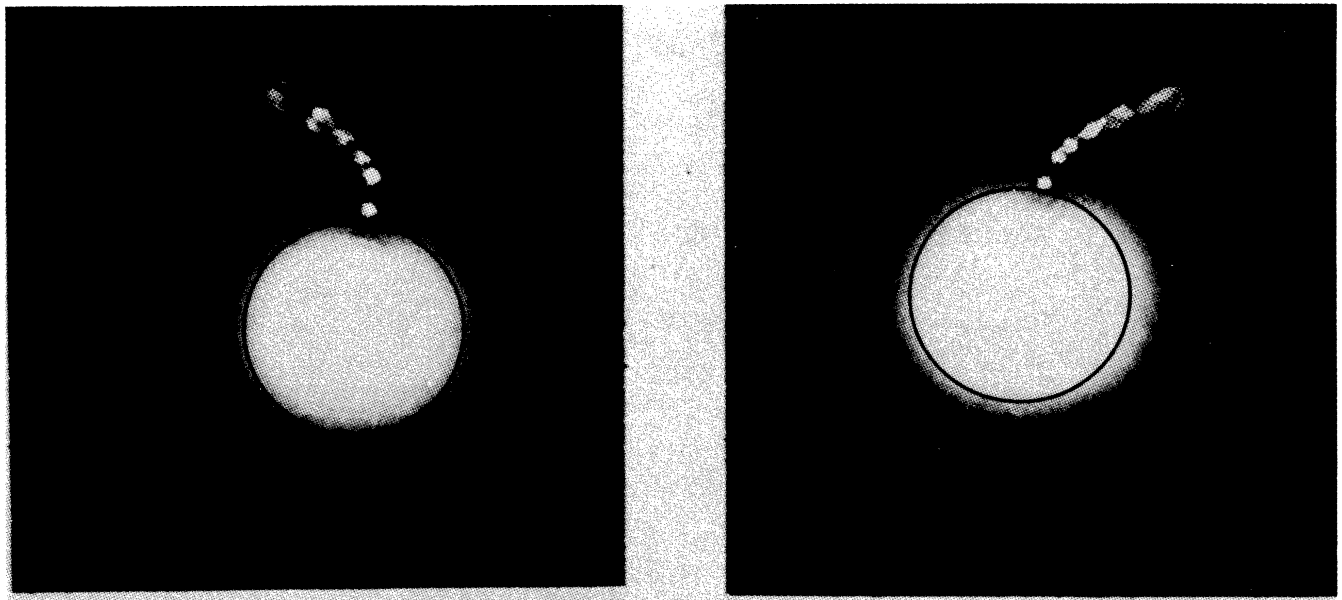

ϕ_a = 312 V. , I_a = 203 ma., I_m = 1.25 A.

ϕ_{BEAM} = 500, 710, 1000, 1480, 1980, 2810, 4020 V.

FIG. E.1 TRAJECTRON DATA ABOVE CUTOFF

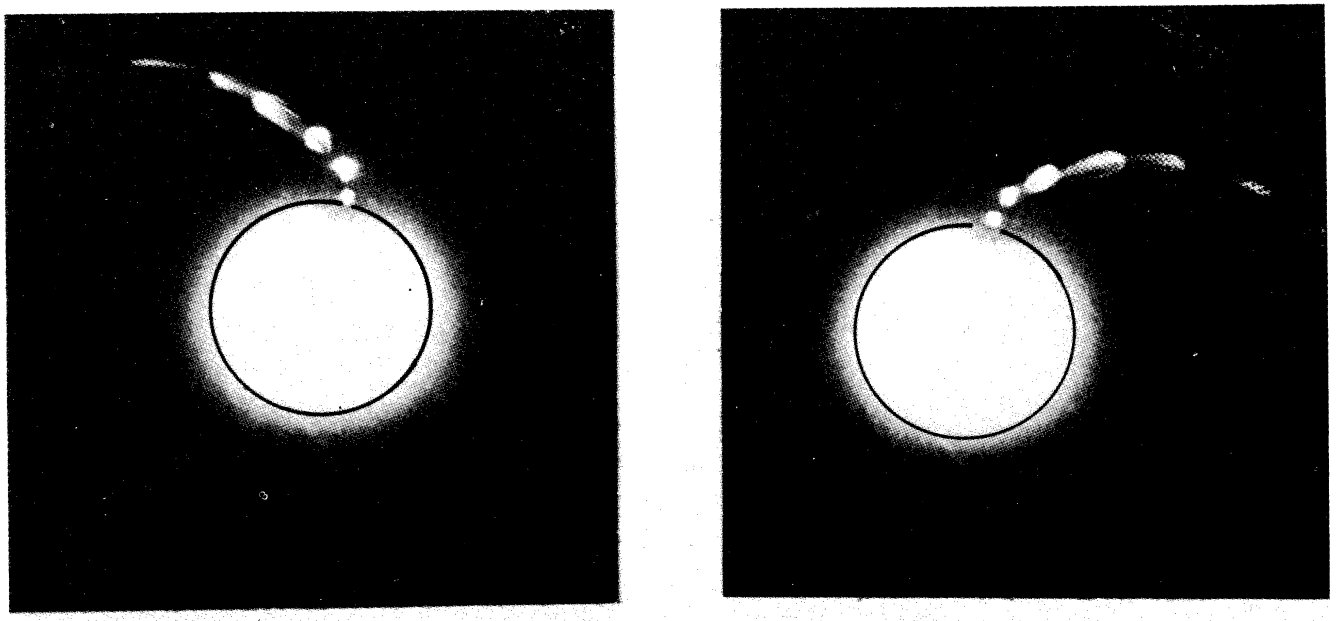

ϕ_a = 322 V. , I_a = 164 ma., I_m = 1.5 A.

ϕ_{BEAM} = 400,500, 710, 1000, 1980, 4020 V.

FIG. E.2 TRAJECTRON DATA AT CUTOFF

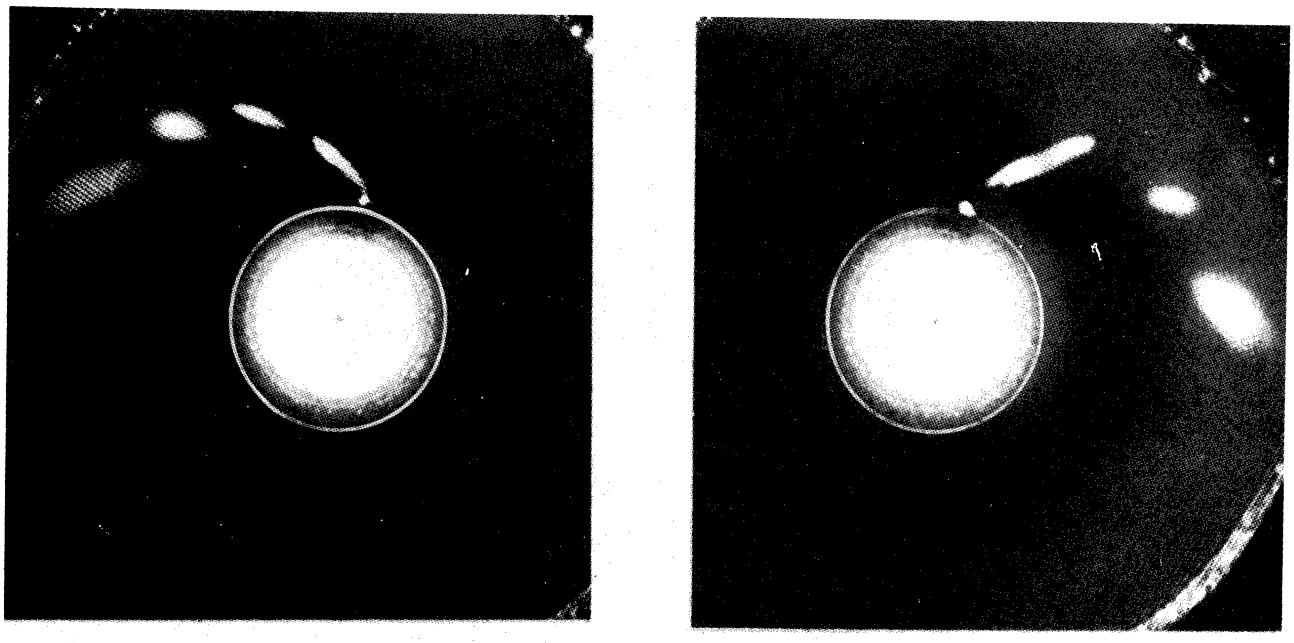

ϕ_a = 1150 V., I_a = 335 ma., I_m = 3 A.
ϕ_{BEAM} = 1000, 1480, 1980, 3520 V.

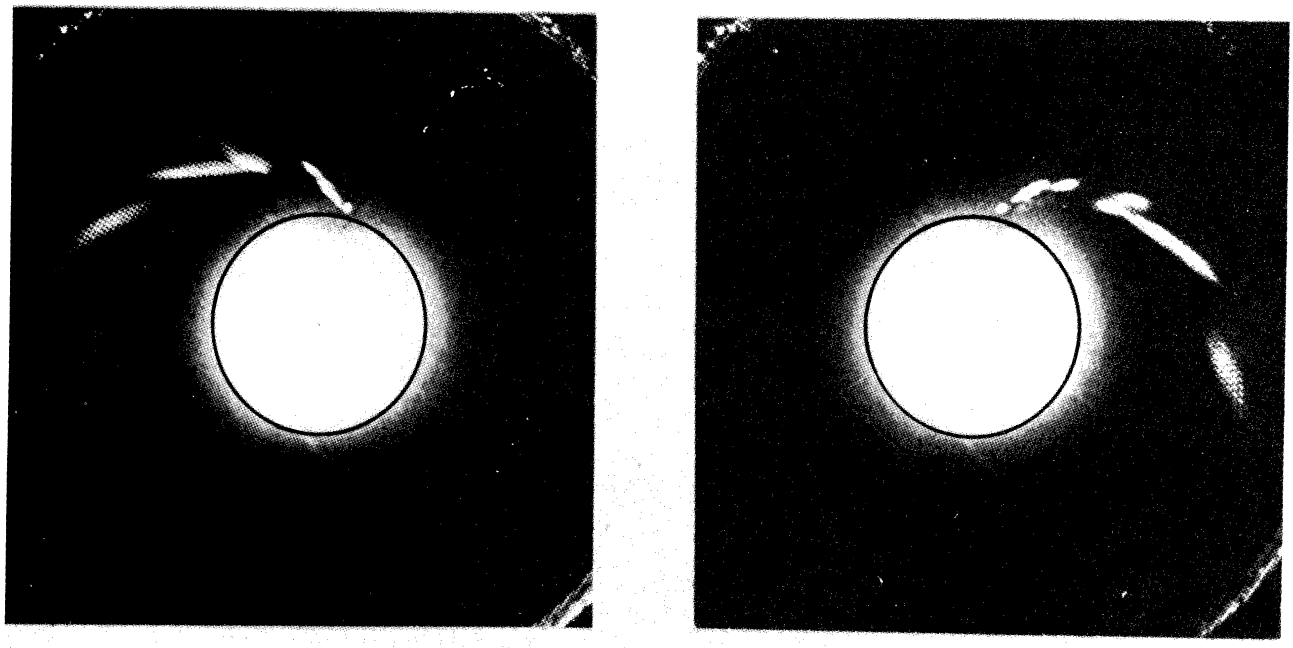

ϕ_a = 1125 V., I_a = 9 ma., I_m = 3 A.
ϕ_{BEAM} = 400, 610, 910, 1380, 2400, 4020 V.

FIG. E.3
TRAJECTRON DATA BELOW CUTOFF

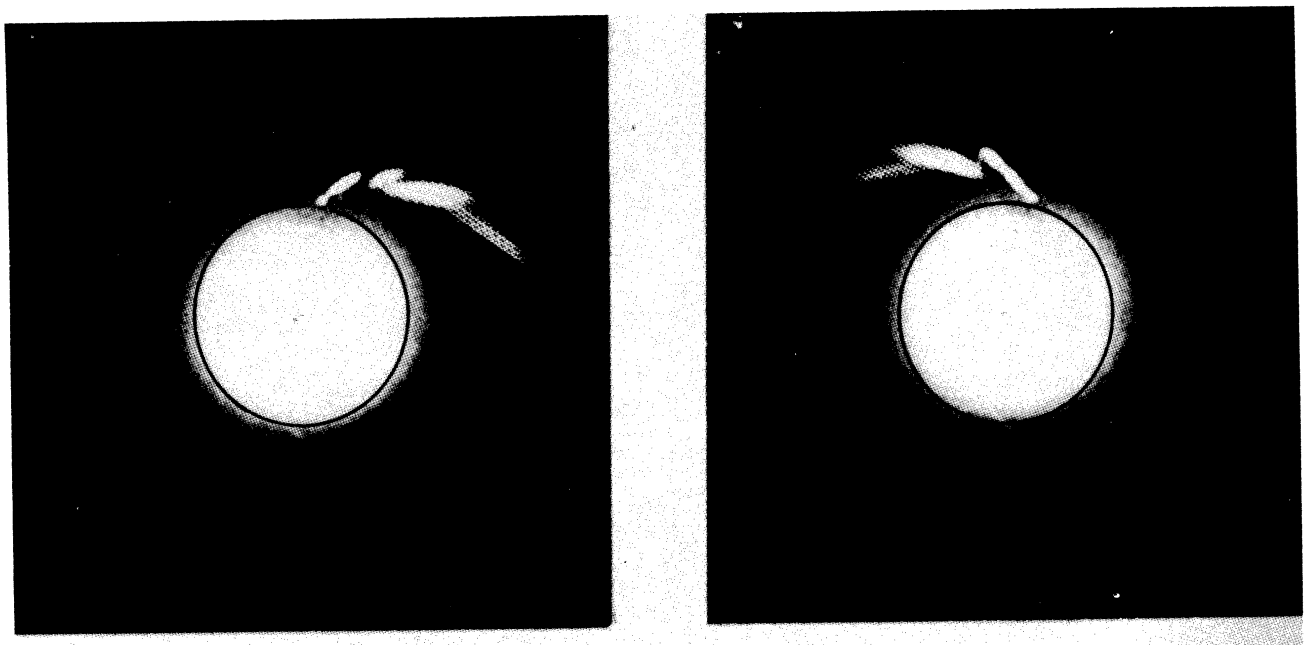

ϕ_a = 870 V. , I_a = 2.2 ma., I_m = 3 A.

ϕ_{BEAM} = 400, 710, 1180, 1980, 4020 V.

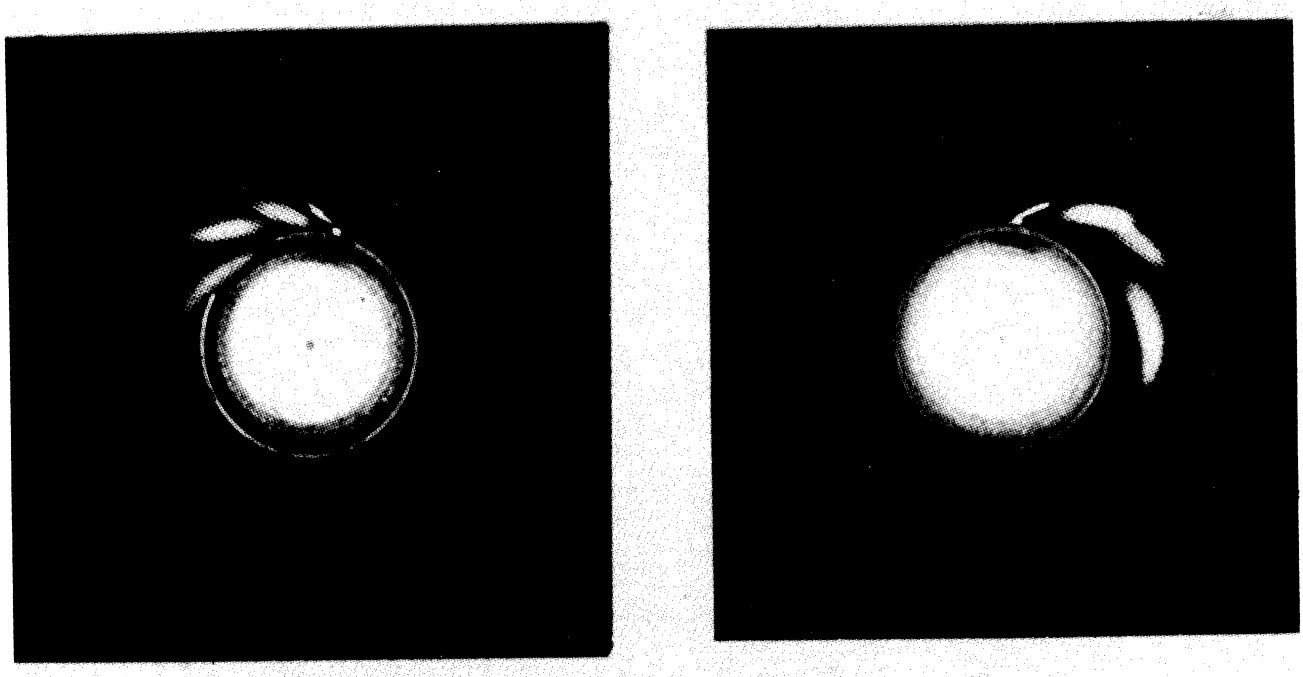

ϕ_a = 655 V., I_a = 0.4 ma., I_m = 3.5 A.

ϕ_{BEAM} = 400, 810, 1580, 3220 V.

FIG. E.4

TRAJECTRON DATA BELOW CUTOFF

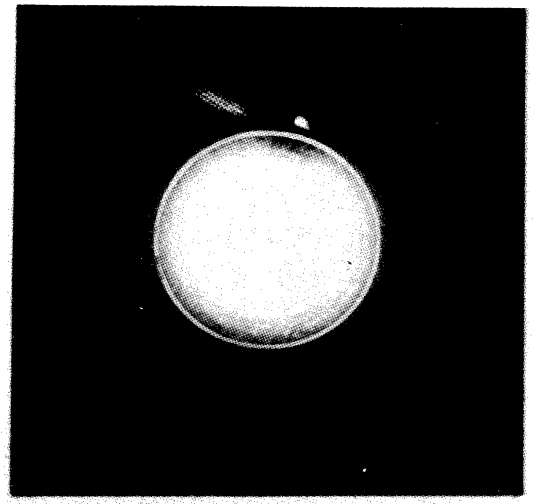

(a.) ϕ_a = 479 V.
I_a = 1.0 ma.

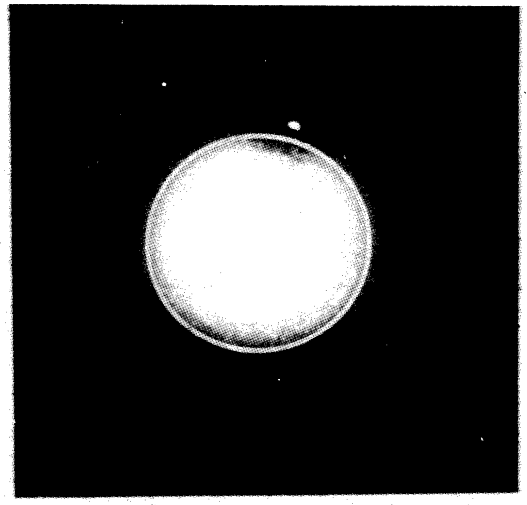

(b.) ϕ_a = 500 V.
I_a = 1.0 ma.

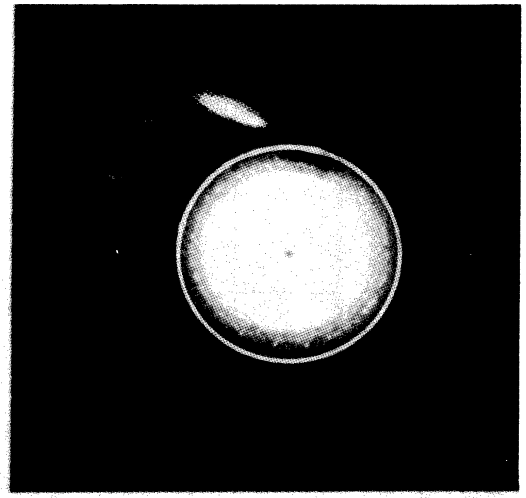

(c.) ϕ_a = 526 V.
I_a = 1.1 ma.

(d.) ϕ_a = 590 V.
I_a = 1.15 ma.

ϕ_{BEAM} = 280, 400, 500, 810 V.
FOR ALL PHOTOGRAPHS

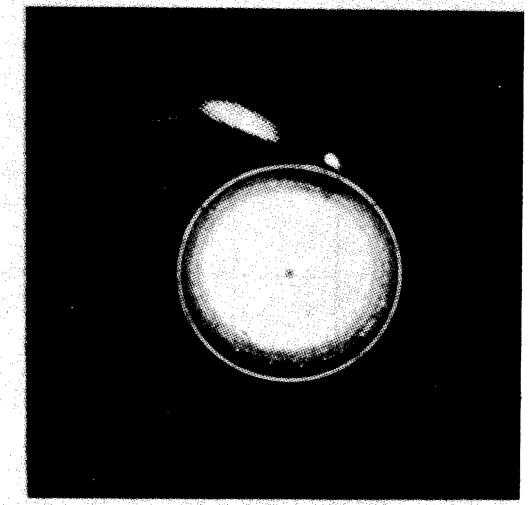

(e.) ϕ_a = 610 V.
I_a = 1.2 ma.

FIG. E.5 TRAJECTRON DATA NEAR ANODE CURRENT INFLECTIONS (SEE FIGURE E.6)

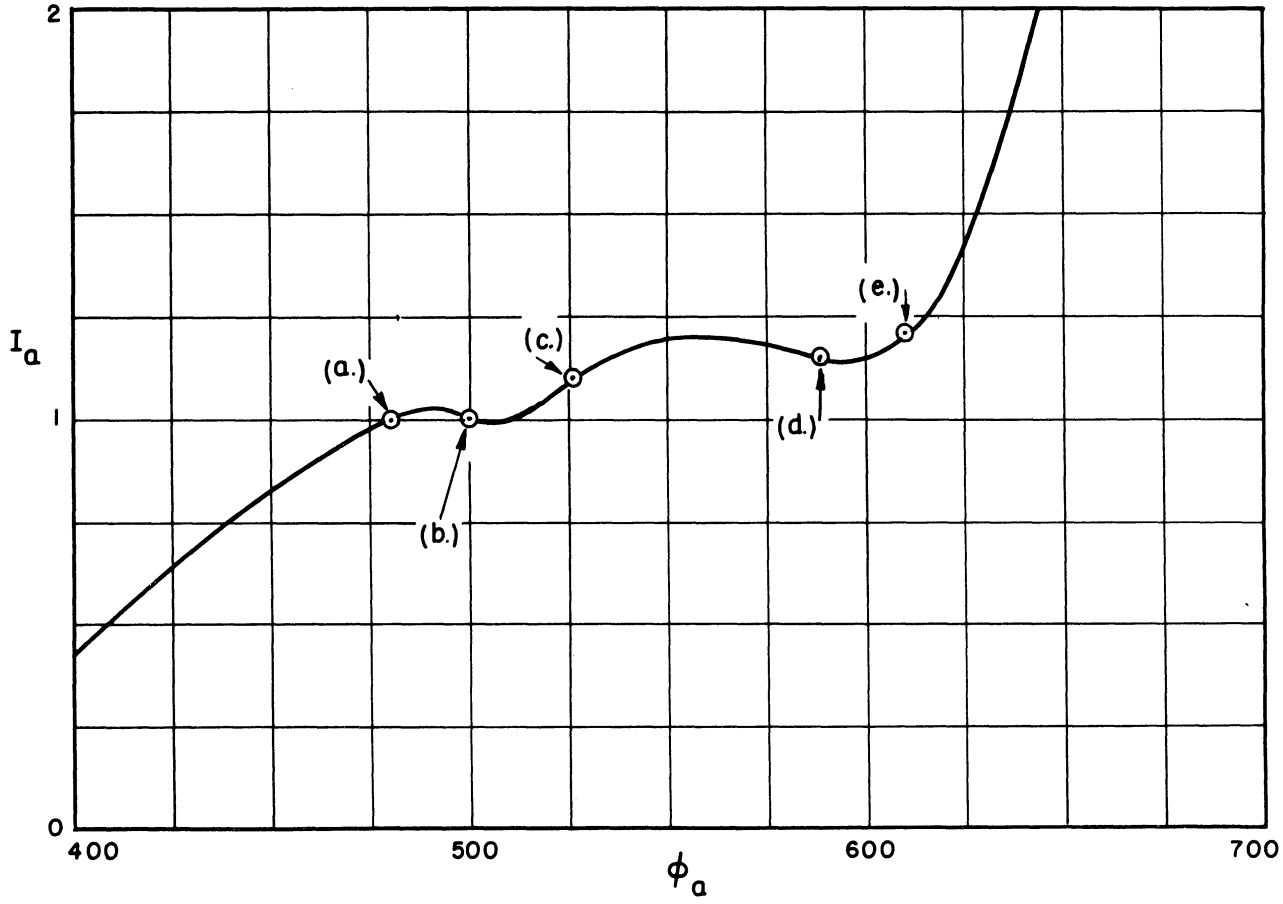

FIG. E.6
ANODE CURRENT – ANODE VOLTAGE
CURVE SHOWING POINTS AT WHICH
THE DATA IN FIGURE E.5 WERE TAKEN

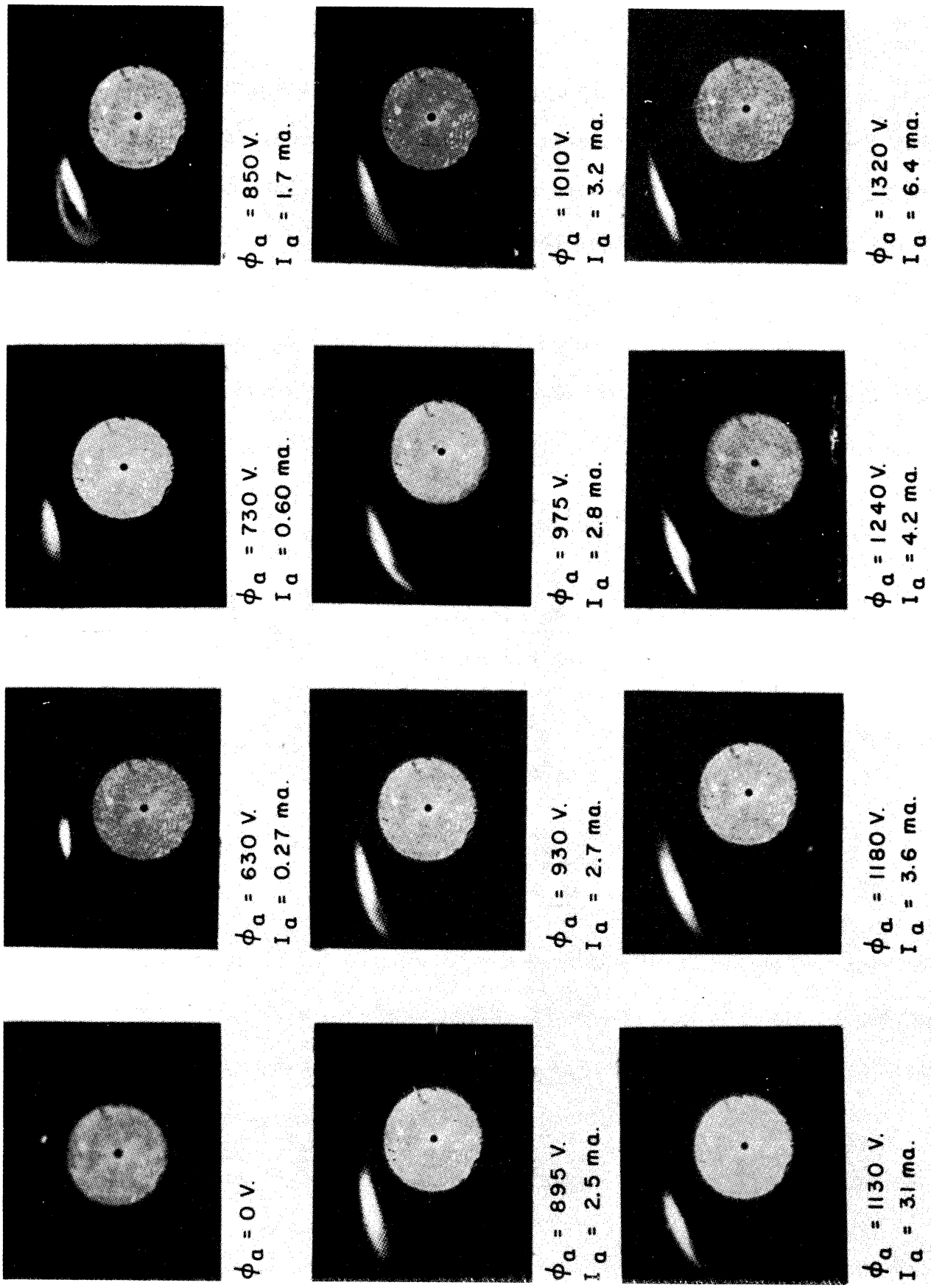

FIG. E. 7 TRAJECTRON BEAM SPOTS WITH FIXED BEAM POTENTIAL AND VARYING ANODE POTENTIAL (I_m = 3.5 A., ϕ_{BEAM} = 810 V.)

APPENDIX F

The purposes of this appendix are (1) to show more rigorously that the trajectron data indicate the presence of space charge outside the Hull radius, and (2) to give some quantitative relations between the amount of space charge outside the Hull radius and the increase in anode potential resulting from the presence of this space charge.

The first step is to derive inequalities concerning the electric field from the equations of motion of beam electrons. Equation (4.27) applies in this case.

$$\frac{\dot{r}^2}{\omega_L^2 a^2} = \frac{\dot{r}_o^2}{\omega_L^2 a^2} + \frac{2e\phi(r,z)}{m\omega_L^2 a^2} - \frac{2e\phi(r_o,z_o)}{m\omega_L^2 a^2} - \frac{r^2}{\omega_L^2 a^2}\left[\frac{P_\theta}{mr^2} + \omega_L\right]^2 + \frac{r_o^2}{\omega_L^2 a^2}\left[\frac{P_\theta}{mr_o^2} + \omega_L\right]^2 - \frac{\dot{z}^2 - \dot{z}_o^2}{\omega_L^2 a^2} \quad . \tag{4.27}$$

$$\frac{2e\phi(r,z)}{m\omega_L^2 a^2} = \frac{2e\phi(r_o,z_o)}{m\omega_L^2 a^2} - \frac{\dot{r}_o^2}{\omega_L^2 a^2} + \frac{\dot{z}^2 - \dot{z}_o^2}{\omega_L^2 a^2} - \frac{r_o^2}{\omega_L^2 a^2}\left[\frac{P_\theta}{mr_o^2} + \omega_L\right]^2 + \frac{r^2}{\omega_L^2 a^2}\left[\frac{P_\theta}{mr^2} + \omega_L\right]^2 \quad . \tag{F.1}$$

The beam was certainly decelerated in the z-direction at least as by the copper mesh at the fluorescent screen as it was accelerated upon entering the diode. Thus $\dot{z}^2 - \dot{z}_o^2$ must be negative. Hence

$$\frac{2e\phi(r,z)}{m\omega_L^2 a^2} < \frac{2e\phi(r_o,z_o)}{m\omega_L^2 a^2} - \frac{r_o^2}{\omega_L^2 a^2}\left[\frac{P_\theta}{mr_o^2} + \omega_L\right]^2 + \frac{r^2}{\omega_L^2 a^2}\left[\frac{P_\theta}{mr^2} + \omega_L\right]^2 , \tag{F.2}$$

or

$$\frac{2e\phi(r,z)}{m\omega_L^2a^2} < \frac{2e\phi(r_o, z_o)}{m\omega_L^2a^2} - \frac{P_\theta^2}{m^2\omega_L^2a^2r_o^2} - \frac{r_o^2}{a^2} + \frac{P_\theta^2}{m\omega_L^2a^2r^2} + \frac{r^2}{a^2} . \qquad (F.3)$$

Rearranging the terms, this can be put in the following form:

$$\frac{2e\phi(r,z)}{m\omega_L^2a^2} < \frac{2e\phi(r_o,z_o)}{m\omega_L^2a^2} + \frac{r^2}{a^2}\left(1 - \frac{a^2}{r^2}\right) - \frac{(P_\theta^2-m^2\omega_L^2a^4)}{m^2\omega_L^2a^2}\left(\frac{1}{r_o^2} - \frac{1}{r^2}\right)$$

$$- \left(\frac{r_o}{a} - \frac{a}{r_o}\right)^2 . \qquad (F.4)$$

By equation (4.2) of Chapter IV,

$$P_\theta = m\omega_L^2\left[(a+h)^2 - s^2\right] \qquad (4.2)$$

where h and s are parameters of the helical path of the beam electron, as described in Figure (4.4). Since h is greater than zero and s smaller than h for all beam electrons,

$$P_\theta < m\omega_L a^2 , \qquad (F.5)$$

and hence the factor $(P_\theta^2 - m\omega_L^2a^4)$ is positive. Since r is greater than r_o, the last two terms in (F.4) are negative. Hence

$$\frac{2e\phi(r,z)}{m\omega_L^2a^2} < \frac{2e\phi(r_o,z_o)}{m\omega_L^2a^2} + \frac{r^2}{a^2}\left(1 - \frac{a^2}{r^2}\right) . \qquad (F.6)$$

The essence of this inequality is that the potential at the maximum radius of a beam electron orbit is equal to the kinetic energy of its tangential motion, which is smaller than it would be if the beam electron had started at rest from the cathode.

A bound on the potential gradient at the maximum radius of the beam electron orbit can be found from the equations of motion:

$$m\ddot{r} - mr\dot{\theta}^2 - e\frac{\partial\phi(r,z)}{\partial r} + eBr\dot{\theta} = 0 \qquad (2.46a)$$

The angular velocity $\dot{\theta}$ can be eliminated by using the angular momentum integral:

$$mr^2\dot{\theta} - \frac{eBr^2}{2} = P_\theta \quad , \quad \text{or}$$
$$mr^2(\dot{\theta} - \omega_L)^2 = P_\theta \tag{2.48}$$

Then equation (2.46a) becomes

$$\frac{e}{m}\frac{\partial \phi}{\partial r} = \ddot{r} - \frac{P_\theta^2}{m^2\omega_L^2 r^3} + \omega_L^2 r \quad . \tag{F.7}$$

By (F.6), $P_\theta < m\omega_L^2 a^2$, and at the maximum radius of the beam electron orbit, $\ddot{r} < 0$. Hence

$$\frac{e}{m}\frac{\partial \phi}{\partial r} < \omega_L^2 \left(r - \frac{a^4}{r^3} \right) . \tag{F.8}$$

This equation states essentially that the magnetic force is greater than the electric force at the turning point.

Now suppose that a beam electron has its turning point at a a radius at least as great as the Hull radius, and suppose there is no space charge outside the Hull radius. Then, given the potential and gradient at the turning point, the anode potential could be calculated. Equations (F.6) and (F.8) give upper bounds on the potential and the gradient, and from them an upper bound on the anode potential can be found.

Equation (F.6) states that the potential at the maximum radius of the beam electron orbit is less than the potential of the B_o solution plus the potential at the point where the beam entered. (This last term is for all practical purposes negligible.) Equation (F.8) states that the gradient at the turning point is less than the gradient of the B_o solution. It follows that if there is no space charge at a radius greater than the maximum radius R_T of a beam electron's orbit, then the

potential at the anode is less than the potential which would occur if there were B_o type space charge in the magnetron with the Hull radius R_h equal to R_T. Anode potential as a function of Hull radius is plotted in Figure 2.10. For example, suppose an electron has its turning point at $R_T = 2$. Then if there is no space charge where $R > 2$, the anode potential must be less than $.067B^2$. (At $R_h = 2$ on the B_o curve in Figure 2.10, $\phi_a = .067B^2$.) If the anode potential is observed to be greater than $.067B^2$, there must be space charge at radius $R > 2$.

The application of this principle to the trajectron data to establish the presence of secular space charge, is now straightforward. The Hull radius is estimated on the basis of Table 5.1 and a data photograph. Judging from Table 5.1, some beam electron has its maximum radius at or slightly beyond the Hull radius. Hence an upper bound for the anode potential can be obtained if it is assumed that there is no space charge outside the Hull radius. The anode potential is observed to be greater than this, and hence it can be concluded that there is space charge outside the Hull radius. This is essentially what was done in Chapter V on page 161.

Next, bounds for the amount of space charge outside the Hull radius will be established. The difference between the potential which occurs and the potential which would occur if there were no space charge outside the Hull radius can be considered as a potential; denote it by $\phi_q(r)$. This potential $\phi_q(r)$ must be zero and have zero gradient at $r = r_h$. At the anode it has the value which is the difference between observed anode potential and the potential which would occur with no space charge outside the Hull radius. If the space-charge distribution is denoted by $\rho_s(r)$, $\phi_q(r)$ satisfies Poisson's equation

$$\frac{1}{r}\frac{d}{dr}\left(r\frac{d\phi_q}{dr}\right) = -\frac{\rho_s(r)}{\epsilon_o} \quad . \tag{F.9}$$

This can be integrated, and

$$\phi_q(r) = -\frac{1}{\epsilon_o}\int_{r_h}^{r}\frac{1}{r}\int_{r'=r_h}^{r'=r} r'\,\rho_s(r')dr'dr \tag{F.10}$$

The integral

$$\int_{r'=r_h}^{r'=r} r'\,\rho_s(r')dr' = \frac{q(r)}{2\pi} \tag{F.11}$$

where $q(r)$ is the amount of space charge between the radius r_h and the radius r. Substituting this in (F.10), and considering only the potential at the anode, (F.10) becomes

$$\phi_q(r_a) = \frac{-1}{2\pi\epsilon_o}\int_{r_h}^{r_a}\frac{q(r)}{r}\,dr. \tag{F.12}$$

The total space charge outside the Hull radius is $q(r_a)$, and the ratio of increase in anode potential to total space charge is

$$\frac{\phi_q(r_a)}{q(r_a)} = -\frac{1}{2\pi\epsilon_o}\int_{r_n}^{r_a}\frac{q(r)dr}{rq(r_a)} \tag{F.13}$$

The ratio $q(r)/q(r_a)$ is monotone increasing and has maximum value unity. It describes the manner in which the space charge is distributed. If all the space charge is concentrated at the Hull radius, $q(r)/q(r_a)$ is identically unity, and the integral (F.13) takes on its maximum value. For that case, equation (F.13) yields

$$\frac{\phi_q(r_a)}{q(r_a)} = \frac{1}{2\pi\epsilon_o}\,\ell n\,\frac{r_a}{r_h} \quad . \tag{F.14}$$

If the space charge density is constant, then by (F.11)

$$q(r) \sim r^2 - r_h^2 \quad , \tag{F.15}$$

and hence

$$\frac{q(r)}{q(r_a)} = \frac{r^2 - r_h^2}{r_a^2 - r_h^2} \quad . \tag{F.16}$$

Then equation (F.13) yields

$$\frac{\phi_q(r_a)}{q(r_a)} = \frac{1}{2\pi\epsilon_o}\left[\frac{1}{2} - \frac{r_h^2}{(r_a^2 - r_h^2)} \ln\frac{r_a}{r_h}\right] \quad . \tag{F.17}$$

Equation (F.14) is certainly an upper bound on the ratio of inc ease in anode voltage to space charge outside the Hull radius. The space-charge density probably decreases as the radius is increased; if so, equation (F.17) is a lower bound on the ratio. The space charge distribution of the B_o solution will lie between these two limits. If r_h is taken as 1.5a and r_a as 3.65a, then equation (F,14) gives $0.89/2\pi\epsilon_o$, equation (F.17) gives $0.31/2\pi\epsilon_o$, and the B_o solution gives $0.38/2\pi\epsilon_o$ as values for this ratio.

BIBLIOGRAPHY

On the DC Magnetron:

1. Allis, W. P. "Theory of the Magnetron Oscillator; Electron Orbits in the Cylindrical Magnetron with Static Fields." Unpublished Radiation Laboratory Special Report 9S, Section 5 (122), M.I.T., 1941.

2. Bellustin, S. V. "On the Theory of Motion of Electrons in Crossed Electric and Magnetic Fields with Space Charge," Physikalische Zeitschrift der Sowjetunion, Vol. 10 (1936), pp. 251-256.

3. Benham, W. E. "Electronic Theory and the Magnetron Oscillator," Proc. Phys. Soc. (London), Vol. 47 (January, 1935), pp. 1-53.

4. Bethenrod, J. "Sur la variation du courant d'espace dans un magnétron sous l'action du champ magnétique," Comptes Rendus de l'Académie des Sciences, Vol. 209 (December 4, 1939), pp. 832-834.

5. Boutry, G. A., and Delcroix, J. L. "La charge d'espace dans un magnétron en régime statique de coupre: magnétron plan ou quasi plan," Comptes Rendus de l'Académie des Sciences, Vol. 232 (April 9, 1951), pp. 1413-1415.

6. Braude, S. J. "The Motion of Electrons in Electric and Magnetic Fields Taking into Consideration the Action of the Space Charge, Physikalische Zeitschrift der Sowjetunion, Vol. 7 (1935), pp. 565-571.

7. Braude, S. J. "On the 'Cutoff' in the Plane Magnetron with Space Charge," Physikalische Zeitschrift der Sowjetunion, Vol. 8 (1935), pp. 584-586.

8. Brillouin, L. "Electronic Theory of the Plane Magnetron," Advances in Electronics, ed. by L. Marton, Vol. 3. New York: Academic Press, 1951, pp. 85-144.

9. Brillouin, L., and Bloch, F. "Electronic Theory of the Cylindrical Magnetron," Advances in Electronics, ed. by L. Marton, Vol. 3. New York: Academic Press, 1951, pp. 145-181.

10. Delcroix, J. L., and Boutry, G. A. "Le magnétron plan en régime statique de charge d'espace," Comptes Rendus de l'Académie des Sciences, Vol. 230 (March 30, 1950), pp. 1046-1048.

11. Delcroix, J. L., and Boutry, G. A. "La charge d'espace dans un magnétron en régime statique de coupure: magnetron cylindrique," Comptes Rendus de l'Académie des Sciences, Vol. 232 (April 30, 1951), pp. 1653-1655.

12. Delcroix, J. L. "Le magnétron en régime statique de coupure: passage du cas cylindrique au cas plan," Comptes Rendus de l'Académie des Sciences, Vol. 232 (June 18, 1941), pp. 2298-2300.

13. Delcroix, J. L. "Le magnétron en régime statique de charge d'espace: magnétrons à anode centrale," Comptes Rendus de l'Académie des Sciences, Vol. 233 (August 20, 1951), pp. 546-547.

14. Delcroix, J. L. "Le magnétron en régime statique de coupure: étude expérimentale," Comptes Rendus de l'Académie des Sciences, Vol. 234 (June 9, 1952), pp. 2347-2349.

15. Delcroix, J. L. "Le magnétron en régime statique de coupure: étude expérimentale. II. Influence de l'inclinasion du champ magnétique sur l'axe du magnétron," Comptes Rendus de l'Académie des Sciences, Vol 235 (November 3, 1952), pp. 1018-1020.

16. Delcroix, J. L. Étude des propriéties statiques des charges d'espace du type magnétron. Doctoral thesis, University of Paris, June, 1953.

17. Doehler, O. "Sur les propriéties des tubes a champ magnétique constant," Part I, Annales de Radioélectricité, Vol. 3 (January, 1948), pp. 27-39.

18. Dow, W. G. Microwave Electron Tubes. New York: Wiley (in preparation).

19. Engbert, W. "Die Potentialverteilung im Magnetron," Hochfrequenztechnik und Electroakustik, Vol. 51 (January, 1938), pp. 44-52.

20. Fechner, P. "Étude sur le magnétron à l'étate bloqué," Annales de Radioélectricité, Vol. 7 (April, 1952), pp. 83-105.

21. Gabor, D. "Stationary Electron Swarms in Electromagnetic Fields," Proc. Roy. Soc. (London), Series A, Vol. 183 (June 18, 1945), pp. 436-453.

22. Glagolev, V. M. "The Passage of Steady Current in a Cylindrical Magnetron," Zhurnal Teknicheskoi Fiziki (U.S.S.R.), Vol. 19 (August, 1949), pp. 943-951. (Also N.R.L. Translation No. 318.)

23. Guénard, P., and Huber, H. "Étude expérimentale de l'interaction par ondes de charge d'espace au sein d'un faisceau électronique se déplaçant dans des champs électrique et magnétique croisés," Annales de Radioélectricité, Vol. 7 (October, 1952), pp. 252-278.

24. Hartree, D. R. Unpublished British Reports C.V.D. Mag. 1, 1941; 3, 1941; 6, 1941; 12, 1942; 23, 1942; 30, 1943.

25. Harvey, A. F. High Frequency Thermionic Tubes. New York: Wiley, 1943.

26. Hull, A. W. "The Effect of a Uniform Magnetic Field on the Motion of Electrons between Coaxial Cylinders," Phys. Rev., Vol. 18 (July, 1921), pp. 31-61.

27. Hull, A. W. "The Paths of Electrons in the Magnetron," (Abstract), Phys. Rev., Vol. 23 (January, 1924), p. 112.

28. Hok, G. "A Statistical Approach to the Space Charge Distribution in a Cut-Off Magnetron," Jour. App. Phys., Vol. 23 (September, 1952), pp. 983-989.

29. Hok, G. "Space-Charge Equilibrium in a Magnetron--A Statistical Approach," Unpublished Technical Report No. 10, Electron Tube Laboratory, University of Michigan, July, 1951.

30. Linder, E. G. "Excess Energy Electrons and Electron Motion in High Vacuum Tubes," Proc. I.R.E., Vol. 26 (March, 1938), pp. 346-371.

31. Lindsay, P. A., and Sims, G. D. "Application of the Thermodynamics of Irreversible Processes to the Theory of the Magnetron," Proc. Phys. Soc. (London), Vol. 66 (May, 1953), p. 423.

32. Möller, H. G. "Elektronenbahnen und Mechanismus der Schwingungserregung," Hochfrequenztechnik und Elektroakustik, Vol. 47 (March, 1936), pp. 115-117.

33. Möller, J. "Messung des Elektronenringstromes im Magnetron," Hochfrequenz und Elektroakustik, Vol. 48 (October, 1936), pp. 141-142.

34 Moullin, E. B. "Considerations of the Effect of Space Charge in the Magnetron," Proc. Cambridge Phil. Soc., Vol. 36 (1940), p. 94.

35. Page, L., and Adams, N. I. "Space Charge in Plane Magnetron," Phys. Rev., Vol. 69 (May 1-15, 1946), pp. 492-493.

36. Page, L., and Adams, N. I. "Space Charge in Cylindrical Magnetron," Phys. Rev., Vol. 69 (May 1-15, 1946), pp. 494-500.

37. Pidduck, F. B. "Electrical Notes: VII Space Charges in a Magnetic Field," Quarterly Journal of Mathematics (Oxford Series), Vol. 7 (September, 1936), pp. 201-209.

38. Reverdin, D. L. "Electron Optical Exploration of Space Charge in a Cutoff Magnetron," Jour. App. Phys., Vol. 22 (March, 1951), pp. 257-262.

39. Slater, J. C. Microwave Electronics. New York: Van Nostrand, 1950, pp. 333-354.

40. Spiwak, G. V., and Zrebny, P. E., "On the Magnetron Cutoff Curve," Comptes Rendus de l'U.R.S.S., Vol. 24 (1939), pp. 237-241.

41. Stoner, E. C. Unpublished British Reports C.V.D. Mag. 8, 1941; 16, 1942; 17, 1942; 25, 1942.

42. Svenssen, R. "An Experimental Investigation of the Electron Orbits in a Magnetron," Proc. I.R.E., Vol. 39 (July, 1951), p. 838.

43. Tonks, L. "Motion of Electrons in Crossed Electric and Magnetic Fields with Space Charge," Physikalische Zeitschrift der Sowjetunion, Vol. 8 (1935), pp. 572-578.

44. Twiss, R. Q. On the Steady State and Noise Properties of Linear and Cylindrical Magnetrons, Doctoral thesis, M.I.T., 1949.

45. Twiss, R. Q. "On the Steady-State Theory of the Magnetron," Advances in Electronics, ed. by L. Marton, Vol. 5, New York: Academic Press, 1953, pp. 247-289.

46. Warnecke, R., Huber, H., Guénard, P., and Doehler, O. "Oscillations d'un magnétron sans fente liées à l'amplification par ondes de charge d'espace," Comptes Rendus de l'Académie des Sciences, Vol. 235 (August 25, 1952), pp. 493-494.

47. Warnecke, R., Huber, H., Guénard, P., and Doehler, O. "Amplification par ondes de charge d'espace dans un faisceau électronique se déplaçant dans des champ électrique et magnétique croisés," Comptes Rendus de l'Académie des Sciences, Vol. 235 (August 18, 1952), pp. 470-472.

48. Wasserman, I. I. "Rotating Space Charge in a Magnetron with Solid Anode" (in Russian), J. Tech. Phys. (U.S.S.R.), Vol. 18 (1948), p. 785.

49. Watanabe, Y., and Katsura, S. "The Cut-off Characteristic and the Potential Distribution of the Magnetron Tube," Technology Reports of the Tohoku University (Sendai, Japan), Vol. 14, No. 1 (1949), pp. 10-26.

50. Wigdortschik, I. M. "Die Geschwindigkeitsverteilung der Elektronen unter dem Einfluss Eines Magnetischen Feldes im Hochvacuum," Physicalische Zeitschrift der Sowjetunion, Vol. 10 (1936), pp. 245-250.

Other Works Cited in the Text:

A. Attwood, S. S. Electric and Magnetic Fields. Third Edition. New York: Wiley, 1949.

B. Dow, W. G. Fundamentals of Engineering Electronics. Second Edition. New York: Wiley, 1952.

C. Dow, W. G. Fundamentals of Engineering Electronics. First Edition. New York: Wiley, 1937.

D. Goldstein, H. Classical Mechanics. Cambridge, Mass.: Addison-Wesley, 1950.

E. Jahnke, E., and Emde, F. Tables of Functions. Fourth Edition. New York: Dover, 1945.

F. Schiff, L. I. Quantum Mechanics. New York: McGraw-Hill, 1949.

G. Spangenberg, K. R. Vacuum Tubes. New York: McGraw-Hill, 1948.

H. Strong, J. Procedures in Experimental Physics. New York: Prentice-Hall, 1938.

I. Webster, A. G. The Dynamics of Particles, and of Rigid, Elastic, and Fluid Bodies. Second Edition. Leipzig: B. G. Teubner, 1912.

LIST OF SYMBOLS USED IN THE TEXT

a	cathode radius
A	vector potential of the magnetic field
A_x, A_y, etc.	components of vector potential
b	constant proportional to current (p. 40)
B	magnetic flux density
B_o, B_1, etc.	types of solutions of magnetron equations (p. 5)
e	charge of an electron
E	energy of an electron
F	electric field strength
h	distance from cathode to axis of helical path of a beam electron (p. 105)
I	current per unit length in a cylindrical magnetron
I_a	anode current in the trajectron
I_m	magnet solenoid current
J	current density
k_1, k_2, etc.	constants in hypothetical secular space charge distributions (p. 61)
ℓ	length of trajectron diode
ℓn	natural logarithm
m	mass of an electron
P_x	canonical x-momentum (p. 20)
P_θ	canonical angular momentum (p. 33)
$Q(R)$	normalized secular space charge distribution (p. 61)

LIST OF SYMBOLS USED IN THE TEXT (cont.)

r	radial distance from axis of cathode
r_a	anode radius
r_h	Hull radius; i.e., maximum radius reached by an electron initially at rest on the cathode (p. 36)
r_o	initial radial displacement
$\dot{r}_o$	initial radial velocity
$R = r/a$	normalized radial distance
$R_a = r_a/a$	ratio of anode radius to cathode radius
$R_h = r_h/a$	normalized Hull radius
R_M	normalized radius of outside edge of spot at its maximum deflection (p. 159)
R_m	normalixed radius of inside edge of spot at its maximum deflection (p. 159)
s	radius of helical path of a beam electron (p. 105)
t	time
$T = \omega_L T$	normalized time
W	distance between successive zeros in velocity in a planar magnetron (p. 26)
x, y, z	rectangular coordinates (p. 18)
$\dot{x}, \dot{y}, \dot{z}$	velocity components in the rectangular system
x_o, y_o, z_o	initial position coordinates
$\dot{x}_o, \dot{y}_o, \dot{z}_o$	initial velocity components
y_h	Hull displacement in a planar magnetron; i.e., maximum displacement of an electron initially at rest on the cathode (p. 22)
y_a	distance between cathode and anode

LIST OF SYMBOLS USED IN THE TEXT (cont.)

α	time constant defined on page 126
γ	time constant defined on page 104
δ	initial angular position of a beam electron in its helical path (p. 105)
ϵ_o	dielectric constant of free space
ϕ, $\phi(r)$, $\phi(r,z)$, $\phi(y)$	electric potential
$\psi(r)$	effective potential for the cylindrical magnetron (p. 128)
ρ	space charge density
ρs	secular space charge density
θ	angular coordinate
$\dot{\theta}$	angular velocity
θ_o	initial angular displacement
$\dot{\theta}_o$	initial angular velocity
$\omega_L = \frac{eB}{2m}$	Larmor angular velocity

The units used in all equations are MKS unless otherwise noted. When numerical values of B or ϕ_a/B^2 are given, B is measured in gauss.

Since R = r/a, any function of r defines a function of R and vice versa. The same notation is used for both functions: for example, $\phi(r) = \phi(R)$ is the potential in a cylindrical magnetron at radius r = aR.

DISTRIBUTION LIST

20 copies - Director, Evans Signal Laboratory
Belmar, New Jersey
FOR: Chief, Thermionics Branch

10 copies - Chief, Bureau of Ships
Navy Department
Washington 25, D.C.
ATTENTION: Code 930A

10 copies Chief, Engineering and Technical Service
Office of the Chief Signal Officer
Washington 25, D.C.

10 copies Director, Air Materiel Command
Wright Field
Dayton, Ohio
ATTENTION: Electron Tube Section

2 copies - Mr. John Keto
Director, Aircraft Radiation Laboratory
Air Materiel Command
Wright Field
Dayton, Ohio

2 copies - Document File
Electronic Defense Group
Engineering Research Institute
University of Michigan
Ann Arbor, Michigan

1 copy - H. W. Welch, Jr., Project Supervisor
Electronic Defense Group
Engineering Research Institute
University of Michigan
Ann Arbor, Michigan

Engineering Research Institute File
University of Michigan
Ann Arbor, Michigan

W. E. Quinsey, Assistant to the Director
Engineering Research Institute
University of Michigan
Ann Arbor, Michigan

W. G. Dow, Professor
Department of Electrical Engineering
University of Michigan
Ann Arbor, Michigan

Gunnar Hok, Professor
Department of Electrical Engineering
University of Michigan
Ann Arbor, Michigan

J. R. Black, Research Engineer
Engineering Research Institute
University of Michigan
Ann Arbor, Michigan

J. S. Needle, Assistant Professor
Department of Electrical Engineering
University of Michigan
Ann Arbor, Michigan

Bell Telephone Laboratories
Murray Hill, New Jersey
ATTENTION: S. Millman

Microwave Research Laboratory
University of California
Berkeley, California
ATTENTION: Professor D. Sloan

Air Force Cambridge Research Laboratories
Library of Geophysics Directorate
230 Albany Street
Cambridge, Massachusetts
ATTENTION: Dr. E. W. Beth

Air Force Cambridge Research Laboratories
Library of Radiophysics Directorate
230 Albany Street
Cambridge, Massachusetts

Collins Radio Company
Cedar Rapids, Iowa
ATTENTION: Robert M. Mitchell

Columbia Radiation Laboratory
Columbia University
Department of Physics
New York 27, New York

Department of Physics
Cornell University
Ithaca, New York
ATTENTION: Dr. L. P. Smith

Industry and Science Department
Enoch Pratt Free Library
Baltimore 1, Maryland

Vacuum Tube Department
Federal Telecommunication Laboratories, Inc.
500 Washington Avenue
Nutley 10, New Jersey
ATTENTION: A. K. Wing, Jr.

General Electric Co.
General Engineering Laboratory Library
Building 5, Room 130
1 River Road
Schenectady 5, N. Y.

General Electric Research Laboratory
Schenectady, New York
ATTENTION: Dr. A. W. Hull

General Electric Research Laboratory
Schenectady, New York
ATTENTION: P. H. Peters

Mr. A. C. Gable
Ind. and Trans. Tube Dept.
General Electric Co. (Bldg. 269)
Schenectady, New York

Mrs. Marjorie L. Cox, Librarian
G-16, Littauer Center
Harvard University
Cambridge 38, Massachusetts

Cruft Laboratory
Harvard University
Cambridge, Massachusetts
ATTENTION: Professor E. L. Chaffee

Electron Tube Laboratory
Research and Development Laboratory
Hughes Aircraft Company
Culver City, California
ATTENTION: G. R. Brewer

Electron Tube Laboratory
Department of Electrical Engineering
University of Illinois
Urbana, Illinois

Mr. R. Konigsberg
Radiation Laboratory
Johns Hopkins University
1315 St. Paul's Street
Baltimore, Maryland

Department of Electrical Engineering
University of Kentucky
Lexington, Kentucky
ATTENTION: Professor H. Alexander Romanowit

Gift and Exchange Division
University of Kentucky Libraries
University of Kentucky
Lexington, Kentucky

Mr. R. E. Harrell, Librarian
West Engineering Library
University of Michigan
Ann Arbor, Michigan

Department of Electrical Engineering
University of Minnesota
Minneapolis, Minnesota
ATTENTION: Professor W. G. Shepherd

Document Office - Room 20B-221
Research Laboratory of Electronics
Massachusetts Institute of Technology
Cambridge 39, Massachusetts
ATTENTION: John H. Hewitt

National Bureau of Standards Library
Room 203, Northwest Building
Washington 25, D. C.

Dr. D. L. Marton
Chief, Electron Physics Section
National Bureau of Standards
Washington 25, D. C.

Mr. Stanley Ruthberg
Electron Tube Laboratory
Bldg. 83
National Bureau of Standards
Washington 25, D. C.

National Research Council of Canada
Radio and Electrical Engineering Division
Ottawa, Ontario
Canada

Dr. O. S. Duffendack, Director
Phillips Laboratories, Inc.
Irvington-on-Hudson, New York

Polytechnic Institute of Brooklyn
55 Johnson Street
Brooklyn 1, New York
Attention: Dr. E. Webber

Department of Electrical Engineering
Pennsylvania State College
State College, Pennsylvania
ATTENTION: Professor A. H. Waynick

Radio Corporation of America
RCA Laboratories Division
Princeton, New Jersey
ATTENTION: Fern Cloak, Librarian

Mr. C. L. Cuccia
RCA Laboratories Division
Radio Corporation of America
Princeton, New Jersey

Radio Corporation of America
RCA Laboratories Division
Princeton, New Jersey
ATTENTION: Mr. J. S. Donal, Jr.

Radio Corporation of America
RCA Victor Division
415 South 5th Street
Harrison, New Jersey
ATTENTION: Hans K. Jenny

Raytheon Manufacturing Company
Research Division
Waltham 54, Massachusetts
ATTENTION: W. M. Gottschalk

Magnetron Developement Laboratory
Power Tube Division
Raytheon Manufacturing Company
Waltham 54, Massachusetts
ATTENTION: Edward C. Dench

Magnetron Development Laboratory
Power Tube Division
Raytheon Manufacturing Company
Waltham 54, Massachusetts
ATTENTION: W. C. Brown

Sanders Associates, Inc.
135 Bacon Street
Waltham 54, Massachusetts
ATTENTION: Mr. James D. LeVan

Sperry Gyroscope Company
Library Division
Great Neck, Long Island, New York

Department of Electrical Engineering
Stanford University
Stanford, California
ATTENTION: Dr. S. Kaisel

Sylvania Electric Products, Inc.
70 Forsyth Street
Boston 15, Massachusetts
ATTENTION: Mrs. Mary Timmins, Librarian

Sylvania Electric Products, Inc.
Woburn, Massachusetts
ATTENTION: Mr. Marshall C. Pease

Department of Electrical Engineering
Yale University
New Haven, Connecticut
ATTENTION: Dr. L. P. Smith

J. A. Boyd, Assistant Supervisor
Electronic Defense Group
Engineering Research Institute
University of Michigan
Ann Arbor, Michigan

Dr. J. H. Findlay
Director of Research
Electronic Products Company
111 E. 3 Street
Mount Vernon, New York